IST-4-027756 WINNER II

D2.3.3 – v1.00

Link level procedures for the WINNER System

Contractual Date of Delivery to the CEC:	**30 November, 2007**
Actual Date of Delivery to the CEC:	**30 November, 2007**
Editor:	David Falconer
Author(s):	Daniel Aronsson, Gunther Auer, Steffen Bittner, Ivan Cosovic, Florence Danilo-Lemoine, David Falconer, Bernard Hunt, Ming Jiang, Chan-Tong Lam, Adrian Langowski, Hongju Liu, Yi Ma, Maryam Sabbaghian, Fayyaz Siddiqui, Mikael Sternad, Tommy Svensson, Alexander Tyrrell, Kai Yu
Participant(s):	*CTH, CU, DoCoMo, ALUK, PRL, PUT, SEUK, TUD, UniS, UU*
Workpackage:	*WP2*
Estimated person months:	**27**
Security:	**PU**
Nature:	**R**
Version:	1.0
Total number of pages:	211

Abstract: In this deliverable, channel estimation algorithms, pilot design, measurement and signalling concepts, link and network synchronisation techniques, and the effects and remedies for RF impairments are described and evaluated for effective application in all WINNER modes, multiple access techniques and deployment scenarios, for SISO and MIMO systems.

Keyword list: Channel estimation, approximation of channel estimation errors, pilot design, measurements, RF impairments, link layer synchronisation, network synchronisation

Executive Summary

This document describes and evaluates link level procedures which are essential to multi-user transmission, spatial processing, and adaptive efficient spectrum use in the WINNER II reference system. These procedures include:

- pilot-aided channel estimation and associated pilot design
- requirements and capabilities for channel measurements
- link-level and network synchronisation.

The proposed procedures have evolved through earlier WINNER I and II studies, and are evaluated for WINNER local (LA), metropolitan (MA) and wide area (WA) scenarios, taking into account relevant link level channel and interference models, and also realistic models of RF impairments.

Effective estimation of channel parameters, usually carried out at the receiving end of links, is essential for detection and decoding of received data with low error probability, as well as for multi-user channel resource scheduling and adaptive transmitter array processing. Channel estimation (CE) is aided by pilot signals that are multiplexed with data. WINNER pilot pattern arrangements in a scattered frequency- and time-multiplexed grid are described, with rationales, for frequency division duplexing (FDD), time division duplexing (TDD), frequency-adaptive, and frequency-non-adaptive modes for the LA, MA and WA scenarios. Pilot locations in the time-frequency grid are distinct from those of data, and also from pilot locations of other user spatially separated or multiplexed terminals in the same sector sharing the same chunk. In downlinks, common pilots (i.e. shared by several user terminals) per beam or per antenna are used, depending on whether spatial multiplexing, beamforming or spatial precoding is used. Dedicated pilots per transmitting antenna are used for uplink transmission. Optimized pilot patterns for one full uplink chunk shared by one or two users, or several adjacent chunks, are found by a least squares linear interpolation analysis. Optimization of system capacity with respect to pilots' power as well as their frequency-time arrangement is also carried out for MIMO-OFDM.

The basic CE process carried out at the receiver involves interpolation in frequency and time from pilot locations to all data-occupied locations in the time-frequency grid. Derivations of CE error models for SISO and MIMO provide insight into the design of pilot arrangements and interpolation process. Simulation studies show channel estimation mean squared error (MSE) and SNR penalty (for a given frame error rate, relative to the case where the receiver knows all received users' channels exactly) due to pilot-based CE. Results are presented for single- and multi-user/multi-antenna cases, for all the generalized multicarrier multiple access techniques considered by WINNER: full-bandwidth and chunk-based OFDM and DFT-precoded OFDM, IFDMA, B-EFDMA and B-IFDMA. Enhancements to the basic pilot-based interpolation CE process are also described and evaluated: iterative joint channel estimation (ICE) and in-cell interference rejection; joint turbo channel estimation and MIMO detection aided by genetic algorithms (GA); least-squares (LS) equalization to reject low-level inter-cell interference; and prediction of channel state information over multiple frames.

Good channel estimation is vital for satisfactory detection and decoding, equalization, interference rejection and diversity combining in WINNER system receivers. Frequency and time interpolation from pilot signal outputs, aided by ICE, can reduce the receiver's CE SNR penalty of full bandwidth single input single output (SISO) systems to close to zero under realistic channel conditions, and with relatively low pilot overhead. The SNR penalty for multiple-input-multiple-output (MIMO) or space division multiple access (SDMA) systems is somewhat larger, since there are more channels to estimate. It is increased slightly further by out-of-cell user signals interfering with pilots as well as data. For the "sub-chunk" transmission modes proposed in WINNER II (IFDMA, B-IFDMA and B-EFDMA), there is little or no possibility of frequency/time interpolation from pilot locations which experience uncorrelated fading. As a result, these transmission modes experience significant CE SNR losses, which diminish (but do not negate) their net diversity gains over their full-bandwidth or "local" FDMA counterparts.

Good channel estimates fed back from receiver to transmitter are also important for spatio-temporal coding and multiplexing schemes. Simulations of 2X2 MIMO systems with linear space-time transmitter processing show that the Alamouti space-time block coding scheme is significantly less sensitive to CE errors than are transmitter minimum MSE (MMSE) processing or vertical Bell Labs Layered Space Time (V-BLAST) spatial multiplexing.

On a broader system-level scale, channel estimation in the form of *channel measurement* is also an essential prerequisite for link adaptation strategies which efficiently marshall space, frequency, time and

power resources for transmissions to and from multiple user terminals. Channel measurement and signalling allows nodes within the system to understand other nodes of the system, signals within the system, and their context. This information can be used to aid various system functions, from initial system discovery to link adaptation and handover. WINNER measurement capabilities and requirements are listed and analyzed. The knowledge so gained can be employed to optimize measurement and signalling in a full system design. An exemplary analysis of the impact of feedback quantization on 2X2 spatio-temporal schemes was carried out, showing that MIMO downlink performance is very sensitive to quantization errors in the channel information fed back from the receiver to the transmitter.

Cost-effective design of advanced wireless systems requires awareness and minimization of the harmful effects on performance of RF impairments such as high power amplifier (HPA) nonlinearities, frequency offset and phase noise. HPA nonlinearities create the need for transmitter power backoff, which reduces power efficiency, and raises cost. These issues are of crucial importance to user terminals. For a proposed WINNER spectral mask, HPA power backoff requirements are shown to depend mainly on the HPA nonlinear input/output characteristic (or to the extent to which it can be linearized by adaptive feedback or other means). DFT-precoded OFDM permits consistently lower HPA backoff than corresponding OFDM waveforms – the main reason for its choice by WINNER for uplink non-frequency-adaptive transmission. Other signal transmitter processing techniques can be used to reduce peak to average power ratio (PAPR) for all types of OFDM and DFT-precoded OFDM, but they only lower backoff requirements if the HPA is linear up to its saturation value. Phase noise is another RF impairment that can cause inter-subcarrier interference (ICI) in OFDM and other multicarrier waveforms. Decision feedback receiver phase noise compensation techniques are proposed and found by simulation to significantly reduce WINNER receiver performance sensitivity to phase noise and frequency offset, thus permitting the use of lower-quality (and hence cheaper) oscillators in user terminals. Furthermore, analytical expressions are derived and evaluated for the effects of frequency synchronisation and timing errors on OFDM reception.

Synchronisation is a basic requirement in communications systems. On a link level, a receiver cannot know precisely when a message is transmitted, because of the propagation delay between the two nodes. Furthermore there is a frequency misalignment between both local oscillators. Therefore the receiver needs to align in time and frequency with the transmitter in order to perform proper decoding. Generally the link-level synchronisation problem is defined as estimating at the receiver the mismatch in time, frequency and phase, in order to recover when the message was emitted, at what frequency and with which phase. In this document two approaches are proposed and evaluated for symbol and frame synchronisation and for frequency acquisition in WINNER systems. The first, called “T-pilot”, requires one OFDM symbol in the superframe preamble, offers low PAPR, and is effective and simple when narrowband interference (such as might be encountered in license-exempt spectrum-sharing scenarios) is not a problem. When such interference is problematic, another downlink superframe preamble structure, occupying three OFDM symbol lengths, and synchronisation processing is proposed and found to be effective.

On a network level, nodes need to agree on a common time reference for transmission, which indicates the beginning of a super-frame. Within a cellular network, base stations are in charge of maintaining users’ synchronisation, and inter-cell synchronisation is necessary. In the peer-to-peer mode where a base station may not be present, synchronisation among participants needs to be achieved in a decentralised manner. Obtaining a synchronised network can be done in a centralised manner if a global reference time is provided. This can be done by relying on the Global Positioning System (GPS) or the European Satellite Navigation System (Galileo). However this synchronisation technique is not well suited for the WINNER system due to constraints on cost and size.

This document investigates a self-organised network synchronisation algorithm for WINNER, inspired by synchronisation of illumination of fireflies. No central entity is responsible for inter-cell synchronisation, and user terminals and base stations align their time reference by following simple rules, using long synchronisation messages that fit in the superframe preamble structure. A system of *N nodes* starting from a totally unsynchronised condition is always able to reach an agreement on a common time reference within 5 periods for a local area type of network composed of four base stations. This coarse network synchronisation phase is similar to an acquisition phase, and should serve as a basis for self-organised network synchronisation. Through the simulation results, it is shown that the optimal coupling to synchronise depends on the number of user terminals that participate to the network synchronisation. Therefore a base station should know how many user terminals in its vicinity are transmitting uplink Sync words, so that synchrony is reached quickly. Following acquisition, tracking is done in a similar fashion. Tracking is done by nodes emitting synchronisation words periodically during the super-frame preamble. Thus the same synchronisation principle is applied both for acquisition and tracking. As a result nodes follow the fastest oscillator.

Authors

Partner	Name	Phone / Fax / e-mail
Carleton University (CU)		
	Florence Danilo-Lemoine	email : fdanilo@sce.carleton.ca
	David Falconer	Phone : +1-613-520-5722
		Fax : +1-613-520-5727
		email : ddf@sce.carleton.ca
	Chan-Tong Lam	email : lamc@sce.carleton.ca
	Maryam Sabbaghian	email: msabbagh@sce.carleton.ca
	Fayyaz Siddiqui	email : fasiddiq@sce.carleton.ca
Chalmers University of Technology (CTH)		
	Tommy Svensson	Phone : +46 31 772 1823
		Fax: +46 31 772 1782
		Email: tommy.svensson@chalmers.se
NTT DoCoMo Euro Labs (DoCoMo)		
	Gunther Auer	Phone:+49 89 5682 4219
		Fax: +49 89 5682 4301
		e-mail: auer@docomolab-euro.com
	Ivan Cosovic	Phone: +49 89 5682 4229
		Fax: +49 89 5682 4301
		e-mail: cosovic@docomolab-euro.com
	Alexander Tyrrell	Phone:+49 89 5682 4235
		Fax: +49 89 5682 4301
		e-mail: tyrrell@docomolab-euro.com
Alcatel-Lucent UK (ALUK)		
	Angeliki Alexiou	Phone : +44 1793 776620
		Fax.: +44 1793 776725
		Email : alexiou@alcatel-lucent.com
	Kai Yu	Phone : +44 1793 776783
		Fax. : +44 1793 776725
		Email : kaiyu@alcatel-lucent.com
Philips Research Labs (PRL)		
	Bernard Hunt	Phone : +44 1293 815055
		Fax : +44 1293 815024
		Email : Bernard.hunt@philips.com
Poznan University of Technology (PUT)		
	Adrian Langowski	Phone : +48 61 665 3916
		Fax : +48 61 665 3823
		e-mail : alangows@et.put.poznan.pl
Samsung Electronics UK (SEUK)		
	Ming Jiang	Phone: +44 1784 428 669
		Fax : +44 1784 428 628
		email : ming.jiang@samsung.com
	Thierry Lestable	Phone: +44 1784 428 720
		Fax: +44 1784 428 628
		email: thierry.lestable@samsung.com
Technical University of Dresden (TUD)		

	Steffen Bittner	Phone : +49 351 463 41042 Fax: +49 351 463 37255 Email: bittner@ifn.et.tu-dresden.de

University of Surrey (UniS)

	Hongju Liu	Phone :+44 1483 68 3600 Fax : +44 1483 68 6011 Email : H.Liu@surrey.ac.uk
	Yi Ma	Phone :+44 1483 68 3427 Fax : +44 1483 68 6011 Email : Y.Ma@surrey.ac.uk

Uppsala University (CTH/UU)

	Mikael Sternad	Phone: +46 704 250 354 Fax: +46 18 555 096 e-mail: mikael.sternad@signal.uu.se
	Daniel Aronsson	Phone:+46 18 471 3071 Fax: +46 18 555 096 email: Daniel.aronsson@signal.uu.se

Table of Contents

List of Acronyms and Abbreviations

1D	One dimensional
2D	Two dimensional
3G	3rd Generation (Cellular System)
3GPP	3G Partnership Program
3GPP-LTE	3GPP Long Term Evolution
m-PSK	Phase shift keying with *m* constellation points (*m*=2,4,8,)
m-QAM	Quadrature amplitude modulation with *m* constellation points (*m*=4,16,64,256)
AMC	Adaptive Modulation and Coding
AP	Access Point
AWGN	Additive white Gaussian noise
BER	Bit Error Rate
B-EFDMA	Block equidistant frequency division multiple access
B-IFDMA	Block interleaved frequency division multiple access
BLAST	Bell Labs layered space time
BLDPC	Block Low Density Parity Check codes
BS	Base Station
CDC	Common data channel
CE	Channel estimation
CG	Concept Group
CIR	Channel Impulse Response
CP	Cyclic Prefix
CPE	Common phase error
DPA	Common pilots per antenna
CPB	Common pilots per beam
CQI	Channel Quality Information
CS	Coding Scheme
CSC	Cumulative Sub-Cost
CSI	Channel State Information
CSIR	Channel State Information at Receiver
CSIT	Channel State Information at Transmitter
CTF	Channel Transfer Function
DAC	Direct Access Channel
DE	Dominant Eigenmode
DFE	Decision Feedback Equalizer
DFICE	Decision feedback iterative channel estimation
DFT	Discrete Fourier Transform
DL	Downlink
DPA	Dedicated pilots per antenna
DPA-FB	Dedicated pilots per antenna over the full band
DPB	Dedicated pilots per beam
ECSI	Effective Channel State Information
EXIT	Extrinsic Information Transfer
FD	Frequency Domain
FD-CTF	Frequency Domain Channel Transfer Function
FDD	Frequency Division Duplex
FDM	Frequency Domain Multiplexed
FDSPT	Frequency domain superimposed pilots
FEC	Forward Error Correction
FEQ	Frequency Equalization
FER	Frame Error Rate
FET	Frequency expanding technique
FFT	Fast Fourier Transform
FIR	Finite impulse response
FR	Frequency Replacement
GA	Genetic Algorithm

GMC	Generalized Multi-Carrier
GoB	Grid of (fixed) beams
HARQ	Hybrid Automatic Repeat Request
HPA	High power amplifier
IBDFE	Iterated block decision feedback equalization
IBI	Inter-block interference
ICE	Iterative Channel Estimation
ICI	Inter-channel interference
ICU	In-cell user
IDFT	Inverse Discrete Fourier Transform
IFDMA	Interleaved frequency division multiple access
IFFT	Inverse Fast Fourier Transform
IP	Interference Power
ISI	Inter-Symbol Interference
LA	Local Area
LDC	Linear dispersion code
LDPC	Low Density Parity Check (codes)
LE	Linear equalizer
L-FDMA	Localized frequency division multiple access
LLR	Log-Likelihood Ratio
LMMSE	Linear minimum mean squared error
LoS or LOS	Line of Sight
LPIF	Lowpass Interpolation Filter
LS	Least squares
LT	Long term
MA	Metropolitan Area
MAC	Medium Access Control
MAP	Maximum A posteriori Probability
MBMS	Multimedia Broadcast Multicast Service
MCS	Modulation and Coding Scheme
MIMO	Multiple Input Multiple Output
ML	Maximum Likelihood
MMSE	Minimum Mean Square Error
MSE	Mean Square Error
MU-MIMO	Multi-User Multiple Input Multiple Output
MUD	Multi-User Detector
MUI	Multi-User Interference
NIP	Noise plus Interference Power
NloS	Non Line of Sight
OCI	Out-of-cell interferer/interference
OF	Objective Function
OFDM	Orthogonal Frequency Division Multiplexing
OFDMA	Orthogonal Frequency Division Multiple Access
OHRSA	Optimized Hierarchy Reduced Search Algorithm
OS	Objective Score
OSTBC	Orthogonal space time block code
PACE	Pilot assisted channel estimation
PAPR	Peak to Average Power Ratio
PLM	Physical Layer Mode
PS	Pilot spacing
PSD	Power spectral density
PSK	Phase-Shift Keying
QAM	Quadrature Amplitude Modulation
QoS	Quality of Service
QPSK	Quaternary phase shift keying (4-QAM)
RAN	Radio Access Network
RAP	Radio Access Point
RLC	Radio link control
RRM	Radio Resource Management

RSS	Received Signal Strength
RVQ	Random Vector Quantisation
RX	Receiver
SC	Single Carrier
SDMA	Spatial Division Multiple Access
SF	Superframe
SiSo	Soft-input Soft-ouput
SINR	Signal-to-Interference plus Noise Ratio
SISO	Single Input Single Output
SM	Serial modulation or spatial multiplexing
SMMSE	Successive Minimum Mean Square Error
SMUX	Spatial Multiplexing
SNDR	Signal to nonlinear distortion ratio
SNR	Signal-to-Noise Ratio
SOPHIE	Soft-output Optimized Hierarchy
ST	Short term
SVD	Singular Value Decomposition
TD	Time Domain
TDC	Targetted data channel
TDD	Time Division Duplex
TDM	Time domain multiplexed
TdoA	Time Difference of Arrival
ToA	Time of Arrival
TEQ	Turbo Equalisation
THP	Tomlinson-Harashima Precoding
Tx	Transmitter
UL	Uplink
UT	User Terminal
V-BLAST	Vertical Bell Labs Layered space time
WA	Wide Area
WHT	Walsh Hadamard Transform
WIF	Wiener Interpolation Filter
ZF	Zero Forcing

1. Introduction

This report presents and assesses techniques for link level procedures for the WINNER system. These techniques are essential for higher level radio access procedures, which rely on estimation of the channel parameters and on the fact that system elements are synchronised. The present document reports the progress since previous investigations and summarises recent research results achieved within the entire WINNER Phase 2 on various topics such as pilot design, channel estimation, measurement and signalling, RF and synchronisation imperfections, link-level and self-organised synchronisation. It also provides a final specification of pilot design, channel estimation schemes, and synchronisation methods for the WINNER system transmission modes.

1.1 Generic System Model

Chapter 2 presents a background overview of the WINNER generic system model. Sections 2.1, 2.2 and 2.3 respectively describe WINNER transmitter and receiver structures, MAC framing and multiple access techniques. The need for channel estimation affects the overall error rate and efficiency of wireless systems. Assessment criteria in the form of spectral and power efficiency are discussed in Section 2.4. Later sections of the document also show performance in terms of bit error probability and frame error probability. Another measure of channel estimation performance, mean squared estimation error, can be modelled analytically in some scenarios, as discussed in Section 2.5 and Appendix B .

1.2 Pilot Design

Pilots are used for implementing certain physical layer support functions, e.g. connection setup, synchronisation, mobility support, power control, CQI measurements and most importantly channel estimation. However, in addition to supporting channel estimation and other functions, pilots add overhead and consume transmission power. Thus, a proper pilot design should from one side enable successful channel estimation and from other side should keep at minimum induced spectral and power efficiency loses.

WINNER system is a multi-antenna concept that incorporates various spatial processing schemes intended to be used in different transmission environments leading to combination of dedicated pilots per flow, common pilots per cell/sector, common pilots per antenna and common pilots per beam are required. In Chapter 3 WINNER pilot design is presented. In Section 3.2 reference pilot design is described which covers all WINNER scenarios, WA, MA and LA, and all reference multiple-antenna configurations. In Sections K.1 and K.2 optimum pilot placement for uplink is considered assuming single chunk and multiple-consecutive chunks scenarios. The pilot grid and pilot power allocation that optimizes spectral efficiency of MIMO-OFDM is derived in Section K.3..

1.3 Channel Estimation

Effective estimation of channel parameters, usually carried out at the receiving end of links, is essential for detection and decoding of received data with low error probability. On a broader system-level scale, channel estimation (CE) in the form of *channel measurement* is also an essential prerequisite for link adaptation strategies which efficiently marshals space, frequency, time and power resources for transmissions to and from multiple user terminals.

In the WINNER system, channel estimation is aided by the transmission of pilots, frequency-multiplexed with data. Pilots create extra overhead, and it is therefore important to use channel estimation techniques which make most efficient use of a limited number of pilots. WINNER channel estimation techniques are presented in Chapter 4. Sections 4.2 and 4.3 describe respectively, noniterative CE techniques which interpolate frequency response estimates from pilot measurements and enhanced iterative CE techniques which supplement the pilot-aided estimates. Prediction of future channel characteristics aids channel-specific adaptation at the transmitter, and is discussed in Section 4.4. Section 4.5 describes the reference design for channel estimation. Simulation-based assessment of channel estimation techniques is reported in Section 4.6, in the form of SNR degradation relative to the case of ideal channel knowledge. In Section 4.7 the impact of CE errors is derived for Alamouti space-time coding and for spatial multiplexing.

1.4 Measurements

Measurements play an important role in modern communications systems, allowing nodes within the system to understand other nodes, signals within the system, and their context. This information can be used to aid various system functions, from initial system discovery to link adaptation and handover. Since

the node which desires certain measurement information may not be the node which is able to perform that particular measurement, signalling of some measurement information is also necessary. In practical communications systems, design of measurement procedures and associated signalling consists of a trade off between a number of factors, such that performance gains are not taken up by increased overheads.

Through knowledge of the overall channel frequency response, discussed in chapter 4, it is possible to derive a large proportion of the measurement metrics required within a communications system. Additionally, a list of measurement metrics required by other components of the WINNER system, in order to carry out their functionality, is given. These measurement matters are detailed in Section 5.2. Although the trade-off of performance vs. overheads for measurement and signalling procedures is a matter for specific system design and implementation, an example study is given in Section 5.3 on the impact of different signalling on multi-antenna transmission techniques.

1.5 RF Imperfections

The need for compensation of RF and synchronisation impairments comes from the non perfect RF components and from mismatches between transmitters and receivers.

In Chapter 6, three different schemes related to general aspect of impairments are discussed. Firstly, the effects of HPA nonlinearities are evaluated by means of HPA output power spectrum measurements, which are an indicator of the required power backoff. Secondly, phase noise causes inter-symbol interference in multi carrier systems, as well as common phase rotation. In single carrier systems it causes a slowly varying phase rotation to the data symbols. However, in both systems the impact of the phase noise can be estimated, tracked and compensated as presented in the corresponding sections. Finally, the SNR degradation due to interference is evaluated in 6.5 and Appendix L. Here two cases are considered. First of all, interblock interference caused by previous or subsequent OFDM is evaluated. Secondly, intercarrier interference due to frequency offset is investigated.

1.6 Link Layer Synchronisation

Synchronisation in communications systems is necessary on two levels. On the link level, a receiver cannot know precisely when a message is transmitted, because of the propagation delay between the two nodes. Furthermore there is a frequency misalignment between both local oscillators. Therefore the receiver needs to align in time and frequency with the transmitter in order to perform proper decoding. Additional difficulty for successful synchronisation appears if system operates in the presence of interference from other system as in, e.g., license exempt case.

To perform successful link level synchronisation in WINNER systems two algorithms are proposed: an algorithm suitable in case when WINNER does not suffer from any outer world interference and an algorithm suitable in case when such interference exists. Link level synchronisation procedures connected to such scenarios as well as WINNER reference design of synchronisation preamble are described in Chapter 7.

1.7 Self-Organised Network Synchronisation

For the WINNER system concept, a self organised network is considered, so no global coordination unit which manages the behaviour of terminals is assumed. On a network level, synchronisation is defined in the sense of aligning local timing units, such that all nodes agree on a common super-frame start. To this end, it is possible to define a global slot structure, in the way that the beginning and end of a super-frame are global parameters.

To do so in a self-organised manner, similar rules to the ones used in nature by fireflies are applied: each node maintains a time reference, referred to as the phase function, which is updated upon reception of a pulse from other nodes. Chapter 8 presents and adapts the firefly synchronisation algorithm to fit into the WINNER frame structure. Further constraints such as the presence of relays and the necessity to include the access to a Primary Reference Clock in large networks are taken into account.

2. Overview on Generic System Model

2.1 Transmitter and Receiver Structure

Figure 2-1 and Figure 2-2 illustrate the generic transmitter and receiver structures, respectively, in the WINNER system [WIN1D210].

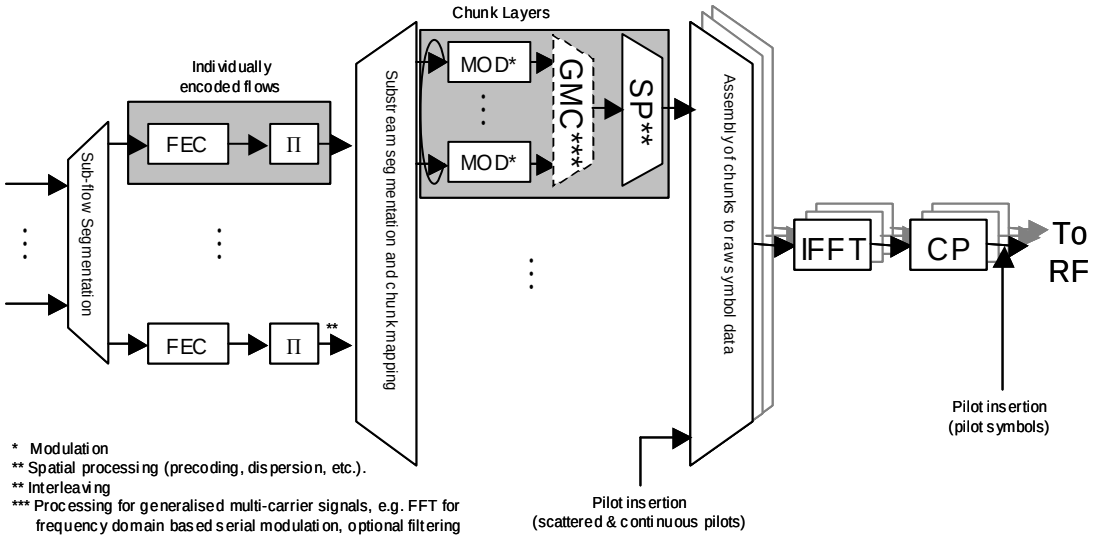

Figure 2-1: Transmitter structure

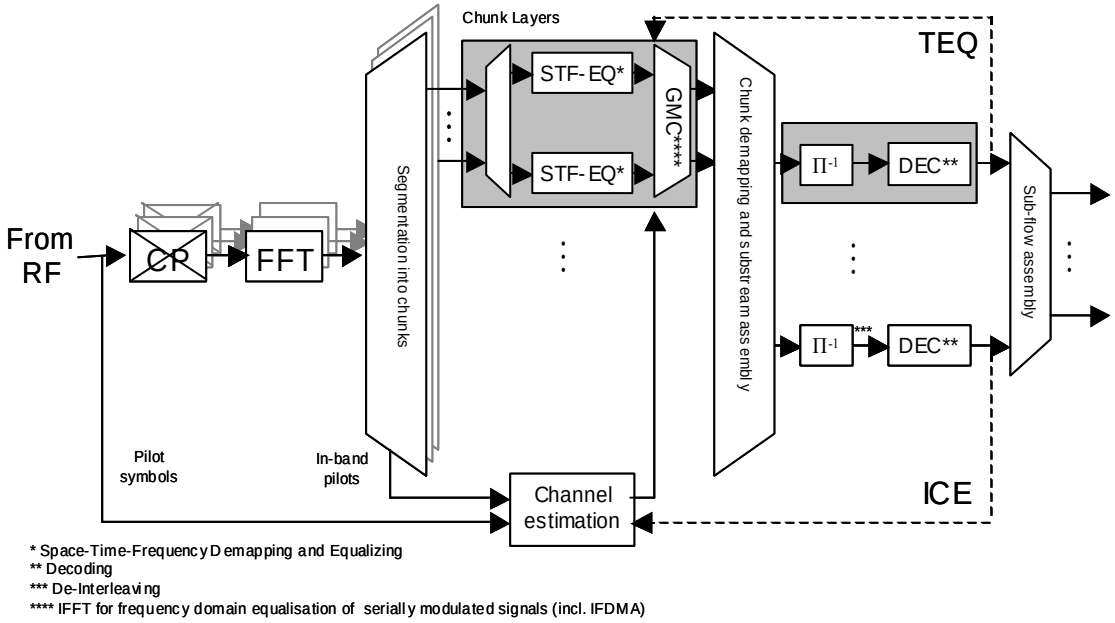

Figure 2-2: Receiver structure

The used air interface parameters are adopted from The WINNER reference system. The OFDM/GMC parameters are presented in Appendix A, which are similar to those used in WIN2D482 except for the number of occupied sub carriers in an OFDM symbol. The difference is small, and does not lead to significant performance differences. An OFDM symbol is a sequence of frequency domain or time domain samples, which are generated by a discrete Fourier transform (DFT) operation from coded, interleaved and constellation-mapped data symbols. The term "OFDM symbol" will be used for all the multicarrier signal variants used in WINNER, including GMC, OFDM, OFDMA, DFT-precoded OFDM, SM, IFDMA B-EFDMA and B-IFDMA.

2.2 MAC Framing

The basic time-frequency unit for resource allocation is the chunk as specified in [WIN2D6137]. In the FDD physical layer modes, chunks comprise 8 subcarriers by 12 OFDM symbols or 312.5 KHz x 345.6 μs. In the TDD physical layer mode, the chunk dimension is 8 subcarriers by 15 OFDM symbols, or 390.62 KHz x 345.6 μs. Compared to [WIN2D6131] the number of subcarriers per chunk is halved from 16 to 8 in order to adapt to the frequency selectivity encountered in metropolitan outdoor scenarios, such as the microcellular test case.

The chunks are organised into *frames*. In the TDD mode, each frame consists of a downlink transmission interval followed by an uplink transmission interval, denoted *slots*, or *time-slots*. In FDD, the frame is also split into two intervals, denoted *slots*, or *time-slots*. Half-duplex terminals may be separated into two groups, where one group has downlink transmission in the first slot and transmits in uplinks in the other, while the other group use the opposite scheme. FDD base stations work in full duplex.

The frame duration has been set equal in the two physical layer modes (PLM)s, to facilitate inter-mode cooperation. With a frame duration of 691.2 μs, an FDD frame consists of two chunk durations, with one chunk per slot. A TDD frame consists of two chunks and two duplex guard intervals, organised into a downlink slot and an uplink slot. With downlink-uplink asymmetry 1:1, the TDD chunks are 15 OFDM symbols long, both in uplink and downlink. Figure 2-3 illustrates FDD and TDD chunks for the reference system parameters of [WIN2D6137].

The *super-frame* (SF) is a time-frequency unit that contains pre-specified resources for all transport channels; It comprises a *preamble* followed by n_f frames. Here n_f = 8, resulting in super-frames of approximate duration 5.6 ms. (It could be extended to e.g. 16 frames, if required). The available number of chunks in the frequency direction could vary with the geographical location. It is assumed that for the FDD DL and UL as well as for TDD, there exist frequency bands that are available everywhere. The preamble is transmitted in those commonly available bands. The remainder of the super-frame may use other spectral areas that are available at some locations, or to some operators, but not to others. All of these spectral areas are spanned by one FFT at the receiver and are at present assumed to span at most 100 MHz.

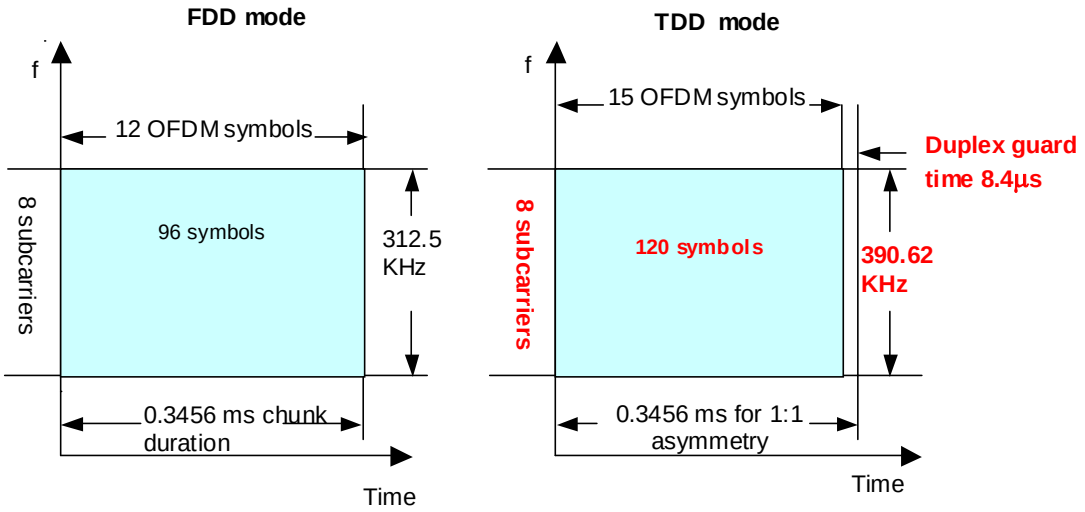

Figure 2-3: Summary of assumed chunk sizes in the two physical layer modes. The figures show a slot (half of the frame) in each case, assuming 1:1 TDD asymmetry

The super-frame structure that has been assumed in the investigations within WINNER II was designed within WINNER phase 1 and is illustrated e.g in Figure 3.4 of [WIN2D6137]. The main part of this super-frame is shared by the contention-based direct access channel (DAC), the scheduled data channels common data channel (CDC) and targeted data channel (TDC), and their related control signalling. It also contains time-frequency-spatial resources that are not to be used, due to interference avoidance

constraints. The resource partitioning (allocation) is performed in terms of chunks. It is performed on a super-frame basis but it may be changed between super-frames. The DAC resource is used both for the DAC channel and for the peer-to-peer transmission. It is organised as a constant set of frequencies over the whole super-frame, to enable the use of carrier-sense multiple access contention based transmission.

The super-frame of the final WINNER concept is described in Section 4.7 of [WIN2D61314]. It has been modified as follows:

- The contention-based DAC channel is not included in the final WINNER II concept.
- The downlink physical broadcast channel and the uplink physical random access channel are no longer included in the preamble of each superframe, but are instead placed within the main part of the super-frame. This increases the flexibility, since the time-scale of broadcast transmission and random access opportunities are decoupled from the superframe timescale.
- To eliminate unused frequency resources, the downlink and uplink network synchronisation pilots have been moved into the first frame of the superframe, in the beginning of the downlink and the uplink slot, respectively of that frame. They only utilize spectral bands that are available over a wide geographical area, to facilitate multi-cell coordination. They each comprise three consecutive OFDM symbols. This corresponds to the minimum B-EFDMA block size of the reference design (cf. Section 2.3 below) so it fits well into the WINNER II frame structure.
- Both the FDD and the TDD super-frame preambles include one OFDM symbol that contains uplink pilots.

2.3 Multiple Access

The WINNER multiple access schemes have in [WIN2D461]. Been developed in a form that has rather little dependence on the main deployment scenarios and modes: WA versus MA or LA and cellular FDD versus cellular TDD. A main conclusion from WINNER phase 1 was that the key distinguishing feature for the choice of multiple access scheme for a particular scheduled flows turns out to be not the deployment scenario, but instead the choice of one of two transmission strategies: **frequency-adaptive transmission** and **non-frequency-adaptive transmission**.

For frequency adaptive transmission, ***chunk-based TDMA/OFDMA*** was identified as the baseline scheme in WINNER phase I. Frequency adaptive transmission utilizes the fine-grained channel variations, by relying on the prediction of the SINR within each chunk (layer). These channel variations will differ between channels to different user terminals. We therefore obtain significant multi-user scheduling gains when flows can be allocated to chunks that provide the best channel gains and interference conditions. A basic requirement for frequency-adaptive transmission is that a transmitter must send pilots scattered over the whole frequency contention band so that the receiver can estimate and predict favorable (high SINR) portions of the frequency band for the transmitter to use in the near future. For the downlink, this requirement is satisfied by common pilots transmitted from the base station. For the uplink, each user terminal would have to transmit multiple pilots outside as well as inside its current transmission chunks, thus leading to significant pilot overhead increases.

With non-frequency-adaptive allocation, bits from each flow are allocated onto sets of chunks that are dispersed in frequency and/or space. Forward Error Correction (FEC) coding and interleaving are used to combat the small-scale frequency selective fading. No feedback from receiver to transmitter is necessary, and pilot overhead will be less; however transmission performance will not benefit from adaptivity and multiuser scheduling gain as it does for frequency-adaptive transmission.

In [WIN2D461] section A4.1, a comparison is made between the different options in of DFT-precoded FDMA/TDMA for uplink, including a variant of DFT-precoded block FDMA with frequency hopping. The conclusion is that IFDMA is the best candidate, especially due to its capability to take advantage of large frequency diversity in the channel without the need for a large pilot overhead, since compared to frequency hopping, interpolation of the channel state in time is made possible. Investigations on sleep mode in [WIN2D461] claimed UT power efficiency gains if intra-chunk sleep mode is supported, i.e. the UT is given the possibility to enter sleep mode in a fraction of the chunk duration. The proposed reference design of the multiple access scheme for the non-frequency adaptive uplink is called Block Interleaved

Frequency Divison Multiple Access (B-IFDMA) [SFF+07]. It is outlined below and described in more detail in [WIN2D461]. It aims at maximizing frequency diversity, while enabling micro-sleep within chunks and simultaneously providing low envelope variations of transmitted uplink. It may also be more robust than IFDMA to interference among frequency-interleaved uplink user signals when there is frequency offset or phase noise.

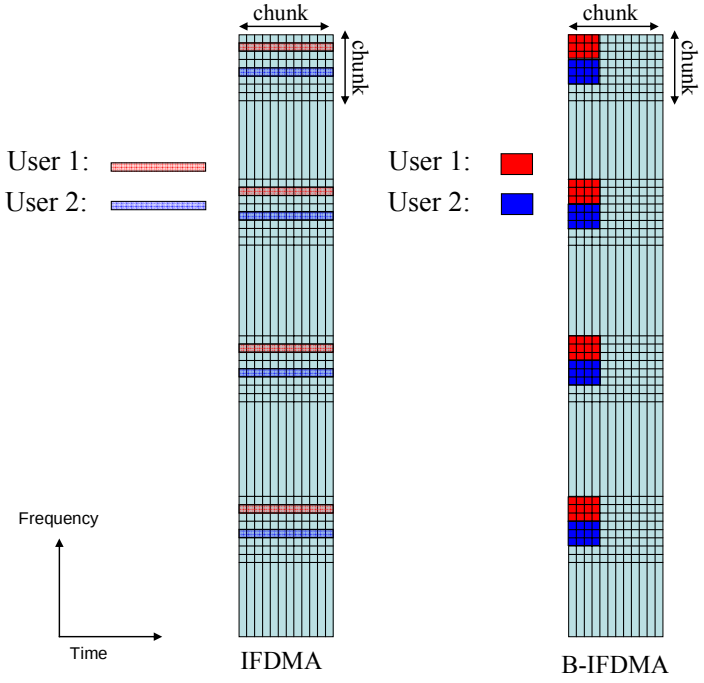

Figure 2-4 Example of B-IFDMA based on FDD chunk size.

In Figure 2-4, B-IFDMA is illustrated in comparison with IFDMA. In B-IFDMA, equidistant blocks of subcarriers in contiguous OFDM symbols are allocated in a chunk duration (slot in FDD). DFT-precoding is performed to make the envelope variation of the transmitted signal low. The same amount of data carrying OFDM subcarrier symbols are allocated in B-IFDMA as in IFDMA to a flow in a chunk duration (equals a frame slot in the current FDD assumptions). By allocating a block of adjacent subcarriers over several contiguous OFDM symbol durations within a chunk, the pilot overhead should be the same as for IFDMA, assuming the chunk is essentially frequency flat. The block based subcarrier allocation also offers the same frequency diversity as IFDMA and a smaller sensitivity to frequency offsets among the uplink UTs compared to IFDMA. The equidistant block allocation in B-IFDMA gives the same advantage and drawback as in IFDMA; it limits the flexibility for the resource allocation, but it enables a smaller resource addressing overhead. B-IFDMA can be used in FDD as well as in TDD, and is proposed for all the deployment scenarios wide area, metropolitan area and local area.

Using the current FDD numerology as an example, in the case of IFDMA; one subcarrier within equidistantly spaced chunks, spanning all 12 OFDM symbols of the chunk duration, is used.[1] The channels at adjacent utilized subcarriers then become rather uncorrelated.

With B-IFDMA, a few adjacent subcarriers are used and only a fraction of the OFDM symbols in a chunk. This enables the UT to enter sleep mode in a fraction of the chunk duration. The appropriate size of the blocks is to be investigated further, but the assumption in Figure 2-4 is to use a block size of 3 subcarriers times 4 OFDM symbols. Larger block sizes are also feasible, and may be preferable from the standpoint of channel estimation and pilot overhead efficiency, as pointed out in section 4.6. Note that several short blocks may also be combined together to further exploit frequency diversity. Using an even number of OFDM symbols enables use of Alamouti space-time coding and using equidistant blocks each

[1] IFDMA can also be used with less than 12 consecutive OFDM symbols assigned to a specific user. The minimum possible number of OFDM symbols is 2. The first used for pilot transmission, the second for data.

of 3 subcarriers should give a power amplifier backoff penalty less than 1dB, since that can be achieved even with blocks of 4 subcarriers. This enables the UT to be in sleep mode for more than half of the chunk duration.

Note that B-IFDMA does not define the resource unit per chunk duration (FDD slot) based on the chunk size, but rather as a function of the block size, repetition distance and bandwidth allocated for non-frequency adaptive transmission. The chunk concept is however still useful; it defines the common resource unit for resource allocation between adaptive and non-frequency adaptive transmission and resource partitioning between access points in case effective frequency reuse distance larger than one is used. Furthermore, it is a common entity for channel estimation due to its property of being essentially flat in time and frequency.

The DFT-precoding assumed in B-IFDMA is of no use in the downlink and to highlight this difference, the multiple access scheme for the non-frequency adaptive downlink is called Block Equidistant Frequency Division Multiple Access (B-EFDMA) and it is the same as for the uplink except the missing DFT-precoding. B-EFDMA can be used in FDD as well as in TDD, and is proposed for all the deployment scenarios wide area, metropolitan area and local area.

2.4 Overall Assessment Criteria

It is the objective of Task 3 to assess the degradation in performance if estimates and measurements are not perfect. Therefore, it appears meaningful to assess the performance of different estimation approaches relative to an **ideal reference system having perfect estimates as well as no overhead due to pilot symbols**.

As the channel capacity is fundamentally determined by bandwidth and SNR, the performance degradation of a candidate estimation algorithm relative to a reference system with perfect estimates and no overhead due to pilots is determined by three factors:

- **Increase in signal to noise ratio needed to achieve a given bit or frame error probability** as a result of non-perfect channel state information and errors in channel estimates.
- **Loss in Spectral Efficiency**: The loss in spectral efficiency or bandwidth efficiency is proportional to the bandwidth consumed by the pilot symbols relative to the total bandwidth.
- **Loss in Power Efficiency:** Assuming a constant overall power budget the degradation in power efficiency is also dependent on the proportion of the total transmit power allocated to pilot transmission.

2.4.1 Spectral Efficiency

For estimation, synchronisation, and measurements purposes pilot symbols are commonly used. In general, one chunk carries N_{pilot} pilot and N_{data} data symbols, so the number of symbols per chunk is $N_{\text{data}} + N_{\text{pilot}}$. In the case that a cyclic prefix is inserted the equivalent total number of symbols per frame becomes $N_{\text{data}} + N_{\text{pilot}} + N_{\text{CP}}$, where N_{CP} represents the number of potential extra data symbols per chunk 'lost' due to the transmission of a cyclic prefix instead. The insertion of a cyclic prefix is likely to incur higher loss than the insertion of pilot symbols.

The spectral efficiency is defined as

$$\eta = \frac{N_{data}}{N_{data} + N_{pilots} + N_{CP}} \tag{2-1}$$

The loss in spectral efficiency is therefore $\eta_{ref} - \eta$, where the spectral efficiency of the reference system is defined by

$$\eta_{ref} = \frac{N_{data,ref}}{N_{data,ref} + N_{CP,ref}} \tag{2-2}$$

If the reference system, or both systems, do not employ a cyclic prefix then $N_{CP}, N_{CP,ref}$ should be set to zero as appropriate.

2.4.2 Power Efficiency and Signal to Noise Ratio Definition

The accuracy of estimates may be improved by a pilot power boost S_p. With an average received energy of a pilot symbol set to $E_p = S_p E_d$, unless constrained by a transmit power or spectral mask limit, where E_d is the average received energy of a data symbol, the SNR at the input of the channel estimation unit is improved by a factor of S_p. On the other hand, if the overall transmit power is kept constant, the useful transmit power of the payload information is reduced.

The power efficiency is defined as

$$\eta_{pow} = \frac{N_{data}}{(N_{data} + N_{pilots} S_p)(1 + F_{CP})} \tag{2-3}$$

where $F_{CP}=N_{CP}/(N_{data}+N_{pilots})$ is the cyclic prefix overhead ratio. The loss in power efficiency is therefore $\eta_{pow,ref} - \eta_{pow}$, where the power efficiency of the reference system is

$$\eta_{pow,ref} = \frac{N_{data,ref}}{N_{data,ref} + N_{CP,ref}} \tag{2-4}$$

As above, $N_{CP}, N_{CP,ref}$ should be set to zero wherever a cyclic prefix is not employed.

The pilot overhead is defined by $\Omega_p = N_{pilots} / N = N_{pilots} /(N_{data} + N_{pilots})$.
From the above analysis it follows that the power dedicated to pilot symbols is determined by the pilot overhead Ω_p, and the pilot boost S_p. The energy per data symbol E_d for the system with pilots, is less than E_s, which is the total average received energy from the data, pilots and cyclic prefixes in a transmitted frame. The ratio of these energies per symbol is

$$\frac{E_d}{E_s} = \frac{1}{1 + \Omega_p (S_p - 1)} \tag{2-5}$$

The term $1 + \Omega_p (S_p - 1)$ is a measure for the pilot insertion loss relative to a reference system assuming perfect channel knowledge and no overhead due to pilots.

The total averaged received energy from the data, pilots and cyclic prefixes is denoted E_s. The total received energy of an FFT block plus its cyclic prefix is thus

$$\begin{aligned} E_{tot} &= E_s (N_{data} + N_{pilots})(1 + F_{CP}) \\ &= E_d (N_{data} + N_{pilots} S_p)(1 + F_{CP}). \end{aligned} \tag{2-6}$$

For Noise power spectral density N_0, the signal to noise ratio is defined as

$$SNR = \frac{E_s}{N_0} = \frac{N_{data} + N_{pilots} S_p}{N_{data} + N_{pilots}} \frac{E_d}{N_0} = \frac{N + N_{pilots}(S_p - 1)}{N} \frac{E_d}{N_0} \tag{2-7}$$

Note that the number of pilots, N_{pilots}, includes all pilots in the FFT block, from all transmitting antennas.

The quantity E_b/N_0, where E_b is the average received energy devoted to a data bit, is a common measure for coding evaluations, independent of the presence of pilots or cyclic prefix. We can define

$$\frac{E_b}{N_0} = \frac{E_d}{N_0} \cdot \frac{1}{r \log_2 M}, \text{ where } r \text{ is code rate and } M \text{ is constellation size,}$$
$$= \frac{N_{data} + N_{pilots}}{N_{data} + N_{pilots} S_p} \cdot \frac{1}{r \log_2 M} \cdot \frac{E_s}{N_0} = \frac{N}{N + N_{pilots}(S_p - 1)} \cdot \frac{SNR}{r \log_2 M}. \quad (2\text{-}8)$$

2.5 Methodology for performance evaluation

The proposed channel estimation techniques are assessed via frame error rate (FER) versus E_s/N_0 and mean square error (MSE) assuming agreed-upon WINNER Phase II channels models [WIN2D112] derived in WINNER phase I [WIN1D54]. The channel estimation techniques can also be approximayely evaluated analytically using a channel estimation error model. This analysis is briefly sketched in Section 2.5.1 and presented in detail in Appendix B. In the case where the estimation error is dominated by noise, the performance degradation can be parameterized by effective noise variance. When the interpolation error dominates, the explicit parameterization is less accurate, and the exact performance should be verified via simulation.

2.5.1 Channel estimation error model

The channel estimation error of subcarrier n and OFDM symbol ℓ, denoted by $\varepsilon_{n,\ell}$ associated to the channel estimate $\hat{H}_{n,\ell} = H_{n,\ell} + \varepsilon_{n,\ell}$, is modelled as an additive Gaussian noise term, with variance equal to the MSE of the channel estimates $\sigma_\varepsilon^2[n,\ell]$. By defining an *equivalent system model* including the channel estimates, the effective SNR including channel estimation errors, as well as consumed resources by pilot symbols (in terms of bandwidth and power) is in the form:

$$\gamma = \frac{E_d}{N_0 + E_d \sigma_\varepsilon^2[n,\ell]} \quad (2\text{-}9)$$

With E_d/E_s given by (2-5), the SNR loss attributed to pilot aided channel estimation schemes can be conveniently expressed as:

$$\Delta\gamma = \frac{\gamma_0}{\gamma} = 1 + (S_P - 1)\Omega_P + \gamma_0 \sigma_\varepsilon^2[n,\ell] \quad (2\text{-}10)$$

Means to expresse the MSE of the channel estimates $\sigma_\varepsilon^2[n,\ell]$ in a parameterized form, as well as the extension of the channel estimation error model to multiple spatial streams, is described in Appendix B.

3. Pilot Design

3.1 Introduction

Pilots are used for implementing certain physical layer support functions, e.g. connection setup, synchronisation, mobility support, power control, CQI measurements and most importantly channel estimation. On the other hand, pilots add overhead and consume transmission power. Thus, a proper pilot design should enable accurate and reliable channel estimation and on the other hand keep the induced spectral and power efficiency loses at an acceptable level. In WINNER phase I pilot aided channel estimation (PACE) for OFDM was extensively studied and serves as a basis for the WINNER pilot design. For channel estimation purposes, the following means for **multiplexing pilots** are foreseen [WIN1D21], [WIN1D23] and [WIN1D210]:

- For OFDM downlink and uplinks a **scattered pilot grid** is used for channel estimation and channel prediction. The pilot grids are specified in Section 3.2.
- For uplink (frequency domain generated) serial modulation, pilot patterns may be generated in the frequency domain equivalent to OFDM, as described in Section 3.2.4. This enables the use of a scattered pilot grid, and therefore establishes a common framework for the pilot grid of generalized multi-carrier (GMC) signals.

The WINNER system concept heavily relies on provision of accurate channel state information (CSI) at both receiver and transmitter. To this end, two types of channel estimation must be distinguished:

- Channel estimation for data reception, where the receiver needs to measure the effective channel (ECSI), including the effect of the spatial processing at the transmitter, referred to as effective CSI (ECSI).
- Channel estimation (or more accurately channel prediction) for adaptive transmit processing based on CSI at the transmitter (CSIT), typically provided through return link feedback or measurements, where an additional extrapolation/prediction in time is required.

One key issue for pilot design is the spatial transmit processing, which is selected based on the available CSI or CQI at the transmitter. The following combinations of available CSI/CQI are considered in the WINNER system concept [WIN2D341]:

Short-term CSIT: an accurate estimate of the full instantaneous channel matrix is assumed, i.e. the channel responses between all transmit and receive antennas. Short-term CSIT allows for the most advanced MU-MIMO schemes, but requires a slowly fading channel, i.e. it is applicable only to users with pedestrian velocities.

Long-term CSIT / short-term CQI: Long term CSIT refers to the spatial structure of the channel expressed by the averaged transmit correlation matrix while short term CQI is a measure of the instantaneous channel gain, e.g. the received SINR. Frequency adaptive transmission with some kind of beamforming is possible.

No CSIT / short-term CQI: only the instantaneous CQI is available at the transmitter, but no knowledge of the channel spatial structure is assumed, enabling frequency adaptive transmission with linear dispersion codes (LDC).

No CSIT / long-term CQI: only average CQI is available at the transmitter, reflecting the channel characheristics due to path-loss and shadowing. Here the transmitter resorts to non-frequency adaptive transmission.

The pilot design for any specific embodiment of MU-MIMO is a challenging task on its own, and the optimum choices for the specific MU-MIMO schemes may be fundamentally different. Moreover, various flavours of multiple antenna transmission schemes are to be flexibly combined with opportunistic multi-user scheduling, and link adaptation, within the same air interface. To this end, a straightforward combination of the individual best choices would result in a combination of a large number of types of pilots (dedicated / common pilots per beam / antenna), which inevitably leads to prohibitive overheads. Hence, the objective of the WINNER pilot design is to reuse pilots for as many different functions as possible.

Section 3.2 describes the pilot design for the WINNER system concept. The WINNER pilot design is a modular concept consisting of basic building blocks defined on the chunk level. These building blocks are:

- The **pilot pattern** specifies the position of pilots on the chunk. The pilot positions is chosen such that a globally regular pilot pattern is obtained, i.e. a two dimensional (2D) grid with equidistantly spaced pilots by D_f and D_t in time and frequency, which is advantageous for channel estimation by interpolation.
- The **pilot type** specifies whether pilots include user specific transmit processing or not.
- The **orthogonal pilot set** specifies whether pilots associated to different spatial streams are orthogonally separated in time and/or frequency, or pilots are spatially reused, i.e. pilots of two spatial streams are placed on the same subcarriers.

This modular concept avoids that several pilot patterns corresponding to different pilot types are inserted within a frame. Instead only one pilot grid is inserted in the frame and the pilot type is determined by the chunk specific spatial transmit processing. Thus, a highly flexible and adaptive system concept can be supported with a modest pilot overhead.

The pilot grids for FDD and TDD modes as well as the super-frame pilot preamble are described in Section 3.2.6. Furthermore, the realization of the WINNER pilot design for the reference design of "wide area", "metropolitan area" and "local area" deployment are addressed in Sections 3.2.7, 3.2.8 and 3.2.9.

Appendix K.1 analyzes the optimal pilot placement for dedicated pilots in a single and Appendix K.2 for the multiple consecutive chunks scenario.

Section K.3 studies the attainable spectral efficiency of MIMO-OFDM with pilot aided channel estimation. For the case of no channel knowledge at the transmitter the optimum pilot grid is derived in terms of placement of pilots in time and frequency, as well as the power allocation for the pilots, such that the channel capacity is maximized. The performance is assessed for the FDD mode using the C2 wide area channel model. Finally, Section 3.3 presents the conclusions.

3.2 Pilot design for the WINNER system concept

3.2.1 Types of Pilots for Single-Antenna Transmission

Dependent on the transmit direction (uplink / downlink) and the kind of spatial processing being used, several types of pilots are being distinguished [WIN1D210]:

- ***Common pilots,*** have the property not to include user-specific transmit processing and thus the interpolation in frequency is restricted by the specific channel estimation algorithm (i.e., related to the estimator complexity) and not by chunk specific constraints. Since the downlink represents a point-to-multipoint connection, common pilots can generally be used on the downlink.
- ***Dedicated pilots*** are required for the uplink of a multi-user system.
    - ***Dedicated pilots over the full bandwidth (DP-FB)*** having identical weights for all chunks in frequency dimension dedicated to a particular user. Therefore interpolation over these chunks is possible. DP-FB allow interpolation for all users, similar to common pilots. However, since pilots cannot be shared between users, the pilot overhead is typically about N_u times higher than the corresponding overhead for common pilots, where N_u is the number of users.
    - ***Chunk-specific dedicated pilots (DP)*** where different weights are applied to each chunk. This is usually the case for FDMA on chunk basis. Hence, interpolation over adjacent chunks is not possible, which potentially degrades the channel estimation performance.

Since the pilot overhead of DP is typically N_u time lower than for DP-FB, it is expected that the choice between DP and DP-FB depends on the number of users, N_u. Typically, for N_u exceeding 4, DP are of advantage. It should be noted, that requirements for CSI at the transmitter so to support adaptive transmission, may also influence the choice of dedicated pilots.

For common pilots channel estimation by interpolation in time and frequency based on a scattered pilot grid is considered to be an efficient solution for an OFDM-based radio interface [WIN1D21] and [WIN1D23].

During the start of communication, interpolation techniques with limited information about the channel conditions must be used. A robust interpolation filter which only assumes knowledge about the CP duration and the maximum velocity expected in a certain environment is another possible choice. During

operation, statistical knowledge about the power delay profile and the Doppler spectrum is accumulated. Channel interpolation utilizing this knowledge can improve performance significantly.

Especially in case of dedicated pilots, purely pilot aided techniques may have severe limitations. Conventional channel estimation by interpolation may then require a significant degree of over-sampling. Advanced solutions, such as iterative channel estimation, aim to make an excessive oversampling redundant, at the expense of increased complexity. If an iterative receiver structure is already in place, iterative channel estimation offers a good compromise between performance and complexity.

3.2.2 Types of Pilots for Multi-Antenna Transmission

Compared to the discussion in Section 3.2.1, spatial processing brings along additional requirements. In particular we need to distinguish the following pilot types [WIN1D27]:

- ***Common pilots*** have the property not to include user-specific transmit processing and thus the interpolation in frequency is possible. In case of user-specific transmit processing, the amplitude and phase induced on common pilots by fading channel deviates from those of the data symbols which are induced by combination of user-specific transmit processing and fading channel, and therefore the receiver cannot detect those based on common pilots. Different variants of common pilots exist
    - ***Common pilots per antenna (CPA)*** are used to obtain the unweighted channel matrix **H** which describes the propagation channel between any combination of transmit and receive antennas in the MIMO case.
    - ***Common pilots per beam (CPB)*** are useful to estimate the effective channel (including the beamforming weights) and perform CQI measurements for the associated beam for fixed beamforming approaches. Note that measurements on such pilots in neighbouring beams could then be used for beam handover. Also, the common pilots per beam benefit from the beamforming gain, which reduces the transmit power required for a target channel estimation error and coverage area.
- ***Dedicated pilots*** may be required if user-specific transmit processing (i.e. a user-specific adaptation of amplitude and phase) is applied to the data symbols. These pilots are subject to the same transmit processing as the data symbols and therefore allow the receiver to estimate the effective channel $\mathbf{H}_U \cdot \mathbf{f}_U$ of user U. The use of dedicated pilots for other purposes, like CQI measurements, is limited, since they contain a user specific component, giving rise to biased measurements. Two different types of dedicated pilots can be distinguished:
    - ***Dedicated pilots per antenna (DPA and DPA-FB)***, which might be either chunk specific (DPA) or over the full band (DPA-FB) as explained in Section 3.2.1.
    - ***Dedicated pilots per beam (DPB and DPB-FB)***, which also might be either chunk specific (DPB) or over the full band (DPB-FB). DPB are useful to estimate the effective channel (including the beamforming weights) and perform CQI measurements for the associated beam for adaptive beamforming approaches. While DPB-FB allow for interpolation over frequency, the resulting pilot overhead may be prohibitive for multi-user MIMO-OFDM.

Due to the fact that common pilots can be used by several users, they are appealing for the downlink processing, since the overall energy to perform the associated functions has only to be spent once and the pilot symbols can be spread over all resources. Also they provide a basis for un-biased CQI measurements. However, certain user-specific spatial processing techniques require to estimate the effective channel (the channel including the spatial precoding), which is typically provided by dedicated pilots. To this end, when user-specific spatial processing is combined with multi-user OFDMA, even on the downlink an increasing amount of dedicated pilots is needed. On the other hand, dedicated pilots fail to deliver unweighted CSI and CQI estimates that are needed for adaptive transmission in a straightforward way. Note that a method to deliver unweighted CQI based on dedicated pilots and use of Kalman filtering is described in Section 4.4.

3.2.3 Pilot grid design at the transmitter for adaptive modulation

Adaptive transmission requires channel prediction for resource allocation. Channel prediction can be based on common pilot symbols that are also used for other purposes. It should utilise the channel correlation in time and frequency. With these methods, adaptive transmission becomes possible in the WINNER system at vehicular velocities. The channel prediction accuracy estimates (covariances) are furthermore important inputs in the design of the link adaptation and resource scheduling schemes.

For adaptive transmission, CSI and/or short-term CQI at the transmitter are required. In OFDM that use adaptive transmission, channels from many users have to be estimated and predicted in each chunk. The following means for providing short term CSI and CQI at the transmitter are possible:

- **Uplink pilots:** In this case, full-band dedicated pilots per antenna (DPA-FB) are transmitted on the uplink [WIN1D24]. The drawback of DPA-FB is the high overhead, as the number of users in a cell/sector is typically rather large. To reduce the resulting overheads, DPA-FB may only be transmitted on the super-frame preamble, and/or to separate groups of users into so called competition bands, where users are only allowed to access a part of the available bandwidth. While the former essentially limits the velocities that can be supported, the latter reduces the possibility to exploit multi-user diversity.
- **Common downlink pilots** provide the UT with short term CSI and CQI. The CQI is compressed as described in [WIN1D24] and fed back to the BS. This allows for adaptive transmission on the downlink. Furthermore, in TDD mode common downlink pilots also provide the necessary CQI for adaptive transmission on the uplink, due to the TDD channel reciprocity.
- Another alternative is to insert common pilot only in the superframe preamble and dedicated pilot per beam (DPB) into each chunk. Then based on these two types of pilots and on Kalman filtering channel prediction can be done and used for the purposes of obtaining CQI (see Section 4.4.2).

Unfortunately, the preferred choice among the above described schemes very much depends on the considered deployment scenario. For instance, consider the LA deployment with n_T=32 BS antennas but very low user velocities. It is obvious that in this case common pilots would result in prohibitive overheads, since first, pilots for n_T transmit antennas need to be inserted; and second, *each* user needs to feed back the channel gains for *all* n_T transmit antennas. What is more, for MU-MIMO with CSIT common pilots do not provide the UT receiver with the effective channel, so dedicated pilots per beam would be needed on top of the common pilots. On the other hand, only one or two uplink pilots per chunk need to be transmitted to provide the BS with the full CSI of all n_T BS antennas. Due to the TDD mode and the low velocities the channel coherence time will exceed a super-frame duration. Hence, in this case, uplink pilots are the clear choice here. As further example, consider mobile users in metropolitan area deployment. While uplink pilots could be used to get CSI or CQI for the downlink, the feedback rate needs to be once every frame. As full-band dedicated pilots are required and the number of users is potentially large, here the resulting overhead is very high. Furthermore, the battery of the UT are drained since a significant fraction of the transmit power is wasted for sending pilots. Here common pilots have a clear advantage, as the number of active BS antennas is much lower, and since common pilots are shared for all users.

3.2.4 Multiplexing of pilots for GMC

Pilots may be time- or frequency-multiplexed with data. Both types of pilots have been considered previously in [WIN1D210]. Time division multiplexed pilots allow a reduction in power backoff for DFT-precoded GMC, The DFT-precoded waveforms with frequency division multiplexed (FDM) pilots still have lower power variation and backoff requirements than those of comparable OFDM signals, but the difference margin from OFDM is reduced by 1 to 2 dB [WIN1D210]. Note that this slightly increased backoff requirement only applies to blocks which contain FDM pilots. If the power in the data components is reduced in those blocks to achieve their reduced backoff, the *average* data energy per bit over a frame is reduced by only a small fraction of a dB, since only a fraction of blocks contain FDM pilots; e.g. 2 or 3 out of 12. Thus the performance penalty of using FDM pilots, but with the same backoff as that of TDM pilots is very small. For example, if 2 out of 12 blocks contain FDM pilots, and if ¼ of the symbols in those blocks are pilots, then a simple calculation shows that the average energy per data bit is decreased by only about 0.2 dB if pilot blocks are backed off by 1 dB without reducing power devoted to pilots. Disadvantages of time multiplexed pilot blocks include a slightly higher overhead penalty since they require their own cyclic prefixes, and also their use would also slightly complicate frame formatting. Accordingly, only frequency multiplexed pilots will be considered in the rest of this document.

There are two variations of frequency multiplexed pilots: the frequency expanding technique (FET) and the frequency domain superimposed pilot technique (FDSPT). FET preserves and rearranges data-carrying subcarriers to accommodate pilots, while FDSPT obliterates data-carrying subcarriers where pilots are to be inserted. Applied to OFDM or SM, FET is equivalent to a scattered pilot grid, where data symbols are inserted at subcarriers where no pilots are present. It is also called pilot-assisted channel estimation (PACE). FDSPT on the other hand, can be viewed as a puncturing of the data symbols. So, data symbols are inserted on all subcarriers, and subsequently pilots are superimposed on a subset of frequencies, replacing data on those frequencies. This effectively results in an increased code rate at the

expense of slightly degraded performance resulting from the imposition of channel frequency response nulls (see Appendix C.2 and [FDL+07a]).The FET (scattered pilot grid) pilot concept is proposed for WINNER II. To this end, there is no need to distinguish between CP serial modulation and OFDM, when it comes to the design of the pilot grid, although certain approaches might be favourable for one or the other.

Because of the close kinship in the GMC framework between OFDM and SM signals with frequency domain pilots, and because of their somewhat lower overhead than corresponding SM signals with time domain pilots, there is interest in reducing the peak to average power ratio (PAPR) in SM systems with frequency domain pilots. One possible approach is for the transmitter to choose one of a finite set of possible pilot sequences, instead of one fixed sequence, to multiplex with data [GEP06]. The sequence giving the minimum PAPR is chosen. This technique can also be (and has previously) been applied to OFDM with frequency multiplexed pilots. [LFD07] shows that this technique can also be applied to SM signals with FDM pilots, with significant power backoff improvement if the HPA is nearly linear up to the saturation point.

3.2.5 Pilot design with interference

For a multi-cell system where each cell is equipped with several antennas users needs to distinguish the pilots originating from the various cells and antennas/beams. In particular, we distinguish inter-beam interference that is encountered when spatially multiplexing several streams per chunk, discussed in Section 3.2.5.1; and inter-cell interference between pilots within the cell (in-cell pilots) and pilots originating from adjacent cells (out-of-cell pilots), as described in Section 3.2.5.2.

Generally speaking there are two possible means for separating interference between pilots:

- ***Orthogonal separation in time and/or, frequency***. Pilots are orthogonally separated so to distinguish the pilots originating from the various cells and/or antennas/beams. Orthogonal separation of pilots therefore mitigates interference on pilot symbols. This however is traded with a substantial increase in pilot overhead.
- ***Scrambling of pilot sequences***. This will randomize the interference from adjacent beams/cells. To this end, the interference is not mitigated but the pilot overhead stays equivalent to the corresponding overhead of a SISO system operating in an isolated cell. Provided that the interference is significantly below the useful signal part beam/cell specific scrambling of pilot sequences may be used to randomize the residual interference. An excessive number of orthogonal pilot sets, consuming a significant amount of the available resources, may therefore be avoided.

While orthogonal separation of pilots implies high overhead, scrambling by cell/beam specific pilot sequences suffers from excessive interference. To this end, a combination of both schemes similar to the grouping of users for SDMA [WIN2D341] appears reasonable. The WINNER pilot design allows for a number of so-called *orthogonal pilot sets*. Pilots associated to spatial streams that cause high inter-beam interference are orthogonally separated in time and/or frequency, otherwise pilots may be spatially multiplexed, as described in Section 3.2.5.1. On the other hand, separation between in-cell and out-of-cell pilots is exclusively achieved by scrambling with cell-specific pilot sequences as elaborated in Section 3.2.5.2.

3.2.5.1 Spatial multiplexing of in-cell pilots

A scattered pilot grid with orthogonally spaced pilot symbols in time and frequency was proposed in [WIN1D21] and [WIN1D210]. This however, may result in prohibitive pilot overheads for advanced MIMO schemes. For instance, in local area deployment a distributed antenna array with up to 32 antenna elements is foreseen. Fortunately, spatial precoding schemes forming beams that are spatially well separated allow to spatially reuse pilot symbols.

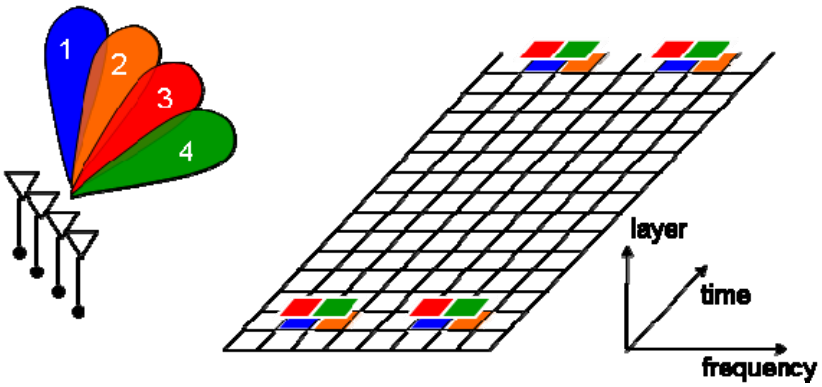

Figure 3-1: Scattered pilot grid. Pilots are orthogonally separated in time and frequency. Furthermore, Pilots associated to beams that are well separated are spatially multiplexed.

Figure 3-1 illustrates a scattered pilot grid. Pilots associated to beams that are spatially well separated are multiplexed. For instance, pilots 1 and 3 as well as 2 and 4 do not spatially overlap, so they are located on the same subcarrier, yielding a pilot reuse of two. On the other hand, pilots associated to beams with significant spatial overlap (in Figure 3-1 pilots 1 and 2, 2 and 3, as well as 3 and 4) need to be orthogonally separated in the time or frequency, i.e. placed on a different subcarrier.

3.2.5.2 Dealing with inter-cell interference between pilots

Scrambled pilots are compared with orthogonally separated pilots in [WIN2D341], Section 2.4.4 and Appendix C.1.2. In a multi-cell multi-user MIMO system, the number of required pilots for orthogonal separation may be rather large. To this end, a compromise between orthogonal separation and scrambling of pilots needs to be taken. For all cells, in-cell users' (ICU) pilots are appropriately assigned to the orthogonal pilot sets as illustrated in Figure 3-1. Out-of-cell users' interference (OCI) affects ICU pilots, but the average ICU to OCI power ratio is to be maintained sufficiently high by employing a suitable interference mitigation scheme. The requirement of low inter-cell interference power can be satisfied by frequency reuse partitioning or by a dynamic channel assignment scheme achieved by inter-cell coordination [WIN2D472]. This hybrid approach offers a lower overhead than fully orthogonal inter-cell pilots, while guaranteeing sufficient SINR for in-cell pilots.

The use of SDMA and aggressive frequency reuse strategies give rise to high levels of co-channel interference which are to be mitigated by spatial processing. However, all studies that involve SDMA in a cellular system in [WIN2D473] and [WIN2D341] ignore the presence of channel estimation errors. Taking into account realistic channel estimation may severely affect the attainable system performance. To this end, in section 4.3.2 multi-cell SDMA uplink transmission based on DFT-precoded OFDM in wide area uplinks including channel estimation is addressed. A SDMA scenario is considered, where several user terminals within a sector, each with one antenna, are simultaneously transmitting to a base station that has multiple antennas. The resulting in-cell user interference due to SDMA is suppressed by linear minimum mean squared error (MMSE) processing of the base station's array output on each subcarrier. This linear array processing can be enhanced by interference cancellation in the form of iterative block decision feedback equalization (IBDFE), or preferably, turbo equalization. Provided accurate estimates of each in-cell user's channel frequency response, these techniques effectively suppress the in-cell multi-user interference (MUI). To ensure accurate channel estimates, frequency-multiplexed pilots, orthogonal for each in-cell user are required.

We note that even low-level inter-cell interference to pilots will degrade channel estimates. It is not worth trying to explicitly estimate inter-cell interferers' channels, due to their low power levels and the complexity involved. However as described in Section 4.3.2, a least squares (LS) decision-directed adaptive equalization method can be used to reduce the effects of inter-cell interference. Asuming 4 OCIs, each on the order of 15 to 18 dB below the in-cell users' signal powers (which may be achieved by frequency reuse partitioning or by dynamic channel assignment achieved by inter-cell coordination [WIN2D472]), simulation results presented in Appendix C.4 suggest that the SNR degradation due to the uncompensated OCIs is on the order of 1 to 2 dB. Relative to the case of known channel state information for all in-cell users, the increase in required SNR to achieve a frame error rate of 10^{-2} is about 4.7 dB for a IBDFE receiver with non-iterative estimation of in-cell users' channels. The use of iterative channel estimation (ICE) reduces this SNR degradation to about 3.2 dB, and the use of the least squares technique reduces it further to about 2.2 dB. Interestingly, the interference on the pilots tended to have more effect on the performance than the inter-cell interference on data symbols. As these studies where restricted to

uplink SDMA, the impact on inter-cell interference on pilot design and channel estimation remain for further study.

3.2.6 Reference pilot design

3.2.6.1 In-band pilot patterns

A generic framework for pilot patterns is briefly summarized by:

- Pilot symbols in frequency and time, with respective spacings D_f and D_t should be placed sufficiently close to satisfy the sampling theorem [WIN1D21] allowing to reconstruct the channel response through interpolation. To allow for realizable filters oversampling factors should be at least 20% and 100% for common and dedicated pilots, respectively.
- The pilot pattern only determines the position of the pilots within the frame. The type of pilot being used (CPA, CPB, DPA or DPB as described in Section 3.2.2) is determined entirely by the spatial transmit processing scheme that is used in a particular chunk (grid of beams (GoB), successive MMSE (SMMSE) or linear dispersion codes (LDC)). This accomplishes that only one pilot grid is necessary to support all flavours of MU-MIMO schemes, and is therefore the key to keep the resulting pilot overheads at an acceptable level. The receiver implicitly knows which type of pilots is transmitted, as it is uniquely determined by the spatial scheme selection and the transmission mode (FDD or TDD).
    - An important requirement to allow for a chunk specific selection of the pilot type, is that the pilot spacing in frequency D_f is chosen such that the chunk width is an integer multiple of D_f.
- Pilots from different spatial streams are reused if the associated beams are well spatially separated, as described in Section 3.2.5. In case of overlapping beams or unweighted transmit signals, pilots are to be orthogonally multiplexed in time and frequency.
- For TDD and half-duplex FDD systems pilots should be placed near the beginning and end of a frame in time direction. The rationale here is that interpolation between pilots exhibits a smaller estimation error than extrapolation near the beginning and end of the frame.
- Dedicated pilots should be placed near the corners of a chunk, as interpolation between pilots exhibits a smaller estimation error than extrapolation at the chunk edges.

The pilot patterns for the FDD mode is illustrated in Figure 3-2 and described in Section 3.2.6.1.3.The pilot patterns for the TDD mode is illustrated in Figure 3-3 and described in Section 3.2.6.1.4 for the downlink and in Section 3.2.6.1.5 for the uplink. Furthermore, the dedicated uplink pilot patterns for B-IFDMA are illustrated in Figure 3-5 and described in Section 3.2.6.1.6. A table with the associated pilot spacings D_f and D_t in frequency and time as well as the resulting overheads is given in Table 3-1.

Table 3-1: Pilot spacings and overheads for the WINNER pilot design. The overhead is given as a function of the number of orthogonal pilot sets P_n.

	FDD[2]	TDD[3]	B-IFDMA
D_f	4	4	4
D_t	10	12	3
Ω_p	$4.16\% \cdot P_n$, ($5.2\% \cdot P_n$), $P_n=\{1,2,3,4\}$	$3.33\% \cdot P_n$, ($1.67\% \cdot P_n$), $P_n=\{1,2,3,4\}$	$8.33\% \cdot P_n$, $P_n=\{1,2\}$

Up to 4 orthogonal sets of pilots are allocated. Due to spatial reuse of pilots, the actual number of spatial streams can be significantly higher than 4. In many cases the number of spatial streams is below 4 and/or the associated beams are well separated; in this case, the number of orthogonal pilot sets, P_n, that are actually used may be smaller than 4. For instance, for SISO only one orthogonal pilot set is used, while for LDC with two antennas 2 orthogonal pilot sets are required.

[2] Pilot overhead in brackets correspond to chunks of high velocity users with speed exceeding 150km/h, where additional pilots are inserted.

[3] Pilot overhead in brackets correspond to chunks of low velocity users with speed below 10km/h.

In Table 3-1 it is seen that the pilot spacing in frequency is always $D_f = 4$. This is due to the chunk dimension in frequency of 8 subcarriers. With $D_f = 4$ there are 2 pilots in frequency per chunk, and a globally regular pilot pattern is retained, where the pilot locations are independent relative to the start of the chunk. This is the key requirement for the WINNER pilot design, as it allows selecting the pilot type (common / dedicated pilot per beam / antenna) on the chunk level. A further advantage of having D_f an integer multiple of the chunk duration is for uplink transmission: if a user is allocated several adjacent chunks, interpolation over frequency on those chunks is possible in case of dedicated pilots per antenna. This is particularly beneficial for relay enhanced cells (REC), as a relay is forwarding data of several users on the uplink in a localized sub-band, so interpolation in frequency over that sub-band is possible.

3.2.6.1.1 Pilot sequences

Given the pilot indices $n_p = \{1,\cdots,\lfloor N_c / D_f \rfloor\}$ and $\ell_p = \{1,2\}$ in frequency and time, the position of the pilot (subcarrier n and OFDM symbol ℓ) within the frame is determined by the following relation:

$$\begin{pmatrix} n \\ \ell \end{pmatrix} = \begin{pmatrix} D_f & d_{0f} \\ 0 & D_t \end{pmatrix} \cdot \mathbf{d}_p + \begin{pmatrix} d_{ort,f} \\ d_{ort,t} \end{pmatrix}, \quad \text{with} \quad \mathbf{d}_p = \begin{pmatrix} n_p - 1 \\ \ell_p - 1 \end{pmatrix} \tag{3-1}$$

where the pilot spacing in frequency is set to $D_f = 4$, while the pilot spacing in time is for FDD mode $D_t = 10$ and for TDD mode $D_t = 12$. In **(3-1)** the parameter $d_{0f} = \{-1,1\}$ specifies the shift in subcarriers between $\ell_p = 1$ and 2, while the vector $\mathbf{d}_{ort} = [d_{ort,f}, d_{ort,t}]^T$ specifies the orthogonal separation of pilots associated to different transmit antennas or beams. The entries of $\mathbf{d}_{ort}$ are within the range $\{d_{ort,f}, d_{ort,t}\} = \{1,2\}$. For the 4 orthogonal pilot sets the following parameters are chosen:

	Orthogonal pilot set			
	1	2	3	4
d_{0f}	1	-1	1	-1
$d_{ort,f}$	1	2	1	2
$d_{ort,t}$	1	1	2	2

The pilot pattern from **(3-1)** allows pilots from multiple beams share the same orthogonal pilot set, which causes inter-beam interference. Moreover, as described in Section 3.2.5, interference from adjacent cells further corrupts the pilots. Hence, pilots originating from the various cells and beams that are spatially multiplexed are randomized through a cell *and* beam specific scrambling sequence, $\tilde{X}^{cell}_{n,\ell}\ \tilde{X}^{\mu}_{n,\ell}$, both of length $2 \cdot N_c / D_f$, where μ is the beam index, n and ℓ are the subcarrier and OFDM symbol position of the pilot from **(3-1)**. The scrambling does not remove the inter-beam and inter-cell interference, but decorrelates the pilots. In order to reduce the peaks inherent to multi-carrier signals, the pilot signal should preferably exhibit a uniform envelope and power spectrum. The recommendation for the pilot sequence is the DFT of a Chu sequence (or the DFT of a sequence with similar properties), as it produces a Chu sequence in the time domain.

3.2.6.1.2 Pilot boost

The effect of a pilot boost on the performance of a MIMO-OFDM system is investigated in Section K.3.2. Only the link level was studied, so cellular interference is not taken into account. The optimum pilot boost derived in (K.25) is shown to be decreasing as the number of transmit antennas increase. In [CCA07] the same observation for multiple antenna systems with beamforming was observed: the higher the beamforming gain, the lower the optimum pilot boost. However, due to practical constraints the pilot boost should be fixed, which means that we need to resort to a sub-optimum boost. Fortunately, most of the attainable gains of a pilot boost are captured by setting the pilot boost to $S_p = 3$ dB.

In [WIN2D341] system level simulations were conducted to assess the benefits of a pilot boost in a cellular system. A pilot boost was shown to be effective only for an irregular pilot pattern, i.e. non-rectangular grid. The irregular pilot pattern was arranged by means of a Costas array in the way that in-cell pilots interfere with out-of-cell data and vice versa. The disadvantage of this approach is that the improvement in SINR on the pilot subcarriers through power boosting is traded with the degradation of SINR on data subcarriers that are hit by out-of-cell pilots. To this end, studies for relay enhanced cells in [WIN2D353] suggest that power boosting of pilots cancels out the gains of soft frequency reuse for cell-edge users.

In any case, due to practical constraints, it appears difficult to ensure that out-of-cell pilots will never interfere with in-cell pilots. For instance, for B-IFDMA there are so few eligible positions to place pilots (see Figure 3-5) that interference between in-cell and out-of-cell pilots can hardly be avoided. Generally speaking, in case of dedicated pilots an irregular pilot patter is likely to cause degradation in channel estimation accuracy, as pilots can no longer be placed near the corners of the chunk. Moreover, for DFT-precoded OFDM, a pilot boost is expected to increase the PAPR and required backoff, thus jeopardizing the benefits of its low PAPR.

In summary, due to the limitations of a pilot boost in a cellular system, and the potential negative implication on the uplink, a pilot boost should not exceed $S_p = 3$ dB in the WINNER system.

3.2.6.1.3 Pilots in FDD mode

On the downlink common pilots per antenna/beam (CPA and CPB) are used, while on the uplink dedicated pilots per antenna (DPA) are used. Since common pilots are not subject to user specific processing, interpolation in frequency is possible, and edge effects are less problematic. According to the WINNER pilot design, the selection of CPA or CPB is determined by the spatial processing within a particular chunk: for GoB we choose CPB, while for LDC we choose CPA. On the other hand, the pilot design is independent of the used multiple access scheme, i.e. whether OFDMA or B-EFDMA is used.

The pilot spacings in frequency and time are $D_f = 4$ and $D_t = 10$. The WINNER 2D grid for the FDD model is illustrated in Figure 3-2 and the position for subcarrier n and OFDM symbol ℓ relative to the first symbol in the chunk at (1,1), denoting earliest OFDM symbol and lowest frequency within a chunk, are given in Table 3-2. Note that in the case of LDC with 2 transmit antennas only two sets of orthogonal common pilots are required.

Table 3-2: Pilot symbol location for the FDD mode relative to the first symbol in the chunk at (1,1). Up to 4 orthogonal pilot sets are supported[4]

$\begin{pmatrix} n \\ \ell \end{pmatrix}$	Orthogonal pilot set							
	1		2		3		4	
	$\begin{pmatrix}2\\1\end{pmatrix}$	$\begin{pmatrix}6\\1\end{pmatrix}$	$\begin{pmatrix}3\\1\end{pmatrix}$	$\begin{pmatrix}7\\1\end{pmatrix}$	$\begin{pmatrix}2\\2\end{pmatrix}$	$\begin{pmatrix}6\\2\end{pmatrix}$	$\begin{pmatrix}3\\2\end{pmatrix}$	$\begin{pmatrix}7\\2\end{pmatrix}$
	$\begin{pmatrix}4\\6\end{pmatrix}$		$\begin{pmatrix}5\\6\end{pmatrix}$		$\begin{pmatrix}4\\7\end{pmatrix}$		$\begin{pmatrix}5\\7\end{pmatrix}$	
	$\begin{pmatrix}3\\11\end{pmatrix}$	$\begin{pmatrix}7\\11\end{pmatrix}$	$\begin{pmatrix}2\\11\end{pmatrix}$	$\begin{pmatrix}6\\11\end{pmatrix}$	$\begin{pmatrix}3\\12\end{pmatrix}$	$\begin{pmatrix}7\\12\end{pmatrix}$	$\begin{pmatrix}2\\12\end{pmatrix}$	$\begin{pmatrix}6\\12\end{pmatrix}$

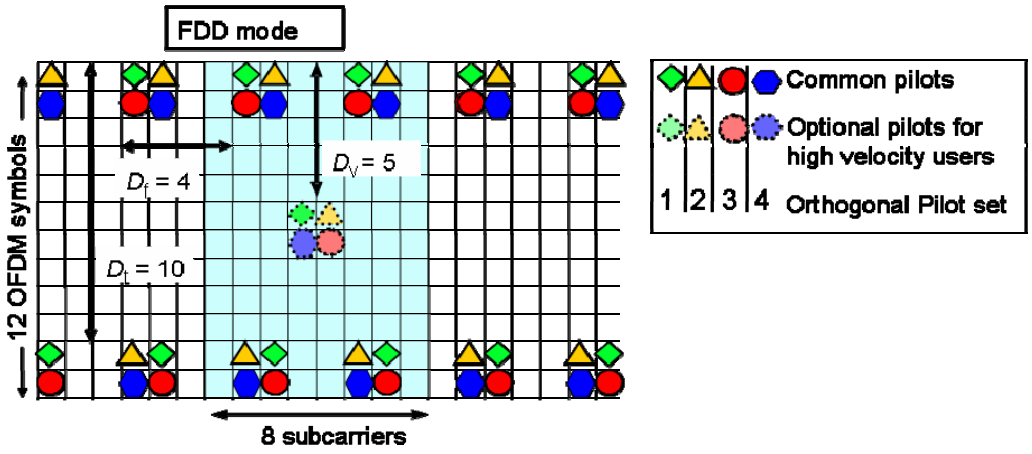

Figure 3-2: Pilot grids for the FDD mode.

[4] The pilots near the center of the chunk are optionally inserted for high mobility users with velocities > 150 km/h.

For chunks associated to high velocity users with speeds exceeding 150 km/h, one additional pilot per orthogonal pilot set is inserted to better track the high time variations on the channel response.

3.2.6.1.4 Downlink Pilots in TDD mode

For the TDD mode 4 pilots per chunk per orthogonal pilot set are arranged in a rhombus shape. The spacing in the time direction D_t should be adjusted to the used uplink/downlink asymmetry ratio. With a link asymmetry ratio of 1:1, the pilot spacings become $D_f = 4$ and $D_t = 12$ in frequency and time. For low mobility users with velocities below 10 km/h, one pilot in time direction is sufficient, i.e. the pilots corresponding to pilot index $\ell_p = 2$ in **(3-1)** may be omitted, which cuts the pilot overhead by a factor of 2.With spatial reuse of pilots, the $P_n = 4$ orthogonal pilot sets allow for a number of spatial layers of up to 32, with a modest pilot overhead of $\Omega_p = 13.3\%$ and 6.7% for mobile and pedestrian velocities.

The pilot spacings in frequency and time are $D_f = 4$ and $D_t = 12$. The WINNER 2D grid for the TDD model is illustrated in Figure 3-3 and the position for subcarrier n and OFDM symbol ℓ relative to the first symbol in the chunk at (1,1) are given in Table 3-3.

Table 3-3: Pilot symbol location for the TDD mode relative to the first symbol in the chunk at (1,1). Up to 4 orthogonal pilot sets are supported[5]

$\begin{pmatrix} n \\ \ell \end{pmatrix}$	Orthogonal pilot set							
	1		2		3		4	
	$\begin{pmatrix}2\\1\end{pmatrix}$	$\begin{pmatrix}6\\1\end{pmatrix}$	$\begin{pmatrix}3\\1\end{pmatrix}$	$\begin{pmatrix}7\\1\end{pmatrix}$	$\begin{pmatrix}2\\2\end{pmatrix}$	$\begin{pmatrix}6\\2\end{pmatrix}$	$\begin{pmatrix}3\\2\end{pmatrix}$	$\begin{pmatrix}7\\2\end{pmatrix}$
	$\begin{pmatrix}3\\13\end{pmatrix}$	$\begin{pmatrix}7\\13\end{pmatrix}$	$\begin{pmatrix}2\\13\end{pmatrix}$	$\begin{pmatrix}6\\13\end{pmatrix}$	$\begin{pmatrix}3\\14\end{pmatrix}$	$\begin{pmatrix}7\\14\end{pmatrix}$	$\begin{pmatrix}2\\14\end{pmatrix}$	$\begin{pmatrix}6\\14\end{pmatrix}$

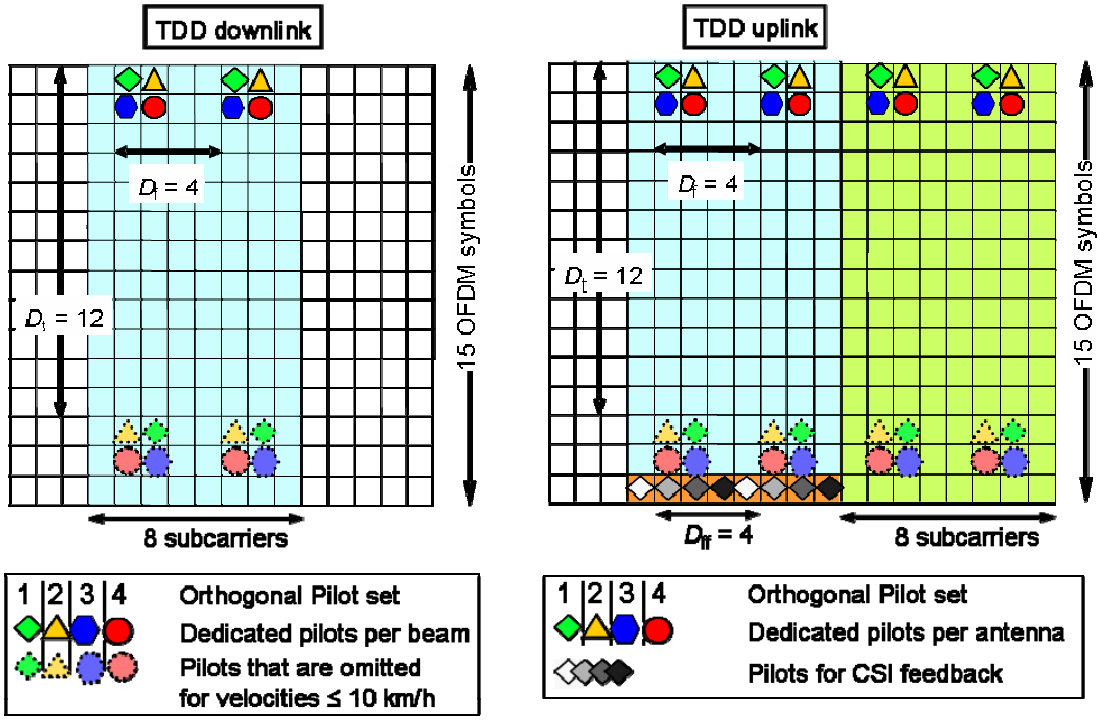

Figure 3-3: Pilot grids for the TDD mode.

In case of spatial precoding at the BS the pilots are weighted with the same beamforming vector as the corresponding data symbols of that spatial layer, i.e. *dedicated pilots per beam* (DPB) are transmitted. However, for MIMO schemes without spatial precoding, the pilots are transmitted as *common pilots per*

[5] For low mobility users with velocities ≤ 10 km/h, one pilot in time direction is sufficient, i.e. the pilots corresponding to pilot index $\ell_p = 2$ in **(3-1)** may be omitted

antenna (CPA). The receiver implicitly knows whether dedicated or common pilots are transmitted on a certain chunk, as it is uniquely determined by the spatial scheme selection.

The recommendation for placing dedicated pilots with a pilot spacing in frequency of $D_f = 4$, may not be immediately apparent. A frequency pilot spacing of $D_f = 6$ as proposed in [WIN2D6137] would place pilots closer to the corners of a chunk. On the other hand, $D_f = 4$ allows for coexistence of dedicated and common pilots. Interestingly, the channel estimation error in terms of MSE per subcarrier for $D_f = 6$ (pilots placed on subcarriers 1 and 7) and $D_f = 4$ (pilots placed on subcarriers 2 and 6) are quite similar as shown in Figure 3-4. There $D_f = 4$ is slightly superior for the FDD mode (channel model C2), while $D_f = 6$ is somewhat better for the TDD mode (channel model B1-NloS). In summary $D_f = 4$ is preferred due to its compatibility with common pilots, i.e. $D_f = 4$ produces a globally regular pilot pattern, which is preferable for common pilots.

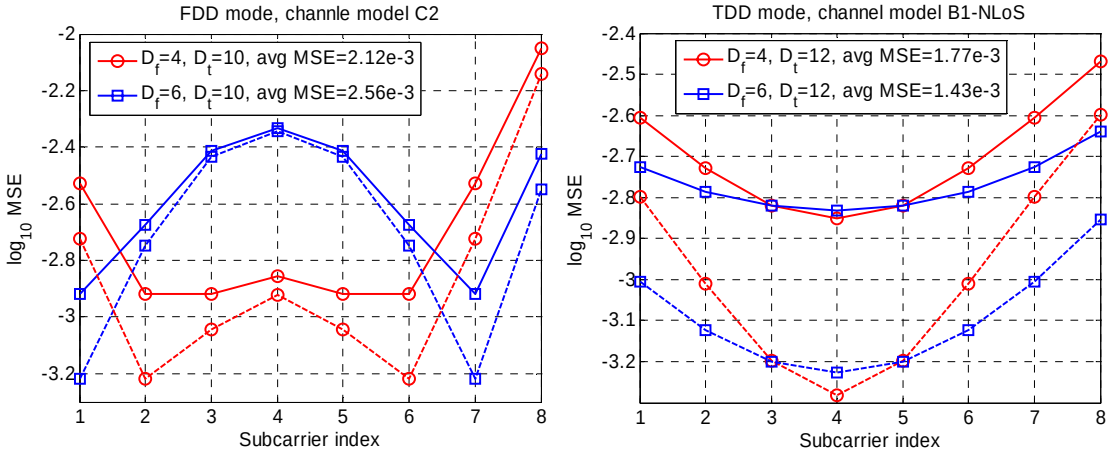

Figure 3-4: MSE against subcarrier index for chunk-wise channel estimation using dedicated pilots. Solid and dashed lines show the OFDM symbol with the best and worst MSE, respectively.

It is seen in Figure 3-4 that for $D_f = 4$ the MSE of subcarrier 8 is significantly degraded. The reason is that on subcarrier no. 8 extrapolation over 2 subcarriers is necessary. To combat the degradation of edge subcarriers, the pilot patterns for both TDD and FDD mode is changed from a rectangular shape to a rhombus, as shown in Figure 3-3 and Figure 3-2.

3.2.6.1.5 Uplink Dedicated Pilots in TDD mode

It is apparent from Figure 3-3 that the pilot pattern for TDD uplinks closely follows the TDD downlink. Dedicated pilots per antenna (DPA) are always used on the uplink.

The difference to the downlink is an additional set of pilots on the last OFDM symbol. For MU-MIMO schemes with spatial precoding based on short term CSI at the transmitter (CSIT) on the downlink, the last uplink OFDM symbol of each chunk is reserved for CSI transfer of downlink streams. As typically users that receive on the downlink typically do not transmit data on the uplink, the uplink pilots can in general not be used for updating the spatial precoding matrix at the BS. UTs insert 2 pilots with frequency spacing $D_{ff} = 4$ per UT antenna on the last OFDM symbol of uplink slots, on those chunks where this UT is receiving data on the downlink. These pilots are transmitted unweighted, and their position in the uplink chunk is $(n, \ell) = \{(b_{ff}, 15), (b_{ff} + D_{ff}, 15)\}$ in (frequency, time), where b_{ff} is the beam index of the corresponding downlink transmission. With 8 subcarriers per chunk up to 4 orthogonal pilot sets are available, which is sufficient to provide CSIT for the 4 spatial layers on the downlink. This means that users that are scheduled for CSIT spatial precoding on the downlink are reserved the last OFDM symbol of the corresponding uplink chunk to transmit pilots. These pilots provide the BS with the necessary CSI to update the spatial precoding matrix for the next downlink transmission.

3.2.6.1.6 Uplink dedicated pilots for B-IFDMA in both FDD and TDD modes

When using the B-EFDMA and B-IFDMA scheme for non-frequency adaptive transmission [WIN2D461], one pilot symbol is included within each ***block,*** if possible located near the centre of the block. The assumed block size is 4 subcarriers by 3 OFDM symbols (abbreviated by 4x3 block). The resulting pilot pattern is depicted in Figure 3-5. A larger number of pilots (one per 4x3 block per layer instead of four pilots per chunk layer) are thus required for the non-frequency adaptive transmission, as compared to the frequency-adaptive transmission. With 8 blocks per chunk in FDD and 10 blocks/chunk

in TDD, the pilot overhead becomes 8/96 and 10/120, respectively. With the specifications for B-IFDMA it is recommended that not more than 2 spatial layers should be used. The reasons are: first, high pilot overheads; and second, the dedicated pilots cannot be placed near the centre of a chunk, which severely affects the channel estimation accuracy.

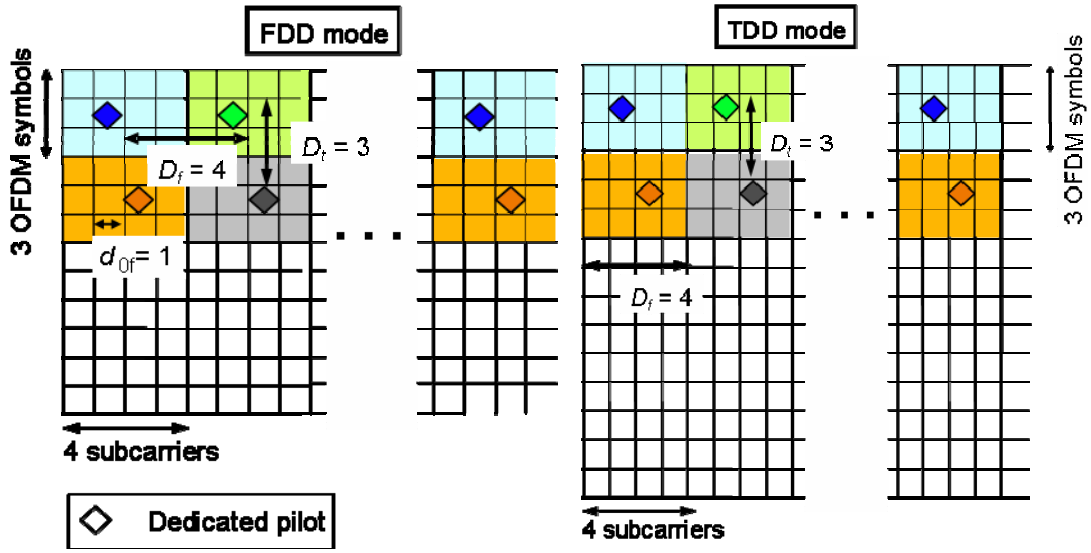

Figure 3-5: Uplink pilot grids for non-frequency adaptive transmission with B-IFDMA.

3.2.6.2 Uplink superframe pilot preamble

The dedicated pilot symbols per stream alone provide estimates of effective channel gains, i.e., channel gains affected by the spatial precoding scheme. To provide the BS with short-term CSI and CQI an uplink pilot preamble is inserted in the beginning of each superframe in both FDD and TDD modes, as shown in Figure 3-6, so to obtain estimates of the unweighted channel matrix. As uplink pilots over the full-band are very expensive in terms of overhead and UT power consumption, these full band pilots are inserted at a lower rate (once per superframe). This essentially limits the maximum velocity for adaptive transmission to 10 km/h. Only users with sufficiently low velocities, and which are scheduled by the BS for adaptive transmission transmit pilots at the superframe preamble. Pilots are orthogonally multiplexed in frequency. With a pilot spacing of $D_f = 8$ up to 8 such users can be supported per competition band.

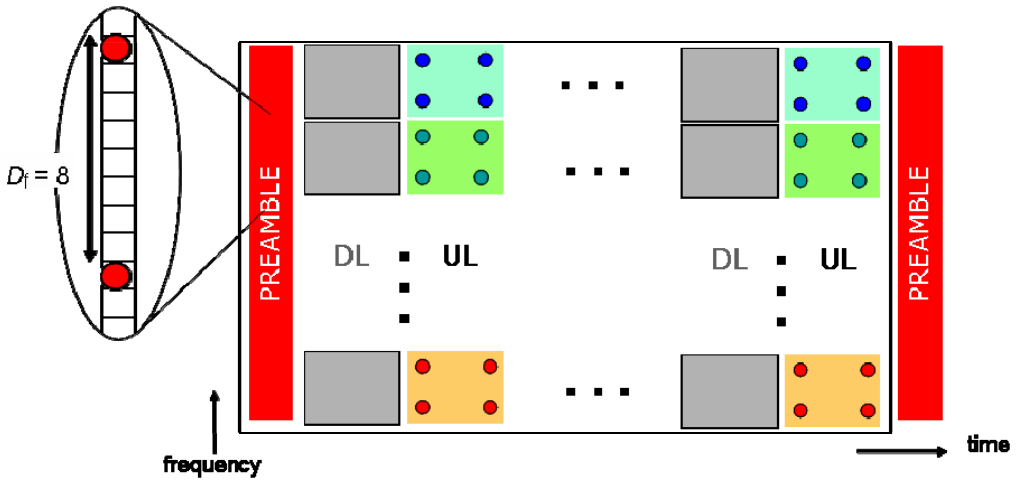

Figure 3-6: Position of uplink full-band dedicated pilots in superframe preamble.

We note that frequency adaptive transmission with mobile velocities up to 50km/h is possible through the downlink pilots in TDD mode. Hence, these mobile users do not insert pilots in the preamble. Pilots for channel estimation are frequency-multiplexed inside OFDM symbols, as described in Section 3.2.6.1.

3.2.7 Pilot design for wide area deployment

Wide area (WA) deployment is characterized by large macro-cells where BS antennas are mounted above rooftop. The pilot grids for the FDD mode apply, shown in Figure 3-2 and specified in Section 3.2.6.1.3. Furthermore an uplink super-frame pilot preamble (see Figure 3-6) as described in Section 3.2.6.2 is foreseen to enable adaptive transmission on FDD uplinks for slowly moving users.

For the reference design the BS is equipped with 4 cross-polarized antenna elements, giving $n_T = 8$ transmit antennas, while the UTs exhibits $n_R = 2$ cross-polarized antenna elements [WIN2D61310].

3.2.7.1 Downlink

The wide-area channels typical for macro-cell deployment are characterized by their small angular spread (assuming BS antennas above rooftop) [WIN2D112]. Beamforming with a grid of fixed beams (GoB) exploits small angular spreads, which makes it possible to focus a large portion of the transmitted energy to a restricted angular zone, and is therefore the preferred spatial transmit processing scheme for wide area downlinks. The reference design employs two GoBs with 4 antennas each (2x4 GoB). Common pilots per beam (CPB) are inserted. With a spatial pilot reuse of 2 and $P_n = 4$ orthogonal pilot sets up to 8 beams can be supported. CPB allow for interpolation over the whole frequency band, the pilots benefit the same beamforming gain as the data symbols, and CQI estimates at the UT can be determined. As the pilot overhead of $\Omega_p = 16.7\%$ is within acceptable limits (see Table 3-1), CPB offer an attractive choice for the WA reference design.

On chunks where data is broadcast without beamforming (e.g. control information or MBMS services) common pilots per antenna (CPA) are used. We note that on a certain chunk CPA are never inserted together with CPB, rather CPA *or* CPB are picked dependent on the chosen spatial transmit processing scheme.

3.2.7.2 Uplink

In WA uplinks dedicated pilots per antenna (DPA) are used. For OFDMA the pilot pattern specified in Figure 3-2 are used, while for B-IFDMA the pattern shown in Figure 3-5 are used. For non-frequency adaptive transmission no other pilots are necessary, i.e. users do not transmit uplink pilots in the super-frame preamble.

Slowly moving users that are scheduled for frequency adaptive transmission transmit need to transmit uplink pilots in the super-frame preamble to enable the BS receiver to scan for those chunks with the best CQI over the entire band. The uplink super-frame pilot preamble contains unweighted dedicated pilots per antenna over the full band (DPA-FB). With a pilot spacing of $D_f = 8$ up to $N_u = 8$ users can share the preamble. In case, $N_u > 8$ competition bands are introduced, which means that a certain user may access only a fraction of the available bandwidth. Therefore, DPA-FB pilots only need to be inserted in the corresponding competition band.

3.2.8 Pilot design for metropolitan area deployment

The micro-cell deployment in metropolitan area (MA) utilizes the TDD mode [WIN2D61311]. Hence, the pilot grids for the TDD mode apply, shown in Figure 3-3 and specified in Section 3.2.6.1.4 for the downlink and in Section 3.2.6.1.5 for the uplink. Furthermore an uplink super-frame pilot preamble (see Figure 3-6) as described in Section 3.2.6.2 is foreseen to enable MU-MIMO with CSIT on the downlink for slowly moving users.

For the reference design the BS is equipped with 4 cross-polarized antenna elements, giving $n_T = 8$ antennas, while the UTs exhibits $n_R = 2$ cross-polarized antenna elements.

3.2.8.1 Downlink

For the reference design the BS is equipped with $n_T = 8$ transmit antennas, and up to 4 spatial streams per chunk can be simultaneously transmitted. In MA downlinks a number of MIMO schemes need to be supported:

- SMMSE with short term CSI at the transmitter (CSIT) with up to 4 spatial streams per chunk. Target are slowly moving users (velocity ≤ 10 km/h) with high median SNR [WIN2D61311].
    - *In-band dedicated downlink pilots*: beamforming is applied to pilots in the same way as to payload data. If the beams are sufficiently spatially separated, i.e. the cross-talk between beams is below a certain threshold, an orthogonal pilot set can be reused.

- *Uplink pilots for CSI transfer*: In case a user transmits and receives data on both uplink and downlink, the necessary CSI for spatial precoding at the BS is readily available by the in-band uplink pilots. Unfortunately, users that receive on the downlink typically do not transmit data on the uplink. In this case, the UTs insert 2 pilots per UT antenna on the last OFDM symbol of uplink slots, on those chunks where this UT is receiving data on the downlink. These pilots facilitate transfer of CSI to the BS transmitter and are transmitted unweighted.
- *Uplink super-frame pilot preamble*: the preamble contains unweighted dedicated pilots per antenna over the full band (DPA-FB). With a pilot spacing of $D_f = 8$ up to $N_u = 8$ users can share the preamble. In case, $N_u > 8$ competition bands are introduced, which means that a certain user may access only a fraction of the available bandwidth. Therefore, DPA-FB pilots only need to be inserted in the corresponding competition band.

- Spatial multiplexing (SMUX) with per antenna rate control (PARC) with up to 2 spatial streams per chunk. Target are users with medium speed (velocity ≤ 50 km/h) with high SNR. No spatial transmit processing, i.e. the payload data is transmitted unweighted.
  - *In-band downlink pilots*: Like the payload data, pilots are transmitted unweighted. On these chunks the pilot grid in Figure 3-3 is then transformed to common pilots per antenna with a regular pilot spacing of $D_f = 4$ and $D_t = 12$ in frequency and time. For each spatial stream one orthogonal pilot set is used.
  - *CQI feedback*: The UTs can generate CQI estimates on all chunks where unweighted downlink pilots are transmitted. These CQI estimates are compressed as described in [WIN1D210] and transmitted to the BS. This enables frequency adaptive transmission on both uplink and downlink, due to the TDD channel reciprocity.
  - *Uplink super-frame pilot preamble*: Due to the high velocities of users associated to SMUX, no uplink pilots are inserted in the preamble.
- Linear dispersion codes by two antenna transmit diversity, the well known Alamouti scheme, applicable to low SNR and/or high velocities.
  - *In-band dedicated downlink pilots*: Pilots are transmitted unweighted, and for each active transmit antenna one orthogonal pilot set is used. In analogy to SMUX the pilot grid in Figure 3-3 is then transformed to common pilots per antenna with a regular pilot spacing of $D_f = 4$ and $D_t = 12$ in frequency and time.
  - *Uplink super-frame pilot preamble*: No uplink pilots are inserted in the preamble for users associated to LDC.

The MA downlink is characterised by a variety of MIMO schemes. The fact that all these MIMO schemes are to be flexibly combined imposes great challenges for the reference design. Figure 3-7 illustrates how the reference pilot design facilitates the coexistence of all considered flavours of MU-MIMO.

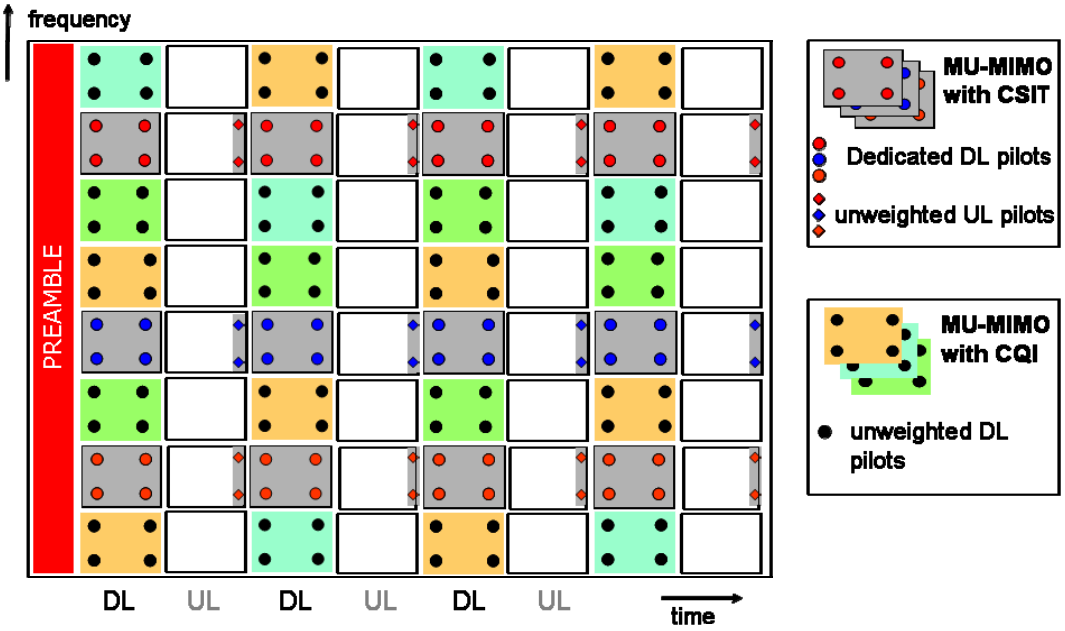

Figure 3-7: Pilot design to enable MU-MIMO in metropolitan area.

Figure 3-7 illustrates the chunk allocation and the coexistence of the considered MU-MIMO schemes. The chunk allocation works as follows:

- Downlink users scheduled for MU-MIMO with CSIT transmit uplink pilots in the super-frame preamble.
- The BS selects up to 4 users that transmit simultaneously in one chunk. The most appropriate chunks for these users are assigned, and the spatial precoding matrix is computed.
  ➔ The chunk allocation for MU-MIMO persists until the next super-frame pilot preamble is transmitted. This is reasonable since the low mobility suggests that the channel conditions do not significantly change during one super-frame. More importantly, now the user specific uplink pilots for CSI transfer only need to be transmitted on the allocated downlink chunks, and not over the full competition band. *This is a key requisite to keep the pilot overhead for CSI transfer on the uplink at an acceptable level*, while maintaining a regular update of the spatial precoding matrix on a frame-by-frame basis.
- The remaining chunks are then assigned to MU-MIMO without CSIT, but with CQI at the transmitter (short-term or long-term).
  ➔ Since these users transmit unweighted downlink pilots, UTs can measure the CQI on all those remaining chunks that are not reserved for MU-MIMO with CSIT. In other words, unbiased CQI is available at the UTs as no user-specific spatial precoding is applied to the pilots, which is a key requirement for multi-user scheduling based on short-term CQI on a frame-by-frame basis.
- CQI is reported to the BS on the uplink as encoded data packets, by DCT (discrete cosine transform) based data compression [WIN1D24], [WIN1D210].
  ➔ This is a key enabler for frequency adaptive transmission up to mobile velocities. We note that no uplink pilots for CSI transfer are needed for high velocity users, avoiding prohibitive overheads for feedback on the uplink.

To conclude, flexible operation and coexistence of various flavours of MU-MIMO is established on the downlink, the overall burden on the uplink for feedback of CQI and CSI is kept remarkably low.

3.2.8.2 Uplink

In MA uplinks dedicated pilots per antenna (DPA) are used. For OFDMA the pilot pattern specified in Figure 3-3 are used, while for B-IFDMA the pattern shown in Figure 3-5 are used. The reference design for downlink and uplink is designed such that the spatial processing schemes chosen for downlink and uplink have the same requirements in terms of signalling. We therefore benefit from the same pilot design for both downlink and uplink reference design [WIN2D341].

As the MU-MIMO schemes with CSIT on the downlink require uplink pilots to update the spatial precoding matrix, the last OFDM symbol is reserved for pilots of those users which require short-term CSI at the BS on that chunk. As this applies only a subset of users, one bit of signalling per chunk per super-frame is necessary, so to inform the UT whether the last OFDM symbol of a particular chunk is reserved for CSI feedback or not.

3.2.9 Pilot design for local area deployment

Indoor deployment in local area (LA) utilizes the TDD mode [WIN2D61312]. Hence, the pilot grids for the TDD mode apply, shown in Figure 3-3 and specified in Section 3.2.6.1.4 for the downlink and in Section 3.2.6.1.5 for the uplink. Furthermore an uplink super-frame pilot preamble (see Figure 3-6) as described in Section 3.2.6.2 is foreseen to enable MU-MIMO with CSIT on the downlink. As in LA deployment all users can be considered slowly moving, the coherence time of all users' channels are expected to exceed the duration of a super-frame. On the other hand, a distributed antenna array with up to n_T=32 BS antennas together with the most advanced MIMO schemes that are able to serve up to 30 users simultaneously on one chunk are considered for LA [WIN2D341], [WIN2D61312]. To this end, one pilot in time direction may suffice, i.e. the pilots corresponding to pilot index $\ell_p = 2$ in **(3-1)** may be omitted, which cuts the pilot overhead by a factor of 2.

3.2.9.1 Downlink

Unlike the MA reference design, the spatial processing in LA deployment is always MU-MIMO with CSIT. The challenge for LA is the potentially very large number of simultaneously served users per chunk. With the 4 orthogonal pilot sets, the spatial reuse of pilots in LA can be up to 8. Since, distributed antenna arrays are considered which decorrelate users and alleviate the near far problem, even such a high spatial reuse of pilots is feasible.

The general rules for the pilot design follow the MA section 3.2.8. The uplink pilot super-frame preamble provides the BS with the necessary CSI of all active users, which is used for chunk allocation and user grouping. Due to the low velocities and the resulting long channel coherence times, users may not need to send pilots on each super-frame preamble. Together with the provision of competition bands, this keeps the pilot overhead for signalling within acceptable limits. Likewise the spatial precoding matrix may not necessarily be updated every frame, so the feedback rate of pilots for CSI transfer on the uplink may also be reduced.

3.2.9.2 Uplink

The pilot design for the uplink closely follows the downlink case described above. Instead of downlink dedicated pilots per beam, dedicated pilots per antenna are used in the uplink. Similar to the downlink, the super-frame preamble provides the BS with the CSI of the uplink users. After chunk allocation and user grouping based on the super-frame preamble the in-band uplink pilots the short-term CSI for the spatial receiver processing at the BS.

3.3 Conclusions

In Section 3.2 the pilot design for the WINNER system concept was established. A modular concept was proposed that allows to flexibly support various flavours of multi-user MIMO schemes in combination with GMC based multiple access schemes. The basic building blocks are the *pilot pattern*, the *pilot type* and the *orthogonal pilot sets*. The pilot pattern defines the position of pilot symbols within the chunk, and at the same time resembles a regular 2D grid with equidistantly spaced pilots on the macroscopic view of the OFDM frame. The spatial transmit processing scheme then defines the pilot type that is inserted on a particular chunk. The introduction of orthogonal pilot sets specifies whether pilots associated to different spatial streams are orthogonally separated in time and/or frequency, or, in case the spatial separation between beams is sufficient, the pilot symbol can be reused. Thanks to this modular concept the pilot overhead stays within acceptable limits. The price to be paid for the low pilot overheads is the increased signal processing at the receiver. Due to the spatial reuse of pilots as well as the use of dedicated pilots, which inevitably compromises the attainable accuracy of pilot aided channel estimation, iterative channel estimation schemes studied in Section 4.3 are identified as a compulsory part of the WINNER system concept.

In Appendices K.1 and K.2, the optimum placement of pilots within a chunk as well as over consecutive multiple chunks is addressed, such that the channel estimation error (including the interpolation error and the noise-induced error) in terms of MSE is minimized. While the optimum pilot placement for one or two transmit antennas is different from the WINNER reference pilot design specified in Section 3.2.6, for 4 transmit antennas the WINNER reference pilot design is optimum.

In Appendix K.3 a framework for pilot grid design in MIMO-OFDM without CSI at the transmitter was developed and applied to determine the pilot spacing and boost, so to maximize the capacity of the target MIMO-OFDM system, including channel estimation errors and pilot symbols overhead. It is shown that the capacity is maximized by placing pilots equidistantly at Nyquist rate. However, the derived bound can only be achieved assuming infinitely long pilot sequences and filters. Furthermore, a semi-analytical procedure was proposed to maximize the capacity for realizable and possibly sub-optimum channel estimation schemes. That is, pilot symbols should be inserted sparsely, but sufficiently often to maintain a small enough interpolation error. Then, with an appropriately chosen pilot boost the capacity is maximized. Numerical results indicate that optimized placement and power allocation of pilot symbols have a significant impact on the attainable channel capacity.

4. Channel Estimation

4.1 Introduction

Channel estimation (CE), generally performed on received signals, is essential for satisfactory performance of equalizers, smart antennas, multi-user scheduling, transmitter array processing and precoding, optimum or near-optimum detection and decoding, and signal quality estimation. In most of the cases relevant to WINNER, channel estimation is explicit, producing estimates of the frequency response (channel transfer function) between transmitters (with or without spatial processing) and receivers. These estimates are then used in the algorithms that perform the abovementioned functions. In some cases, channel estimation is implicit, producing estimates of receiver parameters directly; an example of this is the least squares adaptation for suppressing low level out-of-cell interference, described in section 4.3.2. In the WINNER system, channel estimation is aided by the transmission of pilots, frequency-multiplexed with data. Pilots create extra overhead, and it is therefore important to use channel estimation techniques which make most efficient use of a limited number of pilots.

Sections 4.2, 4.3.1 and 4.3.2 describe respectively, noniterative CE techniques which interpolate frequency response estimates from pilot measurements; genetic algorithm-aided iterative techniques for OFDM which supplement the pilot-aided estimates; and decision-directed iterative techniques for DFT-precoded OFDM, which suppress in-cell and out-of-cell interference with the aid of least squares adaptation. In Section 4.4 channel prediction methods are presented. Section 4.5 describes the CE reference design. Section 4.6 presents simulation results for Wide Area (WA) and Metropolitan Area (MA) scenarios for the techniques described in section 4.3. Section 4.7 analyzes the effect of errors on channel estimates fed back from receiver to transmitter in 2X2 MIMO scenarios. Finally, section 4.8 presents conclusions.

4.2 Noniterative Channel Estimation Techniques

Channel estimation is based on mismatched 2D Wiener filter interpolation that has been applied to pilot aided channel estimation (PACE). PACE is optionally followed by iterative channel estimation (ICE). PACE estimates are used as initial estimates for ICE. For PACE, a cascaded channel estimator is used, consisting of two one dimensional (1D) estimators, termed 2x1D PACE. First, channel estimation is performed in frequency direction at OFDM symbols containing pilot symbols, yielding tentative estimates for all subcarriers of that OFDM symbol. The second step is to use these tentative estimates as new pilots, in order to estimate the channel for the entire frame. It was demonstrated in [HKR97], that 2×1 D-PACE is significantly less complex to implement with respect to optimum 2D channel estimation, while there is little degradation in performance.

Let the FIR filter in time and frequency direction be denoted by $\mathbf{w}''(\ell)=[W''_1(\ell),\cdots,W''_{M_t}(\ell)]$ and $\mathbf{w}'(n)=[W'_1(n),\cdots,W'_{M_r}(n)]$, then the estimator for 2×1 D PACE is obtained by using the Kronecker product, so $\mathbf{w}(n,\ell)=\mathbf{w}''(\ell)\otimes\mathbf{w}'(n)$ of dimension $M_r M_t\times1$. The optimal filter in the sense of minimizing the MSE is the Wiener filter [Kay93]. The estimators $\mathbf{w}'(n)$ and $\mathbf{w}''(\ell)$ are obtained by solving the Wiener-Hopf equation in frequency and time direction, respectively [HKR97].

The filter $\mathbf{w}(n,\ell)$ is designed such that it covers a great variety of power delay profiles and Doppler power spectra. A rectangular shaped power delay profile with maximum delay τ_w and a rectangular shaped Doppler power spectrum with maximum Doppler frequency $f_{D,w}$ are used. The parameters of the robust estimator should always be equal or larger than the worst case channel conditions, i.e. largest propagation delays and maximum expected velocity of the mobile user, so $\tau_w\geq\tau_{max}$ and $f_{D,w}\geq f_{D,max}$. Furthermore, the average SNR at the filter input, which is used to generate the filter coefficients, γ_w, should be equal or larger than actual average SNR, so $\gamma_w\geq\gamma$.

The filter coefficients of such so called Wiener filter with model mismatch are generated with the following prior knowledge about channel statistics:

- The maximum delay of the channel is set equal to the CP-length, $\tau_{\mathrm{w}} = T_{CP} > \tau_{\max}$,
- Max. expected velocity is set with respect to a certain environment (LA: 3km/h, MA: 70km/h, WA: 250km/h),
- SNR is assumed to be perfectly known.

The Wiener filter with model mismatch is closely related to a lowpass interpolation filter (LPIF), in the way that signals with spectral components within the range $[0, \tau_{\mathrm{w}}]$ and $[0, f_{\mathrm{D,max}}]$ pass the filter undistorted, while spectral components outside this range are blocked. In fact, it can be shown that a mismatched WIF approaches an ideal LPIF if the number of filter coefficients approaches infinity, $\{M_{\mathrm{f}}, M_{\mathrm{t}}\} \to \infty$ [AuK05].

By using a scattered pilot grid the received OFDM frame is sampled in two dimensions, with rate D_{f}/T and $D_{\mathrm{t}} T_{\mathrm{sym}}$ in frequency and time, respectively. In order to reconstruct the signal, there exists a maximum spacing of D_{f} and D_{t}, dependent on the filter parameters, $\tau_{\mathrm{w}} \geq \tau_{\max}$, and $f_{\mathrm{D,w}} \geq f_{\mathrm{D,max}}$, that is [HKR97]

$$\frac{D_{\mathrm{f}}\,\tau_{\mathrm{w}}}{T} = \frac{1}{\beta_{\mathrm{f}}} < 1, \qquad 2\,D_{\mathrm{t}}\,f_{\mathrm{D,w}}\,T_{\mathrm{sym}} = \frac{1}{\beta_{\mathrm{t}}} < 1 \tag{4.1}$$

where β_{f} and β_{t} denote the oversampling factor in frequency and time. The sampling theorem states that the theoretical limit is approached by an ideal LPIF, having a rectangular shaped filter transfer function, so $D_{\mathrm{f}} \leq T/\tau_{\mathrm{w}}$ and $D_{\mathrm{t}} \leq 1/(2\,f_{\mathrm{D,w}}\,T_{\mathrm{sym}})$. In order to allow for a realizable filter with finite M_{f} and M_{t}, however, the oversampling factors β_{f} and β_{t} should be larger than one.

Multiple in-cell users (ICUs) may share common frequency-time channels; i.e. they may occupy different layers of the same chunk. Each such interfering ICU has dedicated frequency-time resources for its pilots, which are used for channel estimation. Thus ICUs' pilots are orthogonal and do not interfere with one another. However ICU pilots may be interfered by out-of-cell interferers, which as a result of frequency reuse partitioning strategies, are at relatively low average received power levels. Basic channel estimation strategies thus use the above 2X1D PACE interpolation algorithm with orthogonal ICU pilots, and ignore low-level out-of-cell interference. The following describes a linear equalization MMSE algorithm, using estimated ICU channels, and estimated noise variance, to compensate for frequency selectivity and for ICU interference for the uplink DFT-precoded OFDM.

Assuming that there are N_T interfering transmitters, the frequency domain output of a N_R-receiving antenna array is

$$\mathbf{R}_f = \mathbf{H}_f \mathbf{A}_f + \mathbf{N}_f = \sum_{\ell=1}^{N_T} \mathbf{H}_f(\ell) A_f(\ell) + \mathbf{N}_f \tag{4.2}$$

where $\mathbf{R}_f, f = 0,1,2,...M-1$ is a N_R-dimensional vector at frequency f, M is the FFT size, $\mathbf{H}_f(k), f = 0,1,2,...M-1,\ k = 1,2,..N_T$ is the N_R-dimensional channel frequency response vector from the kth transmitter, $\mathbf{H}_f, f = 0,1,2,...M-1$ is the N_R by N_T matrix whose columns are $\{\mathbf{H}_f(k)\}$, $A_f(k)$, f=0,1,2,...M-1, k=1,..N_T is the kth transmitter's frequency domain data component at frequency f; i.e. it is the M-point DFT of the data symbol sequence $\{a_{m,k}\}$. $\mathbf{A}_f$ is the N_T-dimensional vector of data, and $\mathbf{N}_f$ is a vector of white Gaussian noise samples, whose variance is σ^2.

The frequency domain output of a linear equalizer, characterized at frequency f by the N_R-dimensional vector $\mathbf{W}_f^{(0)}(k)$ for transmitter k, is

$$U_f^{(0)}(k) = \mathbf{W}_f^{(0)}(k)^* \mathbf{R}_f\,, \tag{4.3}$$

where the asterisk denotes conjugate transpose. The superscript (0) is inserted since this equation also defines the starting point for the iterative block decision feedback algorithm. The corresponding time domain output is the inverse DFT

$$u_m^{(0)}(k) = \frac{1}{\sqrt{M}} \sum_{f=0}^{M-1} U_f^{(0)}(k) \exp(j2\pi fm / M), \text{ for } m=0,1,..M\text{-}1. \tag{4.4}$$

The mean square error is minimized by the standard Wiener-Hopf solution:

$$\mathbf{W}_f^{(0)}(k) = (1 - \mu_f^{(0)}(k)) \left[\mathbf{H}_f \mathbf{H}_f^* + \sigma^2 \mathbf{I}_{N_R} \right]^{-1} \mathbf{H}_f(k) \tag{4.5}$$

where

$$1 - \mu_f^{(0)}(k) = \frac{1}{\frac{1}{M} \sum_{f=0}^{M-1} \mathbf{H}_f(k)^* \left[\mathbf{H}_f \mathbf{H}_f^* + \sigma^2 \mathbf{I}_{N_R} \right]^{-1} \mathbf{H}_f(k)} \tag{4.6}$$

is a normalizing factor that constrains a unit gain for the kth transmitter:

$$\frac{1}{M} \sum_{f=0}^{M-1} \mathbf{W}_f^{(0)}(k)^* \mathbf{H}_f(k) = 1. \tag{4.7}$$

The corresponding minimum mean square error at the linear equalizer's output can be shown to be

$$\sigma^{(0)2}(k) = -\mu_f^{(0)}(k) = \frac{1}{\frac{1}{M} \sum_{f=0}^{M-1} \mathbf{H}_f(k)^* \left[\mathbf{H}_f \mathbf{H}_f^* + \sigma^2 \mathbf{I}_{N_R} \right]^{-1} \mathbf{H}_f(k)} - 1. \tag{4.8}$$

4.3 Iterative Channel Estimation Techniques

A turbo receiver consists of an inner and outer receiver which exchange extrinsic information [WIN1D21], [BA06], [AB07]. For iterative channel estimation (ICE) the channel estimation unit is included in the turbo loop. A non-joint, i.e. separated approach, is adopted in which initial channel estimates are provided by PACE. At subsequent iterations channel estimates are refined by utilizing fed back symbol estimates, which serve as auxiliary pilot symbols. A separated approach is more computationally efficient and allows for a flexible and modular receiver design, where the channel estimation unit and the detector/decoder are mostly independent building blocks. Moreover, since an initial estimate already exists, ICE may be implemented optionally, e.g. for high-end terminals. On the other hand, the data symbol estimates are subject to decision feedback errors, which, in particular for low SNR, may cancel out parts of the potential performance gains of ICE. Feedback is derived from **a posteriori** information, as shown in Figure 4-1. As shown in Appendix C.1 using a posteriori information is superor in comparison to using extrinsic information. Note that all results reported in previous deliverables [WIN1D23], [WIN1D210] assume exchange of extrinsic information. The channel estimator component shown in the bottom-left part of Figure 4-1 can potentially be extended to a Genetic Algorithm (GA) aided joint ICE and multi-user detector (MUD), to be introduced in Section 4.3.1, which targets at the multi-user MIMO scenario, where channel estimation is more challenging than that in the SISO scenario. With the aid of the turbo processing framework illustrated in Figure 4-1, the performance of the GA-ICE can be further improved at the expense of a relatively higher computational complexity. Details of the GA-ICE are provided in Section 4.3.1.

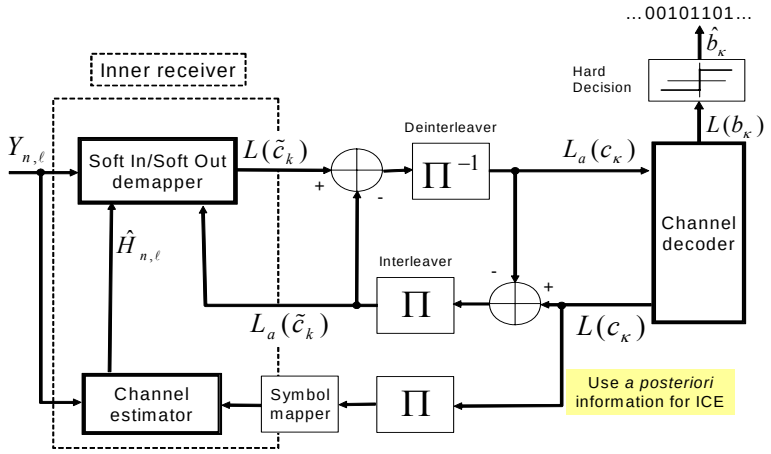

Figure 4-1: Iterative receiver structure. A posteriori information is used for ICE.

4.3.1 Iterative multi-user MIMO channel estimation using genetic algorithms

4.3.1.1 System Overview

As indicated by the terminology, a MIMO system employs multiple transmitter and receiver antennas for delivering parallel data streams. For example, in Figure 4-2 the schematic of an uplink MIMO channel model is provided, where each of the N_t User Terminals (UTs) is equipped with a single transmit antenna and the BS employs N_r receiver antennas. Specifically, at the k^{th} subcarrier during the n^{th} OFDM symbol duration, we have

$$\mathbf{x}[n,k] = \mathbf{H}[n,k] \cdot \mathbf{s}[n,k] + \mathbf{n}[n,k] \tag{4.9}$$

where the $(N_r \times 1)$-dimensional vector $\mathbf{x}$, the $(N_t \times 1)$-dimensional vector $\mathbf{s}$ and the $(N_r \times 1)$-dimensional vector $\mathbf{n}$ are the received, transmitted, and noise signals, respectively. Note that in this specific application example we have assumed a multi-user scenario, where each UT exploits a single antenna. However, the proposed technique can be straightforwardly applied to the scenario, where each UT employs multiple antennas. In such a case, each antenna at the UT can be equivalently treated as an individual "user" shown in the example of Figure 4-2.

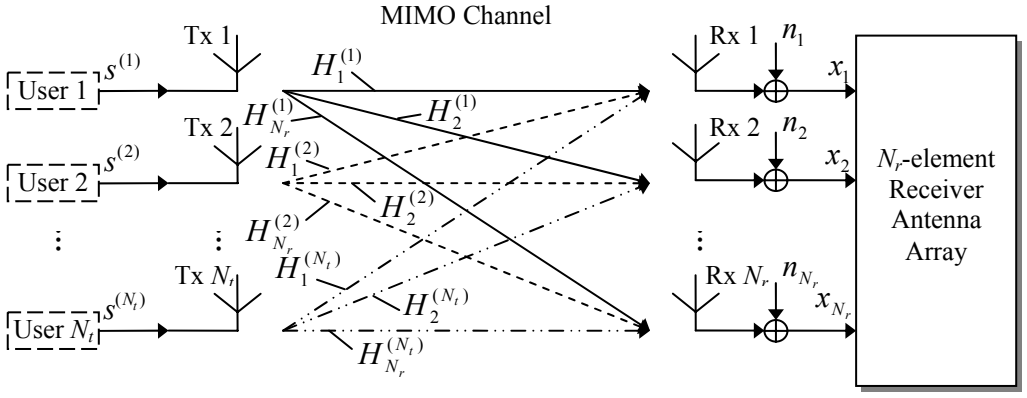

Figure 4-2: Schematic of an uplink MIMO channel model where each of the N_t mobile users is equipped with a single transmit antenna and the BS employs N_r receiver antennas.

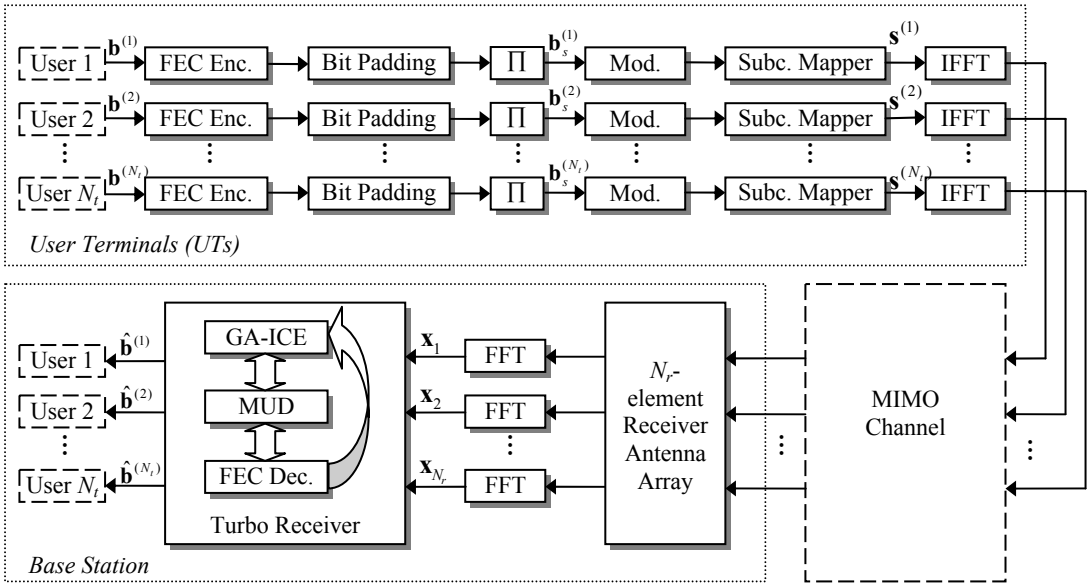

Figure 4-3: Schematic of an uplink multi-user MIMO OFDM system employing the proposed GA-ICE aided turbo receiver.

The schematic of an uplink multi-user MIMO OFDM system using the proposed GA-ICE aided turbo receiver is depicted in Figure 4-3. As shown in the upper half of Figure 4-3, the information bit blocks $\mathbf{b}^{(n_t)}(n_t = 1,\cdots,N_t)$ of the N_t number of UTs are first encoded by the N_t independent Forward Error Correction (FEC) encoders, followed by the corresponding bit padding operations, where zero bits are appended to each user's bit sequence for being conformable to a specific size. The number of padding bits depends on frame size, number of OFDM subcarriers, codeword length, modulation scheme, etc. The resultant appended coded bits are then interleaved and mapped to Quadrature Amplitude Modulation (QAM) or Phase-Shift Keying (PSK) constellation symbols, which are modulated by the length-K Inverse Fast Fourier Transform (IFFT) based OFDM modulators following the subcarrier mapping operation, as seen in Figure 4-3. Then each user's signal is independently transmitted over the MIMO channel described in Figure 4-2. Note that at any time each of the N_t UTs use all the K subcarriers for transmission, except those allocated for other UTs' pilot signals, in order to maximize the system throughput. In other words, the different users' transmitted signals excluding pilot symbols are overlapped across the same time-frequency resource available to the system.

At the BS illustrated at the lower half of Figure 4-3, the received signal constituted by the noise-contaminated superposition of all users' transmitted signals, is first subject to Fast Fourier Transform (FFT) based OFDM demodulation at each of the N_r receiver antenna elements. Finally, the OFDM-demodulated signal is forwarded to the turbo receiver for iterative channel estimation, Multi-User Detection (MUD), and channel decoding, as will be detailed in Section 4.3.1.3.

4.3.1.2 Genetically inspired optimization

The GAs [HOL75], [GOL89], [MIT96], [WHI94], [FOR93] were first introduced by Holland [HOL75] during the 1960s. Since then, a growing interest in Gas resulted in a rapid development in this area [GOL89], [MUH91], [GB89], since Gas have been shown to perform well in numerous robust global search and optimization problems, which may not be conveniently solved by using traditional search methods. A brief introduction of the GAs is provided as follows in the context of channel estimation in multi-user MIMO OFDM systems.

More specifically, at the beginning of the GA-based optimization process, an initial *population* consisting of X number of *individuals* is created, each representing a possible solution of the optimization problem considered, with the aid of a priori knowledge concerning the optimum solution. In our case the goal is to optimize the Frequency-Domain (FD) Channel Transfer Functions (CTFs) such that they sufficiently closely match their true counterparts, if not exactly the same as them. The x^{th} individual of the population of the y^{th} *generation*, is expressed as

$$\begin{cases} \tilde{\mathbf{s}}_{(y,x)}[n,k] & = & \left[\tilde{s}^{(1)}_{(y,x)}[n,k], \tilde{s}^{(2)}_{(y,x)}[n,k], \cdots, \tilde{s}^{(N_t)}_{(y,x)}[n,k]\right] \\ \tilde{\mathbf{H}}_{(y,x)}[n,k] & = & \begin{bmatrix} \tilde{H}^{(1)}_{1,(y,x)}[n,k] & \tilde{H}^{(2)}_{1,(y,x)}[n,k] & \cdots & \tilde{H}^{(N_t)}_{1,(y,x)}[n,k] \\ \tilde{H}^{(1)}_{2,(y,x)}[n,k] & \tilde{H}^{(2)}_{2,(y,x)}[n,k] & \cdots & \tilde{H}^{(N_t)}_{2,(y,x)}[n,k] \\ \vdots & \vdots & \ddots & \vdots \\ \tilde{H}^{(1)}_{N_r,(y,x)}[n,k] & \tilde{H}^{(2)}_{N_r,(y,x)}[n,k] & \cdots & \tilde{H}^{(N_t)}_{N_r,(y,x)}[n,k] \end{bmatrix} \end{cases} \quad (4.10)$$

which can be an arbitrary combination of a length-N_t multi-user constellation symbol vector $\tilde{\mathbf{s}}_{(y,x)}[n,k]$ and a ($N_r \times N_t$)-dimensional FD-CTF matrix $\tilde{\mathbf{H}}_{(y,x)}[n,k]$. Then the GA's task is to find an individual, which is considered optimum or near-optimum in terms of minimizing the Objective Function (OF) defined by

$$\Omega\left(\tilde{\mathbf{H}}[n,k], \tilde{\mathbf{s}}[n,k]\right) = \left\|\mathbf{x}[n,k] - \tilde{\mathbf{H}}[n,k] \cdot \tilde{\mathbf{s}}[n,k]\right\|^2 \quad (4.11)$$

For each individual, the OF's output, referred to as *Objective Score (OS)*, is converted to a corresponding *fitness* value, which indicates the fitness of the specific individual in the sense of (4.11). Then a number of individuals that have the highest fitness values are selected for creating a so-called *mating pool*, based on specific criteria such as those used in [GOL89]. The individuals in the mating pool will be appropriately paired as *parents* for producing *offspring*. More explicitly, for each pair of the parents, the genetic operations referred to as *cross-over* and *mutation* [MIT96] are invoked, which follow specific rules to exchange, combine, and change parts of the parent individuals, resulting in offspring individuals having statistically better fitness values.

The genetic operation cycle mentioned above forms the basis of the GA-aided optimization, yielding an offspring population having an improved average fitness. This evolution continues, until the generation index reaches its maximum. Then the operation of the GA is terminated and the highest-fitness individual of the last population will be considered as the final solution, which is a specific combination of the symbol vector and the FD-CTF matrix, which contains the jointly optimized estimates of the transmitted multi-user symbols and the associated FD-CTFs, respectively, for the specific OFDM subcarrier considered.

4.3.1.3 Turbo MIMO OFDM receiver using GA-aided iterative channel estimation

In this section, we elaborate on the proposed design of the turbo receiver portrayed in Figure 4-3, which is further detailed in Figure 4-4. More specifically, the receiver consists of two major parts, namely the outer loop associated with the channel decoder, as well as the inner loop with the channel estimator and the MUD, as shown at the left- and right-hand side of Figure 4-4, respectively.

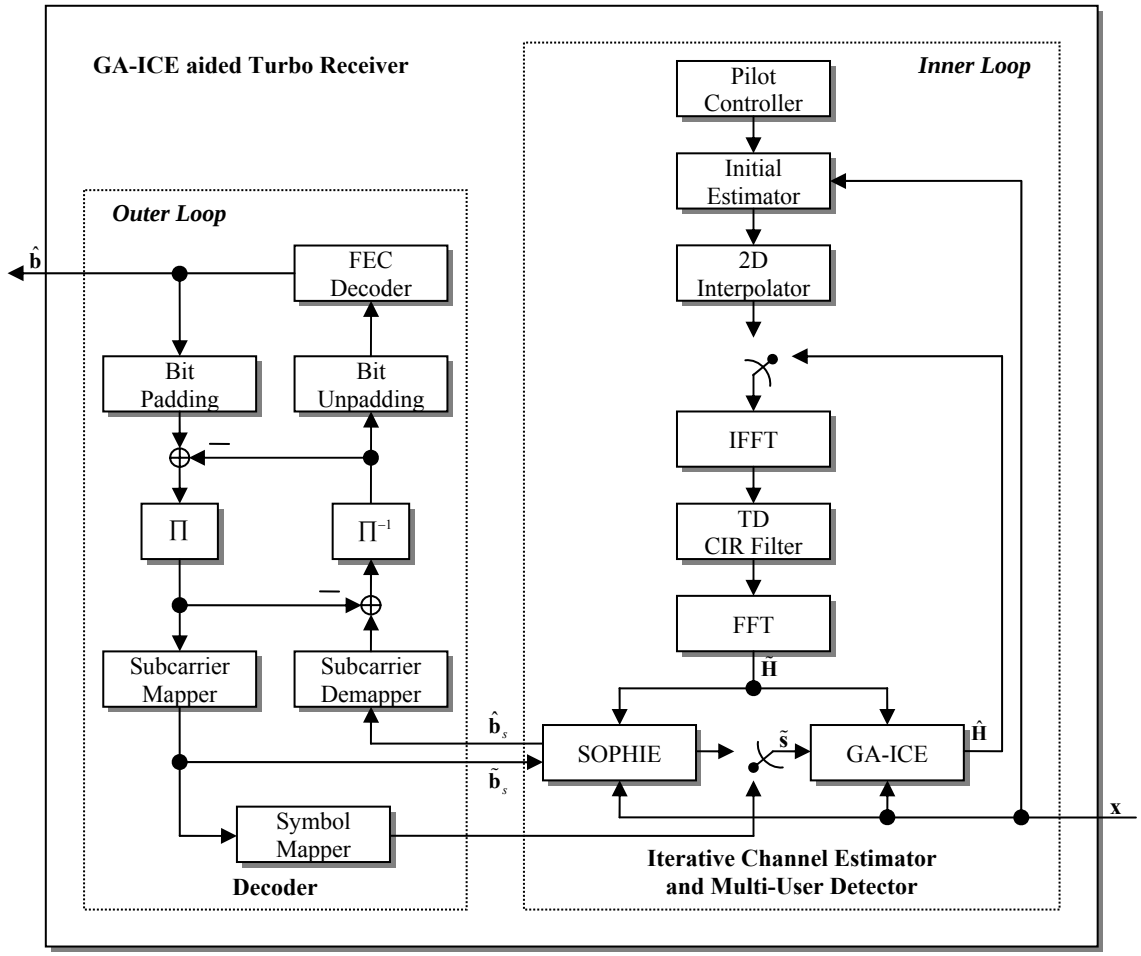

Figure 4-4: The structure of the GA-ICE aided turbo MIMO OFDM receiver.

4.3.1.3.1 Iterative channel estimation and multi-user detection

As seen on the top of the inner loop block plotted in Figure 4-4, as the first step the pilot controller provides known pilot symbols for assisting the initial estimation process invoked at the pilot subcarriers. A pilot pattern based on the WINNER proposal for Time Division Duplexing (TDD) mode [WIN1D210] was used, which is similar to the pattern specified in [WIN2D6137], with the slight modification that additional pilots are inserted at frame edges in both Time Domain (TD) and FD for the sake of improving frame edge performance. Furthermore, the pilot symbols of different users are allocated to orthogonal subcarriers, as also mentioned in Section 3, for the sake of eliminating Multi-User Interference (MUI).

With the aid of the orthogonal multi-user pilots, the initial estimates of the FD-CTFs associated with all the $N_t \times N_r$ UT-receiver links can be generated by

$$\hat{H}_{n_r}^{(n_t)}[n_{p_t}, k_{p_f}] = \frac{(s_{\mathrm{p}}^{(n_t)}[n_{p_t}, k_{p_f}])^*}{|s_{\mathrm{p}}^{(n_t)}[n_{p_t}, k_{p_f}]|^2} \cdot x_{n_r}[n_{p_t}, k_{p_f}], \quad n_t = 1, \cdots, N_t; n_r = 1, \cdots, N_r \quad (4.12)$$

where $s_{\mathrm{p}}^{(n_t)}$ is the pilot symbol from the $(n_t)^{th}$ UT, while $n_{p_t} = p_t D_t$ and $n_{p_f} = p_f D_f$ indicate the pilot subcarriers' locations on the time-frequency grid, and $(\cdot)^*$ denotes complex conjugate. Furthermore, p_t and p_f are the pilot indices in TD and FD, respectively, while D_t or D_f denotes the interval between two consecutive pilots in the corresponding domain. Then a simple two-dimensional (2D) linear interpolation process shown in Figure 4-5 is triggered, generating the initial FD-CTF estimates at the data subcarriers as

$$\begin{cases} \hat{H}_{n_r}^{(n_t)}[n',k] = \hat{H}_{n_r}^{(n_t)}[n_{p_t},k] + \dfrac{n'-n_{p_t}}{D_t}\left(\hat{H}_{n_r}^{(n_t)}[n_{p_t+1},k] - \hat{H}_{n_r}^{(n_t)}[n_{p_t},k]\right), & n_{p_t} \le n' < n_{p_t+1} \\ \hat{H}_{n_r}^{(n_t)}[n,k'] = \hat{H}_{n_r}^{(n_t)}[n,k_{p_f}] + \dfrac{k'-k_{p_f}}{D_f}\left(\hat{H}_{n_r}^{(n_t)}[n,k_{p_f+1}] - \hat{H}_{n_r}^{(n_t)}[n,k_{p_f}]\right), & k_{p_f} \le k' < k_{p_f+1} \end{cases} \quad (4.13)$$

After obtaining the initial channel estimates across the entire frame, an OFDM symbol based TD Channel Impulse Response (CIR) filtering operation is invoked, as portrayed in the middle of Figure 4-4, for the sake of reducing the noise existing in the FD-CTF estimates. Without loss of generality, in Figure 4-5 we illustrate the filtering process in the context of the $(n_r)^{th}$ receiver antenna during the n^{th} OFDM symbol duration. More specifically, for the $(n_t)^{th}$ user, the K number of initial FD-CTF estimates $\hat{H}_{n_r}^{(n_t)}[n,k](k=1,\cdots,K)$ are first subjected to a length-K IFFT, resulting in the set of K uncorrelated CIR-related taps $\hat{h}_{n_r}^{(n_t)}[n,k](k=1,\cdots,K)$. Then, only the first K_0 CIR tap coefficients are retained with the rest set to zero, where K_0 is set to be equal to the number of samples within the OFDM cyclic prefix. Then the retained CIR-related coefficients $\hat{h}_{n_r}^{(n_t)}[n,k](k=1,\cdots,K_0)$ are converted to the noise-reduced *a posteriori* FD-CTF estimates $\tilde{H}_{n_r}^{(n_t)}[n,k](k=1,\cdots,K)$ by the Fast Fourier Transform (FFT).

As indicated in the lower part of Figure 4-4, the cleansed FD-CTF estimates $\tilde{H}_{n_r}^{(n_t)}[n,k](k=1,\cdots,K)$ are forwarded to the MUD for assisting the detection process. Compared with [JAG+06a], [JAG+06b], where the Optimized Hierarchy Reduced Search Algorithm (OHRSA) [HK06], [AH06a] aided MUD was employed, in our system the Soft-output Optimized Hierarchy (SOPHIE) [HK06], [AH06b] aided MUD is exploited. The SOPHIE detector is capable of approaching the near-optimum performance of the OHRSA-aided Log-MAP detector, while imposing a modest computational complexity [HK06], [AH06b]. The output of the SOPHIE MUD as well as the channel estimates provided by the TD filter of Figure 4-5 are then forwarded to the GA-ICE, where they are genetically optimized, as described in Section 4.3.1.2. Moreover, the GA-improved FD-CTF estimates can be fed back to the TD filter for further enhancement. The more accurate channel information is therefore expected to help the SOPHIE MUD improve the quality of the symbol estimates. Such an interactive channel estimation and symbol detection process can continue for a predefined number of iterations, or until satisfactory results are achieved.

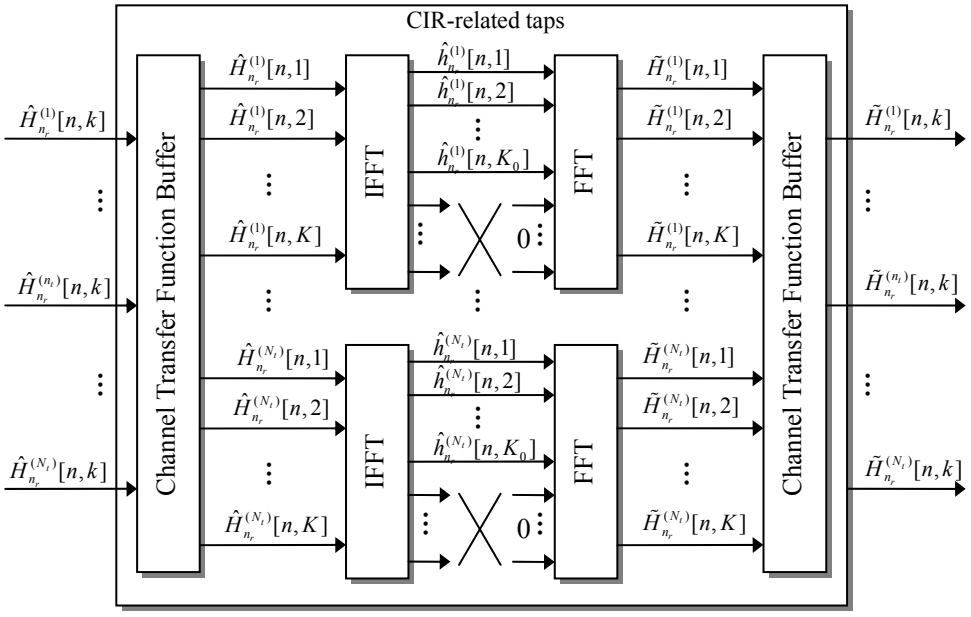

Figure 4-5: Time-domain filtering at the $(n_r)^{th}$ receiver antenna.

4.3.1.3.2 Soft-input Soft-output Turbo Processing

The output of the inner-loop operations discussed in Section 4.3.1.3.1 is constituted by the *a priori* soft bits of the different users, or widely known as Log-Likelihood Ratios (LLRs), which are generated by the SOPHIE MUD [HK06], [AH06b]. As the input to the outer-loop routine, each individual user's soft information is sequentially forwarded to the subcarrier demapper, deinterleaver, and unpadding operator, resulting in the unpadded coded bits to be decoded by the FEC decoder, as observed at the left-hand side of Figure 4-4. Furthermore, extrinsic LLRs can be generated by subtracting the *a priori* LLRs from the *a posteriori* LLRs provided by the FEC decoder. Then the extrinsic soft bits are subject to inverse procedures involving the bit padding, interleaving, and subcarrier mapping operations, before they are mapped to the corresponding constellation symbols, which are used for facilitating the next-round channel estimation process invoked in the GA-ICE within the inner loop. Note that the above-mentioned turbo processing is separately invoked for each of the N_t users for a number of outer iterations I_o.

Naturally, with the aid of the FEC decoder, the accuracy of the detected signal can be substantially enhanced, which is expected to assist the GA-ICE in improving the channel estimates and vice versa. Benefited from the exchange of soft information between the inner and the outer iterations, the system's achievable performance can be significantly boosted, as to be detailed in Appendix D. Main results are also summarized in Table 4.4 in Section 4.6.

4.3.2 Iterative block decision feedback equalization, and channel estimation for uplink multi-user DFT-precoded OFDM, including least squares compensation of out-of-cell interference

The basic linear receiver structure for DFT-precoded OFDM (or serial modulation) can be iterated [BT02], [DGE03], so that at each iteration, estimated cochannel and intersymbol interference, derived from soft detector outputs, is subtracted. This structure is called IBDFE (iterated block decision feedback equalizer). This soft intersymbol interference subtraction yields substantially lower error probability for frequency selective channels, as shown in the above references. When the iteration loop includes soft outputs from the decoder, it is turbo equalization [NLF07]. IBDFE can also include soft cancellation of cochannel interference as well as intersymbol interference for DFT-precoded OFDM [SDF07]. The IBDFE algorithm with cochannel interference, at the ith iteration, for user k (k=1,2,…N_T), based on previous iteration equalizer outputs $\{u_{m,k}^{(i-1)}\}$, is summarized as follows:

$$
\begin{aligned}
&P_{m,k}^{(i-1)} = E(\left|a_{m,k}\right|^2 \left| u_{m,k}^{(i-1)}\right.) \quad \text{for } k = 0,1,..N_T - 1; \quad m = 0,1,..M-1; \\
&P_f^{(i-1)}(k) = \text{FFT of } \{P_{m,k}^{(i-1)}\} \quad (\text{independent of } f \text{ for } f = 0,1,...M-1) \\
&S_{m,k}^{(i-1)} = E(\left|d_{m,k}\right|^2 \left| u_{m,k}^{(i-1)}\right.) \\
&\text{where } d_{m,k}^{(i-1)} = a_{m,k} - \overline{a}_{m,k}^{(i-1)} \\
&\text{and } \overline{a}_{m,k}^{(i-1)} = E(a_{m,k} \left| u_{m,k}^{(i-1)}\right.) \\
&S_f^{(i-1)}(k) = \text{FFT of } \{S_{m,k}^{(i-1)}\} \quad (\text{independent of } f) \\
&\mathbf{S}_f^{(i-1)}(k) = \text{diag}(S_f^{(i-1)}(1), S_f^{(i-1)}(2),...S_f^{(i-1)}(N_T)) \quad (\text{independent of } f)
\end{aligned}
\tag{4.14}
$$

$$
\mu_f^{(i)}(k) = P_f^{(i-1)}(k) - \frac{1}{\frac{1}{M}\sum_{f=0}^{M-1} \mathbf{H}_f(k)^* \left[\mathbf{H}_f \mathbf{S}_f^{(i-1)}(k) \mathbf{H}_f^* + \sigma^2 \mathbf{I}_{N_R}\right]^{-1} \mathbf{H}_f(k)} \tag{4.15}
$$

Where N_R is the number of receiving antenna elements, and N_T is the number of users, each with one transmitting antenna.

The forward equalizer for transmitter k at the ith iteration is given by

$$
\mathbf{W}_f^{(i)}(k) = (P_f^{(i-1)}(k) - \mu_f^{(i)}(k)) \left[\mathbf{H}_f \mathbf{S}_f^{(i-1)}(k) \mathbf{H}_f^* + \sigma^2 \mathbf{I}_{N_R}\right]^{-1} \mathbf{H}_f(k) \tag{4.16}
$$

and the equalizer frequency domain output at frequency f for the kth user is

$$U_f^{(i)}(k) = \mathbf{W}_f^{(i)}(k)^*[\mathbf{R}_f - \sum_{\ell=1}^{N_T} \mathbf{H}_f(\ell)\overline{A}_f^{(i-1)}(\ell)] + \overline{A}_f^{(i-1)}(k) \tag{4.17}$$

where $\overline{A}_f^{(i-1)}(k)$ is the M-point DFT of the the $\{\overline{a}_{m,k}^{(i-1)}\}$. The equalizer time domain output samples are

$$u_m^{(i)}(k) = \text{IFFT}(\{U_f^{(i)}(k)\}) \tag{4.18}$$

and the minimum mean squared error at iteration i can be shown to be

$$\sigma^{(i)2}(k) = -\mu_f^{(i)}(k)\,. \tag{4.19}$$

Expressions for the above conditional expectations depend on the signal constellation. For example for QPSK,

$$\overline{a}_{m,k}^{(i-1)} = \frac{1}{\sqrt{2}}\left[\tanh\left(\frac{\sqrt{2}\,\text{real}(u_m^{(i-1)}(k))}{\sigma^{(i-1)2}(k)}\right) + j\tanh\left(\frac{\sqrt{2}\,\text{imag}(u_m^{(i-1)}(k))}{\sigma^{(i-1)2}(k)}\right)\right]. \tag{4.20}$$

The above expressions use the current estimates of the channels $\mathbf{H}_f$ and of the noise variance σ^2. It is likely that in most scenarios of interest, the out-of-cell interferers' (OCI) channels are difficult to measure, because their received signal powers are low. If only the in-cell users' (ICU) channels are known, N_T is the number of in-cell transmitters, and the out-of-cell interferers are ignored, acting as added noise.

If decision feedback iterative channel estimation (DFICE) is employed, decoder hard decisions on interfering in-cell data (obtained after several IBDFE iterations) are used to remove estimated interference, and the frequency domain channel estimate is obtained from the residual; i.e. at the jth channel estimation iteration, for the kth channel, after i iterations of IBDFE,

$$\mathbf{X}_f^{(j,i)}(k) = \mathbf{R}_f(k) - \sum_{\substack{\ell=1,\\ \ell\neq k}}^{N_T} \hat{\mathbf{H}}_f^{(j-1)}(\ell)\hat{A}_f^{(j,i)}(\ell) \tag{4.21}$$

where $\hat{A}_f^{(j,i)}(k)$ is the DFT of the receivers hard decisions for the jth in-cell user at the ith iteration,

and $$\hat{\mathbf{H}}_f^{(j)}(k) = \frac{\mathbf{X}_f^{(j,i)}(k)}{\hat{A}_f^{(j,i)}(k)}\quad, \tag{4.22}$$

followed by Wiener frequency domain smoothing. A possible problem is noise enhancement at frequencies where $\hat{A}_f^{(j,i)}(k)$ has a small magnitude. This problem can be avoided by replacing $\hat{\mathbf{H}}_f^{(j)}(k)$ by its initial estimate derived from pilots, or its estimate from a previous OFDM symbol if $\left|\,\hat{A}_f^{(j,i)}(k)\,\right|$ is less than a certain threshold. This is an *ad hoc* but relatively simple approach. An alternative, but more complex approach is to use least squares channel estimation over several successive OFDM symbols.

Adaptive suppression of the out-of-cell interference can be done without explicitly estimating out-of-cell interference data or channels by least squares (LS) processing over a series of F successive FFT blocks m=1,2,..F, assuming that channels do not change much over the F blocks. The output of the equalizer for the kth data source after the ith iteration is modified from (4.17) to account for the out-of-cell interference suppression as follows

$$Y_f^{(i)}(k,m) = \mathbf{V}_f^{(i)}(k)^* \hat{\mathbf{X}}_f^{(i)}(m) + U_f^{(i)}(k,m), \quad k=1,2,..N_T, \quad m=1,2,\ldots F, \tag{4.23}$$

where $U_f^{(i)}(k,m)$ for the mth block and the kth in-cell user is given by (4.17), and $\mathbf{V}_f^{(i)}(k)^* \hat{\mathbf{X}}_f^{(i)}(m)$ represents the negative of the estimated out-of-cell interference at the equalizer output in the mth block. The vector $\hat{\mathbf{X}}_f^{(i)}(m)$ is given by

$$\hat{\mathbf{X}}_f^{(j,i)}(m) = \mathbf{R}_f(m) - \sum_{\ell=1}^{N_T} \hat{\mathbf{H}}_f^{(j-1)}(\ell) \hat{A}_f^{(j,i)}(\ell,m)) \tag{4.24}$$

where $\hat{A}_f^{(i)}(k,m)$, which is the FFT of the receiver's *hard decisions* for the kth source in the mth block after the ith iteration The coefficient vector $\mathbf{V}_f^{(i)}(k)$ is obtained by a least squares estimate over F blocks:

$$\mathbf{V}_f^{(j,i)}(k) = \left[\sum_{m=1}^{F} \hat{\mathbf{X}}_f^{(j,i)}(m) \hat{\mathbf{X}}_f^{(j,i)}(m)^* \right]^{-1} \left[\sum_{m=1}^{F} \hat{\mathbf{X}}_f^{(j,i)}(m) [\hat{A}_f^{(j,i)}(k,m) - U_f^{(i)}(k,m)]^* \right] \tag{4.25}$$

One other modification of the iterative equalizer equations, when there are known to be external interferers not accounted for, is to replace the minimum mean squared error $\sigma^{(i)2}(k,m)$ at the ith iteration in the mth block, that is used in calculating the conditional expectations, by an empirical estimate

$$\hat{\sigma}^{(i)2}(k,m) = \frac{1}{M} \sum_{f=0}^{M-1} \left| U_f^{(i-1)}(k,m) - \hat{A}_f^{(i-1)}(k,m) \right|^2. \tag{4.26}$$

4.4 Channel Prediction

4.4.1 Channel prediction for frequency adaptive transmission

In WINNER Phase 1, substantial work was performed on channel prediction. Below we give a short overview of these results for the FDD case as described in more depth in [WIN1D24]. We will also describe how the choice of reference design pilot schemes has affected the feasible terminal velocities for which frequency-adaptive transmission is feasible. We finally illustrate how the prediction performance dependence on the Doppler spectrum of the channel to be predicted. This motivates that separate modelling of channel correlation properties should be performed on-line.

An overview of channel power gain prediction algorithms.

The feedback loop for the FDD system is designed to be as fast as possible, under realistic constraints imposed by computation times and signalling delays. However, channel prediction is needed for non-static users in the scheduling and link adaptation, since extrapolating the present channel estimate would lead to large performance losses at velocities above pedestrian speeds.

The predicted channel power gain within each chunk is an important CQI input variable to the link adaptation and scheduling decisions performed at the transmitter. The question arises how to best predict channel power gains. Extensive investigations of channel power predictors in [Ekm02], [SEA01] and [ESA02] were used as background for the investigations within the WINNER projects. Both theoretical analyses and evaluations on a large set of measured channels with 5 MHz bandwidth were here taken into account. In these investigations, it was concluded that the class of channel power predictors that performed best on measured data was based on *linear* prediction of the complex baseband channel h. It has been shown in Chapter 5.4 of [Aro07] that an MMSE optimal (linear) prediction $\hat{h}$ of the complex channel then provides an MMSE-optimal prediction of the channel power $c = |h|^2$, by using "unbiased" channel power predictor [ESA02]

$$\hat{c} = E|h|^2 = |\hat{h}|^2 + \sigma^2,$$

where σ^2 is the variance of the complex channel prediction $\hat{h}$.

If the noise and interference is assumed Gaussian, then the MMSE optimal channel prediction $\hat{h}$ is provided by the *Kalman predictor*. The Kalman algorithm utilizes the received signals at positions with

known inputs (pilots) and the assumed correlation properties of the channel in time and frequency to optimally extrapolate the channel in time [Aro07]. MMSE predictions of the channel power gains, based on Kalman predictions of the complex channels, have been used and evaluated in the WINNER projects.

In [Ekm02], the most significant taps of the channel impulse response are predicted in the time domain. In [WIN1D24] we have performed the prediction in the frequency domain (The performance of these two schemes can be shown to be equivalent.) A set of linear prediction filters, each responsible for its own subband of the total bandwidth, is utilized. The state space algorithm described in [SA03] is used to predict the complex channel h and the unbiased quadratic predictor is used to predict the channel power c. The predictor utilized the correlation in the time domain of the fading channel. Autoregressive models of order 4 have in [WIN1D24] been used to model the channel correlation in time. They are adjusted to the fading statistics. It also utilizes the correlation of the channel in the frequency domain by predicting p pilot-containing subcarriers in parallel. The number p is a compromise between performance and computational complexity. In the performance results below $p = 8$, spanning 4 chunks, is used. This means that 26 Kalman estimators would be required to cover a band of 104 chunks.

In [SA03] and [Aro07], it is shown that if orthogonally placed pilot signals with *constant modulus*, like 4-QAM are used, then updating of a quadratic state-space Riccati difference equation can be avoided. This update is responsible for the dominant computational load in Kalman algorithms. Instead, one may use pre-computed steady-state solutions to the Riccati equation, either directly, or via the Generalized Constant Gain algorithm [SLA02] that is use in [SA03].

The use of FDD or TDD affects the channel predictor design. In TDD, we may use the channel reciprocity between downlinks and uplinks to estimate the channel of a link based on measurements of the opposite link.[6]

Of the eight possible combinations of FDD/TDD, uplink/downlink and frequency-adaptive/non-frequency adaptive transmission, the case of frequency-adaptive transmission in FDD uplinks represents the most challenging prediction problem. Due to the use of different and widely spaced carrier frequencies for the uplink and the downlink in FDD, channel reciprocity does not hold. Therefore, the uplink channel quality within all potentially useful chunk layers, for channels from all terminals that are in competition for the uplink, have to be predicted at the base station (network) side, based on uplink pilots transmitted by all these terminals. This might easily lead to problems with the total pilot overhead if many active terminals are involved. Either orthogonally placed or overlapping pilots may be used. Overlapping pilots reduce the pilot overhead i.e. the fraction of symbols required for these prediction-specific uplink pilots. A generalization of the Kalman algorithm of [SA03], described in [SA05], can be used to predict the FDD uplink channels from all terminals jointly. Its performance was investigated in [WIN1D24] based on a pilot spacing similar to the downlink prediction. This scheme has been further extended and investigated in [AS07], where also improved overlapping pilot patterns were evaluated.

The numerical complexity of different Kalman-based channel predictors has been assessed in detail in Appendix G of [Aro07], with a summary in [AS07]. To summarize, the complexity is lowest for FDD downlink predictors, higher for FDD uplink predictors based on orthogonal pilot positions and highest for FDD uplink predictors based on overlapping pilots. The latter case requires joint estimation of channels from all users. It was concluded that the computational complexity is within reasonable limits for all these schemes, if the number of simultaneously estimated pilot subcarriers p and the order of the autoregressive model that describes the fading statistics are limited.

The attainable prediction accuracy for a radio link will depend on

- the required prediction horizon, scaled in carrier wavelengths,
- the average SINR of the channel,
- the pilot density and
- the type of fading statistics (the shape of the Doppler spectrum).

The importance of some of these factors will be illustrated below.

[6] This holds for calibrated single-antenna and mulit-antenna systems, if the frame is much shorter than the channel coherence time. However, it should be noted that the interference power at the far-end receiver can in general *not* be inferred from measurements by the near-end receiver.

Prediction performance limits for FDD frequency-adaptive transmission

The prediction accuracy depends on the prediction horizon L scaled in wavelength, which in turn depends on the velocity v, the prediction horizon in time D and the carrier wavelength λ via the relation $L = vD/\lambda$. The prediction accuracy also depends on the SINR. Thus, adaptive transmission to/from a terminal is feasible up to a maximal velocity for a given SINR, or equivalently, down to a limiting SINR at a given velocity.

The prediction accuracy is stated in terms of the normalized mean square prediction error of the complex channel, $\sigma^2 / E|h|^2$, denoted the complex prediction NMSE. The NMSE is shown in Figure 4-6 as a function of the prediction horizon scaled in carrier wavelengths, and as function of the SINR, for the FDD downlink. From earlier investigations of the sensitivity for MCS rate limits to prediction errors, it has been found that if the rate limits are adjusted to take the prediction uncertainty into account, a prediction NMSE of 0.1 for an uncoded system leads to only a minor degradation of the spectral efficiency [FSE+04], [FSS+03], but for coded schemes the sensitivity to prediction errors is slightly larger.

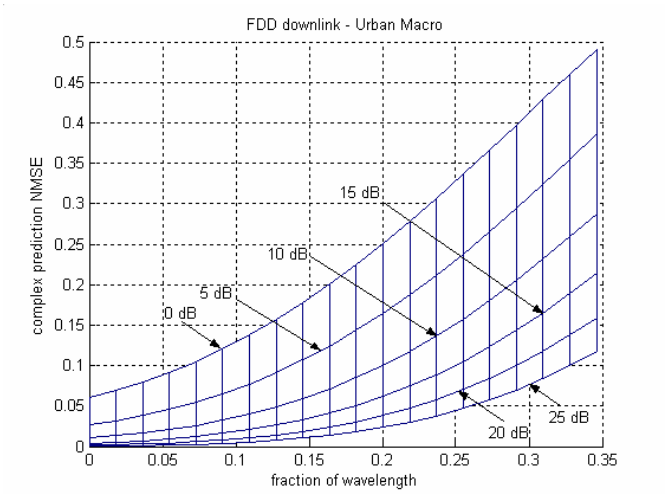

Figure 4-6: Normalized mean square prediction error (NMSE) for the complex channel, as a function of the prediction horizon scaled in carrier wavelengths, and as function of the SINR. Results for a Jakes model Doppler spectrum in a FDD downlink, with full duplex terminals, over WINNER I Urban Macro channels, for a Kalman algorithm utilizing 8 subcarriers.

In FDD downlinks, predictors in the user terminals use downlink pilots in the downlink slot of a frame to predict the downlink slot of the following frame. This is required by the assumed transmission feedback loop delays, see Section 5.2 of [WIN2D61314]. Using the pilot positions assumed in [WIN1D24], this corresponds to a prediction horizon D = 0.843 ms. If an upper limit of 0.15 is assumed for the allowable NMSE when using frequency-adaptive transmission, then we obtain the SINR limits in Table 4.1. These limits are conservative, since the prediction is performed to the far end of the chunk to be allocated, and the prediction accuracy to less distant symbol locations is higher. The results are illustrated for three vehicle velocities and at 5 GHz carrier frequency. At other carrier frequencies *f,* the corresponding velocities would be scaled by 5 GHz/*f*.

Table 4.1: Estimates of the minimum SINR that enable frequency-adaptive transmission. Results for Rayleigh fading channels and 5 GHz carrier [WIN1D24]. The table also shows the corresponding prediction horizons scaled in wavelengths.

SINR, prediction horizon	30 km/h	50 km/h	70 km/h
Downlink	< 0 dB, 0.117 λ	6 dB, 0.195 λ	12.5 dB, 0.273 λ
Uplink, 2 users	*0 dB, 0.117 λ*	*7 dB, 0.195 λ*	*15 dB, 0.273 λ*
Uplink, 8 users	*3.5 dB, 0.117 λ*	*11 dB, 0.195 λ*	*20 dB, 0.273 λ*

The uplink results in Table 4.1 use the required prediction horizons assumed in [WIN1D24], which are still relevant in WINNER II and assume overlapping uplink pilots from all competing users (2 user or 8 users) transmitted within each frame, in all chunks to be predicted. SISO transmission is assumed in all cases. Further and more detailed results on the performance of frequency-adaptive transmission based on channel prediction, and the effect of prediction errors on the performance can be found in [WIN1D24] and in [SS0+07].

Consequences of the choice of pilot schemes in the WINNER reference design

For the WINNER II reference design ***FDD downlink***, the results of Figure 4-6 and Table 4.1 are still valid. Frequency-adaptive transmission in FDD downlinks is thus feasible at vehicular velocities. Note that the carrier frequency used for eavaluation in WINNER II wide-area downlinks has been 3.9 GHz. This improves the predictability, relative to the case at 5 GHz.

A Grid-of-Beam (GoB) deployment is used as the WINNER reference design for FDD wide area deployment [WIN2D61314]. Here, the fading variance will be less than that in the SISO Rayleigh fading scenario assumed above, due to the averaging of the channels from individual antennas performed by the transmit beamforming. This fact is expected to make channel prediction to perform better with GoB deployment, which will result in a better channel prediction performance compared to the estimates in Table 4.1. However, this has not been investigated in the WINNER project.

In the WINNER II reference design ***FDD uplink***, pilots from all terminals are transmitted only once per super-frame in the preamble, to limit the uplink pilot overhead (Section 3.2.6.2). This limits the channel sampling rate and channel sounding energy. As a consequence *frequency-adaptive FDD uplink transmission* would under this assumption be feasible for *pedestrian velocities* only.

For ***TDD systems***, frequency adaptive transmission in downlinks would be integrated with one of several possible a multi-user MIMO-OFDM schemes cf. Section 3.2.8 above.

- For downlinks that use SMMSE with short term CSI at the transmitter, the appropriate pilots to use would be uplink pilots transmitted in the super-frame preamble from all user terminals that take part in the competition for a set of frequency resources. This SMMSE (successive minimum mean square error) multi-user MIMO transmit scheme [WIN2D341] is limited to users below 10 km/h and the super-frame preamble pilots allow frequency-adaptive transmission to be used at these velocities. Section 4.4.2 below presents a Kalman-based algorithm located at the BS side that generates CQI for adapting the downlink transmission, using common (uplink) pilots per antenna from the preamble and also the dedicated (uplink) pilots per spatial stream per chunk.
- Spatial multiplexing with per antenna rate control is the preferred scheme at velocities 10-50 km/h in metropolitan area deployments. In such cases, unweighted pilots would be transmitted from each antenna in each downlink slot. The UTs can generate CQI estimates on all chunks where these downlink pilots are transmitted. These CQI estimates are compressed as described in [WIN1D24] and transmitted to the BS/RN over the uplink. This enables the use of frequency adaptive transmission in both downlinks and uplinks, due to the TDD channel reciprocity, up to velocities determined by the vehicle velocity and the Doppler spectrum properties of each channel.

The influence of the shape of the Doppler spectrum

All of the above results were obtained assuming a Jakes' Doppler spectrum. However, the Doppler spectrum, caused by the angular distribution of local scatters around each terminal, relative to its direction of travel, has a crucial impact on the channel predictability. The dependence of channel prediction performance on the Doppler spectrum has been investigated for the FDD uplink in [AS07]. Some of these results are illustrated in Figure 4-7 below.

The upper plots in Figure 4-7 represent a situation where the Doppler spectrum energy is concentrated close to the maximal and minimal Doppler frequency $\pm v/\lambda$, so the channel variability is almost sinusoidal, with this frequency. This could correspond to a situation when travelling along a street and the dominant interfering electromagnetic waves arrive from the front or the rear direction. Since sinusoids are well predictable, the predictability in this case is much better (the prediction horizon for a given NMSE is much longer) than for the Jakes Doppler spectrum case illustrated in Figure 4-6.

As the other extreme case, the lower plot in Figure 4-7 illustrates the situation for a Doppler spectrum that is flat up to the maximal Doppler frequency. This could correspond to a situation when travelling along a street and the dominant interfering waves arrive from the sides, via reflections from the buildings along the street, while relatively less energy arrives from the forward and backward directions. The channel prediction performance is substantially worse for this case, as compared to a Jake's Doppler spectrum.

It is recommended that a Kalman-based channel predictor is complemented by an estimators of the channel statistics, which estimates a low-order autoregressive models of the Doppler spectrum based on past data. Such a model is useful for two purposes:

1. To assess the predictability of the channel to/from a specific user terminal. This provides input to the decision if a flow is to be transmitted by frequency-adaptive or non-frequency adaptive transmission.
2. To model the time correlation properties of the channel within the Kalman estimator. Use of estimated autoregressive (AR) models of the actual channel variability provide better performance than basing the prediction on a robust fixed model of the time variability, for example an AR model based on a flat Doppler spectrum.

The estimation of low order AR models represents a relatively small increase of the computational complexity of the Kalman predictor. However, it should be noted that the resulting AR models will initially be inaccurate and improve over time.

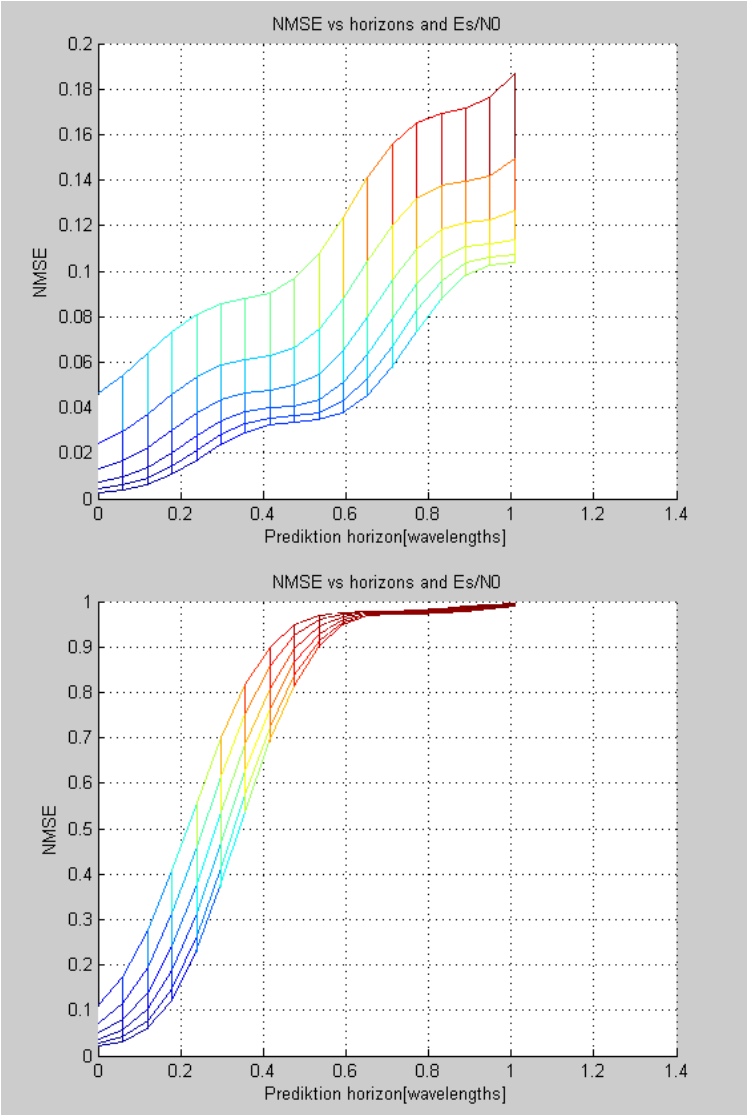

Figure 4-7: Normalized mean square prediction error (NMSE), as a function of the prediction horizon scaled in carrier wavelengths, and as function of the SINR. Results for FDD downlink, full

duplex terminals, over WINNER I Urban Macro channels, with a Kalman algorithm utilizing 8 subcarriers. Results for peaky Doppler spectrum (upper figure) and for a flat Doppler spectrum (lower figure). Compare to Figure 4-6, which is for a Jakes model Doppler spectrum.

4.4.2 Channel prediction using dedicated pilots and Kalman filtering

In this section we describe a method to derive unweighted channel matrix in the TDD mode by exploiting combination of common (uplink) pilots per antenna (CPA) from the preamble, dedicated (uplink) pilots per spatial stream per chunk and Kalman filtering. The so obtained unweighted channel matric is of limited accuracy and can be used for the purposes of calculating CQI. CQI can be used by the scheduler at the transmitter to allocate resources based on it and on requirements of each user. The described method can be used to avoid the need of common pilots per antenna in chunks which are exploited to obtain CQI. Instead, only dedicated pilots per spatial stream per chunk can be applied which are needed to estimate the effective channel information. The corresponding superframe structure which includes CPA in preamble and dedicated pilots per spatial stream per chunk is illustrated in Figure 4-8.

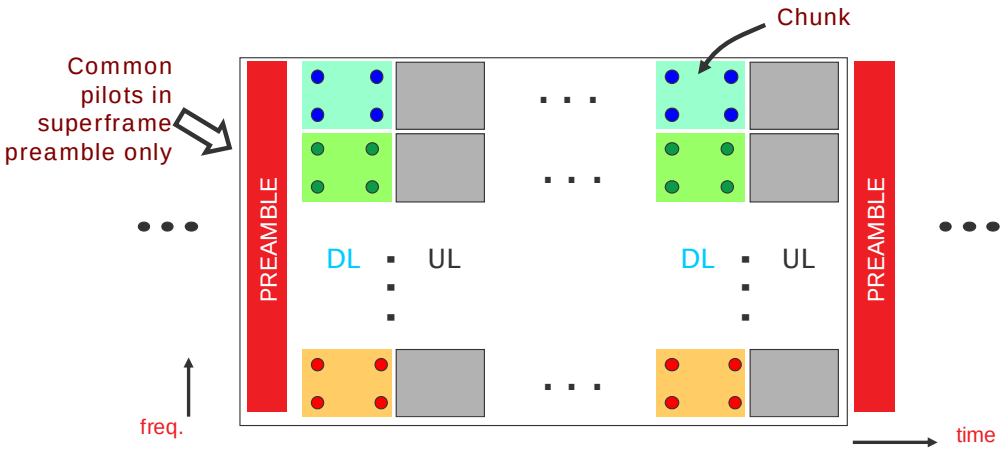

Figure 4-8: Superframe structure: CPA in the preamble and dedicated pilots per spatial stream per chunk.

The procedure for channel prediction via Kalman filtering is summarized in the following:

1. Initial conditions for the Kalman filtering are given by the preamble of each superframe,
2. Prediction of the values in the current step is done using the values from the previous step,
3. Based on the effective channel estimate from the dedicated pilots per spatial stream per chunk and on the Kalman gain, correction step is performed.

The prediction step of the Kalman filtering process is given by

$$\begin{aligned} \hat{\mathbf{h}}_{n,l^-}^{(m_R)} &= a\mathbf{h}_{n,l-1}^{(m_R)} \\ \mathbf{C}_{n,l^-}^{(m_R)} &= |a|^2 \mathbf{C}_{n,l-1}^{(m_R)} + \sigma_w^2 \mathbf{R}_{tx} \end{aligned} \tag{4.27}$$

where $\mathbf{h}$ is channel gains $N_\mathrm{T} \times 1$ vector with N_T denoting number of transmit antennas, a coefficient dependent on the channel evolution model, $\mathbf{C}$ estimate of $N_\mathrm{T} \times N_\mathrm{T}$ error covariance matrix, σ_w^2 noise process variance and $\mathbf{R}_{tv}$ transmit spatial correlation matrix. Furthermore, l is time, i.e., OFDM symbol, index, n is index of subcarriers bearing pilots and m_R denotes index of the receive antenna. Note that Kalman filtering is performed only on the subcarrier - bearing pilots,

The correction step of the Kalman filtering process is given by

$$\begin{aligned}
\mathbf{K}_l &= \mathbf{C}_{n,l^-}^{(m_R)}\mathbf{v}_{tx}(\mathbf{v}_{tx}^T\mathbf{C}_{n,l^-}^{(m_R)}\mathbf{v}_{tx}+\sigma_\varepsilon^2)^{-1} \\
\hat{\mathbf{h}}_{n,l}^{(m_R)} &= \hat{\mathbf{h}}_{n,l^-}^{(m_R)} + \mathbf{K}_l(\hat{h}_{eff\,n,l}^{(m_R)} - \mathbf{v}_{tx}^T\hat{\mathbf{h}}_{n,l^-}^{(m_R)}) \\
\mathbf{C}_{n,l}^{(m_R)} &= (\mathbf{I}_{N_T} - \mathbf{K}_l\mathbf{v}_{tx})\mathbf{C}_{n,l^-}^{(m_R)}
\end{aligned} \tag{4.28}$$

where $\mathbf{v}_{tv}$ is $1\times N_{\mathrm{T}}$ beamforming vector of N_{T} samples, $\mathbf{K}$ is $N_{\mathrm{T}}\times 1$ Kalman gain vector, and σ_ε^2 effective channel MSE. Furthermore, $\mathbf{I}_{N_T}$ is $N_{\mathrm{T}}\times N_{\mathrm{T}}$ identity matrix and h_{eff} effective channel estimate

$$h_{eff\,n,l}^{(m_R)} = \sum_{m_T=1}^{N_T} h_{n,l}^{(m_R,m_T)} v_{tx}^{(m_T)} \,. \tag{4.29}$$

Different downlink chunks can belong to different users and thus interpolation errors between dedicated pilots per spatial stream per chunk will be large. There are two possible ways to overcome this problem:

- At the receiver, the signal received from the pilots of the neighbouring beams is also taken into account. The neighbouring beams have significant overlap and thus the received signal is of sufficient power so that CQI is obtained. The receiver needs to know which chunks use neighbouring beams.
- Non-neighbouring beams that are not sufficiently separated, i.e., whose sidelobes can be further separated applying tapering of beamforming gains [WIN2D341]. Tapering can be used to improve the shape of the beam directivity pattern for SDMA. There are several possible tapering approaches, e.g. Hann, Hamming, Blackmann or Chebyshev window can be applied. Tapering enables re-use of the same chunk by several set of beams so that interpolation error among dedicated pilots per spatial stream per chunk is lower since these pilots are placed closer to each other.

Several numerical results that illustrate performance of this Kalman filtering approach are provided in Appendix C.5.

4.5 Channel Estimation Reference Design

The channel estimation (CE) reference design utilizes a scattered pilot grid as described in Section 3.2.6. Interpolation between pilots over time and frequency by pilot aided channel estimation (PACE) provides initial channel estimates for the entire frame. Interpolation over time and frequency is separated and realized by two one dimensional FIR filters, referred to as 2x1D PACE. As demonstrated in [WIN1D21], [WIN1D23], [WIN1D210] and summarized in Section 4.2, the 2x1D PACE experiences only marginal performance degradation with respect to optimal 2D PACE (i.e. PACE implemented by a two dimensional FIR filter), but significantly reduces the computational cost.

The FIR interpolation filters are implemented by a Wiener interpolation filter (WIF) with model mismatch. The filter coefficients of a WIF with model mismatch are generated with the following prior knowledge about channel statistics: the maximum *delay of the channel* $\tau_{\max}$, *Doppler frequency* $f_{\mathrm{D,max}}$ and *average SINR* are assumed to be known; however, no further knowledge of the 2nd order statistics (i.e. the channel covariance matrices in time and frequency) is assumed. If the required measurements of $\tau_{\max}$, $f_{\mathrm{D,max}}$ and average SINR are unavailable at the receiver, the *worst case* design of the WIF is adopted: the maximum delay of the channel is set equal to the CP-length, the maximum expected velocity is set with respect to a certain deployment scenario (LA: 3km/h, MA: 70km/h, WA: 250km/h), and the highest expected SINR set to 30 dB. We note that the worst case design of the WIF will have significantly poorer performance, so it is recommended to implement and utilize means to measure $\tau_{\max}$ and $f_{\mathrm{D,max}}$.

As the WINNER pilot design in Section 3.2 requires in some cases dedicated pilots as well as allows for spatial reuse of pilot symbols, the attainable performance of PACE may be insufficient to meet the ambitious targets of the WINNER system. Two enhancements for the CE reference design are foreseen:

- **Channel estimation over multiple frames** exploits the correlation in time, in the way that pilot symbols from previous symbols provide significantly improved channel estimates. A Kalman filter is an efficient means to exploit the correlation of pilots over multiple frames as described in Section 4.4.
- **Iterative channel estimation (ICE):** can be efficiently implemented in terminals that contain turbo receiver consisting of an inner and outer receiver that exchange soft information in the

form of log-likelihood ratios (LLRs), as described in Section 4.3. In this case the channel estimation unit is included in the turbo loop and additional computational complexity is acceptable. PACE estimates are used as initial estimates for ICE and feedback needed for ICE is derived from *a posteriori* information, as shown in general iterative receiver structure of Figure 4-1. Application of ICE leads to significant performance improvements over PACE.

Although channel estimation over multiple frames and ICE are both optional extensions of PACE, for the reference CE preferably both extensions should be implemented, to achieve the ambitious spectral efficiency targets of the WINNER system.

In order to improve the performance in a multi-user MIMO scenario where channel estimation is more challenging, ICE can be extended by genetic algorithm (GA) aided joint ICE and multi-user detector (MUD) at the expense of additional computational complexity.

For DFT-precoded OFDM with a decision-directed iterative receiver structure, in-cell and out-of-cell interference is suppressed by means of least squares adaptation. To adaptively suppress out-of-cell interference, without explicitly estimating it, a least-squares processing over several successive FFT blocks can be applied. In order that least-squares processing functions properly, it is required that the channels do not change much over observed blocks.

4.6 Channel Estimation Performance

The effect on error rate performance of channel estimation errors, modelled as Gaussian random variables, is derived and discussed in Appendix B. These models are most accurate at low signal to noise ratios, where the effect of additive noise dominates over interpolation errors. For higher SNR and for iterative channel estimation methods used in the presence of significant Doppler, we must resort to simulated error rate performance for the various channel estimation schemes and modulation, multiple access and coding methods.

We first display a summary of simulation results, from Appendix C for channel estimation schemes, and their penalties relative to the case of perfect channel state information, for the wide area FDD scenario with single input-single output (SISO). Full-band (40 MHz, 40 Mbaud) and 1.25 Mbaud IFDMA, B-EFDMA and B-IFDMA are shown. All results are for QPSK, except for a set of results for 16-QAM B-EFDMA with full-chunk (8X12) blocks. Two channel estimation approaches are used: (1) a non-iterative purely pilot-aided approach using Wiener interpolation in the full band cases case and the single pilot per block without interpolation in the case of B-EFDMA, B-IFDMA and IFDMA; (2) a soft-decision iterative approach (DFICE) to supplement the pilot-aided estimation, using soft decoder outputs. In addition, the improvement available from estimating channel parameters over several successive frames is also shown for full-band DFT-precoded OFDM, B-IFDMA and IFDMA, OFDM and B-EFDMA systems using linear equalization and interference rejection as well as CSI-aware decoding. DFT-precoded OFDM, IFDMA and B-IFDMA systems used iterative block decision feedback equalization (IBDFE), described in Section 4.3.2. Table 4.2 displays the simulation parameters, and Table 4.3 displays the required SNR to achieve a 10^{-2} frame error rate, and also the SNR degradation between ideal CSI and non-ideal CSI with the various channel estimation schemes. The table also shows the pilot overhead percentage for each scheme. More detailed performance results for OFDM, B-EFDMA, DFT-precoded OFDM, IFDMA, and B-IFDMA, assuming different block sizes and modulation schemes as well as including comparisons of PACE and ICE with hard, **extrinsic** or **a posteriori** fed back information are provided in Appendix C.

As indicated in the table, B-IFDMA, B-EFDMA and IFDMA require significantly higher pilot overhead, and exhibit higher SNR degradation due to channel estimation errors than do full-band OFDM and DFT-precoded OFDM. This is mainly due to the reduced opportunity to interpolate pilot estimates and exploit correlation in the frequency domain. There is in fact no frequency domain interpolation in the B-EFDMA, B-IFDMA and IFDMA cases, since for B-(E&I)FDMA there is only one pilot per 4X3 block, and blocks are separated in frequency by more than the correlation bandwidth. The use of larger block sizes (e.g. 8X6), with more pilots, gives more scope for interpolation between pilot locations in frequency and time, while keeping pilot overhead reasonable.

Table 4.3 also shows that iterative channel estimation can yield significant improvement relative to non-iterative estimation, and furthermore that estimation over multiple frames yields 0.5 to 1 dB improvement, at least for the moderate vehicle speed of 50 kph.

Table 4.2: Parameters for single input – single output channel estimation simulations for wide area FDD scenario

Modulation Scheme	QPSK or 16-QAM
Code, decoder	Conv. rate ½ const. length 7, Viterbi decoder
Interleaving	Random
Carrier frequency	3.7GHz
Signal BW	40 MHz
Sub-Carrier spacing	39.0625KHz
Used sub-carriers	1024
Sampling rate	80 MHz
Number of OFDM symbols per chunk	12
Block configuration for B-EFDMA and B-IFDMA	(4 subcarriers) X (3 OFDM symbols) per block. Blocks spaced at 32-subcarrier intervals in frequency
Number of pilots per chunk per OFDM symbol	4 for full-band , 2 for IFDMA, 1 for B-EFDMA and B-IFDMA
OFDM symbols containing pilots	1st and 12th OFDM symbols for full-band and IFDMA, 2nd for 4X3 B-EFDMA and B-IFDMA
Prior information available to interpolator	Channel response<CP length, Vehicle speed<100 kph
Number of receiving elements	N_R=1
Equalization scheme	IBDFE for DFT-precoded OFDM, linear for OFDM
DFICE Iterations	2 or more
Channel, user terminal speed	C2, 50 kph

In SDMA and MIMO scenarios, there is interference from in-cell co-channel users (ICUs) due to the sharing of spectrum among different data streams. In this scenario orthogonal pilot patterns are used in order to avoid interference between the pilot signals from different SDMA streams. Pilot overhead increases as the number of individual streams increases.

Based on the initial channel estimates achieved with the aid of pilots, more accurate estimates are achievable by invoking iterative channel estimation (ICE). More specifically, with the presence of channel coding, turbo-style ICE may be employed, where extrinsic information is exchanged between the channel estimator, symbol detector and channel decoder over a number of outer iterations. Moreover, depending on the algorithm used, additional inner iterations can be carried out within the channel estimator for further performance enhancement.

The results for a 2x2 uplink SDMA OFDM system are summarized in Table 4.4. The turbo-processing assisted genetic algorithm (GA) based ICE introduced in Section 4.3.1 was employed with a pilot overhead of 6.7%. Detailed parameters and configurations can be found in Appendix D. As seen from Table 4.4, the performance of the system improves as the number of inner and/or outer iterations increases. Note that the largest performance improvement was achieved by the first iteration, while the best result attained was a SNR degradation of 1.39 dB in comparison to the ideal CSI aided scenario, when three inner and three outer iterations were employed. Other assumptions are as follows:

- Out-of-cell interference (OCI) not considered
- Two transmit and two receive antennas
- Independent B1 channel links between all antenna pairs
- Half-rate LDPC code [WIN1D210], 4QAM
- Terminal speed of 70km/h
- Perfect synchronisation between all SDMA streams

Table 4.3: SNR and SNR degradation (with respect to perfect CSI) for frame error rate = 10^{-2} for noniterative and iterative channel estimation SISO schemes (wide area scenario)

Pilot Schemes	SNR for ideal CSI (dB) for 10^{-2} frame error rate	SNR (dB) with channel estimation SNR degradation due to channel estimation (dB) (shown in red)		
		Non-iterative channel estimation Wiener pilot Interpolation (W2X1D)		Iterative channel estimation with decoding in iteration loop
QPSK OFDM –full band (4.1% pilot overhead)	10.5	12.0 (1.5)		10.7 (0.2)
QPSK DFT-precoded OFDM-full band (4.1% pilot overhead)	9.4	**1-frame channel est.**	11.5 (2.1)	9.8 (0.4)
		4-frame channel est.	10.9 (1.5)	9.4 (0.0)
QPSK B-EFDMA (4X3 blocks; 32-subcarrier spacing ; 8.3% pilot overhead)	8.2	12.2 (4.0)		11.0 (2.8)
QPSK B-EFDMA (8X6 blocks; 32-subcarrier spacing ; 8.3% pilot overhead)	8.9	12.2 (3.3)		10.7 (1.8)
16-QAM B-EFDMA (8X12 blocks; 32-subcarrier spacing ; 4.1% pilot overhead)	12.2	~16.2 (~4)		13.2 (1.0)
QPSK B-IFDMA (4X3 blocks; 32-subcarrier spacing; 8.3% pilot overhead)	8.4	**1-frame channel est.**	12.7 (4.3)	11.4 (3.0)
		4-frame channel est.	12.0 (3.6)	10.8 (2.4)
QPSK IFDMA (32-subcarrier spacing; 16.7% pilot overhead)	8.5	**1-frame channel est.**	11.3 (2.8)	10.0 (1.5)
		4-frame channel est.	10.4 (1.9)	9.5 (1.0)

Table 4.4: SNR degradation recorded in 2x2 uplink full-band SDMA OFDM with no OCI

	SNR for perfect CSI (dB) for 10^{-2} frame error rate	SNR with channel estimation (dB) (SNR degradation relative to perfect CSI shown in red)			
		Inner (GA) iteration = 0 (i.e. no inner iteration)	Inner iteration = 1	Inner iteration = 2	Inner iteration = 3
Outer (Turbo) iteration = 0 (i.e. no outer iteration)	3.92	6.19 (2.27)	5.83 (1.91)	5.68 (1.76)	5.65 (1.73)
Outer iteration = 1	2.70	4.84 (2.14)	4.43 (1.73)	4.42 (1.72)	4.39 (1.69)
Outer iteration = 2	2.53	4.64 (2.11)	4.42 (1.72)	4.41 (1.71)	4.02 (1.49)
Outer iteration = 3	2.49	4.44 (1.95)	4.08 (1.59)	4.08 (1.59)	**3.88 (1.39)**

In SDMA and MIMO scenarios there may also be interference from out-of-cell interferers (OCIs). OCIs' average received powers at a given base station will depend on their propagation paths to their own base stations. In-cell users are assigned orthogonal pilots; thus there is no in-cell interference to pilots. However to avoid excessive pilot overhead, the same pilots may be assigned to users in other cells; thus there may be pilot interference from adjacent cells.

Inter-cell pilot interference can be minimized by adopting a frequency reuse partitioning strategy, in which user terminals with low path loss to their base stations, but which are in different cells, have frequency reuse of one, while user terminals experiencing higher path loss have a higher frequency reuse factor, and thus experience out-of-cell interference only from more distant cells [WIN2D472], Section 4.3.1. A representative frequency reuse partitioning scenario is presented and analyzed in Appendix A, in which the frequency reuse factors for terminals within and beyond 70% of the cell radius are 1 and 3, respectively. It is shown that based on a WINNER wide area propagation model, average received power from each OCI in this deployment scenario is at least 15 dB below that of in-cell users. Other techniques may be employed to reduce out-of-cell interference, such as dynamic channel allocation and scheduling among base stations [WIN2D472], Section 5, and beamforming [WIN2D473], Section 3.1. For evaluation of channel estimation performance for SDMA with out-of-cell interference, we assume that one or more of these techniques have been applied, so that uplink out-of-cell interferer signals arrive at a victim base station with an average received power of -15 dB relative to the average power of each in-cell received signal.

Table 4.5 is based on simulations, including those reported in C.3, of an uplink DFT-precoded SDMA system with 2 in-cell user terminals sharing a common channel, and (in all but the first row of the table) 4 out-of-cell interferers (OCIs), each with an average received power 15 dB below that of each in-cell user's average received power. The base station has 4 receiving antennas (N_R=4). Independently fading C2 channel models with 50 kph Doppler are assumed between each transmitting/receiving antenna pair. The base station's MMSE-based receiver uses the IBDFE equalization algorithm, for the multi-antenna, multi-user case, described in Section 4.3.2. An exception is in the third row of the table, where a rate ½ regular (3,6) LDPC code with 4608 block length, and turbo equalization, instead of IBDFE, is used [SF06], [NLF07]. As in the SISO cases, non-iterative channel estimation based on interpolation of frequency-multiplexed pilots, is evaluated, as is iterative channel estimation. Both the pilot-based and iterative channel estimation schemes estimate only the in-cell users' channels, while OCIs are ignored. The last column in the table shows results for a least squares (LS) decision directed algorithm (described in Section 4.3.2), which is used in addition to pilot interpolation and iterative ICU estimation. This LS algorithm is aimed at suppressing OCI interference without having to explicitly estimate OCI channels (essentially, the algorithm estimates the out-of-cell interference autocorrelation matrix, instead of out-of-cell interferers' channels). Full-band DFT-precoded OFDM uses 4 orthogonal pilots per chunk per in-cell user. Table 4.5 also shows required SNR and SNR degradation for B-IFDMA with 4X3 blocks and for 8X6 blocks. For the 4X3 case, there are two pilots per block per in-cell user; thus the pilot overhead in this case is 33.3%. For the 8X6 case, there are 4 pilots per block per user; the corresponding total pilot overhead is 16.6%.

Table 4.5: One-Frame Estimation for uplink DFT-precoded OFDM with 2X4 SDMA

MA schemes ↓	SNR for ideal CSI (dB) for 10^{-2} frame error rate	SNR (dB) with channel estimation (SNR degradation due to channel estimation – shown in red)		
		Non-iterative channel estimation	Iterative channel estimation	Iterative channel estimation plus least squares
Full-band DFT-precoded OFDM No OCIs 8.3% pilot overhead	0.3	4.2 (3.9)	3.6 (3.3)	2.3 (2.0)
Full-band DFT-precoded OFDM 4 OCIs, each at -15 dB 8.3% pilot overhead	1.3	6.3 (5.0)	5.0 (3.7)	3.5 (2.2)
Full-band DFT-precoded OFDM with turbo equalization and rate ½ LDPC codes 4 OCIs, each at -15 dB 8.3% pilot overhead	-0.4	3.7 (4.1)	3.0 (3.4)	2.3 (2.7)
B-IFDMA with 4X3 blocks, 32-subcarrier spacing between blocks. 4 OCIs, each at -15 dB 33.3% pilot overhead	-1.0	7.5 (8.5)	5.0 (6.0)	5.0 (6.0)
B-IFDMA with 8X6 blocks, 32-subcarrier spacing between blocks. 4 OCIs, each at -15 dB 16.6% pilot overhead	0.3	6.8 (6.5)	5.4 (5.1)	4.7 (4.4)

Note that "SNR" is signal to noise ratio per receive antenna. It does not include OCI power.

Although this table does not include performance of linear equalization (LE), LE and IBDFE are compared in Section C.3, and the superiority of IBDFE in mitigating cochannel and intersymbol interference is evident. It is also evident from the table that the use of turbo equalization along with LDPC block coding gives a further SNR advantage over IBDFE.

Also, as seen in the table, non-ideal channel estimation causes significant SNR degradation relative to the ideal CSI case, largely due to the OCI interference to the ICU pilots. This is apparent by noting that the SNR degradations in Table 4.5 are significantly worse than those for SISO in Table 4.3. This degradation is reduced by iterative channel estimation, and is further reduced in the full band case by the application of least-squares processing using receiver hard decisions, to suppress OCI interference.

Least squares processing produces no benefit in the 4X3 B-IFDMA case, since the number of OFDM symbols per block (3) is inadequate for the least squares averaging. While the 8X6 B-IFDMA case has 1.3 dB higher required SNR for perfect CSI (due to its slightly diminished frequency diversity), its SNR degradation for non-perfect CSI with ICE and least squares processing is 1.6 dB less than that for the 4X3 case. The main reason for this is the use of 4, instead of 2 pilots in the 8X6 block, allowing better interpolation from pilot estimates, while also reducing overhead. The resulting gain in channel estimation accuracy more than compensates for the reduced diversity of the 8X6 case. The required SNR in this case is 4.7 dB, while for 4X3 it is 5.0 dB. Note that the LDPC/turbo equalization combination reduces required SNR by roughly 1.5 dB, but that the SNR degradation due to non-ideal CSI remains roughly the same.

Comparison of Table 4.5 with Table 4.3 shows that SNR degradation due to channel estimation error is in general larger for the SDMA case, with multiple ICUs and OCIs and multiple receiving antennas. There are several reasons for this:

- The sensitivity of the equalizer output (equation (4.17)) to errors in *multiple* interferers' channels.
- Uncompensated OCI interference to data (unless least squares is used).
- The required SNR per antenna for M=4 antennas to attain a frame error rate of 10^{-2} is much lower than that required for M=1 antenna and one user terminal. Therefore channel estimates at each receiving antenna will be plagued by more noise.
- OCI interference to pilots.
- In the case of B-IFDMA and IFDMA, channel frequency correlation cannot be as effectively exploited to interpolate to non-pilot frequencies and to smooth noise.
- ICE combined with least squares is sensitive to inaccurate subtraction of ICU interference due to ICU channel estimation errors and hard decision errors.
- Least squares equalizer adaptation is less effective for 4X3 B-IFDMA, since there are fewer OFDM symbols for time-averaging.

While the FER performance of B-IFDMA and B-EFDMA with ideal CSI is much better than that of the full band system (due to the enhanced frequency diversity and smaller number of data symbols per frame of the B-IFDMA and B-EFDMA systems), the SNR degradation for non-ideal CSI is significantly larger than that for full-band transmission, even when pilot overhead is about 33%. The use of larger B-IFDMA blocks, with more pilots per block, significantly improves channel estimation accuracy and enables reduced pilot overhead. For relatively low bit rate data streams, B-IFDMA and B-EFDMA, in spite of their less efficient channel estimation properties, exhibit lower frame error rates than local FDMA (L-FDMA) with the same overall bit rate. L-FDMA corresponds to B-IFDMA or B-EFDMA where the blocks are contiguous, instead of being separated in frequency, so the band of frequencies spanned by a L-FDMA signal is much smaller. Separate comparisons of L-FDMA and B-IFDMA (not shown here) indicated the superiority of B-IFDMA for coded QPSK symbol rates up to 5 Mbaud.

4.7 Impact of Channel Estimation Errors on Alamouti and Spatial Multiplexing Transmission Schemes

In this section, we investigate the impact of channel estimation errors on the Spatial Multiplexing and Alamouti schemes. These two schemes only require CSI information at the receive side and we focus on studying the impact of channel estimation errors at the receiver.

4.7.1 System Description

System Model:

Let us assume N_t transmit antennas and N_r receive antennas. The input-output relationship for this narrowband MIMO system can be written as

$$\mathbf{y} = \sqrt{\frac{E_s}{N_t}}\mathbf{H}\mathbf{s} + \mathbf{n}, \tag{4.30}$$

where E_s is the total average energy transmitted over a symbol period, $\mathbf{H}$ is the $N_r \times N_t$ channel matrix, $\mathbf{s}$ is the transmitted symbol vector, $\mathbf{y}$ is the received signal vector, and $\mathbf{n}$ is the additive white Gaussian noise with variance σ^2. Here we assume $\mathbf{H}$ is normalised such that its elements are zero mean complex Gaussian random variables with variance 1, and the averaged symbol energy of $\mathbf{s}$ is unity. For the scenarios that include LOS or dominant components, the mean of $\mathbf{H}$ is no longer zero and is related to the power of the LOS or the dominant components.

Channel Model:

Herein, we use two different channel models to study the impact of channel estimation errors. One is the simplest channel model that models the element of channel matrix $\mathbf{H}$ as independent and i.i.d. zero-mean complex Gaussian variables. Note that model is often valid when the distance between neighbouring elements is large, and the radio environment has rich scattering.

In most scenarios, however, correlations exist at both the transmitter and the receiver. To reflect these characteristics in the real radio scenarios, we also use the WINNER channel models in our simulations. The readers are referred to [WIN2D112] for more details on the WINNER channel models.

4.7.2 Spatio-Temporal Transmission Schemes

4.7.2.1 Spatial Multiplexing

The spatial multiplexing transmits data symbols over parallel spatial subchannels, hence achieves high data rate. This has been demonstrated in [Fos96] [WFG+98] where the Bell Labs Layered Space-Time (BLAST) architectures were proposed along with a coding and decoding scheme. In this subsection, we assume no CSI is available at the transmitter, and the power is equally allocated to each transmit antennas. Four different types of receivers are studied, and we briefly describe these receivers as follows.

Zero-Forcing Receiver: the zero-forcing (ZF) receiver belongs to the linear receiver, and can be expressed as [PNG03]

$$\mathbf{G}_{ZF} = \sqrt{\frac{E_s}{N_t}}\mathbf{H}^{+}, \tag{4.31}$$

where $(\cdot)^{+}$ denotes the Moore-Penrose pseudo inverse.

Minimum Mean Square Error Receiver: this is another type of linear receiver, which can be expressed as [PNG03]

$$\mathbf{G}_{MMSE} = \sqrt{\frac{E_s}{N_t}}(\mathbf{H}^{H}\mathbf{H} + \frac{N_t}{\rho}\mathbf{I}_{N_t})^{-1}\mathbf{H}^{H}, \tag{4.32}$$

where ρ is the average SNR at the receive side.

V-BLAST Receiver: in [WFG+98], the non-linear vertical BLAST (V-BLAST) receiver has been proposed. The main idea is to successively decode the symbols layer by layer. By using symbol cancellation, the interference from the decoded symbols is removed. This approach can be combined with either the ZF or MMSE receivers mentioned above.

4.7.2.2 Alamouti Scheme

Instead of exploiting the spatial multiplexing gain, the well-known Alamouti scheme [Ala98] is designed to exploit the transmit diversity for any system with 2 transmit antennas. It is also a special case of OSTBCs [TJC99], and is the only full rate code available among all OSTBCs. Herein, we focus on studying a 2×2 system using Alamouti scheme.

Let us assume the channel remains constant for two consecutive symbol periods, the input-output relationship for the Alamouti scheme can be expressed as

$$\mathbf{Y} = \sqrt{\frac{E_s}{2}}\mathbf{H}\begin{bmatrix} S_1 & -S_2^{*} \\ S_2 & S_1^{*} \end{bmatrix} + \mathbf{N}, \tag{4.33}$$

where $\mathbf{Y}$ is the received signal matrix, and $\mathbf{N}$ is the noise matrix.

The above expression can also be written using the effective channel matrix, i.e.

$$\mathbf{y}_{eff} = \sqrt{\frac{E_s}{2}}\mathbf{H}_{eff}\mathbf{s} + \mathbf{n}_{eff} \tag{4.34}$$

where $\mathbf{y}_{eff} = [\mathbf{Y}(:,1)^T, \mathbf{Y}(:,2)^T]^T$, $\mathbf{s} = [s_1, s_2]^T$, $\mathbf{N}_{eff} = [\mathbf{N}(:,1)^T, \mathbf{N}(:,2)^T]^T$, and the effective channel matrix $\mathbf{H}_{eff}$ is

$$\mathbf{H}_{eff} = \begin{bmatrix} h_{1,1} & h_{1,2} \\ h_{2,1} & h_{2,2} \\ h_{1,2}^{*} & -h_{1,1}^{*} \\ h_{2,2}^{*} & -h_{2,1}^{*} \end{bmatrix}. \quad (4.35)$$

4.7.3 Channel estimation error at the receiver

In real systems, the channel estimation procedure can never be perfect. Therefore channel estimation errors always exist. The main sources of channel estimation errors include the noise in the estimation procedure, the interpolation process, the quantisation, and the feedback delay. The first two sources have impact over the whole system, while the last two sources impact mainly happen at the transmitter. In this subsection, we focus on the channel estimation errors at the receive side caused by the first two sources.

One popular channel estimation error model is to model the channel estimation error matrix as i.i.d. zero mean complex Gaussian, i.e.

$$\hat{\mathbf{H}} = \sqrt{1-\varepsilon^2}\,\mathbf{H} + \varepsilon\tilde{\mathbf{H}}, \quad (4\text{-}36)$$

where $\hat{\mathbf{H}}$ is the estimated MIMO channel matrix, $\tilde{\mathbf{H}}$ is the normalised i.i.d. zero mean complex Gaussian channel estimation error matrix, and the parameter $\varepsilon \in [0,1]$ measures the accuracy of channel estimation. $\varepsilon = 0$ indicates perfect channel estimation, while $\varepsilon = 1$ indicates a complete failure of channel estimation procedure.

Using the above channel estimation error model, we simulate the Alamouti scheme and the SM scheme for 2×2 systems with one subcarrier, and compare the performance with each other. 1000 channel realisations are generated in our simulations. We further assume that the channels are stationary for 8 successive symbol periods, therefore each channel realisation has been used 8 times for transmission. We use 4-QAM modulation for the SM scheme and 16-QAM modulation for the Alamouti scheme in our simulations in order to keep the same data rate in both transmission schemes.

Figure 4-9 shows the result for the i.i.d. zero mean complex Gaussian MIMO channels. Similar to the results reported in [ZO03], we observe the error floor for the nonlinear V-BLAST receivers is lower than the error floor for the linear ZF and MMSE receivers. When the channel estimation error is small, the error floor for the Alamouti scheme is much lower than the SM scheme.

In Figure 4-10, we have simulated the sub-urban metropolitan scenario using the WINNER C1 model with LOS component. In this type of scenario, the correlations of the channel coefficients are relatively high due to the LOS component. Simulation results show that the performance of different transmission schemes follows the same trend as in
Figure **4-9**, but with higher BER.

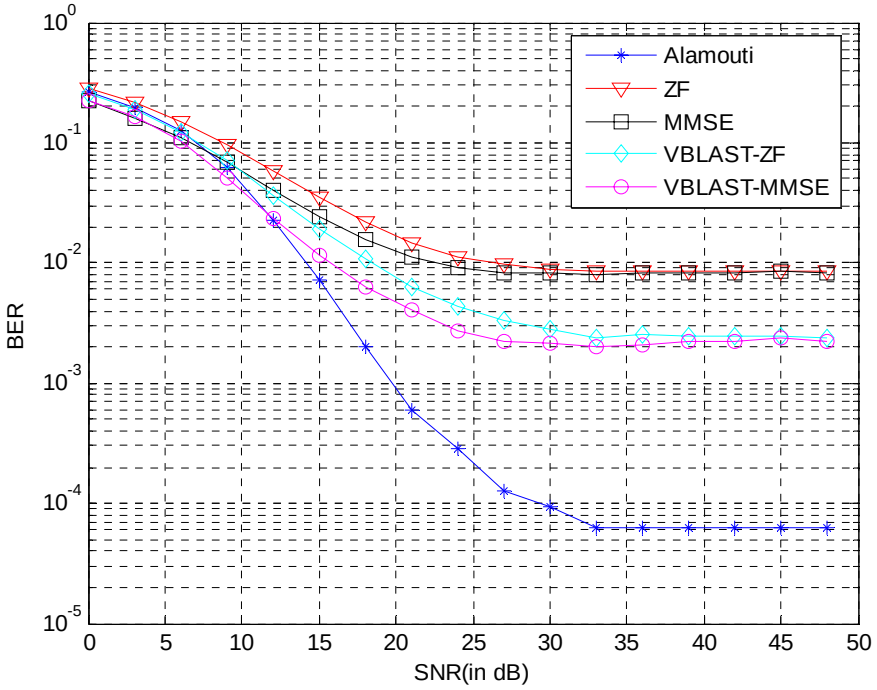

Figure 4-9: Comparison of the Alamouti and SM schemes for 2×2 system with channel estimation errors $\varepsilon = 0.1$, and $\rho_{tx} = \rho_{rx} = 0$.

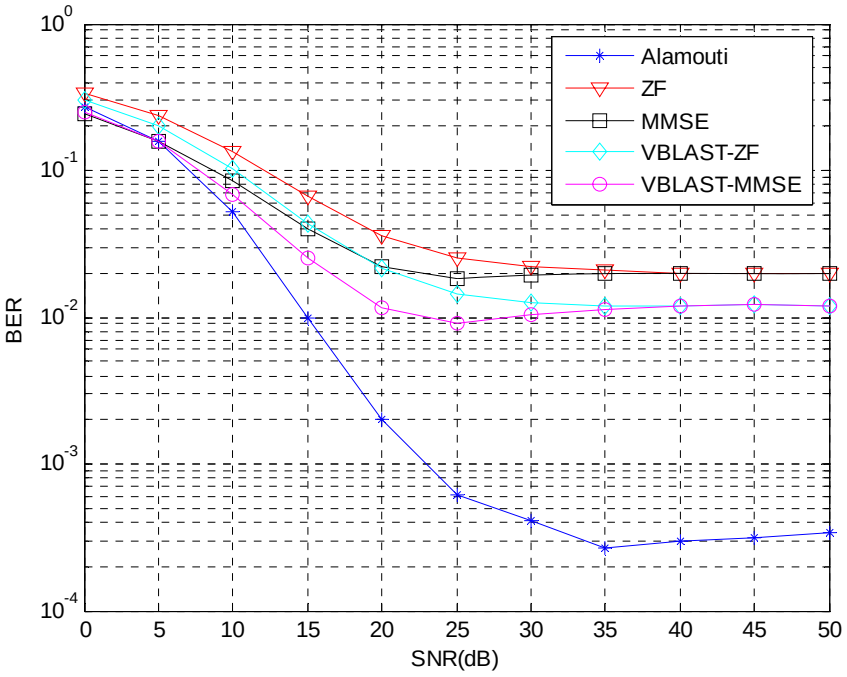

Figure 4-10: Comparison of the Alamouti and SM schemes for 2×2 system with channel estimation errors $\varepsilon = 0.1$, and WINNER C1 LOS scenario.

4.8 Conclusions

It is clear that iterative channel estimation techniques – either by means of genetic algorithms or by means of decision-directed processing – are of great value in reducing the performance degradation that results from imperfect CSI. For this reason, iterative channel estimation techniques are recommended to supplement pilot-based channel estimation in the WINNER reference design.

For full-band transmission, where interpolation and smoothing filtering can be employed over many adjacent subcarriers, the SNR degradation due to non-perfect channel state information can be close to zero dB for single-input single-output. For MIMO and SDMA cases, the SNR degradation is somewhat larger since the receiver must not only equalize, but must also suppress interference using channel estimates. The presence of low level (and therefore hard to explicitly estimate) out-of-cell interferers also degrades channel estimation performance, but this can be reduced to some extent by adding a least squares adaptation step. IFDMA, B-EFDMA and B-IFDMA suffer higher channel estimation error degradation and have higher pilot overhead because of the small size of their blocks, and consequent limited scope for interpolation and filtering in time and frequency over correlated subcarriers. Table 4.3 and Table 4.5 indicated how IFDMA, B-EFDMA and B-IFDMA have lower SNR requirements than full-band transmission when there is perfect CSI, but their SNR requirements increase significantly for even the best channel estimation techniques.

Performance and limitations on channel prediction, using Kalman filter techniques, was evaluated for use in predicting CQI for channel estimation and frequency-adaptive transmission. The Kalman algorithm uses assumed channel time and frequency correlation properties to optimally estimate the future time evolution of the channel. Its use is favoured for channels corresponding to relatively slow mobile terminals, and where auxiliary channel correlation measurements are made.

Finally, channel estimation errors at the receiver were shown to affect spatial multiplexing more than Alamouti single link MIMO systems.

5. Measurements / Signalling

5.1 Introduction

Measurements play an important role in modern communications systems, allowing nodes within the system to understand other nodes of the system, signals within the system, and their context. This information can be used to aid various system functions, from initial system discovery to link adaptation and handover.

Since the node which desires certain measurement information may not be the node which is able to perform that particular measurement, signalling of some measurement information is also necessary. In practical communications systems, design of measurement procedures and associated signalling consists of a trade off between a number of factors, such that performance gains are not taken up by increased overheads.

Through knowledge of the overall channel frequency response, discussed in Section 4, it is possible to derive a large proportion of the measurement metrics required within a communications system. These metrics are tabulated in Section 5.2.1.

Additionally, a list of measurement metrics required by other components of the WINNER system, in order to carry out their functionality, is given in Section 5.2.2.

Although the tradeoffs of performance vs. overheads for measurement and signalling procedures is a matter for specific system design and implementation, an example study is given on the impact of different signalling on multi-antenna transmission techniques in Section 5.3.

5.2 Measurements

5.2.1 Measurement capabilities of WINNER II procedures

In this section we identify the different measurements which are available from, or can be derived from, the other procedures outlined in this document. Most of these measurements relate to the parameters of the channel within the active cell of the measuring node.

A number of key characteristics of each measurement are given, where relevant, since they define the usefulness of the measurement within the overall system design.

In principle, similar procedures could be used to perform measurements of the same parameters of nearby cells. In practice, accurate short term measurements of neighbouring cells requires an inter-cell pilot reuse (orthogonality in time and/or frequency), which is not considered for the WINNER system concept due to high overheads. Additionally the availability and accuracy of such inter-cell measurements would be limited by the relative weakness of the received signals from other cells, and, potentially, interference caused by signals within the active cell.

The following table presents the measurement capabilities of WINNER procedures, and presents for each measurement four categories that are:

- Range of measurement
- Granularity / Accuracy
- Frequency of measurement: how often it can be made/updated
- Timeliness of measurement: delay between the physical event and the availability of measurement of physical event

Name/Description	Range	Granularity	Frequency	Timeliness
Channel matrix	Range of frequency component covers used bandwidth. Range of amplitude component is limited by the Analogue to Digital converter in the implementation. Phase range is 0-360 degrees. Number of links is according to the number of antenna pairs. Resolution of components is subcarrier spacing	Mean Square Error of each component is 1/SNR (in dB) + 1/processing gain (in dB)	Once per OFDM symbol	One OFDM symbol
In Band and Out of Band Channel Frequency Response between each terminal antenna and each RAP antenna		Mean Squared Error is bounded by the larger of: 1/SNR (in dB) + 1/processing gain (in dB) and value from interpolation (order of 10^{-2}, 10^{-3})	Once per OFDM symbol at every used frequency	Typically 1 frame delay

Name/Description	Range	Granularity	Frequency	Timeliness
Channel Impulse Response	Duration of impulse response available is up to the cyclic prefix length. Range of amplitude component is limited by the Analogue to Digital converter in the implementation. Phase range is 0-360 degrees. Number of links is according to the number of antenna pairs. Resolution of components roughly equal to reciprocal of bandwidth.	Mean Square Error of each component is 1/SNR (in dB) + 1/processing gain (in dB)	Once per OFDM symbol	One OFDM symbol
CQI (signalling of various channel related metrics)	According to accuracy of contributing measurement and quantization on signalling.		According to contributing measurement	According to contributing measurement
Multipath delay components (derived from channel matrix / impulse response)	As for Channel Impulse Response	As for Channel Impulse Response	As for Channel Impulse Response	As for Channel Impulse Response
SINR	Between minus 2 and 30 dB	1 dB	Once per frame	One frame
SNR	Between minus 2 and 30 dB	1 dB	Once per frame	One frame
Doppler frequency	Essentially unlimited. Expected values up to the order of ~2.5kHz	Unknown	Perhaps once per superframe.	Perhaps one superframe.

Name/Description	Range	Granularity	Frequency	Timeliness
Propagation delay (can be converted to Ranging)	0 – 20 μS	50 nS	Obtained as part of initial access procedure and handover. Tracked when timing alignment is lost. Additional ranging measurements may be included in location determination procedures.	Less than a superframe.

5.2.2 Measurements required for WINNER II reference design

In this section we present a list of measurements identified as being necessary for the functions of the WINNER II reference design. Each measurement is listed along with a brief supplementary explanation, and one or more examples of use. It is not intended here to give a full description of every use of the measurement, since this is not deemed necessary. Information on the measurements needed for a particular technique is given with the description of that technique, in the appropriate documentation. However, examples of use may aid the understanding of the necessity and role of the measurement within the reference design.

In addition we have identified measurements which need to be signalled between physical nodes, and also whether this signalling needs to be carried on a low latency (< 4 mS) feedback channel. Note that channel channel reciprocity may negate the need for signalling of channel related measurements when TDD is used.

It can be seen that a number of required metrics can be derived from other measurements, rather than requiring their own measurement procedures. Specialised measurement procedures for Location Determination are documented in [WIN2D482], so are not duplicated in this document.

Name	Short description / Comments	Example uses of measurement	Need for signalling?
Channel Quality Indicators (CQI)	Superordinate term for various scalar channel related measurements (no unique definition), e.g., SINR of received streams before or after receive processing	Channel State Information.	Yes, purpose of CQI is to signal channel measurements.
Received SINR (after receive processing)	Received SINR per chunk	Flow and resource allocation, Adaptive Modulation and Coding, Scheduling, Multi-antenna techniques, Handover.	Signalling is required, and is urgent for fully adaptive scheduling (FDD operation)
Received SINR accuracy	MSE of prediction		
Average / Mean SINR	Can be derived from Received SINR		May be required, depending on use.

Name	Short description / Comments	Example uses of measurement	Need for signalling?
Channel State Information (CSI)	channel state information (frequency response of the radio transmission channel) - at transmitter (CSIT) - at receiver (CSIR)	CSIT: assignment of flows and radio resources to subcarriers/chunks; selection of modulation and coding scheme per subcarier/chunk(i.e., prediction of received SINR possible in certain techniques); selection of SDMA scheme; computation of precoding weights in TDD mode CSIR: computation of received beam CQI in fixed beam SDMA techniques; equalization of MIMO channel without transmit precoding (e.g., in FDD uplink)	TDD mode: no signalling when reciprocity can be assumed (calibration needed) FDD mode: CSIT through (quantized) feedback of downlink measurements, only for hybrid schemes adapting spatial codebook
CSI accuracy	Measure of the quality of the available CSI	Selection of frequency-adaptive or non-frequency-adaptive transmission mode	Yes
Effective Channel State Information (ECSI)	Including effect of spatial transmit processing (at receiver)	Equalization of effective MIMO channel acting on data (aka combining)	
Doppler Spectrum	related to CSI accuracy		
Transmit Power		Estimation of expected interference: interference mitigation or avoidance schemes; power sharing algorithms	
Noise plus Interference Power (NIP) at RX		MCS selection, precoding, decoding, equalization, scheduling	
Interference Power (IP)	Frequency dependent	Required if frequency adaptive interference coordination is performed	
Frequency Synchronisation accuracy	Accuracy of carrier frequency in BS and UT	Frequency synchronisation mechanism	
Cell Synchronisation accuracy	Accuracy of the superframe time synchronisation with respect to neighbouring cells	Cell synchronisation mechanism	
Propagation delay	Propagation delay between BS and UT	Timing Advance on the uplink	
ToA TdoA	Time of Arrival and Time Difference of Arrival	Location Determination, UT speed, intermode handover	Non-urgent from UT back to BS, and from BS to location nodes

Name	Short description / Comments	Example uses of measurement	Need for signalling?
UT position		Handover trigger. UT velocity (derived from UT position) could be an inter-mode handover trigger.	
Cell load	Used chunks/Available chunks	Load Balance between modes, congestion control	BS–UT and BS–BS
Inter-cell Received Signal Strength (RSS)		Handover	
Inter-RAN RSS / SINR		Handover between different RAN deployments	
Dominant Inter-cell Interferers identification	Typically only the dominant or the 2 dominant interferers need to be identified. In the downlink this can be done from the average power received from the neighbouring RAPs.	Complexity reduction of inter-cell interference cancellation.	
Inter-cell Interference per chunk	Absolute measure of inter-cell interference per chunk.	Minimum Interference Dynamic Channel Allocation	
Correlation Matrix of the received signal	Correlation matrix of the received signal, including inter-cell interference.	Interference Rejection Combining weights computation	

For details of the example uses of measurements, readers are referred to the following WINNER deliverables: [WIN2D223], [WIN2D341], [WIN2D461], [WIN2D471], [WIN2D472], [WIN2D473], [WIN2D482].

5.3 Signalling

Signalling of measurement results in a radio communications system is one of the tradeoffs necessary in system design.

The amount of information that must be signalled, the accuracy and frequency of signalling and the reliability of signalling all have a system cost in terms of overheads and reduction of useful capacity for end user data. Conversely, given sufficient measurements information, it is possible to use more advanced radio transmission and reception techniques, which increase the available system capacity and performance. This tradeoff can be considered not only in system concept performance assessment, but also in choices of techniques to be included in a system concept.

Analysis of the sensitivity of the full WINNER system concept to accurate signalling tradeoffs is not within the scope of the project, however in this section we study the impact of quantised CSI signalling on spatial-temporal transmission schemes, to gain a better understanding of the types of tradeoffs involved.

We consider the impact of quantised CSI signalling on two spatial-temporal transmission groups, namely single link transmissions and multi-user downlink transmissions. The single link transmissions refer to those transmission techniques used for one transmitter and one receiver. In the multi-user downlink transmission, we assume one transmitter needs to communicate with several users simultaneously.

5.3.1 Single link MIMO transmissions

In this subsection, we study the impact of quantised CSI for dominant eigenmode transmission.

5.3.1.1 System Description

A. System Model

Let us assume N_t transmit antennas and N_r receive antennas. The input-output relationship for this narrowband MIMO system can be written for a given subcarrier as

$$\mathbf{y} = \sqrt{\frac{E_s}{N_t}}\mathbf{H}\mathbf{s} + \mathbf{n}, \tag{5-1}$$

where E_s is the total average energy transmitted over a symbol period, $\mathbf{H}$ is the $N_r \times N_t$ channel matrix, $\mathbf{s}$ is the transmitted symbol vector, $\mathbf{y}$ is the received signal vector, and $\mathbf{n}$ is the additive white Gaussian noise with variance σ^2. Here we assume $\mathbf{H}$ is normalised such that its elements are zero mean complex Gaussian random variables with variance 1, and the averaged symbol energy of $\mathbf{s}$ is unity. For the scenarios that include LOS or dominant components, the mean of $\mathbf{H}$ is no longer zero and is related to the power of the LOS or the dominant components.

B. Channel Model

Herein, we use two different channel models to study the impact of channel estimation errors. One is the simplest channel model that models the element of channel matrix $\mathbf{H}$ as independent and i.i.d. zero-mean complex Gaussian variables. Note that this model is valid when the distance between neighbouring elements is large, and the radio environment has rich scattering.

In most scenarios, however, correlations exist at both the transmitter and the receiver. To reflect these characteristics in the real radio scenarios, we also use the WINNER channel models in our simulations. The readers are referred to [WIN2D112] for more details on the WINNER channel models.

5.3.1.2 The Dominant Eigenmode Spatio-Temporal Transmission Scheme

When the CSI is available at the transmitter, an approach to exploit the diversity gain is the dominant eigenmode transmission. The main idea is to transmit via the subchannel that associated with the largest singular value $\sigma_{\max}$ of channel matrix **H**. Let the singular value decomposition (SVD) of **H** be written as

$$\mathbf{H} = \mathbf{U}\mathbf{D}\mathbf{V}^H. \tag{5-2}$$

Let us assume **w** and **g** are the right and left singular vectors that are associated with $\sigma_{\max}$. The transmitter then multiplies the symbol with the weighting vector **w**, and the received signal is

$$\mathbf{y} = \sqrt{\frac{E_s}{N_t}}\mathbf{H}\mathbf{w}s + \mathbf{n}. \tag{5-3}$$

The received signal is then multiplied with another weighting vector **g**, i.e.

$$z = \mathbf{g}^H\mathbf{y} \tag{5-4}$$

This can be simplified to

$$z = \sqrt{E_s}\sigma_{\max}s + n, \tag{5-5}$$

and the received SNR for the dominant eigenmode transmission is

$$\eta = \frac{\left\|g^H Hw\right\|_F^2}{N_t\left\|g\right\|_F^2}\rho = \sigma_{\max}^2\rho. \tag{5-6}$$

5.3.1.3 Quantised CSI at the transmitter

For dominant eigenmode transmissions, the CSI is required at the transmitter side. In FDD systems, this means a feedback link is necessary for the receiver to send the CSI information back to the transmitter. To do this, the CSI needs to be quantised at the receiver side. Therefore, the transmitter receives the imperfect CSI with quantisation errors.

In this subsection, we consider a simple random vector quantisation (RVQ) scheme [TFF07]. Note that the optimal quantiser for the MIMO system is not known in general, and the RVQ scheme provides a lower bound in terms of performance.

To quantise a vector $\mathbf{h}_k$, let us first obtain the direction of the vector as

$$\widetilde{\mathbf{h}}_k = \frac{\mathbf{h}_k}{\|\mathbf{h}_k\|}. \tag{5-7}$$

We then quantise the direction of $\mathbf{h}_k$ using a random code book, where the 2^B quantisation codewords are chosen from an isotropic distribution on the M-dimensional unit sphere independently, i.e.

$$C_k = \{\mathbf{c}_{k,1},...,\mathbf{c}_{k,N}\} \tag{5-8}$$

with $|C_k| = 2^B$. By minimising the chordal distance, the quantised direction of channel $\mathbf{h}_k$ can be expressed as

$$\hat{\mathbf{h}}_k = \underset{\{\mathbf{C}_{k,j}\}_{j=1,...,N}}{\arg\max} \left|\widetilde{\mathbf{h}}_k \mathbf{c}_{k,j}\right|. \tag{5-9}$$

We have simulated the dominant eigenmode transmission with quantisation errors at transmit side using both the simple uncorrelated complex Gaussian MIMO channel model and WINNER C1 LOS channel model, and quantised the right singular vector **w** using RVQ scheme with 8 bits. The quantised version of **w** is then fed back to the transmitter. Simulation results show the system performance degrades when quantisation errors exist at the transmitter. Mode details can be found in Appendix E of this deliverable.

5.3.2 Multi-User Downlink Transmission using MMSE Precoding

In this subsection , we study the impact of RVQ errors on multi-user downlink transmission using MMSE precoding. Let us assume the base station is equipped with N_t transmit antennas, and each of the *K* users has one receive antenna. The system model can be expressed in the baseband domain at a given subcarrier as

$$\mathbf{y} = \sqrt{\frac{E_s}{N_t}}\beta\mathbf{H}\mathbf{F}\mathbf{s} + \mathbf{n}, \tag{5-10}$$

where $\mathbf{H} = [\mathbf{h}_1^T, \mathbf{h}_2^T, ..., \mathbf{h}_K^T]^T$ is a $K \times N_t$ channel matrix, **F** is the MMSE precoding matrix designed as

$$\mathbf{F} = \mathbf{H}^H(\mathbf{H}\mathbf{H}^H + \alpha\mathbf{I})^{-1}, \tag{5-11}$$

where α and β can be written as

$$\alpha = \left(\frac{E_s}{N_t\sigma_n^2}\right)^{-1}, \ \beta = \sqrt{\frac{E_s}{\mathrm{tr}(\mathbf{F}\mathbf{s}\mathbf{s}^H\mathbf{F}^H)}}. \tag{5-12}$$

By using the MMSE precoding matrix designed above, interference among different users is mitigated significantly. In the high SNR region, the MMSE precoder converges to the ZF precoder and the interferences are completely removed. This means the multi-user downlink channel is separated into K independent parallel channels that are almost orthogonal with each other. Therefore the throughput for the whole system can be calculated as the sum of K independent channels with small amount of interferences from other users.

Systems with one base station (equipped with four transmit antennas) communicating with two users (each equipped with one receive antenna) have been simulated. We assume each user estimates the CSI perfectly and feeds back the quantised CSI to the transmitter. The WINNER B1 NLOS scenario is simulated. We study both the system throughput and BER performance (assuming 4-QAM modulation). Simulation results show that both the BER and the system throughput achieve a floor at high SNR region when 12 quantisation bits are used. Furthermore, the system performance improves when the number of quantisation bits increases. More details can be found in Appendix E of this deliverable.

5.4 Conclusions

In this chapter we have presented an overview of the measurement capabilities of the WINNER II physical layer procedures, and an analysis of the measurement requirements of the WINNER II reference design. Even though the measurement procedures and reference design functions have been developed in parallel, it can be seen that there is a good correlation between the requirements and capabilities, highlighting the radio system know-how which has been utilised in the project. A full system design and specification activity could easily optimise the combinations of capabilities and requirements.

Additionally, an exemplary study on the impact of feedback quantisation on spatial-temporal transmission schemes has been presented, which again would provide useful guidance to a full system design and specification activity.

6. RF Impairments

6.1 Introduction

In this section three themes related to synchronisation impairments are discussed. Firstly the effects of high power amplifier (HPA) nonlinearities on properties of transmitted signals are considered, in particular the transmitted power spectrum. Due to different path losses desired and undesired user spectra may be received with large power variability. Hence, avoidance of adjacent channel interference then requires transmit power backoff and rather stringent spectral masks.

Secondly the modelling and suppression of oscillator phase noise and frequency offsets are addressed for both: OFDM with spatial multiplexing and DFT precoded OFDM. This step is especially important for OFDM systems, as phase noise causes intercarrier interference.

Finally SNR degradation due to interference is evaluated. Two main cases are considered. Firstly, samples from previous and subsequent OFDM symbols are added to desired samples and distort the received OFDM signal resulting in interblock interference (IBI). Secondly, carrier frequency offset between transmitter and receiver causes intercarrier interference (ICI) and degrades the SNR.

6.2 HPA Non-Linearities

Neighbouring desired and undesired user spectra may be received with large power variability due to differing path losses. Avoidance of adjacent channel interference then requires low transmitted power spectral sidelobes and rather stringent spectral masks. For example, allowable interference to adjacent-frequency receivers is usually specified in terms of maximum interference power at a certain distance and at a certain frequency offset from the interferer's carrier. Under typical transmitted power and path loss conditions, this may imply spectral masks with as much as 40 to 60 dB of out of band attenuation. A WINNER spectral mask [WIN1D25], scaled to fit current assumed wide area system bandwidth, is illustrated in the following figures. Control of power spectrum sidelobe levels to obey a spectral mask is normally achieved by an appropriate power backoff at the HPA. Signal processing techniques to reduce the dynamic range of the transmitted waveform can also be used to reduce spectrum sidelobe levels, and have been discussed and evaluated in other WINNER reports [WIN1D21], [WIN1D23] and other references [DFL+07], [FDL+07a].

Minimising the power backoff required for high power amplifiers is very important in terms of cost and battery recharging intervals, especially for mobile terminals. Large required backoff lowers amplifier efficiency and increases the maximum output power required from the HPA, thus increasing its cost, and battery drain.
The minimum required power backoff depends on several factors:

- The distribution of the transmitted signals' amplitude; i.e. its dynamic range. A large dynamic range implies larger minimum to maximum amplitude swings and hence larger backoff to minimise distortion. A commonly used, but not necessarily very useful, criterion is "peak to average power ratio" (PAPR).
- The nonlinear input-output characteristic of the HPA. In our studies, we have used the Rapp model for amplitude to amplitude conversion, which is considered reasonably typical for solid state power amplifiers. The model has one parameter, p. A low value of p; e.g. $p = 2$, results in an input-output characteristic which has a visible nonlinearity below the saturated output. It may be typical of a moderate-cost HPA. A higher quality HPA, or one whose input-output characteristic below saturation is linearized by adaptive pre-distortion, has a higher value of p, such as $p=10$.
- The power spectrum mask to which the HPA output power spectrum must be confined. It is determined by consideration of allowed power leakage into adjacent users' spectral allocations. In this study we use the spectral mask that was derived for WINNER narrowband mobile terminal outputs in [WIN1D25], scaled to the used wide area signal bandwidths of 40 MHz and 10 Mhz.

In general, different nonlinearity characteristics and spectral masks will change the absolute values of backoffs for different types of signals, but would not be expected to change the relative values.

Various OFDMA and DFT-precoded OFDMA signals transmitted through a Rapp model nonlinearity with p=2 and 10 were simulated, and their resulting average output power spectra were measured. Typical results are shown in the figures below. Each signal block is time-windowed with a raised cosine window after the IFFT operation. For each signal, the average power was adjusted by trial and error so that the power spectrum barely grazed the spectral mask. Then the difference between that average power and the saturated output power from the nonlinearity was the signal's required power backoff.

Figure 6-1 shows p=2 HPA output power spectra for full-band 16-QAM OFDM and DFT-precoded OFDM (serial modulation) for 40 MHz nominal bandwidth (50 MHz system bandwidth), Serial modulation requires nearly 2 dB less backoff to comply with the scaled WINNER spectral mask that is shown in the figure.

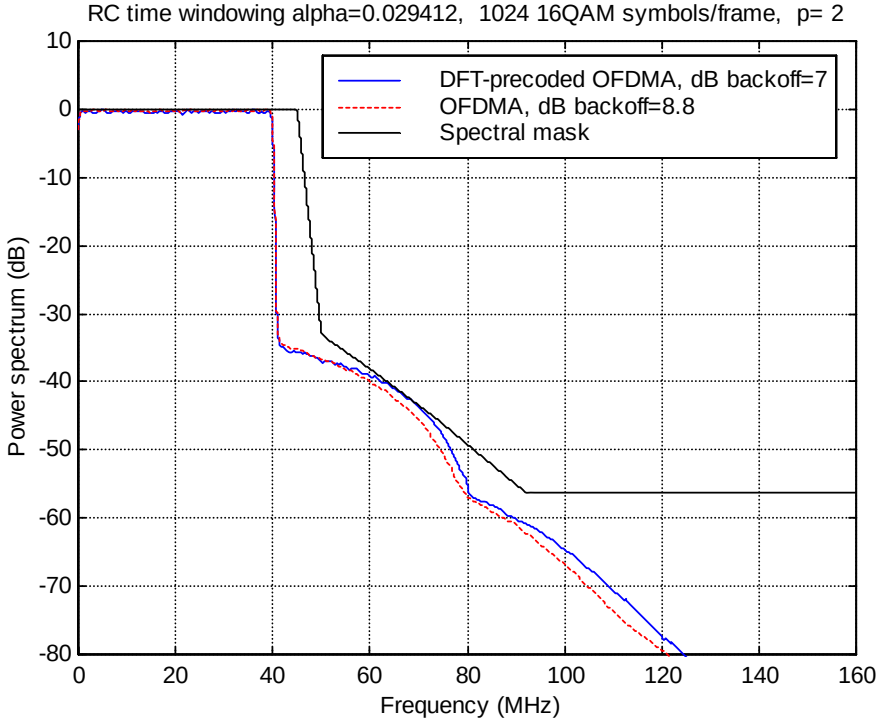

Figure 6-1 HPA output power spectra for full-band (40 MHz) 16-QAM OFDMA and DFT-precoded OFDMA signals. HPA has Rapp model nonlinearity with parameter p=2.

Required backoff is further reduced if the HPA has a nearly linear characteristic below saturation, as exemplified by the power spectra for p=10, shown in Figure 6-2. The backoffs for both signal formats are reduced by 1 dB. The p=10 characteristic produces flatter out of band radiation, but at very low levels. As discussed in [DFL+07], [FDL+07a], there are a number of techniques, which can be applied equally well to OFDM and DFT-precoded OFDM signal waveforms to reduce their PAPR; however it turns out that these techniques are of little value in reducing the required power backoff unless the HPA has a nearly linear characteristic up to its saturation level.

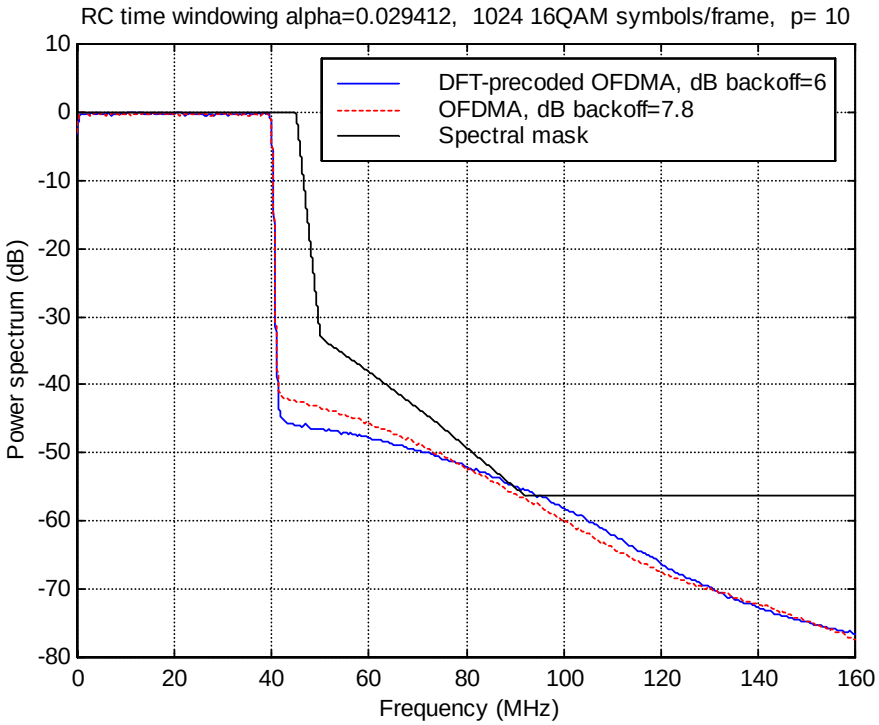

Figure 6-2 HPA output power spectra for full-band (40 MHz) 16-QAM OFDMA and DFT-precoded OFDMA signals. HPA has Rapp model nonlinearity with parameter *p*=10.

It is worth noting that for a typical spectral mask such as the scaled WINNER mask shown in these figures, it is mainly the out of band radiation, rather than nonlinear distortion of the transmitted signal, that determines the required power backoff. For example, for Figure 6-1 and subsequent figures, the in-band distortion of the transmitted signals is at least 30 to 35 dB below the signal power, and total out of band distortion is at least 35 to 40 dB below the signal power. This statement should be modified somewhat for high level modulation, such as 64- and 256-QAM. Figure 6-3 shows HPA output signal constellations for 256-QAM signals emerging from a *p*=10 HPA,. The signal to nonlinear distortion ratios are 37.3 and 38.4 dB, for backoffs of 7.9 dB and 6.1 dB, for OFDM and DFT-precoded OFDM, respectively.

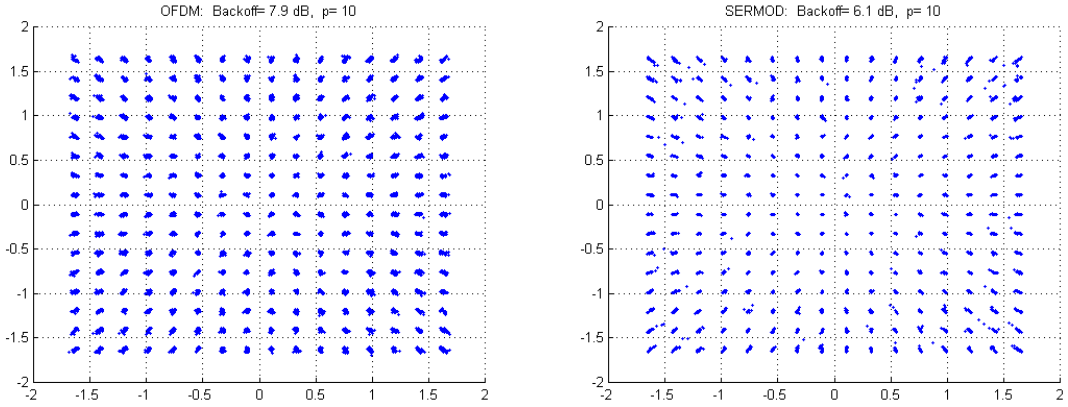

Figure 6-3 Signal constellations for 256-QAM full-band (40 MHz) OFDM and DFT-precoded OFDM (labelled "SERMOD") at the output of a *p*=10 Rapp model HPA. The signal to nonlinear distortion ratios are 37.3 and 38.4 dB for OFDM and DFT-precoded OFDM, respectively.

The backoff requirements for QPSK B-EFDMA and B-IFDMA signals with a 4-subcarrier block width, with 32 blocks spaced at 32 subcarrier intervals, are shown in.Figure 6-4. Although the B-IFDMA signal waveform is not exactly equivalent to a single carrier waveform, its required backoff is close to that of the full-bandwidth case. Results presented in [DFL+07] indicate that IFDMA has similar backoff properties to B-IFDMA and full-band DFT-precoded OFDM.

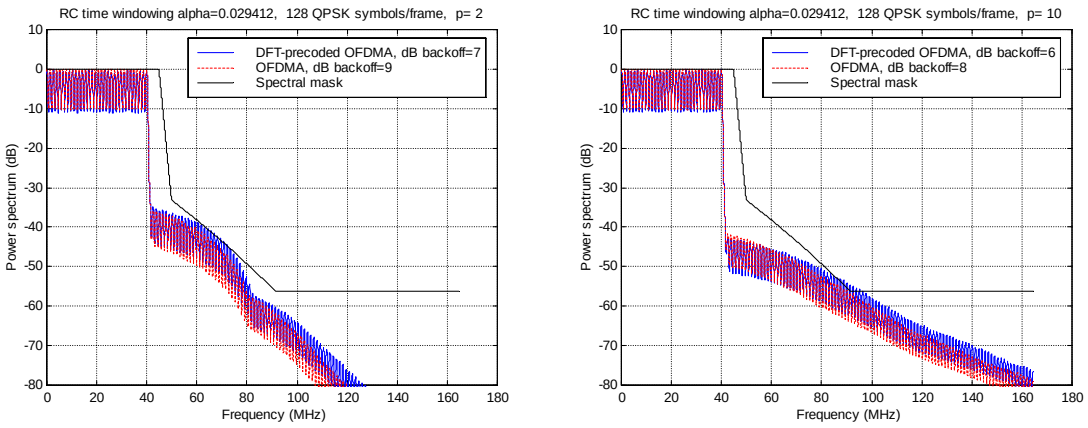

i. (b)

Figure 6-4 HPA output power spectra for QPSK OFDMA and DFT-precoded OFDMA signals, corresponding to B-EFDMA and B-IFDMA respectively, with block width=4 and with 40 MHz nominal bandwidth. (a) HPA has Rapp model nonlinearity with parameter p=2; (b) HPA has Rapp model nonlinearity with parameter p=10;

The power spectra shown above are for signal waveforms which do not include frequency-multiplexed pilots for channel estimation and synchronisation. Full-band and B-IFDMA signals' peak to average ratio and HPA output spectra will be affected, since frequency multiplexed pilots essentially add another waveform to the data waveform. It is to be expected that the power spectrum for B-EFDMA will be little affected by frequency multiplexed pilots, since the signal is the sum of many waveforms in parallel anyway. As shown in [DFL+07], the presence of pilots in the B-IFDMA signal increases the backoff required from 7.0 dB to 7.8 dB, and the difference from B-EFDMA decreases from 1.9 dB to 1 dB. Note that only a fraction of OFDM symbols contain pilots and need this extra backoff. Thus the effect of frequency multiplexed pilots on the required power backoff is minimal.

The effect on output power spectra of adaptive frequency domain resource partitioning was also evaluated. It was found that it has no adverse effect on the emitted power spectrum, relative to the spectral mask. This is because in order for a spectrum to fall within a spectrum mask, power control can only **reduce** power from its spectrum mask limit at a given frequency. Figure 6-5 illustrates this. Note that the backoff difference between OFDMA and DFT-precoded OFDMA is reduced, but is still positive.

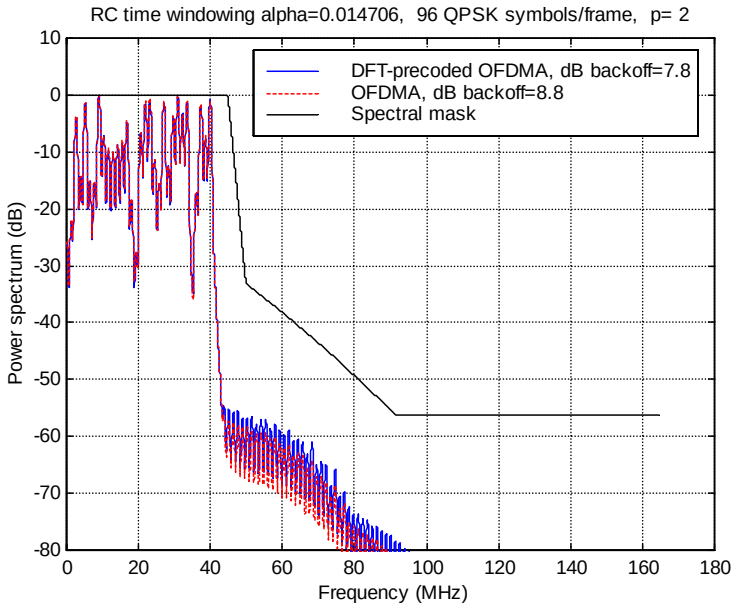

Figure 6-5 Illustration of output HPA power spectrum for nonuniformly-spaced spectrum chunks – typical of frequency-adaptive resource partitioning for OFDMA and DFT-precoded OFDMA, Rapp parameter *p*=2.

Table 6-1 summarizes the results for required power backoff, for in-band signal to nonlinear distortion, and for signal to adjacent user distortion. For the full-band (40 MHz) cases, adjacent user refers to the adjacent 40 MHz frequency band. For B-EFDMA and B-IFDMA, adjacent user means the frequencies occupied by a user whose blocks are immediately adjacent and interleaved in frequency with those of the transmitting user; e.g. the transmitting user occupies subcarriers [1, 2, 3, 4, 33, 34, 35, 36,..] and the adjacent user occupies subcarriers [5, 6, 7, 8, 37, 38, 39, 40,…].

Table 6-1 Required power backoffs and signal to distortion ratios to comply with WINNER spectral mask, for Rapp HPA parameter values *p*=2 and 10

	Rapp parameter *p*=2			**Rapp parameter *p*=10**		
	Required power backoff (dB)	**Signal to in-band distortion Ratio (dB)**	**Signal to adjacent user distortion ratio (dB)**	**Required power backoff (dB)**	**Signal to in-band distortion ratio (dB)**	**Signal to adjacent user distortion ratio (dB)**
QPSK (4-QAM)						
OFDM (full-band)	8.8	32.7	38.6	7.9	40.2	44.7
DFT-precoded OFDM (full-band)	6.8	37.0	39.5	5.7	49.3	51.3
B-EFDMA	9.0	35.7	41.7	8.0	42.9	47.6
B-IFDMA	7.0	36.3	40.2	6.0	44.3	47.9
16-QAM						
OFDM (full-band)	8.8	31,8	38.5	7.8	37.8	44.4
DFT-precoded OFDM (full-band)	7.0	33.3	38.2	6.0	39.6	46.9
B-EFDMA	8.8	29.8	40.8	8.0	32.1	49.1
B-IFDMA	7.3	29.8	39.6	6.5	32.1	49.3
64-QAM						
OFDM (full-band)	8.7	31.5	38.1	7.9	37.5	44.7
DFT-precoded OFDM (full-band)	7.0	32.6	37.8	6.1	38.6	45.8
256-QAM						
OFDM (full-band)	8.7	31.6	38.2	7.9	37.3	44.5
DFT-precoded OFDM (full-band)	7.0	32.6	37.6	6.1	38.4	45.6

To summarise the results:

- The backoff required to satisfy the spectral mask does not increase significantly in going from QPSK to 256QAM.
- The same holds true for backoffs required to maintain a given signal to nonlinear distortion ratio (SNDR). E.g. for p=2 Rapp model nonlinearity, backoffs required to satisfy spectral mask also yield approx. 32 dB SNDR for QPSK through 256QAM. (although it would probably be desirable to have a higher SDNR, and therefore somewhat more backoff, for 256QAM).
- DFT-precoded OFDM and B-IFDMA have 1.5 to 2 dB less required power backoff than do OFDM and B-EFDMA, respectively (~2 dB for QPSK, ~1.5 dB for 256QAM).
- For all modulations, and for Rapp parameter p=10 (HPA approximating an ideal linear clipper), required backoff is roughly 1 dB less than that for p=2 (corresponding to more nonlinearity in the unsaturated region of the HPA). P=10 also reduces SNDR by about 5 dB.
- Thus DFT-precoded OFDM and higher quality (or adaptively-predistorted) HPAs are desirable, especially for uplink transmission high level modulations.
- Required backoff of course depends on the choice of the spectral mask.
- Adaptive resource partitioning for frequency adaptive transmission can only reduce the required backoff to comply with the spectral mask.

6.3 Phase Noise (TUD)

6.3.1 Introduction

Once frame timing and carrier frequency acquisition have been achieved by a receiver, fine carrier phase synchronisation and symbol timing must be carried out. Carrier phase synchronisation is complicated by time variation of the phase of the received carrier – in the form of *frequency offset* and *phase noise* in the transmitter frequency synthesizers and oscillators used for up- and down-conversion. A complex baseband received signal with frequency offset and phase noise can be represented as:

$$\mathrm{Re}\left(s(t)\cdot e^{j\cdot(2\cdot\pi\cdot\delta f\cdot t+\varphi(t))}\right) \qquad (6.1)$$

where δf represents the frequency offset and $\varphi(t)$ represents random phase noise. For cost reasons it is likely that the worst case frequency offset and phase noise impairments will be in the user terminals. Frequency offset and phase jitter cause inter-carrier interference in OFDM systems (see for example [PVM95] and [Sto98]). Avoidance of severe performance degradation requires that frequency offsets be kept lower than about 1% of the subcarrier spacing.

6.3.2 Phase Noise Model

Phase noise is a random process characterised by the power spectral density of $\varphi(t)$. Many studies, such as [PVM95], model it as a Wiener process, with a Lorentzian power spectrum behaving like f^{-2}. More realistic phase noise spectra have somewhat more complex shapes, but still typically exhibit f^{-2} behaviour over part of their range [Lar96]. For simplicity we will restrict ourselves to the case of a free running oscillator (Wiener process). The output of a noisy oscillator is modelled as a stochastic time shift [BRF07]:

$$x_s(t+\alpha(t)) \qquad (6.2)$$

where $x_s(t)$ is the noiseless periodic steady state response of an oscillator. The phase offset at the time instance t is now given as $\varphi(t) = 2\pi f_m\, \alpha(t)$, with f_m as carrier frequency. The properties of the time shift $\alpha(t)$ can be considered as Brownian motion (Wiener) process. The variance of such a process increases linearly with the time at a rate c_{vco} (constant which depends on the oscillator quality), thus the time shift can be expressed using the Wiener process $V(t)$ as follows:

$$\alpha(t) = \sqrt{c_{vco}}\,V(t). \qquad (6.3)$$

The oscillator constant c_{vco} can be determined using the single side power spectrum density $P_{SS}(f)$ which is the Fourier transform of the autocorrelation function $R(t,\tau)$ of $x_s(t+\alpha(t))$ and is given for sinusoidal oscillator by:

$$P_{SS}(f) = 2\sum_{i=\pm 1} X_i X_i^* \frac{f_m^2 i^2 c_{vco}}{\pi^2 f_m^4 i^2 c_{vco} + (f+if_m)^2}. \qquad (6.4)$$

here X_i represents the Fourier components of x_s. The normalised PSD for the carrier frequency f_m is defined as a ratio between the signal power in the 1-Hz bandwidth at the frequency offset f and the total signal power:

$$L(f) = 10\log_{10}\frac{P_{SS}(f_m+f)}{P_{tot}} \qquad (6.5)$$

where for small values of c_{vco} and for $f_m >> f$ usually the following approximation is used resulting in a single side Lorentzian power density spectrum, given as dBc/Hz

$$L(f) \approx 10\log_{10}\frac{f_m^2 c_{vco}}{\pi^2 f_m^4 c_{vco}^2 + f^2}. \qquad (6.6)$$

Finally the oscillator constant c_{vco} is related to the 3dB bandwidth:

$$c_{vco} = \frac{f_{3dB}}{\pi f_m^2}. \qquad (6.7)$$

With f as the subcarrier spacing of an OFDM system, it is common to use the single relevance performance parameter δ_{3dB}as the relative oscillator linewidth with respect to the subcarrier spacing given by:

$$c_{vco} = \delta_{3dB} \frac{f}{\pi f_m^2}. \quad (6.8)$$

The discrete time phase noise model for a free running oscillator is based on a sampled Brownian motion process. The phase noise at the k^{th} sample is related to the previous one as:

$$\varphi(k) = \varphi(k-1) + w \quad (6.9)$$

where w is a Gaussian distributed random variable, with zero mean and variance $\sigma^2 = 4\pi f_m^2 c_{vco} T_S$. In this notation T_S describes the sample interval.

6.3.3 Phase Noise Suppression in OFDM with Spatial Multiplexing

Phase noise induces the following two effects to an OFDM system: first a rotation of the received constellation, which is referred to as common phase error (CPE): second intercarrier interference (ICI). In comparison to the frequency offset (which can be understood as a linear phase shift), phase noise is a random process and changes rapidly within one OFDM symbol. For that reason the complexity of suppressing phase noise is larger than for suppressing frequency offsets, which is normally taken as constant within one burst.

For single-input single-output (SISO) systems a lot of phase noise correction methods are already investigated [PVM95], [WB02], however, phase noise compensation in a MIMO environment is only rarely discussed with exceptions as [LWB06], [STSF04] and [STSF05]. Most of the proposed phase noise correction methods only compensate the common phase error (CPE), which is a common rotation to all subcarriers. However, in the existence of strong phase noise this correction can easily become insufficient, because higher order spectral components of the phase noise process are still present leading to intercarrier interference (ICI). Therefore an extension and optimisation of the phase noise suppression algorithm initially proposed for the SISO case in [PVM95] to the case of multiple transmit and receive antennas.

In a coded MIMO environment it is common to perform detector-decoder iterations in order to achieve near capacity performance. One idea is to inherently use the soft information of the coded bits supplied from the decoder in each iteration to improve the linear minimum mean squared error (LMMSE) estimation of the Fourier coefficients of the phase noise realizations. For the LMMSE estimation a selection based on the soft information is performed to identify the most reliable symbols which are used for the estimation. As stated above phase noise in time domain is a multiplicative distortion resulting in a convolution of the spectra in the frequency domain. In order to not perform multiple transformations the phase noise influence in the frequency domain is compensated by performing a deconvolution with the estimated spectrum.

Considering a MIMO (multiple-input, multiple-output) OFDM transmission with N_{Tx} transmit (Tx) and N_{Rx} receive (Rx) antennas and N_C subcarriers the MIMO-OFDM transmit vector $\mathbf{S}$ given by:

$$\mathbf{S} = \left[\mathbf{S}_1, \ldots, \mathbf{S}_i, \ldots, \mathbf{S}_{N_C}\right]^T \quad (6.10)$$

Whose components $\mathbf{S}_i$ denote the N_{tx} x 1 frequency domain MIMO transmit vectors for subcarrier frequencies.

After direct down-conversion the time domain received OFDM signal at receive antenna rx in the presence of phase noise can be expressed as:

$$r_{rx}(k) = \sum_{tx=1}^{N_{Tx}} \left(s_{tx}(k) * h_{rx,tx}(k)\right) \exp\left(j\varphi(k)\right) + \xi_{rx}(k) \quad (6.11)$$

where *s(k)* is the time domain signal, * stands for convolution and $\xi_{rx}(k)$ represents white Gaussian noise with variance σ^2_k. In this notation $h_{rx,tx}(k)$ describes the time domain channel impulse response between transmit antenna tx and receive antenna rx. At the receiver the CP is removed and a discrete Fourier transform per antenna is performed transforming the received signal back in frequency domain. The overall transmission chain including Fourier transforms is given by the following vector matrix notation:

$$\mathbf{R} = \left(\mathbf{F} \otimes \mathbf{I}_{Rx}\right)\boldsymbol{\Psi}\boldsymbol{\upsilon}\left[\mathbf{h}\boldsymbol{\Theta}\left(\mathbf{F}^{-1} \otimes \mathbf{I}_{Tx}\right)\right]\mathbf{S} + \boldsymbol{\xi} \quad (6.12)$$

where uppercase letters describe frequency domain signals and lowercase letters time domain. The circle cross denotes the Kronecker Product, **F** is the N_C x N_C Fourier matrix. The cyclic prefix is added by multiplication with matrix **Θ** and removed by the multiplication with matrix **Ψ**. The phase noise process is represented by $\boldsymbol{\upsilon} = \mathrm{diag}(e_0,\ldots,e_{N-1})$ with $e_k = \exp(j\,\varphi(k))$ and *N* representing the total number of samples including guard interval. Furthermore the channel is given by the matrix **h** of channel impulse responses. Performing standard matrix manipulation the received signal in the frequency domain can be written as:

$$\mathbf{R} = \mathbf{YHS} + \boldsymbol{\eta} \quad (6.13)$$

where the fact is applied that the circular block matrix **ΨhΘ** can be diagonalised by the IFFT and FFT operation resulting in the $N_C N_{Rx}$ x $N_C N_{Tx}$ block diagonal matrix **H**, which is the frequency domain representation of the channel matrix **h**. Phase noise at the receiver causes intercarrier interference between the received symbols during downconversion, which is modelled by **Y**. The AWGN noise is also transformed in the frequency domain, keeping the same statistic behaviour. The phase noise matrix representation is given by:

$$\mathbf{Y} = \begin{pmatrix} E_0 & E_{-1} & \cdots & E_{-(N_C-1)} \\ E_1 & E_0 & \cdots & E_{-(N_C-2)} \\ \vdots & \vdots & \ddots & \vdots \\ E_{N_C-1} & E_{N_C-2} & \cdots & E_0 \end{pmatrix} \otimes \mathbf{I}_{Rx} \quad (6.14)$$

and

$$E_i = \frac{1}{N_C}\sum_{k=0}^{N_C} \exp\left(-j2\pi ik / N_C\right)\exp\left(j\varphi(k)\right). \quad (6.15)$$

the frequency domain representation of the phase noise process. The main tasks are to compensate the influence of the phase noise and to solve the joint detection problem due to spatial multiplexing on each subcarrier.

Although the phase noise realizations are based on a sampled Wiener process with mean zero, the average phase rotation per OFDM symbol common to all subcarriers is not zero. Since the CPE changes from symbol to symbol an initial correction of the phase error using the preamble is insufficient and does not yield acceptable performance. A possible way to track the phase noise distortion is to use known pilots. The location of the pilots within the transmitted symbols with the vector P. Using the least squares estimation the common phase rotation is given by [PVM95]:

$$\exp(j\Phi_0) \approx E_0 = \frac{\mathbf{A}_P^H \mathbf{R}_P}{\mathbf{A}_P^H \mathbf{A}_P} \quad (6.16)$$

the abbreviation $\mathbf{A}_P = \mathbf{H}_P\mathbf{S}_P$ is used and $\mathbf{R}_P$ is a vector of received pilot symbols.

After initial correction of the common phase error and decoding a first estimation of the transmitted symbols is available. However, this estimation is not very reliable, since each received symbol still suffers from a weighted sum over all other symbols in addition to interstream interference. Therefore, an iterative estimation of higher order harmonics is proposed using the idea of joint linear minimum mean square error (LMMSE) estimation [PVM95]. The key point of the linear MMSE approach as one way to estimate the phase noise is the fact that only a few low frequency components of the phase noise spectrum are usually sufficient to give a reasonable approximation of the phase noise realization during a given OFDM symbol. In order to perform the LMMSE estimation the received signal is written down in a vector matrix notation for a subset of B different receiver symbols, based on their soft values, leading to the following set of linear equations:

$$\begin{bmatrix} \mathbf{R}_{i_1} \\ \vdots \\ \mathbf{R}_{i_B} \end{bmatrix} = \begin{bmatrix} \mathbf{A}_{i_1-u} & \cdots & \mathbf{A}_{i_1} & \cdots & \mathbf{A}_{i_1+u} \\ \vdots & & \ddots & & \vdots \\ \mathbf{A}_{i_B-u} & \cdots & \mathbf{A}_{i_B} & \cdots & \mathbf{A}_{i_B+u} \end{bmatrix} \cdot \begin{bmatrix} E_u \\ \vdots \\ E_0 \\ \vdots \\ E_{-u} \end{bmatrix} + \begin{bmatrix} \zeta_{ICI\,i_1} \\ \vdots \\ \zeta_{ICI\,i_B} \end{bmatrix} + \begin{bmatrix} \boldsymbol{\eta}_{i_1} \\ \vdots \\ \boldsymbol{\eta}_{i_B} \end{bmatrix}. \quad (6.17)$$

The selection of the most reliable subcarriers/symbols is described in [PVM95]. Again the abbreviation $\mathbf{A}_i$ for the product $\mathbf{H}_i\mathbf{S}_i$ on subcarrier i is used and $\mathbf{A}_i$ has the dimension of Rx x 1. The influence of the higher order phase noise harmonics is specified by the optimization parameter u that represents the estimation order (maximal considered frequency) of the phase noise process. During the iteration process the order u is increased and thus higher order harmonics are estimated. In addition, a more accurate estimation of already existing components is performed. To further reduce the number of equations only the best receive antenna per subcarrier are selected which is specified by the maximal row norm of the channel matrix **H**. Hence, the number of equations is in direct relation to u by $B \geq 2u+1$ and does not depend on the number of receive antennas any more.

The estimation of the Fourier coefficients of the phase noise process up to a certain order u can be considered as a Bayesian estimation problem of a parameter vector which is disturbed by the remaining intercarrier interference and Gaussian noise due to the AWGN term. Writing the vector matrix in a more compact form as:

$$\mathbf{R} = \mathbf{A} \cdot \mathbf{E} + \boldsymbol{\varepsilon} \quad (6.18)$$

where $\boldsymbol{\varepsilon}$ represents the effective measuring noise. The LMMSE estimate of the vector **E** is given by:

$$\hat{\mathbf{E}} = \mathbf{M} \cdot \mathbf{R} \quad (6.19)$$

with

$$\mathbf{M} = \boldsymbol{\Phi}_{\mathbf{EE}} \mathbf{A}^{\mathrm{H}} \left(\mathbf{A} \boldsymbol{\Phi}_{\mathbf{EE}} \mathbf{A}^{\mathrm{H}} + \boldsymbol{\Phi}_{\boldsymbol{\varepsilon\varepsilon}} \right)^{-1} \quad (6.20)$$

The evaluation of the correlation matrix $\boldsymbol{\Phi}_{\mathbf{EE}}$, which represents the auto correlation of the vector **E** can be found in [PRF04]. The matrix $\boldsymbol{\Phi}_{\boldsymbol{\varepsilon\varepsilon}}$ represents the correlation matrix of the remaining noise term $\boldsymbol{\varepsilon}$. It is common to approximate the remaining intercarrier interference by the remaining phase noise variance of the not estimated harmonics multiplied by the signal power [PRF04], based on the fact that the channel is passive on average. However, this assumption works for long time observations only and does not hold on a symbol time basis where the instantaneous channel realisation has a strong impact on the remaining noise variance. Hence, considering the instantaneous channel realization the remaining noise variance is given for b = {1, …, B} by:

$$\sigma^2_{\zeta_{ICI,i}} = \sum_{\substack{v=-N_{FFT}/2 \\ v \neq \{-u,\cdots,u\}}}^{N_{FFT}/} \left(\mathbf{A}_{i_b - v} \right)^H \cdot \mathrm{E}\left\{ \left| E_v \right|^2 \cdot \mathbf{I}_{Rx} \right\} \cdot \left(\mathbf{A}_{i_b - v} \right) \quad (6.21)$$

Note that for the LMMSE estimation only the component of the selected receive antenna is needed. Furthermore, the computation of the expectation of the squared norm of the remaining ICI terms is given in [PRF04]. This more accurate variance is also used in the metric computation.

Having the estimated phase noise coefficients available, one possible way to correct the phase noise distortion in the time domain would be the multiplication of the received signal with the complex conjugate time domain representation of the estimated Fourier coefficients. This method, however, is from a computational point of view an inefficient way since the IFFT of the estimated Fourier coefficients has to be performed before multiplication and the modified received signal has to be transformed back to frequency domain after phase noise correction. In order to reduce the number of operations direct phase noise compensation in the frequency domain is performed. Then the already Fourier transformed received symbols and the phase noise distortion can be deconvolved using the frequency reversed conjugate spectrum of the phase noise estimation according to:

$$\hat{\mathbf{R}} = \mathbf{R} \otimes \mathbf{E}^{*} \tag{6.22}$$

This frequency domain compensation is equivalent to the multiplication with the complex conjugate phase noise process in time.

For each subcarrier i the optimal MIMO detector tries to find a valid symbol vector that has been sent with the highest a-posteriori probability conditioned on modified received symbol vector. In the following the subcarrier index i is dropped to increase readability. The L-value of a certain bit $X_{tx,m}$, with m defining one bit in one symbol, is now defined as:

$$\begin{aligned} L\left(X_{tx,m} \mid \hat{\mathbf{R}}\right) &:= \ln \frac{\mathrm{P}\left[X_{tx,m} = +1 \mid \hat{\mathbf{R}}\right]}{\mathrm{P}\left[X_{tx,m} = -1 \mid \hat{\mathbf{R}}\right]} \\ &= \ln \frac{\sum_{\mathbf{X} \in \mathrm{X}_{tx,m+1}} \mathrm{p}(\hat{\mathbf{R}} \mid \mathbf{X}) \cdot P[\mathbf{X}]}{\sum_{\mathbf{X} \in \mathrm{X}_{tx,m-1}} \mathrm{p}(\hat{\mathbf{R}} \mid \mathbf{X}) \cdot P[\mathbf{X}]} \end{aligned} \tag{6.23}$$

where for the second equality sign the Bayes'theorem was applied as well as the assumption of mutually independent bits. The MIMO channel introduces interference among the transmitted signals at the receiver. The conditioned probability density represents the channel influence and is given by the multidimensional Gaussian distribution

$$\mathrm{p}\left(\mathbf{R} \mid \mathbf{S}\right) = \frac{1}{\pi^{Rx} \det\left(\mathbf{\Phi}_{\varepsilon\varepsilon}\right)} \exp\left(-\left(\hat{\mathbf{R}} - \mathbf{HS}\right)^{\mathrm{H}} \mathbf{\Phi}_{\varepsilon\varepsilon}^{-1} \left(\hat{\mathbf{R}} - \mathbf{HS}\right)\right) \tag{6.24}$$

For the L-value computation only the exponential term is relevant – the constant scaling factor cancels out. The second term represents the a-priori knowledge fed into the detector from the outer decoder and is zero at the first iteration. An efficient way to compute the numerator and denominator in of the L-value is to use the so called max-Log approximation. The L-value can therefore be approximated as:

$$\begin{aligned} L\left(x_{tx,m} \mid \hat{\mathbf{R}}\right) \approx & \max_{\mathbf{X} \in \mathrm{X}_{+1}} \left\{ -\left(\hat{\mathbf{R}} - \mathbf{HS}\right)^{\mathrm{H}} \mathbf{\Phi}_{\varepsilon\varepsilon}^{-1} \left(\hat{\mathbf{R}} - \mathbf{HS}\right) + \ln \mathrm{P}\left[\mathbf{x}\right] \right\} \\ & - \max_{\mathbf{X} \in \mathrm{X}_{-1}} \left\{ -\left(\hat{\mathbf{R}} - \mathbf{HS}\right)^{\mathrm{H}} \mathbf{\Phi}_{\varepsilon\varepsilon}^{-1} \left(\hat{\mathbf{R}} - \mathbf{HS}\right) + \ln \mathrm{P}\left[\mathbf{x}\right] \right\} \end{aligned} \tag{6.25}$$

However, even with these simplifications, the computational complexity of the L-value computation is exponential in the number of antennas times the number of bits per symbol. In terms of equalization the most straight forward way to find a suboptimal solution for the closest point problem is to directly invert the channel matrix **H** in order to approximate the original signal that has been sent. This is done by discretisation of the filter output of the so called zero forcing (ZF) equalizer to the values that represent a valid signal. The main advantage of this scheme is that the interference between the signals transmitted over different antennas is totally cancelled out.

However, the main drawback of this approach is that the noise vector is multiplied with the inverted channel matrix. Especially, if the channel is almost singular, this scheme will lead to a strong amplification of the remaining noise, leading to a bad overall detection performance. In order to mitigate this problem it is possible to design a filter matrix **G** with the aim of maximizing the SINR at the filter output. One possible solution is to minimize the mean square error (MSE) between the originally sent signal and the estimated signal leading to the well known (linear) minimum mean squared error equation:

$$\mathbf{G} = \arg\min_{\mathbf{G}} E\left\{ \left\| \hat{\mathbf{S}} - \mathbf{S} \right\|^{2} \right\} \tag{6.26}$$

The solution of this minimization problem is given by the following equation:

$$\mathbf{G}_{MMSE} = \left(\mathbf{\Phi}_{\mathbf{ss}}^{-1} + \mathbf{H}^{H} \mathbf{\Phi}_{\varepsilon\varepsilon}^{-1} \mathbf{H} \right)^{-1} \cdot \mathbf{H}^{H} \mathbf{\Phi}_{\varepsilon\varepsilon}^{-1} \tag{6.27}$$

where $\mathbf{\Phi}_{\mathbf{ss}} = E\{\mathbf{s} \cdot \mathbf{s}^{H}\} = E_s / N_{tx} \cdot \mathbf{I}$ and $\mathbf{\Phi}_{\varepsilon\varepsilon}$ describes the transmit signal covariance matrix and the noise covariance matrix respectively. Since the MMSE solution provides a trade-off between noise amplification and interference reduction between the signals transmitted over different antennas, the estimated symbol $\hat{\mathbf{s}}$ is not unbiased anymore, i.e.:

$$\mathbf{G}_{MMSE} \cdot \mathbf{H} \neq \mathbf{I} \tag{6.28}$$

which leads to a scaling of the decision region in the constellation diagram. This is not a problem for (uncoded) transmission of M-PSK or QPSK. However, the WINNER system uses high order modulation schemes in combination with coding and therefore the impact of the bias has to be considered. For that purpose the filter matrix $\mathbf{G}_{\mathrm{MMSE}}$ has to be modified by a diagonal matrix and finally leading to a new filter matrix given as:

$$\mathbf{G}_{UB} = diag\left(diag^{-1}\left(\mathbf{G}_{MMSE}\cdot\mathbf{H}\right)\right)\cdot\mathbf{G}_{MMSE} \tag{6.29}$$

Using the MMSE approach in a coded environment, the knowledge of the SINR at each layer is of essential importance for the computation of the soft values. Hence, for each layer the SINR is given as the diagonal elements of the error covariance matrix, i.e.

$$SINR_{tx} = \frac{1}{\left(\left(\mathbf{\Phi}_{\mathbf{ss}}^{-1} + \mathbf{H}^{H}\mathbf{\Phi}_{\boldsymbol{\varepsilon\varepsilon}}^{-1}\mathbf{H}\right)^{-1}\mathbf{\Phi}_{\mathbf{ss}}^{-1}\right)_{tx,tx}} - 1 \tag{6.30}$$

As a conclusion, the linear MMSE approach leads to a lower likelihood of performing a wrong detection than the solution obtained by linear ZF equalization.

6.4 Phase Noise Suppression for DFT-Precoded OFDM (Serial Modulation)

6.4.1 Case of no adjacent channel interference

It was pointed out in [WIN1D22], Section 2.1.1.7, that frequency offset and phase noise cause affect the receiver output in serial modulated systems in a different (and more easily-correctable) way than in parallel modulated systems like OFDM. Whereas these impairments cause inter-symbol interference in multicarrier systems, as well as a common phase rotation, they simply cause a slowly varying phase rotation to single carrier (DFT-precoded OFDM) data symbols, which can be easily estimated, tracked and compensated. Figure 6-6 taken from [WIN1D23], illustrates the phase error at the time domain output of a linear frequency domain equalizer in a serial modulation system, with a frequency offset equal to 10% of the inter-subcarrier spacing. It is an almost linear variation in time, with a slope proportional to the frequency offset. There are outliers on the ends, whose effects could be eliminated by not transmitting data on those few symbols, or by extrapolation of the linear slopes towards the edges.. A simple decision-directed technique can easily predict this slow variation of the phase error, enabling it to be corrected.

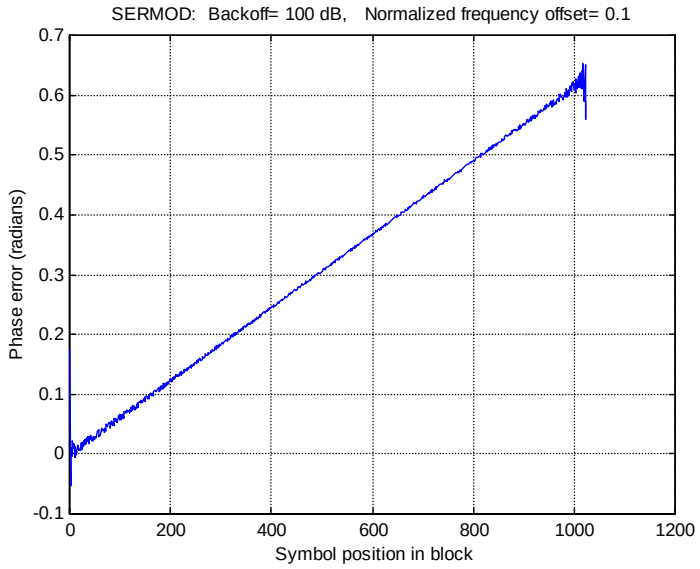

Figure 6-6 Output phase error variation over a 1024-symbol block for serial modulation. Signal is subject to frequency offset equal to 10% of inter-subcarrier spacing.

Phase noise would trace a similar trajectory, but with a slowly and smoothly varying profile instead of the linear increase or decrease of frequency offset. Thus the symbol rate-sampled time domain signal at the equalizer output can be modelled as

$$r_n = c_n e^{j\phi_n} + w_n = c_n e^{j(n\theta + \sum_{k=1}^{n} \varepsilon_k)} + w_n \quad \text{for } n=0,1,..N_{fft}\text{-}1 \tag{6.31}$$

where $\{ w_n \}$ represents uncorrelated Gaussian noise samples, N_{fft} is the DFT size, c_n is the n^{th} transmitted data symbol, $\theta = \frac{2\pi\delta f T}{N}$, δf represents the frequency offset, and $\{\varepsilon_k\}$ are the Gaussian Brownian motion increments of the phase noise process.

The time-varying phase process $\{\phi_n\}$ can be tracked with a second order soft decision directed phase locked loop (PLL), which uses log likelihood ratio (LLR) information from a turbo equalizer. For QPSK, the PLL update at the kth data symbol period is, for ($k = 1,...,N$ and $\phi_i = 0$ for $i \le 0$):

$$\begin{aligned} \phi_k &= \phi_{k-1} + \alpha_1(\phi_{k-1} - \phi_{k-2}) \\ &+ \alpha_2 \frac{\mathrm{Im}\left(r_{k-1}^* e^{j\phi_{k-1}+\frac{\pi}{4}}\right)\sinh\left(t_{R,k-1}\right) + \mathrm{Im}\left(r_{k-1}^* e^{j\phi_{k-1}-\frac{\pi}{4}}\right)\sinh\left(t_{I,k-1}\right)}{\cosh\left(t_{R,k-1}\right) + \cosh\left(t_{I,k-1}\right)} \end{aligned} \tag{6.32}$$

where $t_{R,k}$ and $t_{I,k}$ are defined as:

$$t_{R,k} = \frac{\lambda_{Rk}}{2} + \frac{\lambda_{Ik}}{2} + \frac{2\sqrt{2}}{\sigma_n^2}\mathrm{Re}[r_k^* e^{j\phi_k+\frac{\pi}{4}}] \tag{6.33}$$

$$t_{I,k} = \frac{\lambda_{Rk}}{2} - \frac{\lambda_{Ik}}{2} + \frac{2\sqrt{2}}{\sigma_n^2}\mathrm{Re}[r_k^* e^{j\phi_k-\frac{\pi}{4}}], \tag{6.34}$$

α_1 and α_2 are PLL constants, designed for stability and PLL bandwidth, and λ_{Rk} and λ_{Ik} are respectively the LLRs of the real and imaginary parts of the decoder output.

Simulation results for this approach are shown in [WIN1D22].

6.4.2 Case of adjacent channel interference

The above discussion was for the case where no other user signals occupy immediately adjacent subcarriers. If there are adjacent users, frequency offset and phase noise, which cause inter-subcarrier interference, will obviously cause interference between user signals occupying adjacent subcarriers. Assuming that interference-causing adjacent channel signals are from the same cell or sector, their average received powers will be equal due to power control, and the effect of the adjacent channel interference will be similar to that of same-signal inter-subcarrier interference detailed in 6.3.3. For full band transmission the adjacent channel interference will be mostly concentrated on the subcarriers located at the band edge, and so the effect should be relatively minor. The types of signals most vulnerable to the adjacent channel interference would be those in which different users' signals are interleaved in frequency, such as IFDMA and B-IFDMA. Explicit attempts to compensate would be complicated because each adjacent channel interfering signal will in general have different phase noise and frequency offset. [WIN1D22] includes simulation results showing the effects of uncompensated frequency offset and phase noise on multi-user IFDMA signals.

6.5 SNR Degradation due the Interference

Appendix L derives analytical expressions for SNR degradation due to inter-block interference (IBI) and inter-carrier interference (ICI).

6.6 Conclusions

In the first part of this section the effect of HPA nonlinearity on full band OFDM, DFT-precoded OFDM, IFDMA, B-IFDMA and B-EFDMA signals was evaluated by means of HPA output power spectrum measurements, which are usually more indicative of required power backoff than are signal to nonlinear

distortion ratios. DFT-precoded OFDM, IFDMA and B-IFDMA require less power backoff than OFDM and B-EFDMA. Required backoff is also reduced for all modulations by using a high quality (linear below the saturation level) or an adaptively linearized power amplifier. Also, adaptive resource partitioning for frequency adaptive transmission was found to only reduce the required backoff to comply with the spectral mask

In the second part of this section soft information based equalisation is proposed for iterative phase noise correction in MIMO-OFDM transmission. It is demonstrated that this leads to a more reliable estimate of the instantaneous realisation of the phase noise process. Compared to conventional CPE correction an improved LMMSE estimation of higher order components is introduced. The result is that the bit and frame error floors could be substantially reduced. For serial modulation, correction of in-band frequency offset and phase noise is easier than for OFDM since these impairments directly and slowly affect each output time domain data symbol. Thus simple decision-directed phase estimation can be used. Such a decision-direct procedure applied within a turbo equaliser is described and evaluated. The system can now handle quite severe phase noise and frequency offset.

Finally, an analytic expression of the SNR degradation due to interference is given in Appendix L. Curves showing SNR degradation values for different timing and frequency synchronisation errors are presented.

7. Link Level Synchronisation

7.1 Introduction

Link level synchronisation is an important issue in OFDM transmission. Link level synchronisation can be divided into the following categories:

- time synchronisation, further subdivided into:
  - frame synchronisation,
  - symbol synchronisation,
- frequency synchronisation, further subdivided into:
  - carrier frequency synchronisation,
  - carrier phase synchronisation.

Taking into account the WINNER MAC frame structure, synchronisation algorithms specific for packet or bursty transmission have to be applied.

In this chapter link layer synchronisation procedures for WINNER system are developed. Two scenarios are considered:

- a scenario in which WINNER system does not suffer from any outer world interference which corresponds to the exclusive operation of WINNER in the assigned frequency band and
- a scenario in which WINNER system is affected by some narrowband interference sources, e.g., as in the case of licence-exempt bands or multi-band operation in which several non-continuous frequency bands exist between which other systems emit.

In the next sections it is assumed that the system of interest uses OFDM symbols each with N subcarriers out of which N_U subcarriers are used for data symbol transmission. The time domain samples are given by

$$x_i(n) = \frac{1}{\sqrt{N}} \sum_{k=0}^{N_U-1} X_{i,k} e^{j \cdot \omega_N k \cdot n} \tag{7.1}$$

where i is the index of the OFDM symbol, $X_{i,k}$ is the k-th modulated symbol in frequency domain, and $\omega_N = \frac{2\pi}{N}$.

Section 7.2 describes WINNER reference design of synchrobnisatin preamble. Section 7.3 and 7.4 describe link layer synchronisation algorithms suitable for a scenario in which WINNER system does not suffer from any outer world interference and scenario in which it is affected by outer world interference. Finally, Section 7.5 presents conclusions.

7.2 Reference Design of Synchronisation Preamble

In this section, the reference design of synchronisation preamble is presented. Time and frequency synchronisation should be performed during DL Synch slot in the WINNER MAC super-frame.. The first symbol of the slot, called *T-Pilot*, is dedicated for time and frequency synchronisation and its design must be appropriate for the chosen synchronisation algorithm.

Coarse and fine time and frequency synchronisation algorithms utilize first OFDM symbol of *DL Synch* time slot named *T-Pilot* whose time domain structure is illustrated in.

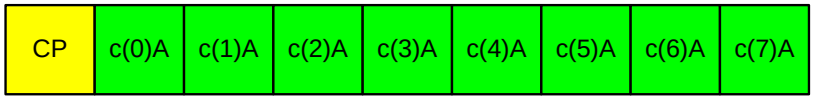

Figure 7-1: Preamble structure defined in 802.16d

The samples $c(m)$ modify the signs of A symbols, and their vector form is defined as follows

$$\mathbf{c} = [c(0), c(1), c(2), c(3), c(4), c(5), c(6), c(7)] = [-1, 1, 1, 1, 1, 1, 1, 1] \tag{7.2}$$

In order to create such preamble, pilot tones should be transmitted on every eighth subcarrier, named here active subcarriers, among all used subcarrier. Moreover some active subcarriers are excluded to ease integer frequency offset estimation. The example of T-Pilot design in the frequency domain is shown in Figure 7-2.

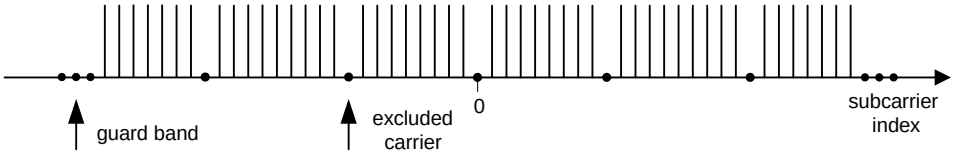

Figure 7-2 The subcarrier power pattern of the T-Pilot. Only every eighth subcarrier is shown. The rest is set to 0.

The preamble should not only have good correlation properties but also low Power-to-Average-Power Ratio (PAPR). The lowest PAPR of the preamble was achieved using Gold sequence of degree 9 and shift registers which states were initiated by 247_{oct} and 503_{oct}. Indices of excluded subcarriers were found using PAPR reduction algorithm [SS06]. The algorithm finds pilot tones that have the greatest influence on PAPR. Those pilots are excluded form the pattern and not predistorted as in original version of the algorithm. The following set of excluded pilot tones indices minimising PAPR was found

$$40, 384, 392, 408, 568, 1480, 1640, 1664, 2008 \tag{7.3}$$

for indoor and micro-cellular scenarios, and

$$88, 96, 264, 464, 488, 1560, 1584, 1784, 1952, 1960 \tag{7.4}$$

for urban scenario. The PAPR of designed preamble is equal to 5.98 dB.

7.3 Link Level Synchronisation: Licensed Case

7.3.1 Coarse symbol timing synchronisation

In order to perform the coarse timing synchronisation only four A symbols of preamble presented in Figure 7-2 are used. The following time metric is applied

$$M(d) = \frac{\left| \frac{1}{3} \sum_{m=0}^{2} c(m) \sum_{n=0}^{L-1} \left[r(d-n-(3-m)L) r^*(d-n-(2-m)L) \right] \right|^2}{\left(\sum_{n=0}^{L-1} |r(d-n-L)|^2 \right)^2} \tag{7.5}$$

where $L = \frac{1}{8} N$. In the above formula the numerator is an averaged value of three cross-correlations computed between four consecutive sample blocks of length L. Thus, it realises noise averaging improving the quality of the time metric. The shape of the time metric calculated with (7.5) and the *T-Pilot* (Figure 7-2) is presented in Figure 7-3

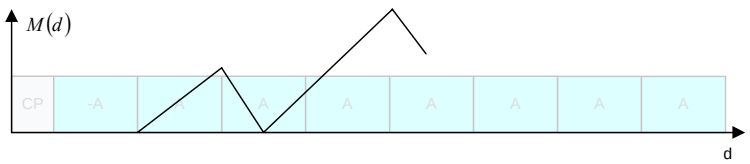

Figure 7-3 The shape of the time metric

In order to detect the second peak of the time metric (7.5) the metric is compared with a detection threshold Γ_m. The middle of the OFDM symbol, i.e. the maximum value of the time metric, is found among all time metrics greater than the detection threshold. Thus, the beginning of the next OFDM symbol is estimated with the following formula

$$\hat{\theta} = \arg\max_{d}\left(M\left(d\right)\right) + N/2, \text{ for } M\left(d\right) > \Gamma_m \tag{7.6}$$

Detection of the maximum value of (7.5) ends coarse timing synchronisation stage. However, fine frequency synchronisation should be performed yet.

7.3.2 Fractional and integer frequency offset estimation

The process of the frequency synchronisation consists of two elements: frequency estimation and frequency correction. A general frequency estimation scheme is shown in Figure 7-4

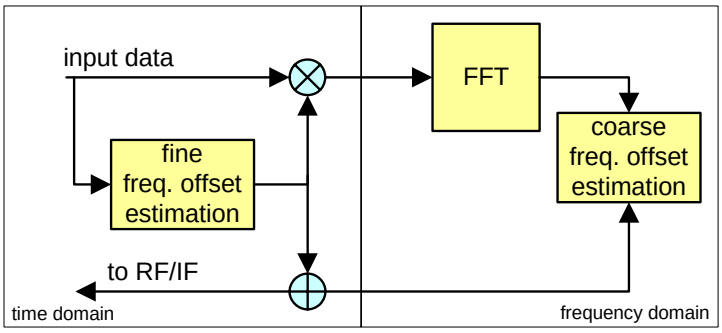

Figure 7-4 Frequency estimation in the time and frequency domains

Having a preamble of the form shown in Figure 7-2 at the beginning of each super-frame we are able to estimate the frequency offset using the same procedure as in timing estimation. This time the argument of the correlation between two subsequent pilot symbols determines the frequency offset, i.e.

$$\gamma(m) = \sum_{n=m}^{m+L-1} r\left(n\right) r^{*}\left(n+L\right) \tag{7.7}$$

$$\hat{\delta f} = \frac{1}{2\pi L}\arg(\gamma(\hat{\theta})) + l\Delta f \tag{7.8}$$

where $\hat{\theta}$ is the estimated symbol timing. Calculating the argument of the correlation function as the basis of the frequency offset estimation we get frequency offset ambiguity due to the fact that the argument is calculated modulo π. Thus, such an algorithm is able to estimate only a fractional part of the frequency offset, whereas its integer part $l\Delta f$ in terms of the multiples of the currently used subcarrier distance Δf must be estimated in another way. The distance between the used subcarriers in the pilot symbols of type A is (Figure 7-2) equal to $8\Delta f$ (assuming every subcarrier of every pilot symbol is used), so $\pm 4\Delta f$ is the maximum frequency offset which can be estimated. The shorter the pilot symbols that are used the wider the range of the frequency offset that is possible to estimate in the time domain. However, shortening the pilots degrades the estimation quality which is achieved during cross-correlation of the pilot symbols. The quality of the frequency offset estimate can be improved by extending the correlation window over two A pilots. Hence, the range of the frequency offsets possible to be estimated is shortened to $\pm 2\Delta f$. The desired frequency offset estimate is achieved after five A pilots, due to the fact that the sign of the first pilot is negated. Thus, the frequency offset estimation quality can be further improved by averaging estimates computed during last three pilot symbols, i.e.

$$\gamma_{2L} = \sum_{n=m}^{m+2L-1} r\left(n\right) r*\left(n+2L\right) \tag{7.9}$$

$$\Delta\hat{f}_A = \frac{1}{A4\pi L}\sum_{n=0}^{A-1}\arg\left(\gamma_{2L}\left(\hat{\theta} - N/2\right)\right) + l\Delta f \tag{7.10}$$

After correcting the fractional part of the frequency offset the integer part can be estimated. The integer frequency offset $l\Delta f$ is equal to an integer multiple of four subcarrier distances Δf . Thus, in order to estimate the remaining frequency offset, a *N/4*-point FFT should be performed on the *T-Pilot*. The resulting frequency-domain symbol will contain every fourth subcarrier only. In case of the *T-Pilot* design presented in Figure 7-2 $N/4 = 2L$, thus, three different blocks of samples $\mathbf{b}_i$ shown in Figure 7-5 can be

used. In order to avoid IBI the last block is shifted *G* samples from the estimated end of the *T-Pilot*. The value of the *G* parameter should be at least the same as the maximum timing synchronisation error.

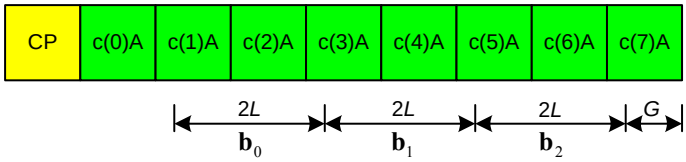

Figure 7-5: Time averaging of A pilot symbols

Before FFT is performed the samples from $\mathbf{b}_i$ blocks are summed averaging the noise, i.e.

$$\mathbf{X}_d = \mathbf{F}\left(\sum_{i=0}^{2}\mathbf{b}_i\right) \tag{7.11}$$

where $\mathbf{X}_d$ is a vector containing every fourth subcarrier and $\mathbf{F}$ is a matrix of Fourier transform coefficients. Next the integer frequency offset is estimated. The estimator block diagram is presented in Figure 7-6

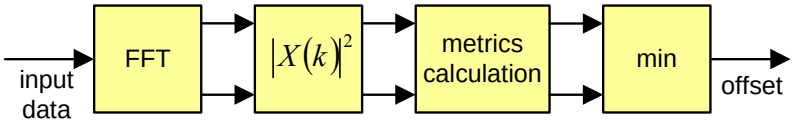

Figure 7-6: Integer part frequency offset estimation

It is possible to create a specific subcarrier pattern in the frequency domain by exclusion of some extra subcarriers in the OFDM pilot symbol, e.g. as shown in Figure 7-2.Knowing this pattern the receiver is able to correlate the instantaneous powers of the received signal samples in the frequency domain with the known pattern and select that set of bins of the FFT demodulator which minimises a cost function [Dlu03],[DW02]. A few cost functions have been investigated for that purpose and in [Dlu03] and [DW02] it is shown that the best cost function is given by

$$M_F(l) = \sum_{\substack{k=-N/2;\\ k\ \text{unused}}}^{N/2-1} \left|X_d(k+l)\right|^2 - \sum_{\substack{j=-N/2;\\ j\ \text{used}}}^{N/2-1} \left|X_d(j+l)\right|^2, l \in \langle -FO, FO\rangle \tag{7.12}$$

where *FO* is assumed maximum frequency offset. In (7.12) the power of used and unused subcarriers on the FFT output for the pilot symbol is calculated. The power of the unused subcarriers has a weighting factor equal to one, whereas the used subcarriers have a weighting factor equal to –1. Note that instantaneous power of each FFT output bin is taken into account in finding the minimum of the cost function. The frequency offset estimation method is blind and "one-shot" and turned out to be very robust against selective fading notches if some carefully selected subcarriers are additionally excluded [Dlu02]. It is also relatively robust against the fractional offset estimation inaccuracy performed in the time domain. After successful frequency offset estimation the frequency correction algorithm simply selects the appropriate subset of the FFT output bins.

7.3.3 Fine symbol timing synchronisation

After coarse symbol timing synchronisation the symbol timing error is equal to

$$e = \hat{\theta} - \theta \tag{7.13}$$

where θ is the ideally estimated start of the OFDM symbol. The error e causes a phase offset in frequency domain and if e is large enough it also causes IBI.

The fine symbol timing synchronisation can be realised by an Energy Detection (ED) algorithm using pilot symbols $p_{i,k}$ multiplexed into *i*-th OFDM symbol on certain subcarriers *k* [YLCC00], [NP02]. First, the least square (LS) estimates of the channel frequency response at pilot subcarrier frequencies are estimated. Let us denote $\hat{p}_{i,k}$ as the *k*-th received pilot tone in the *i*-th OFDM symbol. The channel estimate is given by

$$\widetilde{H}_{i,k} = \frac{\hat{p}_{i,k}}{p_{i,k}},\ k = 0,...,K-1 \tag{7.14}$$

where K is the number of used pilot tones. After applying the Hamming window and zero padding, a $2K$-point IFFT is applied to the channel frequency response in order to obtain the channel impulse response

$$\widetilde{h}_{i,m} = \frac{1}{2K}\sum_{k=0}^{K-1}\widetilde{H}_{i,k}\omega(k)e^{j2\pi\frac{mk}{2K}}, \quad m = 0,..., 2K-1 \tag{7.15}$$

where $\omega(k)$ are the samples of a Hamming window (which is used for reducing IFFT output leakage). Finally the power delay profile $\widetilde{S}_m$ is calculated

$$\widetilde{S}_m = \left|\widetilde{h}_m\right|^2, m = 0,..,2K \tag{7.16}$$

The estimate of the symbol timing error e is computed using the index m of the maximum of the power delay profile as the strongest path delay

$$\widetilde{e} = -\frac{1}{2}\arg\max_m\left(\widetilde{S}_m\right) \tag{7.17}$$

Alternatively, the estimate of the symbol timing error can be computed using the index m of the power delay profile value exceeding desired threshold

$$\begin{aligned}\lambda &= \left(\max_m\left(\widetilde{S}_m\right) - \min_m\left(\widetilde{S}_m\right)\right)\cdot\alpha \\ \widetilde{e} &= -\frac{1}{2}\arg_m\left(\widetilde{S}_m > \lambda\right)\end{aligned} \tag{7.18}$$

where α is a scaling factor. The integer part of the estimate $\widetilde{e}$ is used for correcting the FFT window position and the fractional part of $\widetilde{e}$ is used for the phase shift of the input data in the sampling time error correction algorithm.

Simulation results of both time and frequency synchronisation algorithms, as well as tests results of the performance degradation due to narrowband interference (NBI) are presented in Appendix I.

7.4 Link Level Synchronisation: License-Exempt and Spectrum Sharing Cases

Multi-carrier spectrum sharing systems derive their denomination from the fact that they operate over a bandwidth where other narrowband interference (NBI) signals are allocated. The effect of strong NBI is such that the common approach of using a dedicated training block composed of several repeated parts for timing and frequency acquisition would experience significant degradations in a spectrum sharing system. When NBI is present the signal received over the preamble is not any more symmetrical in time domain making it difficult to apply conventional synchronisation algorithms. Thus, in order to achieve good synchronisation in a spectrum sharing scenario, it is necessary to explicitly take care of NBI.

In the following, to cope with NBI, we pursue the following approach: in the frequency domain we estimate what are the subcarriers occupied by narrowband sources and then we suppress the NBI by setting to zero all interfered sub-carriers.

7.4.1 Observed Scenarios

The synchronisation algorithm developed in this section is suitable for several spectrum sharing scenarios: horizontal sharing (HS) with or without coordination and vertical sharing (VS) scenario. For more details about HS and VS definitions please refer to [WIN2D61311]. Figure 7-7 and Figure 7-8 illustrate spectrum allocation in considered scenarios. HS without coordination corresponds to the license-exempt scenario in which minimal coordination between spectrum sharing systems is done.

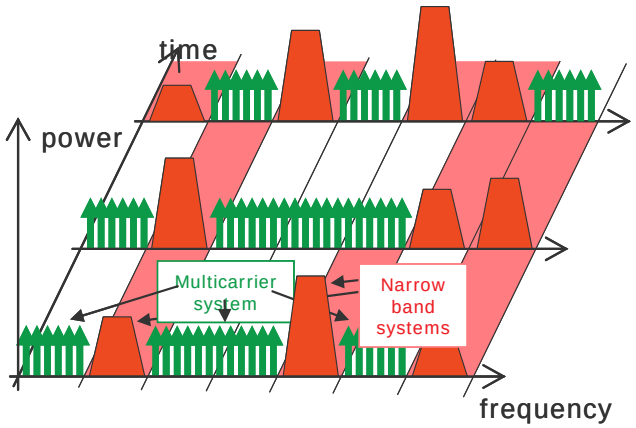

Figure 7-7: Example of multi-carrier WINNER system and narrow-band spectrum sharing systems co-existing in HS scenario with coordination or VS scenario.

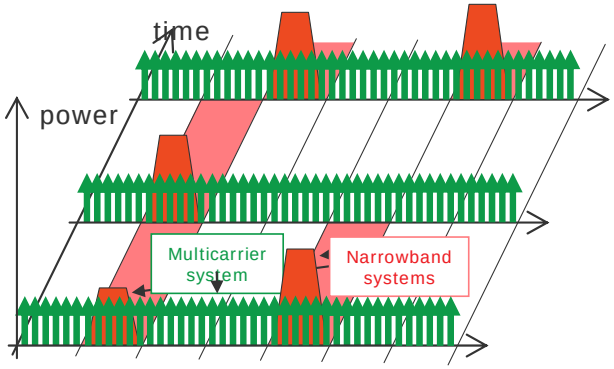

Figure 7-8: Example of multi-carrier WINNER system and narrow-band spectrum sharing systems co-existing in HS scenario without coordination – license-exempt case.

7.4.2 Synchronisation Method for Spectrum Sharing Use

A preamble block composed of 3*N* time domain samples, corresponding to 3 OFDM symbols is used to perform the following operations: detection of NBI sources, timing synchronisation and carrier frequency offset estimation.

After the NBI sources have been detected (NBI detection phase) and the interfered sub-carriers have been set to zero (NBI cancellation phase), the virtually interference-free time domain samples of the preamble are fed to the synchronisation unit. The block diagram of the receiver is shown in Figure 7-9.

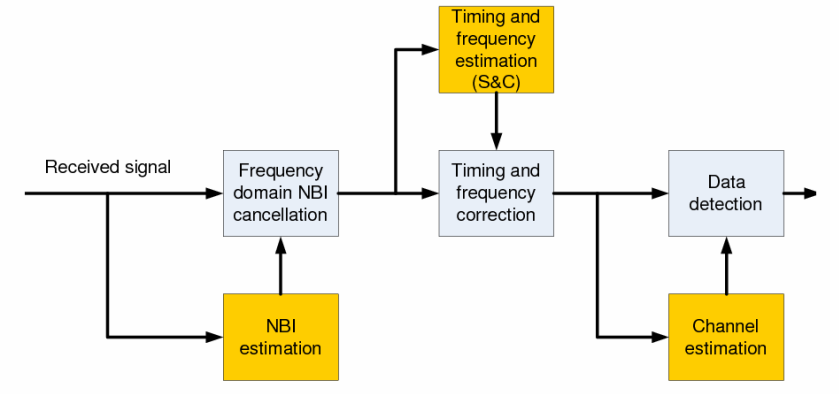

Figure 7-9: Receiver block diagram.

The preamble of length 3*N* is foreseen in preamble part of superframe and its structure is represented in Figure 7-10. It is divided in two half blocks of size 3*N*/2 symbols each. Note having two identical blocks of this size enables robustness to frame-synchronisation errors of up to *N*/2, reduction of size of identical halves would reduce robustness to frame-synchronisation errors. The first half block contains the

sequence $\{b_1(n)\}, n = 1,\ldots,3N/2$ and the second half block contains the sequence $\{b_2(n)\}, n = 1,\ldots,3N/2$, which is a replica of $b_1(n)$ rotated by a frequency corresponding to the subcarrier spacing $\Delta f = 1/(NT)$, i.e.

$$b_2(n) = b_1(n)e^{j\frac{2\pi m}{N}} \tag{7.19}$$

Thus, indicating with $s(n)$ the time domain samples (tds) transmitted in the preamble, it is

$$s(n) = \begin{cases} b_1(n) & n = 1,...,3N/2 \\ b_2(n-3N/2) & n = 3N/2+1,...,3N \end{cases} \tag{7.20}$$

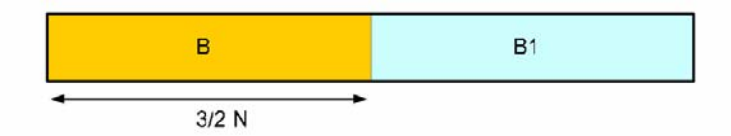

Figure 7-10: Proposed DL synchronisation preamble structure.

7.4.2.1 NBI Detection

The NBI detection algorithm relies on the specific structure of the preamble, which has been built to make the NBI detection algorithm robust to frame-synchronisation error θ up to *N*/2. At the receiver the tds of the preamble are grouped in two *N*-dimensional blocks $\mathbf{r}^{(0)} = [r(1),\ldots,r(N)]^T$ and $\mathbf{r}^{(1)} = [r(1+3N/2),\ldots,r(N+3N/2)]^T$ where $r(n)$ is defined as

$$r(n) = x_\theta(n) + i(n) + n(n) \tag{7.21}$$

where $x_\theta(n)$ is the useful signal at the receiver delayed by θ samples and $i(n)$ are the time samples of NBI signal.

Neglecting noise and carrier frequency offset, $R^{(0)}(m)$, the *m*-th outcome of the DFT of $\mathbf{r}^{(0)}$, is

$$R^{(0)}(m) = H(m)S_\theta^{(0)}(m) + I^{(0)}(m), 0 \le \mathrm{m} \le \mathrm{N}\text{-}1 \tag{7.22}$$

and $R^{(1)}(m)$, the *m*-th outcome of the DFT of $\mathbf{r}^{(1)}$, is

$$R^{(1)}(m) = H(m)S_\theta^{(1)}(m) + I^{(1)}(m), 0 \le \mathrm{m} \le \mathrm{N}\text{-}1 \tag{7.23}$$

where $S_\theta^{(0)}(m)$ is the *m*-th output of the DFT of the vector $\mathbf{s}_\theta^{(0)} = [s(1-\theta),...,s(N-\theta)]^T$, $S_\theta^{(1)}(m)$ is the *m*-th output of the DFT of the vector $\mathbf{s}_\theta^{(1)} = [s(1+3N/2-\theta),...,s(N+3N/2-\theta)]^T$ and $I^{(0)}(m)$ and $I^{(1)}(m)$ are the DFT of the NBI in the two vectors. The channel *H*(*m*) is assumed constant for the duration of the whole preamble.

Since the preamble is built with two sequences that are rotated with respect to each other of a frequency exactly equal to the sub-carrier spacing, there is a cyclic shift of a position between $S_\theta^{(0)}(m)$ and $S_\theta^{(1)}(m)$, i.e.

$$S_\theta^{(1)}(m) = S_\theta^{(0)}(m-1) \tag{7.24}$$

The above property can be exploited to reveal the presence of NBI. The metric $\Lambda(m) = R^{(0)}(m) - R^{(1)}(m-1)$ is

$$\Lambda(m) = S_\theta^{(0)}(m)((H(m) - H(m-1))) + I^{(0)}(m) - I^{(1)}(m-1) \tag{7.25}$$

Assuming that the channel does not exhibit significant variations between adjacent sub-carriers, i.e. $H(m) \approx H(m-1)$, the desired signal is cancelled in previous equation resulting in

$$\Lambda(m) = I^{(0)}(m) - I^{(1)}(m-1) \tag{7.26}$$

Thus, in the following we compare $|\Lambda(m)|^2$ with an adequate threshold to detect the presence of NBI. Figure 7-11-Figure 7-14 show how the NBI detection algorithm works.

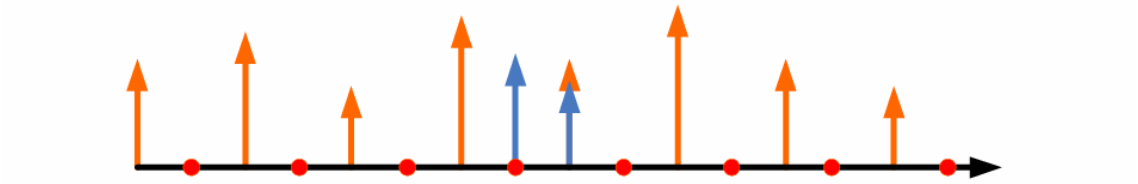

Figure 7-11: NBI detection: DFT of the first received block.

.

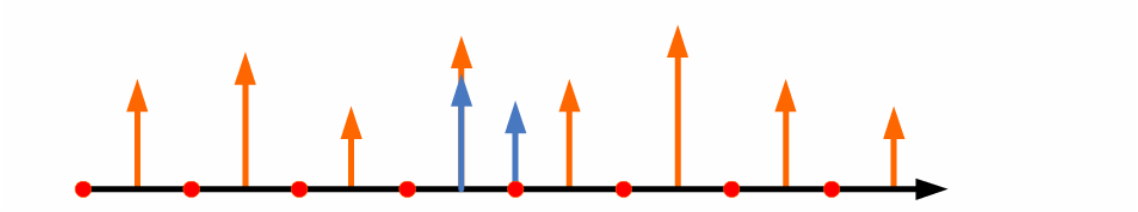

Figure 7-12: NBI detection: DFT of the second received block.

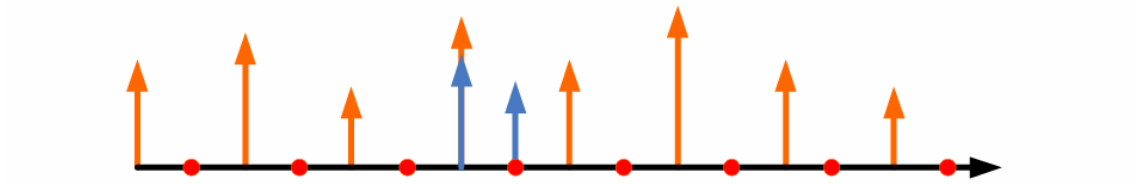

Figure 7-13: NBI detection: Back-shifted DFT of the second block.

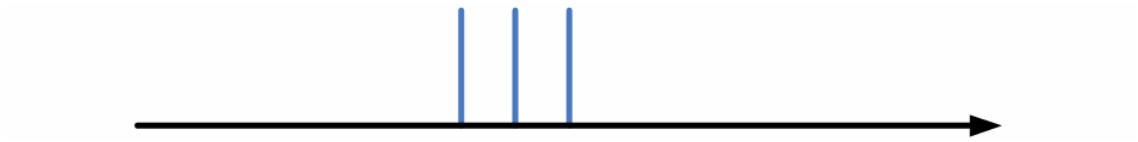

Figure 7-14: NBI detection: Interference detected.

7.4.2.2 Interference Detection in Presence of Carrier Frequency Offset

The synchronisation algorithm has to cope with larger offsets and can be easily adapted to be very robust to any frequency offset. The effect of a frequency offset ν is a fixed phase rotation $\phi = 2\pi\frac{3}{2}\nu$ between corresponding elements of the vectors $\mathbf{s}_\theta^{(0)}$ and $\mathbf{s}_\theta^{(1)}$. Thus being the DFT a linear operator, this fixed rotation phase translates also on $\mathbf{S}_\theta^{(0)}$ and $\mathbf{S}_\theta^{(1)}$ and it is

$$S_\theta^{(1)}(m) = S_\theta^{(0)}(m-1)e^{j\phi} \tag{7.27}$$

Therefore, to remove the effect of the phase offset ϕ, the metric $\Lambda(m)$ needs to be modified in

$$\Lambda(m) = \left|R^{(0)}(m)\right| - \left|R^{(1)}(m-1)\right| \tag{7.28}$$

As illustrated in Figure 7-11 – Figure 7-14, the NBI detection algorithm tends to detect the presence of interference also on the sub-carriers adjacent to those where actually NBI is. Therefore, the NBI cancellation algorithm will remove a number of sub-carriers slightly greater than what is effectively

needed, but this effect is compensated by the large number of sub-carriers in the WINNER system so that the system performance is hardly affected.

7.4.2.3 NBI Cancellation

Let Ψ be the set of the subcarriers that have been detected as interfered, interference is removed by setting to zero the sub-carriers in Ψ so that the timing synchronisation and the carrier frequency estimation algorithms can work reliably. Figure 7-15 shows how NBI cancellation is implemented:

C. The tds $r(n), n = 1, \ldots, N_1$ of the received signal are fed to a DFT device that yields $R(m), m = 1, \ldots, N_1$. The DFT length N_1 is chosen to include the whole synchronisation preamble, so that all the interference is removed at the same time.

- Most of the interference is removed by setting to zero all the subcarriers in Ψ. This operation yields $\tilde{R}(m), m = 1, \ldots, N_1$ such that

$$\tilde{R}(m) = \begin{cases} 0 & m \in \Psi \\ R(m) & \text{otherwise} \end{cases} \tag{7.29}$$

The symbols $\tilde{R}(m)$ are fed to an IFFT device to generate the virtually interference-free tds $\tilde{r}(n)$.

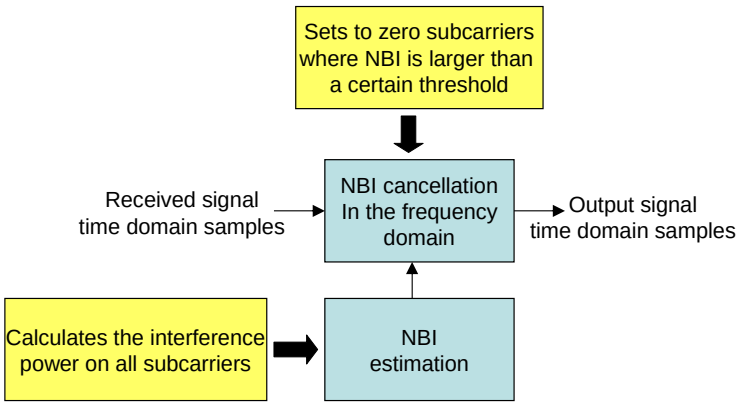

Figure 7-15: NBI cancellation block diagram.

7.4.2.4 Timing Synchronisation and Frequency Estimation

Symbol and timing estimation are performed according the algorithm proposed by Schmidl & Cox (S&C). Since we assume to have cancelled all the NBI, interference does not appear explicitly anymore in the received signal equations.

Signal synchronisation is performed using the same preamble block employed for NBI detection, composed by two semi-blocks of size 3*N*/2 tds each. As already mentioned (see (7.19)), the second semi-block contains the sequence $b_2(n)$ that is a replica of the sequence transmitted in the first semi-block $b_1(n)$ rotated by a frequency corresponding to the subcarrier spacing.

i. Timing estimation

Timing synchronisation is achieved by maximization of the timing metric $\Lambda(d) = |P(d)|^2 / R^2(d)$, i.e.

$$\hat{\theta} = \arg\max\{\Lambda(d)\}. \tag{7.30}$$

The difference with the standard S&C is that the tds of the second semi-block need to be counter-rotated before being correlated with the tds of the first semi-block and thus it is

$$P(d) = \sum_{n=0}^{N-1} \tilde{r}^*(n+d)\tilde{r}(n+d+3N/2)e^{-j2\pi n/N}. \tag{7.31}$$

while $R(d)$ normalizes the timing metric with respect to the energy received on the training symbol, i.e.,

$$R(d) = \sum_{n=0}^{N-1} \left| \tilde{r}(n+d) \right|^2 . \tag{7.32}$$

2) Frequency estimation

The frequency estimation algorithm has to deal with the frequency shift $\Delta f = 1/(NT)$ of the sequence $b_2(n)$ with respect to the sequence $b_1(n)$. In fact, after having estimated the correct timing, the *N*-leg correlation of the tds of the two semi-blocks yields

$$S = \sum_{n=0}^{N-1} \tilde{r}^*(n+\hat{\theta}) \tilde{r}(n+\hat{\theta}+3N/2) e^{-j2\pi n/N} = \sum_{n=0}^{N-1} \left| x(n) \right|^2 e^{j2\pi(3\nu/2+d_0/N)} + w_0 . \tag{7.33}$$

where $d_0 = \hat{\theta} - \theta$ introduces a bias on the frequency estimate. To overcome this problem in the following we assume that the 3*N*/2 tds of $b_1(n)$ are obtained as the three-fold repetition of a primary sequence $b_0(n)$ of *N*/2 tds, so that $b_1(n) = b_0(\mathrm{mod}(n, N/2))$. Exploiting the periodicity of the training sequence, the carrier frequency offset can be estimated as the mean of $\hat{\nu}_1$, the offset estimated on the first semi-block and $\hat{\nu}_2$, the offset estimated on the second semi-block. Thus, let S_1 and S_2 be the *N*/2-leg correlations of the tds of the first and second semi-block, respectively

$$S_1 = \sum_{n=0}^{N/2-1} \tilde{r}^*(n+\hat{\theta}) \tilde{r}(n+\hat{\theta}+N/2) = \sum_{n=0}^{N/2-1} \left| x(n) \right|^2 e^{j\pi\nu N} + w_1 . \tag{7.34}$$

and

$$S_2 = \sum_{n=0}^{N/2-1} \tilde{r}^*(n+\hat{\theta}+3N/2) \tilde{r}(n+\hat{\theta}+2N) = \sum_{n=0}^{N/2-1} \left| x(n) \right|^2 e^{j\pi(\nu+1)N} + w_2 . \tag{7.35}$$

Then, the offset calculated on the first semiblock is $\hat{\nu}_1 = \frac{1}{\pi} \arg\{S_1\}$ and the offset calculated on the second semi-block is $\hat{\nu}_1 = \frac{1}{\pi} \arg\{S_2\} - 1$ and an unbiased estimate of the frequency offset is

$$\hat{\nu} = \frac{\hat{\nu}_1 + \hat{\nu}_2}{2} . \tag{7.36}$$

Simulation results of both time and frequency synchronisation algorithm are presented in Section I.2 of Appendix I.

7.5 Conclusions

In this chapter two link level synchronisation algorithms designed for the WINNER system were introduced. First, the design of low-PAPR synchronisation pilot, termed T-Pilot-based design, of DL Synch slot was proposed together with synchronisation algorithm utilising its properties. Second, an algorithm suitable for application in presence of NBI is developed. The algorithms were tested in various WINNER scenarios and their complexity was also estimated.

Proposed T-Pilot-based synchronisation scheme gives accurate and reliable results if NBI is not present using only one OFDM symbol. Moreover initial channel estimates are computed. The complexity of this solution is smaller then the complexity of IFFT-2048 making it suitable for implementation.

In case when NBI is present, as available in license-exempt systems, T-Pilot-based scheme exhibits large degradations for low SIRs. However, in this scenario, second algorithm that is especially designed to detect and cancel presence of NBI shows much greater robustness than T-Pilot-based scheme. The price to pay for this improvement is that, in the case of the second algorithm, synchronisation preamble requires three symbols to function properly.

8. Self-Organised Network Synchronisation

8.1 Introduction

Slot synchronisation is an enabling component for the WINNER system. It helps producing higher throughput and is useful for coordination in higher layers. The problem of inter-cell slot synchronisation consists of aligning the timing reference of all nodes, so that base stations and user terminals agree on a common start of the super-frame. As direct communication among base stations is not always available in the WINNER concept and cooperation for network synchronisation among all network operators is not mandatory [WIN1D71], it is difficult to rely on a centralised approach to deploy a network slot synchronisation protocol. Thus a self-organised approach is preferred.

One interesting example of self-organised systems in nature has been observed in South-East Asia alongside riverbanks. At dawn, male fireflies gather on trees and synchronise their blinking. It seems as though the whole tree is flashing in perfect synchrony. Mirollo and Strogatz [MS90] derived a theoretical framework for the convergence to synchrony. In their model, which is presented in Section 8.2, no delays are considered between interactions, and nodes communicate through pulses.

The fundamental firefly synchronisation algorithm is extended in Section 8.3 to fit into the WINNER system. A self-organised network is considered, so no global coordination unit which manages the behaviour of base stations and user terminals is assumed. Synchronisation is defined in the sense of aligning local timing units, such that all nodes agree on the beginning and end of a super-frame.

To properly adapt the model of [MS90] to the WINNER concept, the given super-frame structure needs to be respected, which calls for an adaptation of the model, so that two groups form, one composed by base stations and the other by user terminals, and each group helps the other to synchronise.

Thanks to the proposed strategy, the network is able to synchronise starting from any misalignment. When misalignments are not too large, a tracking phase is introduced to limit the listening time of user terminals and save battery consumption. The time needed for the network to synchronise is evaluated through simulations, and results are presented for the local area and metropolitan area scenarios in Appendix J. Furthermore modifications to the presented scheme are presented to include relays, to impose a global reference onto the entire network, which is necessary for cellular networks, and to compensate for propagation delays. In Appendix J.3 simulation results examine the synchronisation accuracy in the wide area scenario.

8.2 Firefly Synchronisation

A firefly is modelled as a pulse oscillator that flashes periodically and interacts with other nodes through pulses. This class of oscillators is termed *pulse-coupled oscillators*. These systems are known to show interesting phenomena ranging from perfect synchrony to pattern formation [GDGLP00].

This section describes how time synchronisation is achieved between pulse-coupled oscillators, i.e. all oscillators pulse simultaneously. First, a mathematical model is associated with these oscillators. Then the scheme and conditions for a system of N oscillators to synchronise are presented.

Mathematical Model

As a simple mathematical representation, a pulse-coupled oscillator is described by its phase function $\phi_i(t)$. This function evolves linearly over time from 0 to a threshold value, which is normalised to 1 for simplicity:

$$\frac{d\phi_i(t)}{dt} = \frac{1}{T} \quad . \tag{8.1}$$

When the phase reaches the threshold value 1, the oscillator is said to *fire*, meaning that it will transmit a pulse and reset its phase. If not coupled to any other oscillator, it will naturally oscillate and fire with a period *T*. Figure 8-1(a) plots the evolution of the phase function during one period when the oscillator is isolated.

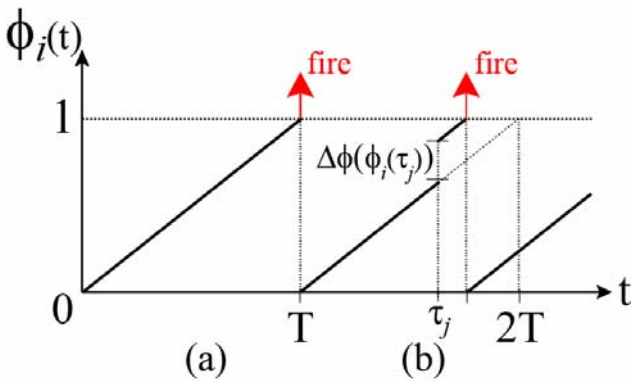

Figure 8-1: Time evolution of the phase function (a) for an isolated node, (b) upon reception of a pulse at instant τ_j.

The phase function can be seen as an internal counter that dictates when a pulse should be emitted. The goal of the synchronisation algorithm is to align all internal counters, so that all nodes agree on a common firing instant. To do so, the phase function needs to be adjusted. In the following, we consider that all nodes have the same dynamics, i.e. clock jitter is considered negligible.

Synchronisation of oscillators

When coupled to others, an oscillator i is receptive to the pulses of its neighbours. Phase adjustment is performed upon the reception of a single pulse, and depends on the current phase value at the receiver. When receiving a pulse at instant τ_j, a node instantly increments its phase by an amount that depends on the current value:

$$\phi_i(\tau_j) \rightarrow \phi_i(\tau_j) + \Delta\phi(\phi_i(\tau_j)) \text{ when receiving a pulse.}$$

Figure 8-1(b) plots the time evolution of the phase when receiving a pulse. The received pulse causes the oscillator to fire early. By appropriate selection of $\Delta\phi(\phi_i)$, a system of *N* identical oscillators forming a fully meshed network is able to synchronise their firing instants within a few periods [MS90].

The phase increment $\Delta\phi(\phi_i(\tau_j))$ is determined by the Phase Response Curve (PRC), which was chosen to be linear in [MS90]:

$$\phi_i(\tau_j) + \Delta\phi(\phi_i(\tau_j)) = \min\left(\alpha \cdot \phi_i(\tau_j) + \beta, 1\right) \quad (8.2)$$

where α and β determine the coupling between oscillators. It was shown in [MS90] that if the network is fully meshed, the system always converges, i.e. all oscillators will agree on a common firing instant, for $\alpha > 1$ and $\beta > 0$. The coupling influences the time to synchrony.

An example of the synchronisation of pulse-coupled oscillators is shown in Figure 8-2.

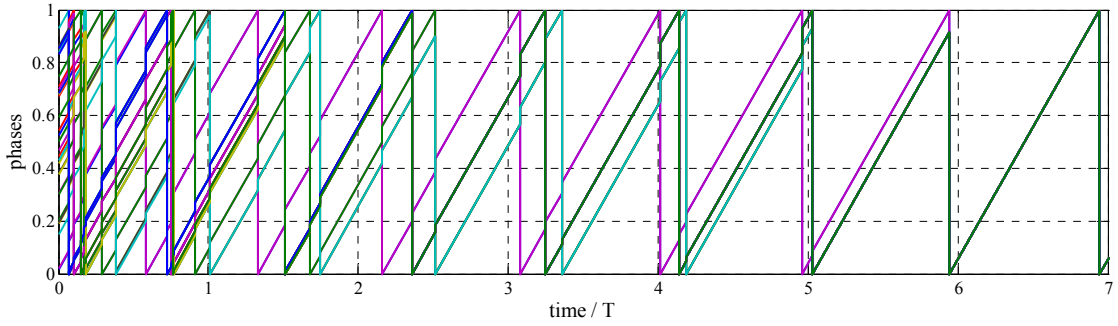

Figure 8-2: Synchronisation emerges from an initially random situation.

In Figure 8-2, initially all nodes start with a random phase, which increments until one phase reaches the threshold. At this instant and each time a phase reaches the threshold value, neighboring nodes increment

their phase. Over time, order emerges from a seemingly chaotic situation where nodes fire randomly, and after 6 periods in Figure 8-2, all nodes fire in synchrony. Thus synchronisation is achieved in a dynamic fashion after several periods.

This synchronisation property is very appealing. Nodes do not need to distinguish between transmitters, and simply need to adjust their internal clock $\phi_i(t)$ by a phase increment when receiving a pulse and transmit a pulse when firing. After some time, synchronisation emerges from an initially unsynchronised situation, and pulses are transmitted synchronously.

Refractory Period

When delays are introduced in the system, such as propagation delays, a system of pulse-coupled oscillators becomes unstable, and the system is unable to synchronise [EPG95]. To regain stability, a refractory period of duration T_{refr} is introduced after transmitting. During this period no phase increment is possible [HS03]. A node's receiver is switched on during this period, but the phase function stays equal to zero even if a synchronisation message is received. This behaviour is shown for one period of node *i* on Figure 8-3. During this period node *i* perceives two pulses at instants τ_j and τ_k. As *i* is in refractory at τ_j, no phase increment occurs, and only the pulse at τ_k causes a phase increment.

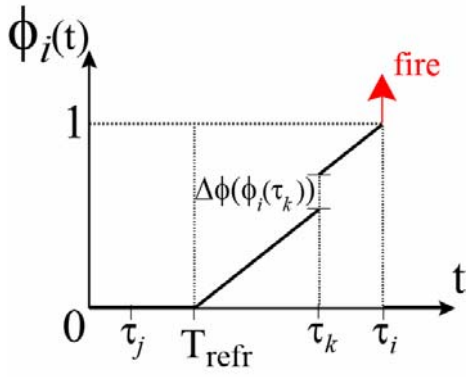

Figure 8-3: Time evolution of the phase function when a refractory period is present.

The appropriate choice of T_{refr} is important. It should be large enough to limit the number of interactions per period and thus for the network to remain stable, but not too large as to prevent some interactions between nodes.

8.3 Network Synchronisation Procedure

Initially when a UT accesses the network, it needs to synchronise with its base station by following its timing reference, so that it does not disturb ongoing transmissions. This Master-Slave type of synchronisation is common for intra-cell synchronisation, and is currently deployed in GSM and UMTS networks. This section presents a slot synchronisation scheme that fits into the WINNER super-frame structure. The synchronisation rules for performing slot synchronisation are based on the detection of uplink and downlink synchronisation words, which is done by the link synchronisation algorithm presented in Section 7, and adjusting internal clocks based on the pulse-coupled oscillator rules presented in Section 8.2.

8.3.1 Preamble Structure and Constraints

Within the first phase of the WINNER project, network synchronisation was integrated into the system. The most noticeable contribution is the inclusion of two synchronisation words within the preamble of the WINNER super-frame.

The super-frame preamble of the WINNER system consists of five consecutive time slots:

- "UL Synch" of duration $T_{\text{UL,Synch}}$: transmission slot for the synchronisation word transmitted by UTs.
- "RAC" of duration T_{RAC} : Random Access Channel.

- "GI" of duration T_{GI} : Guard Interval.
- "DL Synch" of duration $T_{DL,Synch}$: transmission slot for the synchronisation word transmitted by BSs.
- "BCH" of duration T_{BCH} : Broadcast Channel used by BSs to transfer general information to members of the cell.

The sum of these time slots corresponds to the length of the preamble:

$$T_{preamble} = T_{UL,Synch} + T_{RAC} + T_{GI} + T_{DL,Synch} + T_{BCH} \quad (8.3)$$

The super-frame preamble is shown in more detail in Figure 8-4.

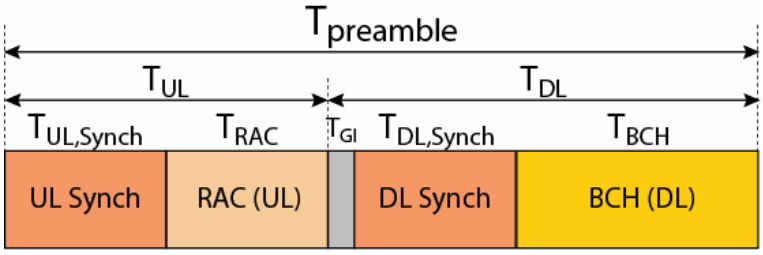

Figure 8-4: WINNER Super-frame Preamble.

Integrating the firefly synchronisation rules into the WINNER superframe structure is performed by utilising the the two synchronisation words as follows. The first sync word, labelled "UL Synch", is used by one group composed of UTs to transmit a synchronisation word that is received by the second group composed of BSs to adjust their phase function and synchronise. In a similar fashion, the second sync word, labelled "DL Synch", is used by the second group to broadcast a synchronisation word that is used by the first group to synchronise. The necessity for having two distinct transmission slots is justified by the fact that nodes cannot receive and transmit simultaneously. Hence one group relies on the other to synchronise, and not on synchronisation words from the same group.

When applying the pulse-coupled oscillator model to wireless systems, delays are critical [TA07]. To minimise the delays between transmission of a synchronisation word and its reception, the slot synchronisation unit is placed close to the link synchronisation unit, which is described in Section 7. The network synchronisation block diagram is shown in Figure 8-5.

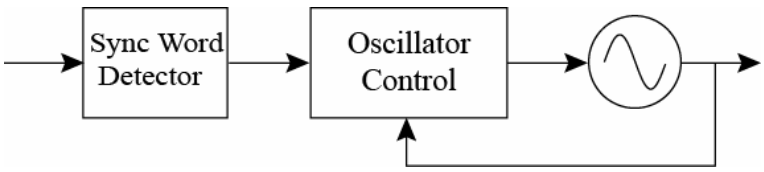

Figure 8-5: Block diagram of the slot synchronisation unit.

The synchronisation word detector described in Section 7 provides the timing of received synchronisation words. Thus in a similar way to the Mirollo and Strogatz synchronisation scheme, this block outputs a series of pulses that are related to the timing of synchronisation words. The oscillator control is further detailed in Sections 8.3.2 and 8.3.3,and is different for BSs and for UTs. The behaviour of each group relies on the firefly synchronisation rules in order to control the slot oscillator, which indicates the beginning and end of a super-frame. In return the oscillator feedbacks the timing to the oscillator control unit in order to indicate state changes.

8.3.2 Coarse Misalignment

The synchronisation of pulse-coupled oscillators presents the advantage that synchronisation emerges from *any* random initial situation, and does not have pre-requisites regarding the distribution of initial firing instants. Thus self-organised synchronisation enables systems to cope with changes in the topology, which is especially interesting in mobile systems, where wireless communications do not guarantee that all nodes in the network are connected.

Given the super-frame structure, Figure 8-6 presents the evolution over time defined for BSs and UTs as well as the super-frame preamble structure, when nodes are synchronised. To force the formation of two groups, one formed by BSs and the other by UTs, the phase function of BSs is adjusted when detecting a transmission from UTs, and vice versa. Hence two distinct synchronisation sequences "UL Synch" and "DL Synch" are used.

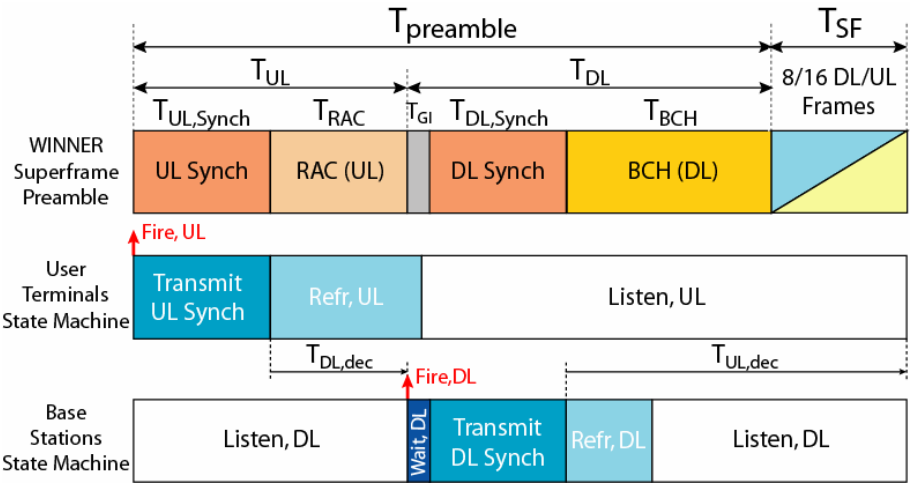

Figure 8-6: Time evolution of the network synchronisation unit for user terminals and base stations in the coarse misalignment mode.

Based on the two behaviors in Figure 8-6, interactions occur between the two groups (BSs and UTs) when a node transmits and nodes from the other group detect this transmission. Detection of the distinct synchronisation words is done by the link level synchronisation procedures described in Section 7. This allows for robust detection and avoids too much additional processing at the receiver.

Based on the super-frame structure, the listening time for user terminals and base stations is equal to:

$$T_{\mathrm{UL,Rx}} = (T_{\mathrm{preamble}} + T_{\mathrm{SF}}) - (T_{\mathrm{UL,Sync}} + T_{\mathrm{refr,UL}}) \tag{8.4}$$

$$T_{\mathrm{DL,Rx}} = (T_{\mathrm{preamble}} + T_{\mathrm{SF}}) - (T_{\mathrm{DL,Sync}} + T_{\mathrm{refr,DL}}) \tag{8.5}$$

Based on the firefly synchronisation rules presented earlier, slot synchronisation requires all nodes to maintain a phase function that is adjusted. Thus all user terminals maintain a phase function, which increments linearly over time:

$$\frac{d\phi_i(t)}{dt} = \frac{1}{T_{\mathrm{UL,Rx}}} \tag{8.6}$$

where $T_{\mathrm{UL,Rx}}$ is the listening period of a user terminal and is to be defined later.

Similarly all base stations maintain a phase function:

$$\frac{d\phi_i(t)}{dt} = \frac{1}{T_{\mathrm{DL,Rx}}} \tag{8.7}$$

where $T_{\mathrm{DL,Rx}}$ is the listening period of a user terminal and is to be defined later.

Key to separating nodes into two predefined groups is done in two parts:

- Coupling at Base Stations: if at instant τ_j, a BS node i is in 'Listen' state, where its phase function ϕ_i linearly increments over time, and a UT node j, which can communicate with i, started transmitting $T_{\mathrm{UL,Synch}} + T_{\mathrm{DL,dec}}$ before, then the receiving BS node i increments its current phase ϕ_i:

$$\phi_i(\tau_j) \rightarrow \phi_i(\tau_j) + \Delta\phi_{\mathrm{BS}}(\phi_i(\tau_j)) \text{ where } \phi + \Delta\phi_{\mathrm{BS}}(\phi) = \alpha_{\mathrm{BS}} \cdot \phi + \beta_{\mathrm{BS}} \tag{8.8}$$

- Coupling at User Terminals: if at instant τ_i, a UT node j is in 'Listen' state, where its phase function ϕ_j linearly increments over time, and a BS node i, which can communicate with j,

started transmitting $T_{\mathrm{DL,Synch}} + T_{\mathrm{UL,dec}}$ before, then the receiving UT node *j* increments its current phase ϕ_j:

$$\phi_j(\tau_i) \rightarrow \phi_j(\tau_i) + \Delta\phi_{\mathrm{UT}}(\phi_j(\tau_i)) \text{ where } \phi + \Delta\phi_{\mathrm{UT}}(\phi) = \alpha_{\mathrm{UT}} \cdot \phi + \beta_{\mathrm{UT}} \tag{8.9}$$

So far propagation delays were neglected for simplicity. Let $\theta_{UT,i,BS,j}$ denote the propagation delay between the *i*-th UT and the *j*-th BS. Then the interaction between these is always delayed by $\theta_{UT,i,BS,j}$, which affects the achieved accuracy. This is problematic for the wide area scenario, and propagation delays needs to be compensated. Advancing of uplink transmission so that alignment in time at the base station is perfect is detailed in Section 8.4.

The decoding delays $T_{\mathrm{UL,Synch}} + T_{\mathrm{DL,dec}}$ and $T_{\mathrm{DL,Synch}} + T_{\mathrm{UL,dec}}$, which are shown in Figure 8-6, are needed to allow for a processing delay in order to perform link synchronisation. These delays need to be constant so that the phase increment at a BS occurs $T_{\mathrm{UL,Synch}} + T_{\mathrm{DL,dec}}$ after a UT has fired, and the phase increment at a UT occurs $T_{\mathrm{DL,Synch}} + T_{\mathrm{UL,dec}}$ after a BS started transmission of a DL Sync word.

Thanks to this strategy, the formation of two groups is controlled: starting from a random initial state, where all nodes fire randomly, after following the simple coupling rules, UTs and BSs separate over time into two groups, all BSs firing T_{UL} after UTs and all UTs firing T_{DL} after BSs. This state corresponds to a synchronised state. Simulation results for this synchronisation strategy are presented for the local area and metropolitan area in Appendices J.1 and J.2.

8.3.3 Tracking

Once coarse network synchronisation is performed and nobody transmits synchronisation words while others transmit payload data, then nodes enter a tracking mode. Switching from one mode to the other is decided by a base station, which can signal it to users in its cell using the BCH for example. This has yet to be defined.

In tracking mode durations of states `Listen,UL` and `Listen,DL` and delay $T_{\mathrm{UL,dec}}$ are diminished by the duration of the data part of the super-frame T_{SF}. The synchronisation unit in tracking mode is suspended during the duration of the payload data. This is done so that nodes do not have to listen continuously, which limits battery consumption.

The tracking mode for UTs and BSs is shown in Figure 8-7.

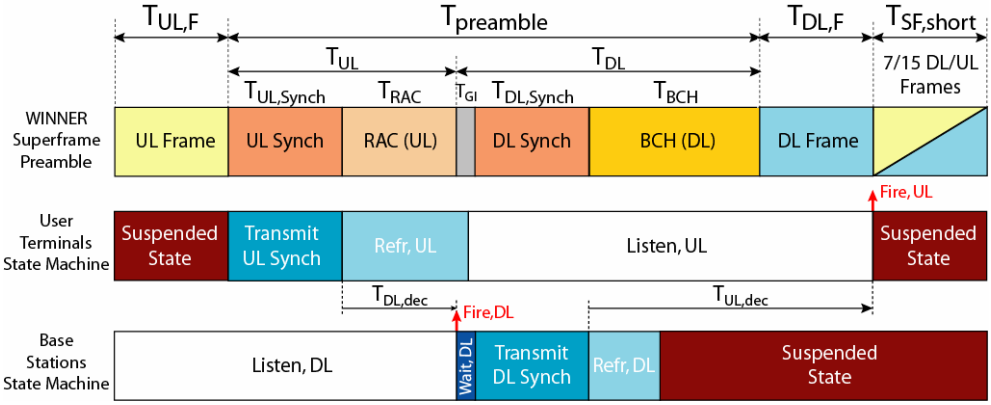

Figure 8-7: Tracking mode of the Network Synchronisation units.

The major difference from the coarse synchronisation mode includes the addition of a `suspended` state where nodes do not have to listen for synchronisation words nor adjust their clock (network synchronisation is switched off). Hence the listening time is diminished by $T_{\mathrm{SF,short}}$, which is equal to $T_{\mathrm{SF}} - T_{\mathrm{DL,frame}}$. Only during `Listen` state do nodes maintain a phase function, which linearly increases over time, and adjust it when detecting a synchronisation word.

In this novel state, nodes only track for short misalignment due to clock imperfections. Given the pulse-coupled oscillator model that was chosen, when clock skew is present in the model, nodes synchronise to the fastest running clock.

8.3.4 Inclusion of relays

Relays need to perform two tasks for the slot synchronisation scheme: update the reference of base stations based on the references of user terminals, and update the reference of terminals that cannot directly communicate with their base station.

Preferably the inclusion of relays into the synchronisation algorithm should be done seamlessly. To do so, Figure 8-8 presents the states followed by relays during coarse synchronisation: relays alternatively transmit the UL Synch word and the DL Synch word and correctly adjust their phase upon detection of either synchronisation word. Thanks to this scheme, there is no need to define a third synchronisation word, and user terminals do not need to distinguish between relays and base stations for performing slot synchronisation.

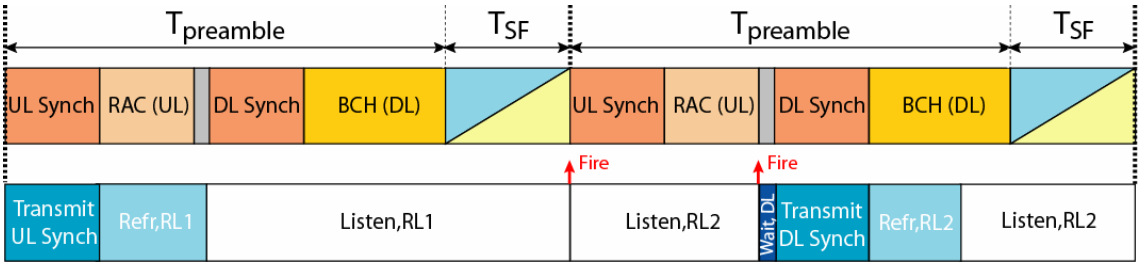

Figure 8-8: Time Evolution of relays.

Contrary to user terminals and base stations, relays need to be able to detect both UL Synch and DL Synch words. However these operations do not need to be performed simultaneously:

- in state `Listen,RL1`, relays detect only DL Synch words,
- in state `Listen,RL2`, relays detect only UL Synch words.

Performance in the Metropolitan Area scenario is presented in Appendix J.2.

8.4 Compensating Propagation Delays: Timing Advance

Propagation delays can be problematic in uplink transmissions when they are large. Indeed, if this delay is larger than the guard interval of an OFDM symbol, then a transmission of the UL Sync word interferes strongly with adjacent slots, i.e. the previous UL slot and the RAC slot. Thus it is particularly important in the Metropolitan Area and Wide Area cases to compensate these. Table 8.1 summarises the maximum propagation delays considered for the three different scenarios in WINNER and the considered guard interval durations [WIN2D6137].

	WA	MA	LA
Guard Interval Duration [µs]	3.20	2.00	2.00
Maximum Inter-node distance [m]	1000	325	100
Propagation delay [µs]	3.33	1.08	0.333

Table 8.1 – Various propagation delays

From this table, compensating for propagation delays on the uplink is essential for the Wide Area case.

A common procedure for compensating for the propagation delay is for terminals to advance their transmission by the propagation delay. The firing instant of timing reference instant of user terminals $\tau_{\mathrm{UT},i}$ is advanced by the propagation delay with its own base station $\theta_{\mathrm{UT},i,\mathrm{BS(i)}}$, so that uplink transmissions are effectively performed according to the new timing reference instant:

$$\tau_{\mathrm{UT},i} \rightarrow \tau_{\mathrm{UT},i} - \theta_{\mathrm{UT},i,BS(i)} \tag{8.10}$$

Evaluation of this technique is presented for the wide area case in Appendix J.3.

8.5 Imposing a Global Reference to Self-Organised Synchronisation

Performing slot synchronisation in a self-organised manner presents a number of advantages such as the robustness against failure of the base station and the adaptation to the network topology.

In a cellular network, an issue with employing such a self-organised synchronisation algorithm is *scalability*. In very large networks, it has been shown that synchronisation can fall apart due to loops in the network, and a synchronised state is never reached.

To prevent this problem, which is likely to occur in WA and MA scenarios, a reference needs to be imposed onto the network. To do so, a few nodes within the network need to have access to a Primary Reference Clock, which is available for example through the Global Positioning System (GPS), and should redistribute this timing reference. Furthermore imposing the stable reference given by the Primary Reference Clock helps avoiding stability issues that are common to oscillators.

Hence, we consider a scenario where only a few nodes have access to an absolute clock reference. The objective is to let these reference nodes impose a global time reference to the entire network.

As only a few nodes are considered to have access to a global reference, these reference nodes need to enforce their timing onto normal nodes. This section presents how this can be done when nodes are following the slot synchronisation strategy presented in Figure 8-6.

8.5.1 Dynamics of forced and forcing oscillators

The dynamics of each node are determined by:

- their internal dynamics, i.e. the state machine and the internal clock;
- the external influence of other nodes, i.e. the phase increments that adjust the internal clock.

A key to achieving synchronisation from any initial condition is that coupling parameters in the Phase Response Curve (PRC) need to be $\alpha > 1$ for the slope of the PRC and $\beta > 0$. Figure 8-9 plots several phase response curves as the slope of the PRC for an initial phase increment $\beta = 0.01$.

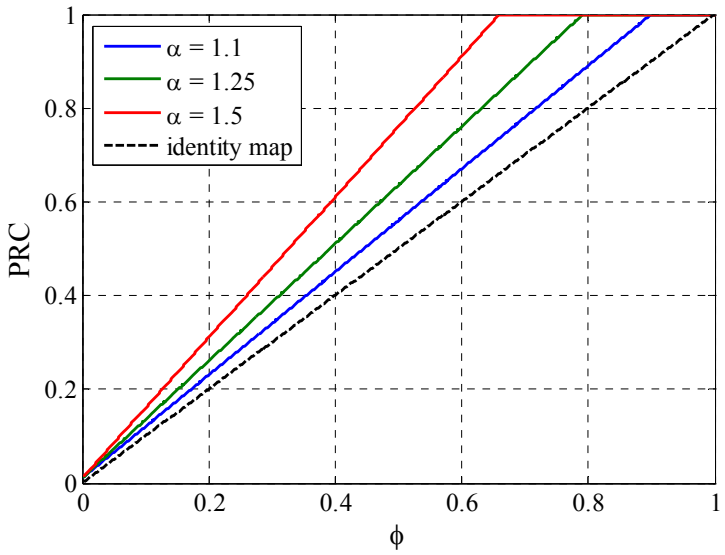

Figure 8-9: Phase Response Curves for different values of α.

A forcing oscillator tries imposing its own reference onto normal oscillators by running at a different frequency, and without ever adjusting its phase as it obtains its reference from an external source.

From Figure 8-9, it is clear that phase increments are always strictly positive. Thus a phase increment always brings a node closer to the firing instant and shortens the remainder of a period, and increases the internal frequency of the receiving oscillator.

Observing this, such an oscillator would not be able to follow a reference oscillator running slower, because the receiving oscillator always tries to catch up, and never slows down, which would be needed to follow a slower oscillator. Therefore a reference oscillator should run faster than normal oscillators in order to impose its timing.

8.5.2 Application to the Network Synchronisation Scheme

A reference node corresponds to an oscillator that periodically transmits the “DL Sync” word at the start of every super-frame without ever modifying its phase. This deafness is problematic if reference and

normal nodes run at the same frequency, and results in normal nodes not being able to follow the timing of reference nodes [TA07].

To counter this undesired effect, reference nodes run at a different frequency. As noted above, this frequency should be higher than the frequency of normal nodes. Thus the super-frame duration of reference nodes needs to be shorter. A means of achieving this is to shorten the duration of the "Wait,DL" state, which is equal to T_{GI}, the guard interval duration, for normal nodes. So for reference base stations, the guard interval is shortened:

$$T_{\mathrm{Wait,ref}} < T_{\mathrm{GI}} \tag{8.11}$$

The time evolution of reference base stations is shown in Figure 8-10 along with the super-frame structure (top) and the state machine of normal base stations (middle).

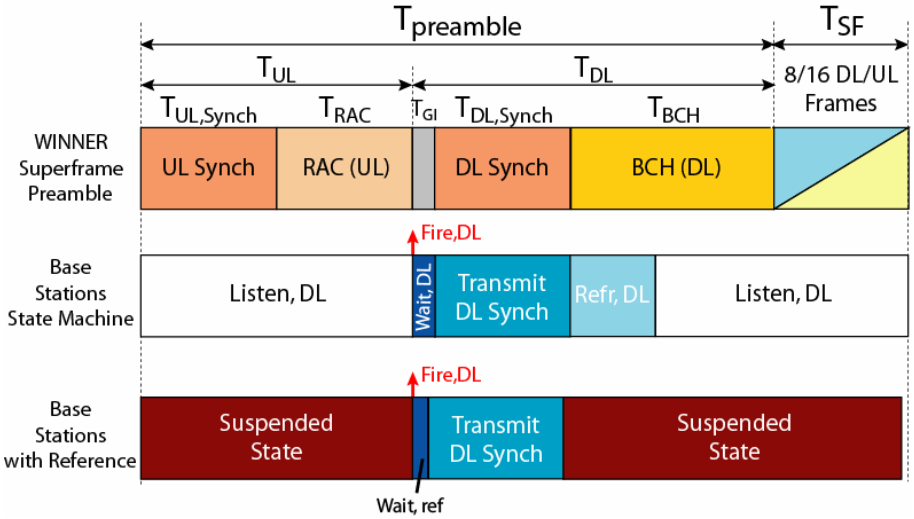

Figure 8-10: Time evolution of Reference Base Stations.

The exact duration of $T_{\mathrm{Wait,ref}}$ is determined by the accuracy of slot oscillators: reference oscillators need to run faster than any normal nodes, so that their timing is always imposed. Although the super-frame duration of reference BSs is shorter than for normal nodes, the scheme fits into the reference design, because only the guard interval duration is shortened and all other transmission durations are kept.

For reference nodes to correctly function, a common start based on the primary reference clock is needed. This should be treated in the translation of the PRC signal to the start of the super-frame common to all reference nodes, and is not elaborated here.

8.6 Conclusions

This section studied the applicability of a self-organised synchronisation algorithm inspired from firefly synchronisation to WINNER using long synchronisation messages and fitting into the super-frame structure. The original algorithm is not directly usable, and a modification was introduced to regain high accuracy and to correctly split base stations to form one group and user terminals to form another.

Thanks to these rules, a system of *N nodes* starting from a totally unsynchronised condition is always able to reach an agreement on a common time reference within 5 periods for a local area type of network composed of four base stations. This coarse network synchronisation phase is similar to an acquisition phase, and should serve as a basis for self-organised network synchronisation.

Through the simulation results presented in Appendix J, it is shown that the optimal coupling to synchronise depends on the number of user terminals that participate to the network synchronisation. Therefore a BS should know how many UTs in its vincinity are transmitting UL Sync words, so that synchrony is reached quickly.

Hearability of the UL Sync word is also an important issue for the network synchronisation scheme. Transmission of this word should not cause too much interference, in case other users are transmitting data, and yet it should be sufficiently robust, so that it can be detected in the presence of high interference. Thus the design of the UL Sync word needs to meet these criteria, and should be further investigated.

Following acquisition, tracking is done in a similar fashion but the listening time is restricted in order to reduce battery consumption and only track clock drift. Tracking is done by nodes emitting synchronisation words periodically during the super-frame preamble. Thus the same synchronisation principle is applied both for acquisition and tracking. As a result nodes follow the fastest oscillator.

9. Summary and Conclusions

9.1 Pilot Design

Pilot design is an important building block of the WINNER system concept, as it enables adaptive transmission and multiple antenna transmission schemes. Several studies aiming to optimize the placement and the power allocation of pilot symbols were conducted. Both dedicated pilots, where only the pilots that are within the chunk can be utilized for channel estimation, as well as common pilots, where interpolation in frequency over consecutive chunks is possible, were addressed. These studies provide valuable insights not only on the placement of pilot symbols, but also on the attainable spectral efficiency of a MIMO-OFDM system taking into account realistic channel estimation schemes.

When it comes to a general framework for the WINNER pilot design, there are many constraints other than the placement of pilots that need to be taken into consideration. As pilot overheads tend to increase when more antennas are allowed into the system, it is crucial that the inserted pilots can be efficiently reused for several functions. Apart from channel estimates at the receiver, these functions are measurements of CQI and CSI which are utilized for link adaptation. The reuse of pilots as well as the flexibility to support various flavours of multi-user MIMO and multiple access schemes is one of the main features of the WINNER pilot design. A modular concept is established that consists of basic building blocks: the pilot pattern, the pilot type and orthogonal pilot sets. The pilot pattern defines the position of pilot symbols within the chunk, and at the same time resembles a regular 2D grid with equidistantly spaced pilots on the macroscopic view of the OFDM frame. The spatial transmit processing scheme then defines the pilot type that is inserted on a particular chunk. The introduction of orthogonal pilot sets specifies whether pilots associated to different spatial streams are orthogonally separated in time and/or frequency, or, in case the spatial separation between beams is sufficient, the pilot symbol can be reused. Thanks to this modular concept the pilot overhead stays within acceptable limits.

9.2 Channel Estimation

Channel estimation (CE) in WINNER II is based on pilot subcarriers placed in a scattered pilot grid, with in-cell users' pilots placed so as not to interfere with one another. When block sizes are large enough to permit several pilots per block, Wiener filter interpolation, in frequency and time over one of more frames, provides channel estimates for all used subcarriers and OFDM symbols. Pilot-based CE can be enhanced by iterative CE (ICE), and, for MIMO and SDMA, can be further aided by application of genetic algorithm (GA) or least squares (LS) techniques. There is always some performance loss (SNR degradation relative to the idealized situation where all channels are known by the receiver) resulting from CE. In general, larger CE performance losses occur:

- when interpolation over a wide range of subcarrier frequencies and OFDM symbol times is not possible; for example for IFDMA, B-IFDMA and B-EFDMA. As a result, the effective diversity advantage, over full-band or local FDMA, of these multiple access schemes, is diminished.
- when interference is imposed to pilots and data transmitters from outside the cell or sector. Such interference should be kept to a low level by frequency reuse partitioning or inter-cell dynamic channel assignment, and can be combated at the receiver by LS techniques which essentially attempt to estimate the autocorrelation matrix of the out-of-cell interference.

Performance and limitations on channel prediction, using Kalman filter techniques, was evaluated for use in predicting CQI for channel estimation and frequency-adaptive transmission. The Kalman algorithm uses assumed channel time and frequency correlation properties to optimally estimate the future time evolution of the channel. Its use is favoured for channels corresponding to relatively slow mobile terminals, and where auxiliary channel correlation measurements are made.

9.3 Measurements

An analysis of the measurement capabilities available from WINNER physical layer procedures has been made. When compared to the measurement requirements of other WINNER functions, it can be seen that there is a good match between the available capabilities and the requirements. Where there is not such a good match, specific measurement capabilities are developed in association with the functions requiring them.

An example study on the impact of feedback quantisation on spatial-temporal processing gives useful indications on the trade-off between signalling overhead and system performance, which can be used for guidance by system designers.

9.4 RF and Synchronisation Imperfections

Regarding high power amplifier the following conclusion can be drawn. Minimising the power backoff required for high power amplifiers is very important in terms of cost and battery recharging intervals, especially for mobile terminals. Large required backoff lowers amplifier efficiency and increases the maximum output power required from the HPA, thus increasing its cost, and battery drain. The effect of HPA nonlinearity was evaluated for different systems. The required backkoff of course depends on the choice of the spectral mask. The proposed phase noise compensation algorithms are summarised as follows. The phase noise compensation algorithm for multi-carrier systems is applicable for any pilot patterns and does not need any additional overhead. For the single carrier case the time-varying phase process can be tracked with a second order soft decision directed phase locked loop (PLL), which uses log-likelihood ratio (LLR) information from a turbo equalizer. For both schemes (multi and single carrier) the complexity of the correction algorithm can be neglected compared to the decoding complexity. Finally, an analytic expression of the SNR degradation due to interference is given. Curves showing SNR degradation values for different timing and frequency synchronisation errors are presented.

9.5 Link Layer Synchronisation

Link layer synchronisation is based on synchronisation symbol placed in the downlink (DL) synch slot of the preamble. In licensed case *T-Pilot* synchronisation scheme is used. The synchronisation is performed in two stages and both are performed during one OFDM symbol. The first one includes coarse timing synchronisation and fractional frequency offset estimation, both utilising modified Schmidl & Cox algorithm. The latter one includes integer frequency offset estimation and fine timing synchronisation, both performed in frequency domain. According to presented simulation results the synchronisation scheme guarantees inter-block interference (IBI) free signal receive and acceptable low inter-carrier interference (ICI), however it is not robust against narrowband interference (NBI).

In presence of NBI, as in license exempt and spectrum Sharing case, the algorithm utilising three OFDM symbols should be used. The algorithm detects and removes the interference in frequency domain. The corrected signal is then used for time and frequency synchronisation in time domain. Simulation results proved the efficiency of the algorithm even for very low signal to interference power ratio.

9.6 Self-Organised Network Synchronisation

Section 8 presented a modified version of the firefly synchronisation scheme that fits into the WINNER frame structure. Thanks to this modification, a network is able is correctly synchronise, i.e. base stations and user terminals agree on a common time slotted structure, starting from any random misalignment. The algorithm was further modified in order to cope with the presence of relays in the network, and with the access to a Primary Reference Clock. This last property is necessary in order to stabilise the network, i.e. avoid synchronisation loops, and in order to reduce scalability issues that are common in self-organised networks. Thanks to these modifications, simulation results shown in Appendix J show that the proposed network synchronisation algorithm is well suited to all WINNER concept groups.

Appendix A. Parameters and Assumptions for Reference Simulations

A. 1 Air Interface Parameters

The used air interface parameters are to be adopted from [WIN2D6137] The OFDM/GMC parameters of [WIN2D6137] are similar to those used in [WIN1D210], except for the number of occupied subcarriers in the FDD mode. The [WIN2D6137] reference system parameters are summarized in Table A-1

	Base Coverage Urban	Micro-cellular	Indoor
Centre frequency (GHz)	3.95 DL/3.7 UL	3.95 (metro area) 5.0 (local area)	
Channel spacing (MHz)	50	100	
Number of used subcarriers	1152	1840	
Sub carrier distance Δf	45 MHz/1152 = 39062.5Hz	89.84 MHz/1840 =48828.125 Hz	
Useful symbol duration T_N	25.6μs	20.48μs	
Guard interval T_G	3.2μs	2.00μs	
Total symbol duration	28.8μs	22.48μs	
used sub carriers	[-576:576]	[-920:920]	
Assumed channel models	C2	B1	A1

Table A-1: "New reference system parameters (from [WIN2D6137])

A. 2 A Proposed Uplink Interference Simulation Scenario

The use of SDMA and aggressive frequency reuse strategies give rise to high levels of co-channel interference which must be mitigated by spatial processing at the receiver. Spatial processing that adapts to desired signals' and interferers' locations and spatial signatures require accurate channel estimation and appropriate allocation of pilot signals. In this section we suggest a scenario for simulation of interference in wide area uplinks. It is based on a frequency reuse partitioning strategy outlined in Appendix L of [WIN2D6137].

Figure A- 1, adapted from [WIN2D6137], Appendix L, shows a system with three-sectored hexagonal cells with maximal radius R. The inner green circles, with radius 0.7 R, represent areas with frequency reuse 1. The outer yellow, blue and grey areas have frequency reuse factor 3, since they would otherwise be more vulnerable to interference from adjacent cells. Thus a common set of transmission channel resources is shared by user terminals in all areas labeled A_1, another set of resources is shared in areas labeled B_1, etc. The resources labeled A_1, B_1, A_2, B_2 etc. are disjoint.

Suppose that in a SDMA scenario, up to K+1 (K=0, 1, 2, ..) user terminals share the same transmission resources, and therefore interfere with one another in any given sector. We distinguish signals and interference from in-cell and out-of-cell user terminals. Thus each user signal has up to K equal-power in-cell interferers. For uplink transmission the average received power from in-cell users is assumed to be equal, as a result of power control, to the power of a user on the edge of a cell or inner circle.

As shown in the figure, users in inner area A_1 also suffer out-of-cell interference from two nearby sectors, also labeled A_1. The maximum number of out-of-cell interferers from these two sectors is 2(K+1). The minimum distance of each of these out-of-cell interferers to the base station is $\sqrt{3}R$. If we assume the WINNER urban coverage propagation exponent of 3.84, a minimum distance out-of-cell interferer in this case has a received average power of $38.4[\log_{10}(0.7/\sqrt{3})] = -15$ dB relative to the average power of any

in-cell user. The maximum out-of-cell interferer distance in this case is 2.7*R*, corresponding to a relative average power of $38.4[\log_{10}(0.7/2.7)] = -22.5$ dB.

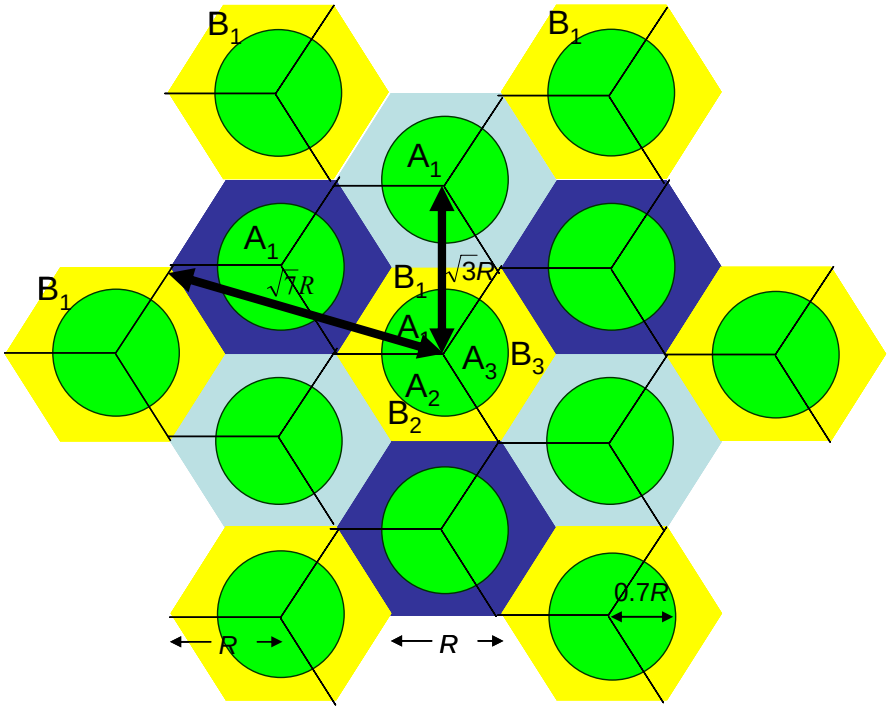

Figure A- 1 Cellular layout, showing frequency reuse zones

For a user in B_1, the nearest out-of-cell B_1 interferer appearing at the base station is at a distance of $\sqrt{7}R$, and the corresponding average power relative to an in-cell user signal is $38.4[\log_{10}(1/\sqrt{7})] = -16$ dB. The maximum out-of-cell interferer distance for B_1 is 4*R*, corresponding to a relative power of $38.4[\log_{10}(1/4)] = -23$ dB. The maximum number of out-of-cell interferers from the three nearest B_1 sectors is 3(*K*+1).

For this scenario with 3-sector hexagonal cells with center reuse-1 circles of radius 0.7 *R*, and outer reuse-3 areas with radius *R*, the ranges of maximum and minimum average out-of-cell interferer powers are the same, to within 1 dB. For purposes of evaluation of SDMA and MIMO channel estimation performance and pilot assignment in MMSE interference rejection combining receivers, we therefore suggest the following interference scenario for link level simulations of SDMA uplinks:

- Number of in-cell interferers (reflecting the degree of spatial multiplexing) =*K* (*K*=0,1,2,…), all with average powers equal to that of the desired signal.
- Number of out-of-cell interferers = 3(*K*+1), with average powers (relative to that of the desired signal) uniformly spaced from -15 dB to -23 dB. For example if there are 6 out-of-cell interferers, their average powers would be: -15 dB, -16.6 dB, -18.2 dB, -19.8 dB, -21.4 dB, and -23 dB.
- The channels between each transmitting antenna and each receiving base station antenna are independent, and they are scaled in relative power as indicated above. Each channel (based on channel models like C2, B1, etc.) is subject to an impulse response with independent Rayleigh coefficients, and is subject to time variation due to Doppler.

Note that pilot overhead for receiver spatial adaptation will increase at least in proportion to *K*+1, the number of in-cell SDMA interferers. Pilot overhead is relatively high for high degrees of spatial multiplexing. As suggested in the above discussion, out-of-cell interferers' powers are relatively low.

Appendix B. Performance Assessment Using Channel Estimation Error Model

B.1 SISO system

In the following the channel estimation error $\varepsilon_{n,\ell}$ associated to the channel estimate $\hat{H}_{n,\ell} = H_{n,\ell} + \varepsilon_{n,\ell}$ is modelled as an additive Gaussian noise term. In order to derive a model taking into account channel estimation errors, we define an equivalent SISO system model including the channel estimate

$$Y_{n,\ell} = X_{n,\ell} H_{n,\ell} + Z_{n,\ell} = X_{n,\ell} \hat{H}_{n,\ell} + \eta_{n,\ell} \tag{B-1}$$

where $X_{n,\ell}$, $H_{n,\ell}$ and $Z_{n,\ell}$ denote the transmitted symbol with energy per symbol E_d, the channel transfer function (CTF), and additive white Gaussian noise (AWGN) with zero mean and variance N_0, respectively. Assuming a normalized average channel gain, $E(|H_{n,\ell}|^2) = 1$, the average signal to noise ratio (SNR) is E_d/N_0. In addition, $\hat{H}_{n,\ell}$ denotes the channel estimation unit output, i.e., the estimate of the CTF, $H_{n,\ell}$, Furthermore, n and ℓ denote n-th subcarrier within a chunk and ℓ-th OFDM symbol within a chunk, respectively.

Solving **(B-1)**, the noise term of the equivalent system model is obtained by $\eta_{n,\ell} = \varepsilon_{n,\ell} X_{n,\ell} + Z_{n,\ell}$, where $\varepsilon_{n,\ell} = H_{n,\ell} - \hat{H}_{n,\ell}$ denotes the channel estimation error. Assuming Rayleigh fading, the channel response $H_{n,\ell}$ is a complex Gaussian random variable. Since the estimation error $\varepsilon_{n,\ell}$ is a weighted sum of Gaussian random variables, $\varepsilon_{n,\ell}$ itself is Gaussian distributed. Assuming an unbiased estimator [Kay93] $\varepsilon_{n,\ell} \sim CN(0, \mathrm{MSE})$ is a Gaussian random variable with zero mean and variance equal to the MSE, denoted by $\sigma_\varepsilon^2[n,\ell] = E(|\varepsilon_{n,\ell}|^2)$. Then the variance of the effective noise term, $\eta_{n,\ell}$, is found to be $\sigma_\eta^2[n,\ell] = N_0 + E_s \sigma_\varepsilon^2[n,\ell]$. The effective noise term whose variance $\sigma_\eta^2[n,\ell]$ is the noise added to the nth coded data symbol in the ℓth block in an OFDM receiver. For a linear serial modulation receiver, the frequency domain samples undergo an inverse FFT operation. The resulting average mean squared error affecting each output coded data symbol from a frequency domain linear equalizer in a serial modulation receiver can be expressed as

$$\mathrm{MSE} = \frac{1}{N_{data}} \left[\sum_{n=0}^{N_{FFT}-1} \left| W_n * H_{n,\ell} - 1 \right|^2 + N_0 \sum_{n-0}^{N_{FFT}-1} \left| W_n \right|^2 \right],$$
$$\text{where } W_n = \frac{\hat{H}_{n,\ell}^*}{\left| \hat{H}_{n,\ell} \right|^2 + N_0}. \tag{B-2}$$

When this expression is expanded, the resulting average output mean squared error turns out to be

$$\mathrm{MSE} = MSE_0 + \sum_{n=0}^{N_{FFT}-1} \sigma_\varepsilon^2[n,\ell] \left| W_n \right|^2 . \tag{B-3}$$

In other words, for serial modulation with linear equalization, the variance of the channel estimation error at each frequency simply adds to the noise power at that frequency.

For purposes of data detection and decoding the loss in SNR due to channel estimation is dependent on two factors: the estimation error $\varepsilon_{n,\ell}$, and the fraction of the total transmit power dedicated to pilot symbols. The reference SNR is $\gamma_0 = E_s / N_0$ where E_s denotes the total averaged received energy from the data, pilots and cyclic prefixes. The effective SNR including channel estimation errors and pilots becomes $\gamma = \dfrac{E_d}{N_0 + E_d \sigma_\varepsilon^2[n,\ell]}$.

With E_d/E_s given by (2-5), the SNR loss is

$$\Delta\gamma = \frac{\gamma_0}{\gamma} = 1 + (S_P - 1)\Omega_P + \gamma_0\sigma_\varepsilon^2[n,\ell] \tag{B-4}$$

Let the channel estimate be performed by a 2D FIR filter $\mathbf{w}$ of dimension $M_\mathrm{f} \cdot M_\mathrm{t}$, utilizing M_f and M_t pilot symbols in frequency and time, denoted by $\hat{H}_{n,\ell} = \mathbf{w}^H\tilde{\mathbf{y}}$. The $M_\mathrm{f}M_\mathrm{t}$ dimension vector

$$\tilde{\mathbf{y}} = [Y_{\tilde{n},\tilde{\ell}}, \cdots, Y_{\tilde{n}+M_\mathrm{f}-1,\tilde{\ell}}, \cdots, Y_{\tilde{n}+M_\mathrm{f}-1,\tilde{\ell}+M_\mathrm{t}-1}]^T$$

accounts for the received pilot sequence in frequency and time. The indices $\{\tilde{n},\tilde{\ell}\}$ indicate the subcarrier and OFDM symbol positions of the pilot symbols.

The MSE of an arbitrary pilot aided scheme with $\hat{H}_{n,\ell} = \mathbf{w}^H\tilde{\mathbf{y}}$ is determined by

$$\begin{aligned}\sigma_\varepsilon^2[n,\ell] &= E[\varepsilon_{n,\ell}\varepsilon_{n,\ell}^*] = E[|H_{n,\ell} - \hat{H}_{n,\ell}|^2] \\ &= E[|H_{n,\ell}|^2] - 2\Re\{\mathbf{w}^H\mathbf{r}_{\tilde{\mathbf{y}}H}[n,\ell]\} + \mathbf{w}^H\mathbf{R}_{\tilde{\mathbf{y}}\tilde{\mathbf{y}}}\mathbf{w}\end{aligned} \tag{B-5}$$

The 2D correlation functions $\mathbf{R}_{\tilde{\mathbf{y}}\tilde{\mathbf{y}}} = E\{\tilde{\mathbf{y}}\tilde{\mathbf{y}}^H\}$ and $\mathbf{r}_{\tilde{\mathbf{y}}H} = E\{\tilde{\mathbf{y}}H_{n,\ell}^*\}$ represent the auto-correlation matrix of the received pilots, $\tilde{\mathbf{y}}$, and the cross-correlation between $\tilde{\mathbf{y}}$ and the desired response $H_{n,\ell}$, respectively.

Assuming that the CTF and the noise are uncorrelated, the auto-correlation function can be expressed as $\mathbf{R}_{\tilde{\mathbf{y}}\tilde{\mathbf{y}}} = \mathbf{R}_{\tilde{\mathbf{h}}\tilde{\mathbf{h}}} + \frac{1}{\gamma_\mathrm{p}}\mathbf{I}$, where $\mathbf{R}_{\tilde{\mathbf{h}}\tilde{\mathbf{h}}}$ is the auto-correlation matrix of the CTF at pilot positions excluding the AWGN term, and $\mathbf{I}$ denotes the identity matrix, all of dimension $M_\mathrm{f}M_\mathrm{t} \times M_\mathrm{f}M_\mathrm{t}$. With the pilot insertion loss of (B-4), the SNR at pilot positions becomes $\gamma_p = S_pE_d / N_0 = \gamma_0 S_p / (1 + (S_p - 1)\Omega_p)$. Inserting the expression for $\mathbf{R}_{\tilde{\mathbf{y}}\tilde{\mathbf{y}}}$ into **(B-5)**, it is seen that the MSE can be separated into a noise error σ_n^2 and an interpolation or lag error σ_i^2 [WIND21].

These parts are uncorrelated and the MSE is the sum of their respective variances $\mathrm{MSE} = \sigma_n^2 + \sigma_i^2$. The noise part is inversely proportional to γ_p and is given by

$$\sigma_n^2 = \mathbf{w}^H\mathbf{w}\frac{N_0}{E_P} = \frac{1}{G_n\gamma_0} \cdot \frac{1 + (S_P - 1)\Omega_P}{S_P} \tag{B-6}$$

where $G_n = 1/(\mathbf{w}^H\mathbf{w})$ defines the estimator gain, which accounts for the ratio of the average noise measured at the output relative to the input of the channel estimation unit.

The interpolation error is independent of the SNR and a function of the used interpolation filters as well as the channel conditions. According to **(B-5)** the variance of the interpolation error is determined by

$$\sigma_i^2 = E\left\{\left|H_{n,\ell}\right|^2\right\} - 2\Re\left\{\mathbf{w}^H\mathbf{r}_{\tilde{\mathbf{h}}H}\right\} + \mathbf{w}^H\mathbf{R}_{\tilde{\mathbf{h}}\tilde{\mathbf{h}}}\mathbf{w} \tag{B-7}$$

The MSE and therefore the noise and interpolation errors in **(B-6)** and **(B-7)** are dependent on the subcarrier index n and OFDM symbol index ℓ. In order to allow for a simple model, we choose to average the MSE over the entire sequence, so $\sigma_\eta^2 \to \overline{\sigma}_\eta^2$. Near the beginning and end of the sequence edge effects result in an increased estimation error. In particular, for high SNR where edge effects are the dominant source of the estimation error, a certain deviation due to this averaging is to be expected.

Substituting the MSE, $\bar{\sigma}_{\varepsilon}^2 = \bar{\sigma}_{\mathrm{n}}^2 + \bar{\sigma}_{\mathrm{i}}^2$ into (B-4), with $\bar{\sigma}_{\mathrm{n}}^2$ being expressed in the parameterized form of **(B-6)** the loss in SNR due to channel estimation can be transformed to

$$\Delta\gamma = \left(1 + (S_P - 1)\Omega_P\right) \cdot \left(1 + \frac{1}{G_n S_P}\right) + \gamma_0 \sigma_i^2 \qquad \text{(B-8)}$$

From above analysis it follows that in order to describe the performance penalty due to channel estimation, only the estimator gain G_{n} and the interpolation error $\bar{\sigma}_{\mathrm{i}}^2$ are required.

B.2 MIMO system

Similar to the analysis provided in the previous section for SISO system, in this section we develop a channel estimation model for MIMO-OFDM without channel state information at the transmitter. The goal of analysis is to provide an expression for equivalent SNR degradation and thus describe effects of channel estimation with a single parameter.

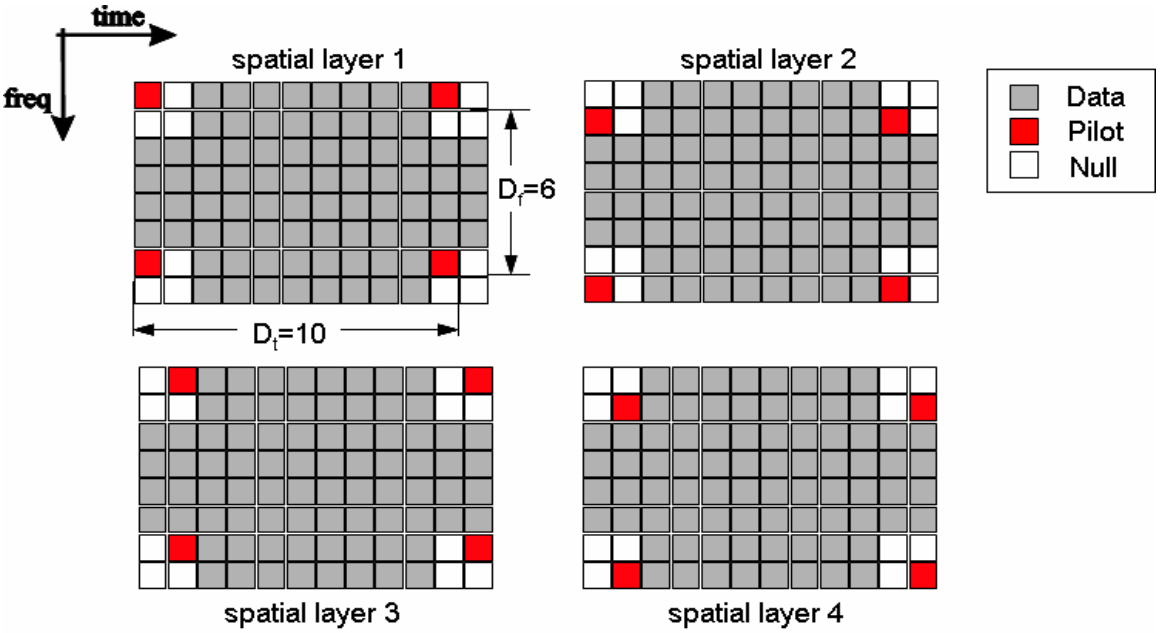

Figure B-1 Dedicated pilot allocation for 4 spatial streams in FDD mode.

Consider a MIMO-OFDM system with N_T transmit and N_R receive antennas. We assume that N_T spatial streams are transmitted and that channel knowledge is not available at the transmitter. The considered pilot pattern for a system with 4 spatial layers is shown in **Figure B-1**. Pilots are orthogonally separated in time and frequency, i.e. when a pilot is transmitted on a spatial stream, all other streams transmit zeros. With the given parameters up to 4 spatial layers can be supported per chunk. Denote with N_c the number of used subcarriers, and with L the number of OFDM symbols per frame. OFDM modulation is performed by N_{DFT} NDFT–point ($N_{DFT} > N_c$) inverse DFT (IDFT), followed by insertion of a cyclic prefix of N_{CP} samples. Assuming perfect orthogonality in time and frequency, the received signal of subcarrier n of the l-th OFDM symbol block and ν -th receive antenna is given by

$$Y_{n,\ell}^{(\nu)} = \sum_{\mu=1}^{N_T} \sqrt{\frac{E_d}{N_T}} X_{n,\ell}^{(\mu)} H_{n,\ell}^{(\mu,\nu)} + Z_{n,\ell}^{(\nu)};\ 0 \le n \le N_c,\ 0 \le \ell \le L,\ 0 \le \nu \le N_R. \qquad \text{(B-9)}$$

where $X_{n,\ell}^{(\mu)}$, $H_{n,\ell}^{(\mu,\nu)}$ and $Z_{n,\ell}^{(\nu)}$ denote the normalized transmitted symbol over transmit antenna μ with $E\left\{\left|X_{n,\ell}^{(\mu)}\right|^2\right\} = 1$, the channel transfer function (CTF) between transmit antenna μ and receive antenna ν, and additive white Gaussian noise (AWGN) at the ν -th receive antenna with zero mean and variance

N_0, respectively. An energy per transmitted data symbol of E_d / N_T and a normalized average channel gain, $E\left\{\left|H_{n,\ell}^{(\mu,\nu)}\right|^2\right\}=1$ is assumed.

The channel estimation unit outputs an estimate of the CTF, $H_{n,\ell}^{(\mu,\nu)}$, denoted by $\hat{H}_{n,\ell}^{(\mu,\nu)} = \mathbf{w}^T \tilde{\mathbf{y}}^{(\mu,\nu)}$. Let M_f and M_t denote the number of pilot symbols in frequency and time used to generate $\hat{H}_{n,\ell}^{(\mu,\nu)}$. The $M_f M_t \times 1$ column vector $\tilde{\mathbf{y}}^{(\mu,\nu)}$ contains the received pilots from transmit antenna μ to receive antenna ν. The $M_f M_t \times 1$ column vector $\mathbf{w}$ represents an arbitrary linear estimator, e.g. a 2D FIR filter.

In order to derive a model taking into account channel estimation errors, we assume a receiver that processes the channel estimates $\hat{H}_{n,\ell}^{(\mu,\nu)} = \mathbf{w}^T \tilde{\mathbf{y}}^{(\mu,\nu)}$ as if these were the true CTF. The effect of channel estimation errors is an increased effective additive noise term $\eta_{n,\ell}^{(\nu)}$, described by the equivalent system model

$$Y_{n,\ell}^{(\nu)} = \sum_{\mu=1}^{N_T} \sqrt{\frac{E_d}{N_T}} X_{n,\ell}^{(\mu)} H_{n,\ell}^{(\mu,\nu)} + Z_{n,\ell}^{(\nu)} = \sum_{\mu=1}^{N_T} \sqrt{\frac{E_d}{N_T}} X_{n,\ell}^{(\mu)} \hat{H}_{n,\ell}^{(\mu,\nu)} + \eta_{n,\ell}^{(\nu)}. \tag{B-10}$$

Solving (B-10), and defining the estimation error by $\varepsilon_{n,\ell}^{(\mu,\nu)} = H_{n,\ell}^{(\mu,\nu)} - \hat{H}_{n,\ell}^{(\mu,\nu)}$, yields

$$\eta_{n,\ell}^{(\nu)} = \sum_{\mu=1}^{N_T} \sqrt{\frac{E_d}{N_T}} X_{n,\ell}^{(\mu)} \varepsilon_{n,\ell}^{(\mu,\nu)} + Z_{n,\ell}^{(\nu)}. \tag{B-11}$$

In the following we assume that the estimation error $\varepsilon_{n,\ell}^{(\mu,\nu)}$ is a Gaussian random variable with zero mean and variance equal to the MSE. We assume that this variance is independent of μ and ν, denoted by $\sigma_\varepsilon^2[n,\ell] = E\left[\left|\varepsilon_{n,\ell}\right|^2\right]$, dropping indices μ and ν. Finally, the variance of the effective noise term, $\eta_{n,\ell}^{(\nu)}$, equals $\sigma_\eta^2[n,\ell] = N_0 + N_T \frac{E_d}{N_T} \sigma_\varepsilon^2[n,\ell]$, also independent of the index ν.

The loss in SNR due to channel estimation is dependent on two factors: the estimation error $\varepsilon_{n,\ell}$ and the overhead in terms of transmit power dedicated to pilot symbols in, given by

$$\Delta\gamma = \frac{\gamma_0}{\gamma} = \frac{1}{\sigma_{\hat{H}}^2}\left(1 + N_T \Omega'_P (S_P - 1) + \gamma \sigma_\varepsilon^2[n,\ell]\right) \tag{B-12}$$

where $\Omega'_P = \Omega_P / N_T$ is the pilot overhead per transmit antenna and the effective SNR including channel estimation reads

$$\gamma = \frac{E_d \sigma_{\hat{H}}^2}{N_0 + E_d \sigma_\varepsilon^2[n,\ell]} \tag{B-13}$$

Note that allowing for arbitrary linear estimators, the model in (B-10) only provides meaningful results for high SNR, where the variance of the channel estimates, $\sigma_{\hat{H}}^2 = E\left[\left|\hat{H}_{n,\ell}^{(\mu,\nu)}\right|^2\right]$, is well approximated by $\sigma_{\hat{H}}^2 \approx \sigma_H^2 = 1$.

Similarly as in SISO case, the MSE can be separated, assuming a linear estimator, into a noise error and an interpolation or lag error

$$\sigma_\varepsilon^2 = \sigma_n^2 + \sigma_i^2 \tag{B-14}$$

The noise part is given by

$$\sigma_n^2 = \mathbf{w}^H \mathbf{w} \frac{N_0}{E_P} = \frac{1}{G_n \gamma_0} \cdot \frac{1 + N_T \Omega'_P (S_P - 1)}{S_P} \tag{B-15}$$

whereas interpolation error is determined by

$$\sigma_i^2 = E\left\{ \left| H_{n,\ell}^{(\mu,\nu)} \right|^2 \right\} - 2\Re\left\{ \mathbf{w}^H \mathbf{r}_{\tilde{\mathbf{h}} H}^{(\mu,\nu)} \right\} + \mathbf{w}^H \mathbf{R}_{\tilde{\mathbf{h}}\tilde{\mathbf{h}}}^{(\mu,\nu)} \mathbf{w} \tag{B-16}$$

The loss in SNR due to channel estimation equals to

$$\Delta\gamma = \left(1 + N_T \Omega'_P (S_P - 1)\right) \cdot \left(1 + \frac{1}{G_n S_P} \right) + \gamma_0 \sigma_i^2 \,. \tag{B-17}$$

Appendix C. Performance Assessment of the WINNER Pilot Design

C.1 Performance of iterative (turbo) channel estimation for OFDM and B-EFDMA

In this section, pilot-aided (PACE) and iterative channel estimation (ICE) is evaluated for non-adaptive OFDM transmission in FDD mode using the parameters described in Appendix A. The performance is evaluated for OFDM where one user is allocated the full bandwidth, OFDMA with chunk size 8x12 and B-EFDMA with sub-chunk (or block) size of 4x3 (subcarriers x OFDM symbols). Channel estimation with common and dedicated pilots is considered. While common pilots can be used in the downlink, in a multi-user scenario where user specific special precoding is used and adjacent chunks are assigned to different users, the channel is to be estimated on a per-chunk basis. The presented results, however, assume one spatial stream and omni-directional antennas. Since the number of pilots per chunk is constrained by the chunk size, PACE will either experience significant performance degradation, and/or a large pilot overhead.

For Wiener filtering, a robust filter design is selected for each mode, according to the specifications in Appendix A.

For OFDM the subcarrier spacings in time and frequency directions are set to D_t=11 and D_f=4 according to the notation shown in Section 3.2.6. For PACE and ICE, the filter orders in frequency directions are set to M_f=8, while in time direction M_t=2 for PACE, since there are only two pilots available, and M_t=L=12 for ICE. The size of a codeword is equivalent to the number of data subcarriers per frame, which is 11264 coded symbols per frame.

For B-EFDMA the pilot spacings are D_t=3 and D_f=4, resulting in one pilot per chunk for block size 4x3, so for PACE M_t=1 and M_f=1, i.e. no interpolation is possible. For ICE, the filter orders are set according to the block size. So, for a 4x3 block we get M_t=3 and M_f=4. For B-EFDMA the size of one codeword amounts to 352, which corresponds to one B-EFDMA block every 32 subcarriers. Hence, the codeword length for B-EFDMA is 32 times less than for full band OFDM.

In the numerical simulations, the channel encoder is a memory 6 CC with generator polynomials (133,171) in octal form. For ICE the performance is evaluated for feedback derived from *a posteriori* information, unless otherwise stated (see Figure 4-1).

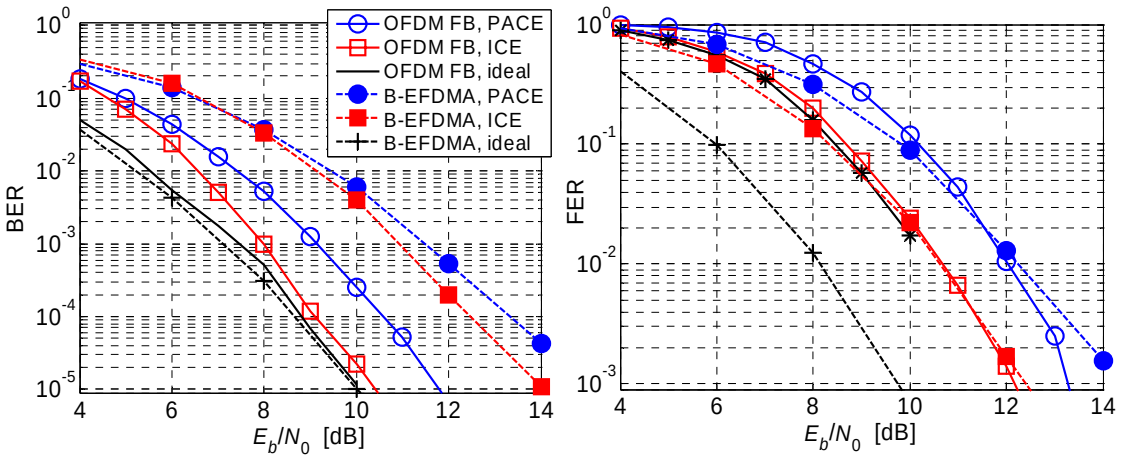

Figure C- 1 Bit and frame error rates for full bandwidth (FB) OFDM (1 user case) and B-EFDMA with 4x3 block size (32 user case)

In Figure C- 1 the BER and FER performance of full bandwidth (FB) OFDM (1 user case) and B-EFDMA with 4x3 block size and 32 users is compared. For perfect channel knowledge (label "ideal") the performance of B-EFDMA is very good. Due to the short codewords, the FER of B-EFDMA outperforms full bandwidth OFDM by 2dB. However, if channel estimation is taken into account the performance of B-EFDMA severely degrades. For B-EFDMA with PACE the performance degradation exceeds 4dB for

BER as well as FER. With ICE the FER of B-EFDMA can be improved by about 1.5dB, while the BER improvement is less than 1dB. However, a gap of about 2.5dB to the FER of B-EFDMA with perfect channel knowledge remains. The reason for this 2.5dB gap of ICE is twofold: first, the poor initial channel estimates since there is only one pilot per block; second, the relative small number of filter coefficients due to the small block size.

For full bandwidth OFDM the performance degradation of PACE and ICE relative to perfect channel knowledge is significantly lower. The FER of ICE even approaches the performance of perfect channel knowledge.

In summary, the choice of multiple access schemes for the WINNER system should not be carried out without taking into account channel estimation.

The next set of figures elaborates on the choice of the block (i.e. sub-chunk) size for B-EFDMA. By increasing the block size, while keeping the number of transmitted symbols per frame constant, less frequency diversity will degrade performance. On the other hand, with an increased block size more pilots can be accommodated per block, yielding improved channel estimates which boost performance. Hence, there clearly exists a trade-off on the optimum block size for B-EFDMA. Unfortunately, this optimum heavily depends on the number of coded symbols per frame (i.e. the size of the codeword), and the modulation cardinality, as well as on other factors. In the following we fix the size codeword length to N_{CW}=352, which is in line with the results in Figure C- 1. For the considered block sizes of 4x3, 8x3, 8x6 and 8x12, this results to one B-EFDMA block every 32, 64, 128 and 256 subcarriers, which corresponds to 32, 16, 8 and 4 blocks per frame, respectively.

It is important to note that for longer codewords the frequency diversity advantage for B-EFDMA with 4x3 blocks will reduce, while the channel estimation error does not. Therefore, the presented results favour small block length.

For block sizes multiple of 4x3, with the B-EDMA pilot spacings of D_t=3 and D_f=4 more pilots fit within one block, and so the filter orders for PACE and ICE can be increased accordingly. For PACE a block size of 8x3, 8x6 and 8x12 amounts to the filter orders in time M_t=1,2 and 4, while the frequency filter orders yields M_f=2. For ICE, the filter orders increase in proportion to the block size, i.e. a $m \times n$ block results in the filter orders M_t=n and M_f=m in time and frequency. The channel estimation unit is generated according to Scenario A in Appendix A, i.e. the maximum channel delays and the maximum Doppler frequency are assumed to be known.

Figure C- 2 shows results for the channel estimation MSE for B-EFDMA using dedicated pilots for various block sizes. It is clearly seen that the channel estimation performance benefits for larger blocks. While significant further performance improvements are provided by ICE, the effect of the B-EFDMA block size on the MSE is similar for both PACE and ICE.

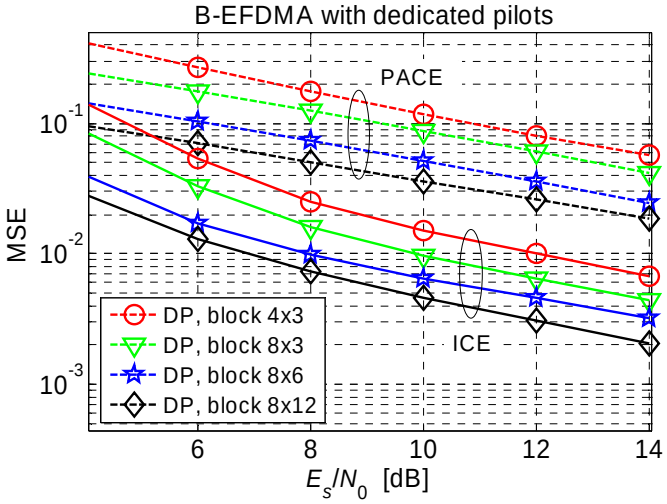

Figure C- 2 Channel estimation MSE for B-EFDMA using dedicated pilots for various block sizes (32 user case). Dashed and solid lines show the performance for PACE and ICE, respectively. The channel estimation unit is generated according Scenario A (see Appendix A)

Figures C-3 and C-4 show the bit and frame error rates for B-EFDMA using dedicated pilots for various block sizes. It is seen that the frequency diversity advantage for B-EFDMA with 4x3 blocks is mostly cancelled out by the degraded channel estimation performance. More specifically, B-EFDMA with large blocks (8x6 and 8x12) is superior for low SNR, while B-EFDMA with small blocks (4x3 and 8x3) is superior for high SNR (E_s/N_0>11dB). Interestingly, there is little different between block size 4x3 and 8x3, so the ability to perform interpolation only in frequency appears to have little effect on the performance. Furthermore, block size 8x12 has poor performance, even when taking account channel estimation. This is due to the fact that there are only 4 blocks per frame for the chosen frame length, compared to 32 blocks for a 4x3 block size.

In summary, for the selected parameters B-EFDMA with 8x6 blocks offers the best trade-off between frequency diversity and channel estimation performance; only for high SNR (E_s/N_0>11dB) B-EFDMA with small blocks (4x3 and 8x3) has a performance advantage. Only for codewords that are even smaller than 352, smaller blocks are are likely to prove superior.

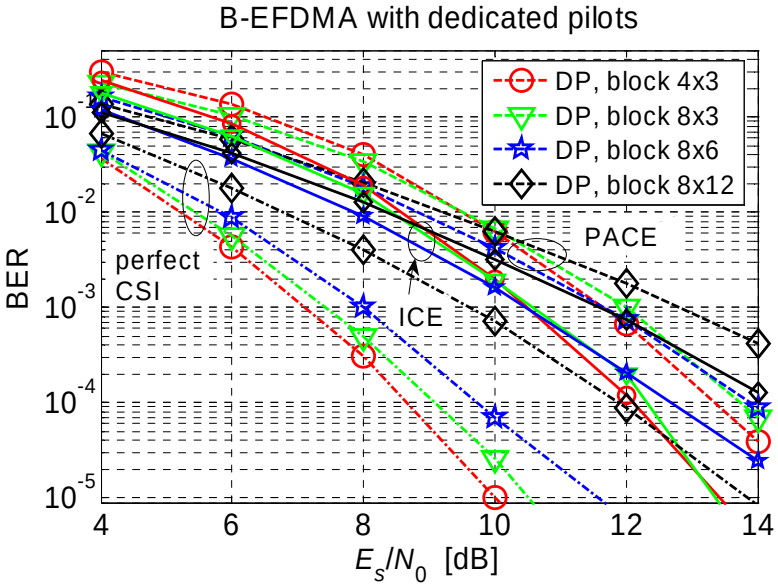

Figure C- 3 Bit error rates (BER) for B-EFDMA with channel estimation using dedicated pilots for various block sizes (32 user case). Dashed, solid and dash-dotted lines show the performance for PACE, ICE, and perfect channel state information (CSI), respectively.

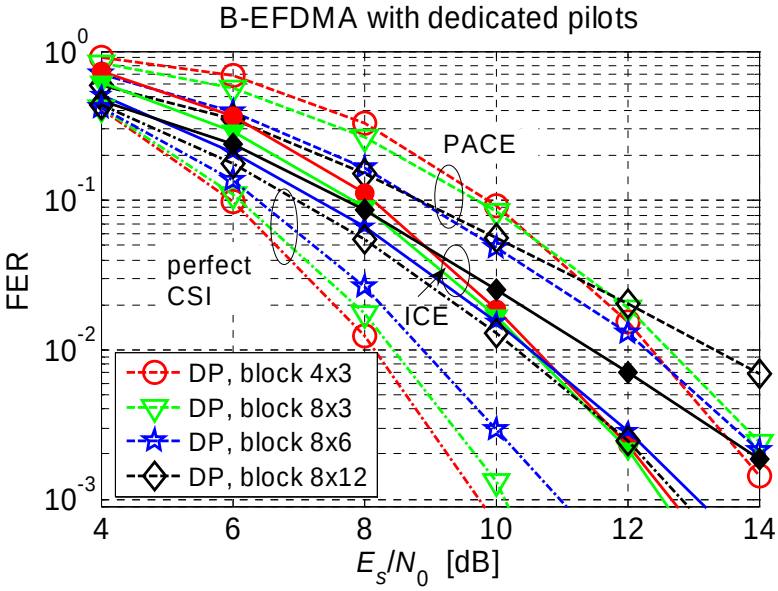

Figure C- 4 Frame error rates (FER) for B-EFDMA with channel estimation using dedicated pilots for various block sizes (32 user case). Dashed, solid and dash-dotted lines show the performance for PACE, ICE, and percect channel state information (CSI), respectively.

According to the discussion in Section 4.3, for ICE the performance is evaluated for feedback derived from **extrinsic** or **a posteriori** information, shown in Figure C-5. Note that all results reported in previous deliverables [WIN1D23], [WIN1D210] assume exchange of extrinsic information.

Furthermore, the performance of two variants of channel estimation units is compared, Scenario A and Scenario C in Appendix A. We note that for Scenario A the maximum channel delays and the maximum Doppler frequency are assumed to be known, whereas Scenario C assumes maximum channel delays equal to the CP duration, and maximum Doppler frequencies corresponding to 100km/h mobile velocities. Simulations suggest that in case dedicated pilots are used, for higher order modulation the high fragmentation of B-EFDMA blocks lead to unacceptable performance. Hence, for subsequent simulation results in Figure C-5 to C-7 we choose the original chunk size as the block dimension, i.e. a block size of 8x12. Also the codeword length is increased by a factor of 4, resulting in a codeword length of 1408 compared to previous plots, so to provide sufficient frequency diversity. In this configuration 8x12 blocks are placed equidistantly, once every 32 subcarriers.

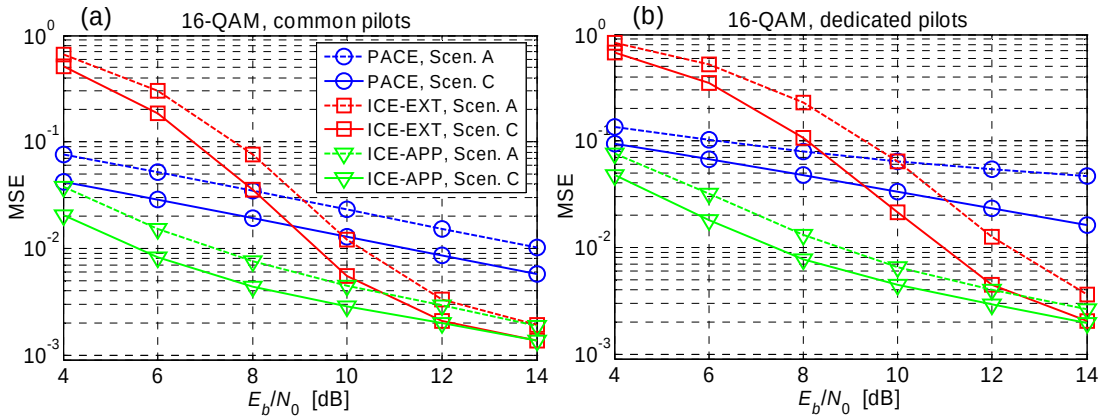

Figure C- 5 MSE vs SNR for PACE and ICE with (a) common and (b) dedicated pilots. 8x12 block size, 16-QAM, SISO, FDD mode, channel C2 NLOS, UT velocity 50 km/h.

Figure C-5 shows the mean squared error (MSE) against the SNR for PACE or ICE in the FDD mode. Due to the superior reliability of a posteriori (APP) feedback from the channel decoder, the MSE using APP feedback is significantly better compared to extrinsic (EXT) feedback in the low SNR regime. This is particularly evident for higher order modulation, as for 16-QAM. In comparison, the MSE improvement for ICE using an estimator according to Scenario A rather than Scenario C is not as significant.

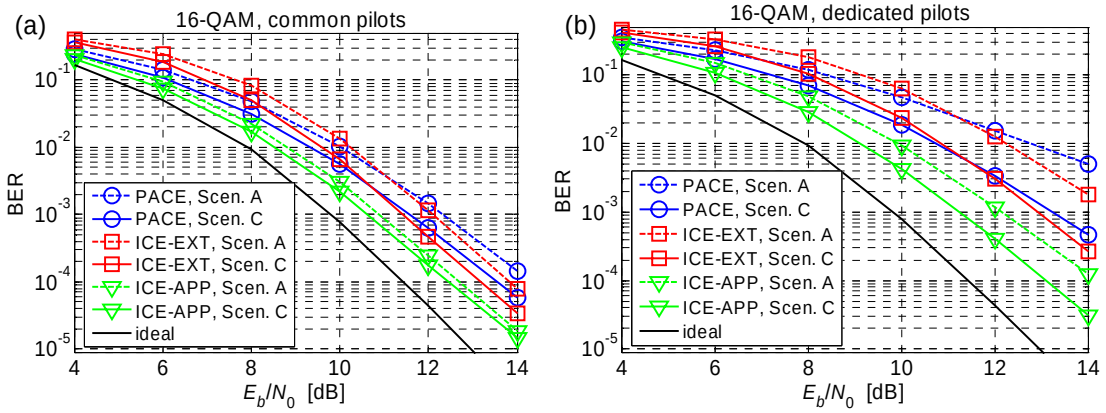

Figure C- 6 BER vs SNR for PACE and ICE with (a) common and (b) dedicated pilots. 16-QAM, SISO, FDD mode, channel C2 NLOS, UT velocity 50 km/h.

Figure C- 6 shows the bit error rate (BER) against the SNR for PACE or ICE for the FDD mode. Due to the superior reliability of the a posteriori (APP) feedback from the channel decoder, ICE APP outperforms ICE with extrinsic information feedback (ICE EXT). As also indicated by the MSE results, ICE APP is very effective for higher order modulation such as 16-QAM. ICE-APP utilizing an estimator

according to Scenario A only deviates about 1 and 1.5 dB from perfect CSI (label "ideal") for common and dedicated pilots, respectively. Interestingly, the degradation of ICE-APP compared to perfect CSI increases when the SNR increases. This is in contrast to the MSE curves in Figure C-5, and suggests that the MSE is not a reliable indicator for BER or FER performance.

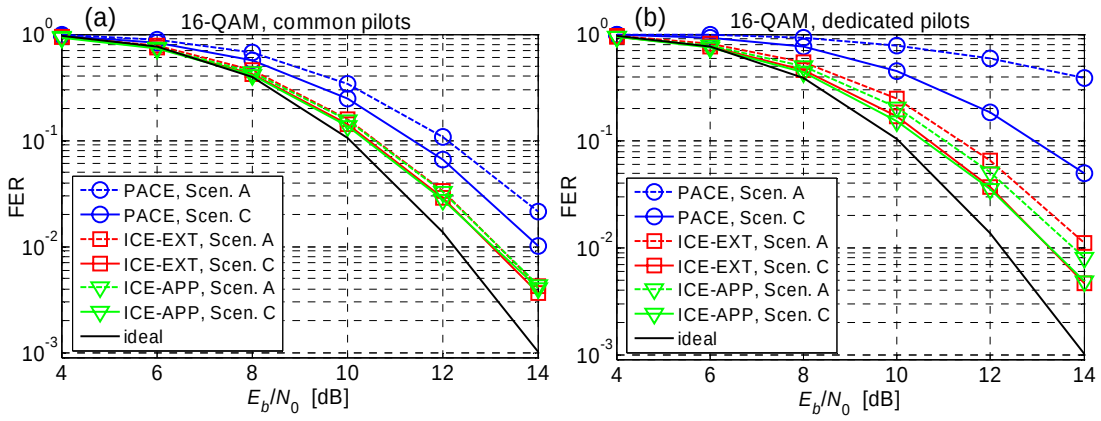

Figure C- 7 FER vs SNR for PACE and ICE with (a) common and (b) dedicated pilots. 16-QAM, SISO, FDD mode, channel C2 NLOS, UT velocity 50 km/h.

Figure C-7 shows the frame rate (FER) against the SNR for PACE or ICE for the FDD mode. For ICE with common pilots the performance of ICE-EXT and ICE-APP is similar; the performance loss relative to perfect channel knowledge does not exceed 1dB. Also no advantage is overserved when using the more sophisticated estimation unit of Scenario A. For chunk based channel estimation with dedicated pilots ICE turns out to be particularly effective. There the degradation with respect to perfect CSI is also bounded by about 1dB, which translates to an improvement exceeding 2dB compared to PACE. This however, requires an estimator which has knowledge about the channel delays and Doppler frequency (Scenario A). On the other hand, ICE-APP with an estimator according to Scenario C is only about 0.5dB worse than a ICE-APP with a Scenario A estimator.

C.2 Noniterative DFT-precoded OFDM performance results – full bandwidth

Results have been obtained for serial modulation (DFT-precoded GMC) for the case of Wiener interpolation in the frequency and time domains (similar to the interpolations used for OFDM-PACE, using the same maximum Doppler and uniform power delay profile assumptions). Three scenarios were investigated, corresponding to three degrees of prior knowledge about channel ststistics:

- Scenario A: known maximum delay spread and maximum vehicle speed
- Scenario B: known maximum delay spread but unknown maximum vehicle speed (100 km/hr assumed)
- Scenario C: assumed maximum delay spread assumed equal to CP length, and 100 km/hr maximum vehicle speed.

Rate ½ convolutional codes with constraint length 7 with QPSK modulation were used in the simulations.The frame error rate performance curves for FET and FDSPT pilots, used with soft DFE (also called IBDFE) equalization, with 4 equalization iterations, are given in Figure C-8 for the case of urban macro channel C2 with a vehicle speed of 50 km./hr. The system parameters used are those shown in Appendix A for the FDD mode. 256 pilots are inserted (in time or frequency) in the first and 12th block of each slot.

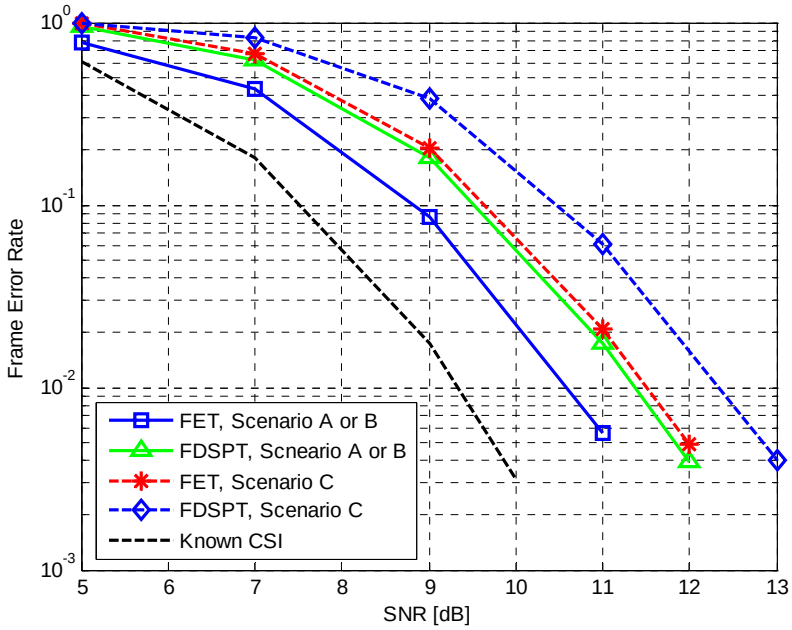

Figure C- 8 Wiener filter, soft iterative DFE results for FET and FDSPT pilots. C2 channel, 50 km./hr. Rate ½ constraint length 7 convolutional code. 2X 1 D Wiener interpolation in time and frequency with frequency window 16 and time window 2

C.3 Noniterative and iterative DFT-precoded OFDM performance results – chunk-based transmission, IFDMA and B-IFDMA

The simulation results shown in C.2 were obtained for non-iterative channel estimation; i.e. channel estimates were obtained solely from Wiener interpolation from pilot positions over one frame, as elaborated in Section 4.2. In this section, we show simulation results for non-iterative, and also for iterative channel estimation (ICE), described in 4.3.2. The interpolation and smoothing in channel estimation is extended beyond one frame. The results also include the chunk-based multiple access schemes IFDMA and B-IFDMA, as well as full-bandwidth transmission, and also a variant of B-IFDMA, called 2B-IFDMA, in which full chunks, equally spaced in frequency are used.

IFDMA was simulated with two FDM pilot arrangements (both FET), shown in Figure C-9. In each case, data- or pilot-carrying subcarriers are spaced by 32 subcarriers (32X39.0625=1250 KHz), enough to yield substantial frequency diversity for channel model C2 in the non-adaptive transmission mode. The designation "FxTy" means that pilot-carrying OFDM symbols contain x pilots per chunk, and that y OFDM symbols per chunk contain pilots. F1T1 incurs a pilot overhead of 1/12 and F1T2 incurs a pilot overhead of 2/12. In each case simulated, a user occupies 12 out of 96 positions in a FDD chunk.

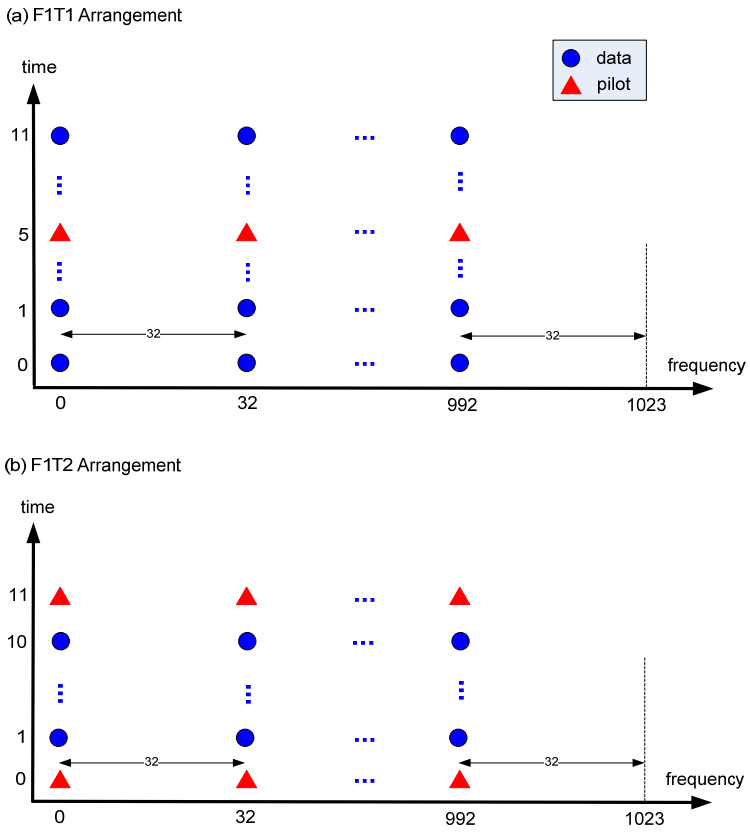

Figure C-9 IFDMA pilot arrangements: F1T1 (pilot overhead=1/12) and F1T2 (pilot overhead=2/12)

B-IFDMA, with the same total number of occupied positions per chunk, was also simulated, in three pilot symbol arrangements, shown in Figure C-10. F1T1, F2T1 and F2T2 respectively incur pilot overheads of 1/12, 2/12 and 4/12. In these arrangements, the same inter-block spacing of 32 subcarriers is used, assuring good frequency diversity between blocks. Another "full chunk" signal format, called 2B-IFDMA, was also simulated, where a user's chunks are spaced by 32 subcarriers and where each occupied chunk is fully populated in all 96 positions, and there are four pilots per chunk, two in each of the first and twelfth OFDM symbols. 2B-IFDMA carries 8 times the data rate of the B-IFDMA cases, and has a pilot overhead ratio of 4/96. Note that comparison of full bandwidth and 2B-IFDMA cases with IFDMA and B-IFDMA is imprecise, since each of these cases involves different numbers of data symbols, and hence different code block sizes.

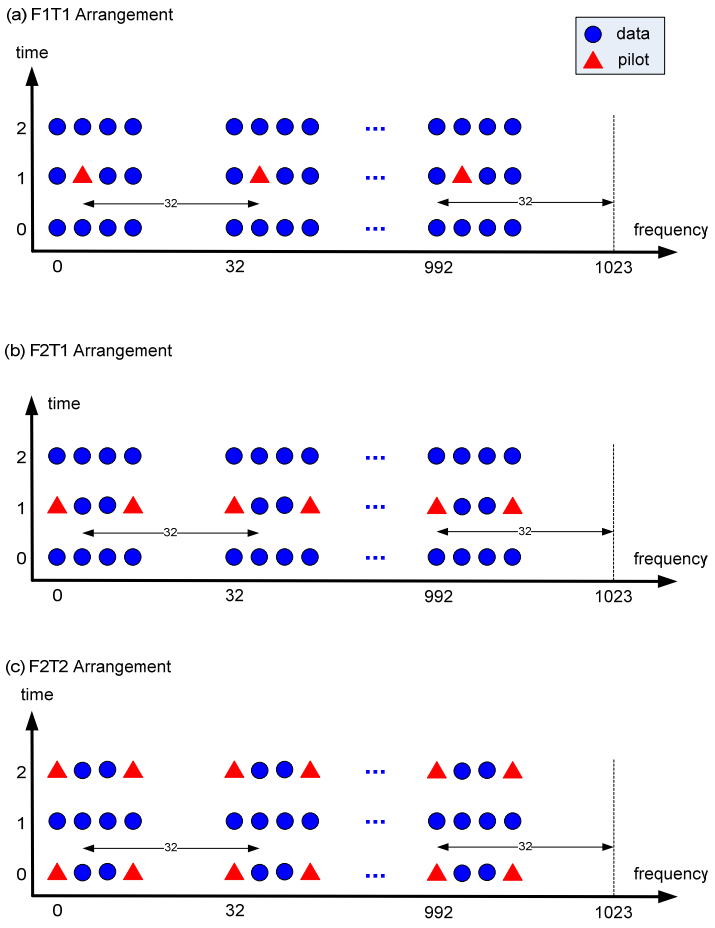

Figure C-10 B-IFDMA pilot arrangements: F1T1 (pilot overhead=1/12), F2T1 (pilot overhead=2/12) and F2T2 (pilot overhead=4/12)

Interpolation and smoothing of channel estimates over more than one frame has the potential to improve channel estimation performance (at the expense of increased receiver delay). Figure C-11 shows pilot arrangements for smoothing over one or more frames. Q is the number of OFDM symbols over which smoothing is performed. For example Q=48 for IFDMA indicates smoothing over 4 successive half-duplex frames, and Q=6 for B-IFDMA indicates smoothing over 2 successive half-duplex frames.

In the simulation results shown here, the receiver uses soft DFE (IBDFE). Non-iterative channel estimation, with Wiener interpolation is signified by "W" in the following figures. For F1T1, there is only one pilot symbol per chunk, and no interpolation is used. For F1T2 there is time interpolation using a Wiener filter with the Doppler assumption of scenario C, specified in C.2. Simulation results were also obtained for scenario A and B, but they are not displayed here for brevity.

IFDMA with the various forms of channel estimation is shown in Figure C-12. Also shown for comparison is the case of known channel state information (indicated by "K-CSI"). Comparison with Figure C-8 shows performance advantages of the extra frequency diversity inherent in the IFDMA signal formats, which partially offsets the higher pilot overhead of the latter. ICE gives roughly a 1 dB improvement over the corresponding non-iterative channel estimation, and smoothing over 4 frames (Q=48) gives about 0.6 to 1 dB improvement over smoothing over just one frame. The FER performance of 4-frame smoothing combined with ICE is about 1 dB worse than the case of known channel state information.

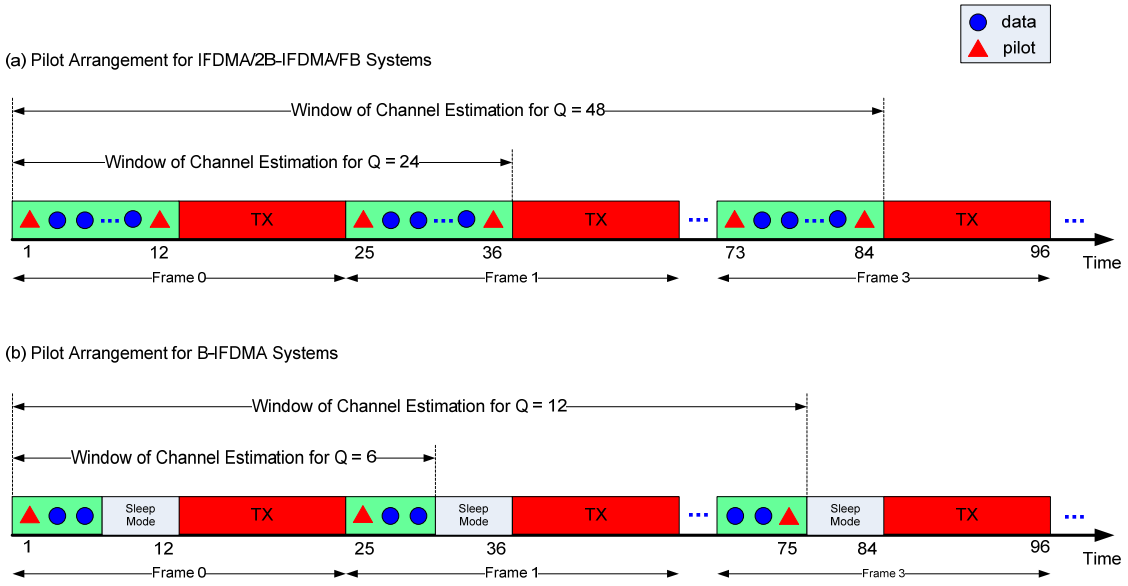

Figure C-11 Pilot arrangements for smoothing over one, two or four half duplex frames for (a) IFDMA and 2B-IFDMA, (b) B-IFDMA. Q is the number of OFDM symbols over which smoothing/interpolation is performed. Red triangle indicates OFDM symbols which contain pilots. Red sections indicate periods in which the half-duplex FDD terminal is transmitting, not receiving.

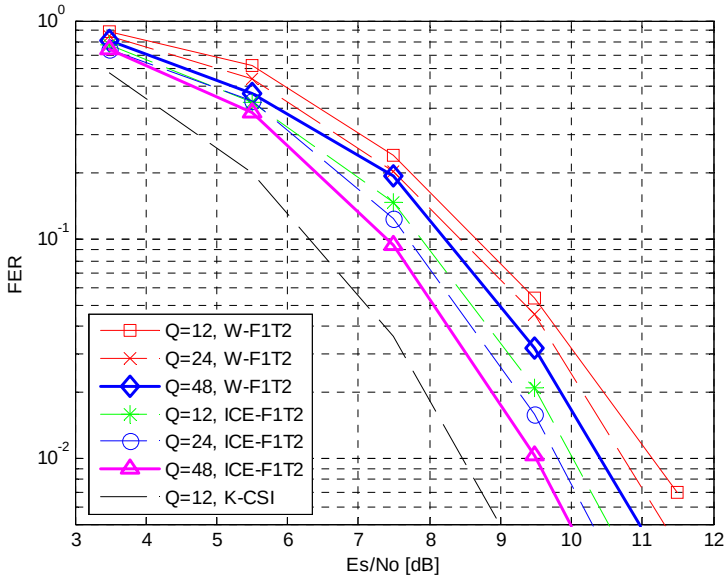

Figure C-12 Frame error rate for IFDMA with pilot arrangement F1T2, with non-iterative (W) and iterative (ICE) channel estimation. Also shown for comparison is the case of known channel state information (K-CSI). Q=number of OFDM symbols used for channel estimation interpolation and smoothing. C2 channel model with vehicle speed=50 km./hr. Scenario C assumptions used: maximum delay spread=CP length; vehicle speed = 100 km./hr.

If full duplex FDD is used, the red transmission periods, shown without pilots in Figure C-11, are eliminated, and smoothing can be more effective. Figure C-13 shows average mean squared channel estimation error for IFDMA for estimation over one (Q=12) , two (Q=24) and four (Q=48) frames, for the half and full duplex cases. The figure legends indicate which OFDM symbols contain pilots. For example "[1 8 16 24]" in the full duplex FDD case means that there are two successive frames (therefore 24 adjacent OFDM symbols) with pilots in the 1st, 8th, 16th and 24th OFDM symbols. "[1 12 25 36]" in the half duplex FDD case means that there is a 12-OFDM symbol gap between two received frames, so pilots

occur in the 1st and 12th OFDM symbol of the first received frame, and also in the 1st and 12th OFDM symbol of the second received frame.

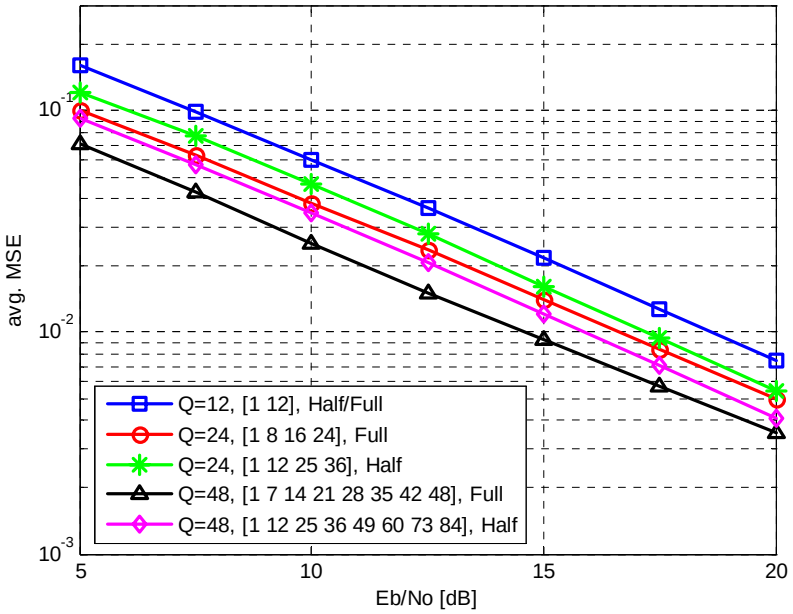

Figure C-13 Average mean square non-iterative channel estimation error for IFDMA for estimation over several frames in half and full duplex cases.

This shows clearly that multi-frame channel estimation is more effective in the full duplex FDD scenario, because successive received frames are adjacent, but there is still some improvement for half duplex FDD. All other simulation results in this section are for the half duplex case.

Frame error rate for multi-frame smoothing with the F1T1 pilot pattern for B-IFDMA is shown in Figure C-14. B-IFDMA is just slightly (~0.1 dB) better than IFDMA for known CSI, but with channel estimation with F1T1, it is 0.6 dB to almost 2 dB worse than the corresponding IFDMA, since B-IFDMA with F1T1 has only one pilot per block, and under the simulation conditions (C2 channel with 50 km./hr, the channel is *not* constant over a 4X3 block. Note that although F1T1 incurs less pilot overhead than F2T1 – 1/12 instead of 2/12, it is considerably more than the full bandwidth system pilot overhead of 4/96.

Figure C-15 shows corresponding results for B-IFDMA with the F2T1 pilot arrangement (same overhead ratio as for the IFDMA case). B-IFDMA still shows up worse than IFDMA with each type of channel estimation, but the difference is less than for the F1T1 case.

The "full-chunk" case, 2B-IFDMA, where fully-occupied chunks are separated by 32 subcarriers, is shown in Figure C-16. The pilot overhead (4/96) is much less than that of the IFDMA and B-IFDMA cases, and the FER performance for ICE with smoothing over 4 frames is about the same as that of IFDMA with the same channel estimation method.

Finally, the full bandwidth case (equivalent to the scenario of Figure C-8) is shown in Figure C-17. The known-CSI performance is slightly worse (about 0.8 dB) than that of IFDMA, but the performance with ICE and 4-frame smoothing is about the same as that of IFDMA. The diversity gains achieved by IFDMA and B-IFDMA are somewhat diminished by their less effective channel estimation capabilities (due to sparse pilot locations) in the C2 channel with 50 km./hr.

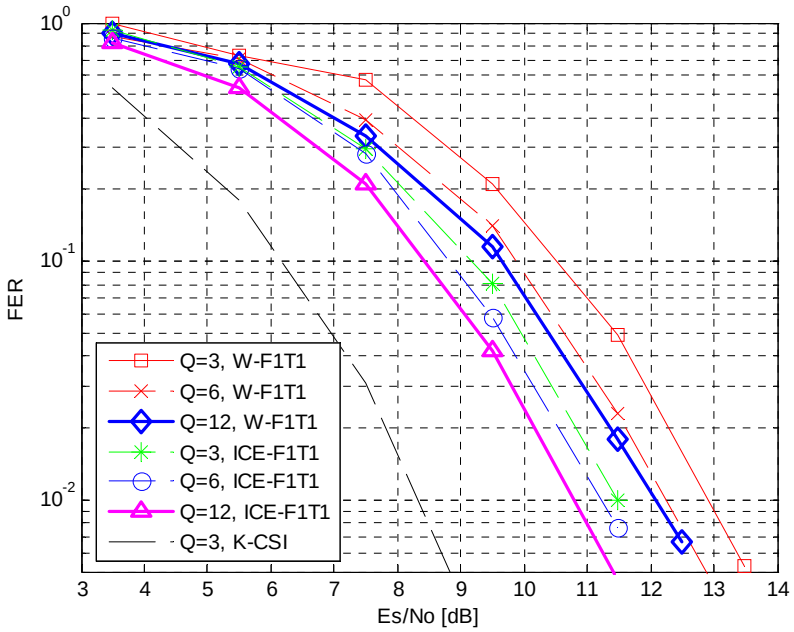

Figure C-14 Frame error rate for B-IFDMA with pilot arrangement F1T1, with non-iterative (W) and iterative (ICE) channel estimation. Also shown for comparison is the case of known channel state information (K-CSI). Q=number of OFDM symbols used for channel estimation interpolation and smoothing. C2 channel model with vehicle speed=50 km./hr. Scenario C assumptions used: maximum delay spread=CP length; vehicle speed = 100 km./hr.

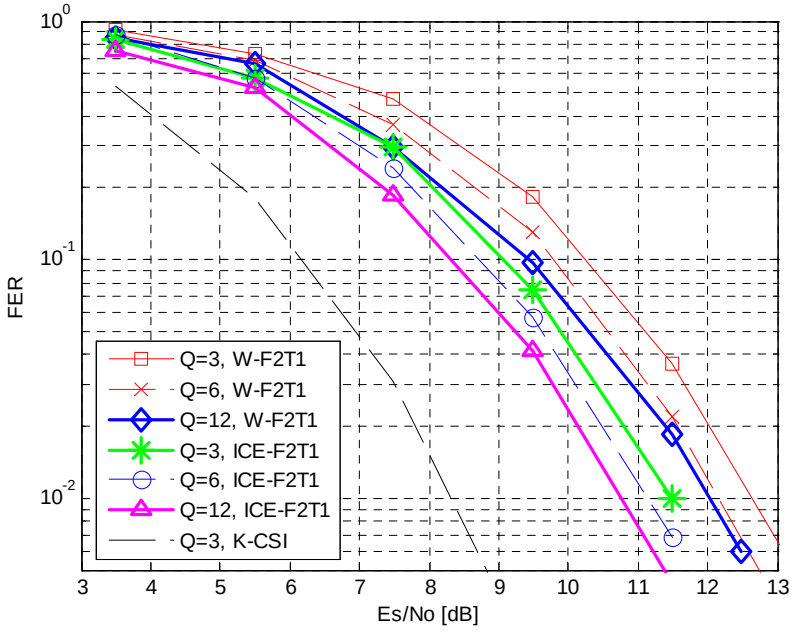

Figure C-15 Frame error rate for B-IFDMA with pilot arrangement F2T1, with non-iterative (W) and iterative (ICE) channel estimation. Also shown for comparison is the case of known channel state information (K-CSI). Q=number of OFDM symbols used for channel estimation interpolation and smoothing. C2 channel model with vehicle speed=50 km./hr. Scenario C assumptions used: maximum delay spread=CP length; vehicle speed = 100 km./hr.

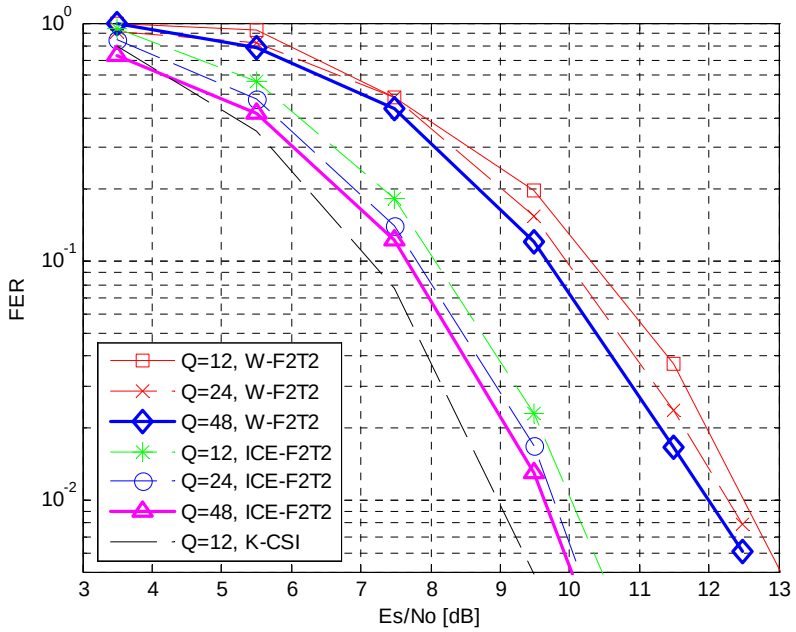

Figure C-16 Frame error rate for 2B-IFDMA with pilot arrangement F2T2, with non-iterative (W) and iterative (ICE) channel estimation. Also shown for comparison is the case of known channel state information (K-CSI). Q=number of OFDM symbols used for channel estimation interpolation and smoothing. C2 channel model with vehicle speed=50 km./hr. Scenario C assumptions used: maximum delay spread=CP length; vehicle speed = 100 km./hr.

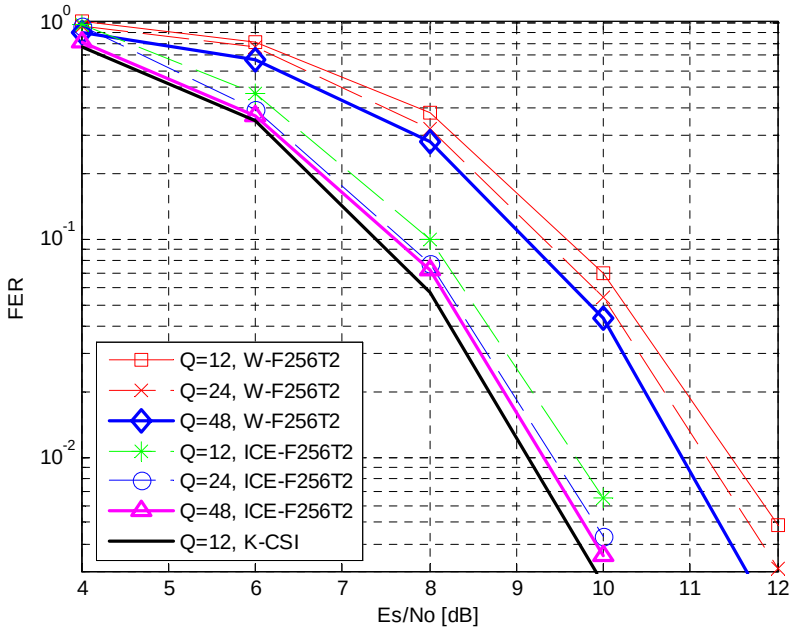

Figure C-17 Frame error rate for full bandwidth system with pilot arrangement F2T2, with non-iterative (W) and iterative (ICE) channel estimation. Also shown for comparison is the case of known channel state information (K-CSI). Q=number of OFDM symbols used for channel estimation interpolation and smoothing. C2 channel model with vehicle speed=50 km./hr. Scenario C assumptions used: maximum delay spread=CP length; vehicle speed = 100 km./hr.

C.4 Performance of Interference Suppression Techniques in a Wide Area Cellular Environment

Several interference suppression and channel estimation techniques were simulated for in-cell SDMA single-antenna users (ICU) transmitting DFT-precoded OFDM (serial modulation) signals to a base station that has M receiving antennas. Each transmitted signal is QPSK with rate ½ constraint length 7 convolutional coding. The average received powers of the ICUs, which transmit simultaneously in a common bandwidth, were assumed equal as a result of the application of power control. As well, there are several out-of-cell interferers (OCI) transmitting to other base stations. The average received power of the OCIs was significantly below that of the ICUs, in accordance with the uplink interference scenario in Appendix A. Each transmission path was modelled as an independent C2 channel. All users' 12-OFDM symbol frames were assumed synchronised. To the first and twelfth OFDM symbol of each frame was added two or more short training blocks containing a Chu sequence of 256 pilot training symbols. The resulting pilot waveform was therefore uniform in amplitude and spectrum. It was shown in [WIN1D210] that an arrangement of time-multiplexed pilots has the same performance as an equivalent arrangement of frequency multiplexed pilots in which a grid of equally-spaced pilots in an OFDM symbol is the result of a DFT of a 256-point Chu sequence. All in-cell pilots were orthogonal and did not interfere with one another. Thus the pilot arrangement was equivalent to one in which each ICU's pilots were allocated to two or more disjoint, uniformly-spaced sets of 256 subcarriers in pilot-carrying OFDM symbols. OCI pilots overlapped the ICU pilots, so that each ICU pilot suffered from low level interference from one or more OCI pilots.

Since ICU pilots were orthogonal, initial channel estimates for each ICU to each receiving antenna were made using the estimation and 2X1D Wiener interpolation procedure described in Section 4.2, neglecting the interference from OCI pilots. From these channel estimates, a linear least squares frequency domain equalizer array $\mathbf{W}(f)$ was derived as in Section 4.2, and soft symbols from this equalizer for each ICU were passed to a decoder, yielding data symbol decisions. An improved equalizer using the iterative block decision feedback equalization (IBDFE) algorithm, with 4 iterations, described in 4.3.2 was also tested. In a further refinement, an iterative decision feedback channel estimation scheme (DFICE) was tested, as described in Section 4.3.2.

Figure C-18 shows the frame error rate as a function of the number of out-of-cell users, for the scenario in which there is K=1 in-cell user, there are two receive antennas, the signal to noise ratio at each antenna is 6 dB, and the OCIs' received average power is either -15 dB or -16.6 dB. Each transmitted signal arrives at each receiving antenna through an independent C2 channel with a vehicle speed of 50 km./hr. OCIs interfere with ICU data and pilot signals, and there was no attempt at compensating for the OCIs. The number of training blocks is NT=2. Two receiver and channel estimation types are compared:

(1) Linear equalization with ICU channels estimated from 2X1D Wiener pilot interpolation (labelled "LE")
(2) IBDFE with ICU channels initially estimated from 2X1D Wiener pilot interpolation and in subsequent iterations by DFICE (labelled "DFICE")

For a frame error rate of 10^{-2}, only one -16.6 dB OCI can be tolerated by the linear equalizer, while two -15 dB or four -16.6 dB OCIs can be tolerated by the DFICE/IBDFE combination. The results demonstrate the effectiveness of DFICE. They also show the system's sensitivity to the number of uncompensated out-of-cell interferers, especially for a fixed amount of pilots and a number of receiving antennas that is less than the total number of interferers. Results (not shown) obtained for training proportional to the number of OCIs show less sensitivity to the number of OCIs, but require a proportional increase in pilot overhead. Results for the case of K=2 in-cell transmitters, with linear equalization and non-iterative channel estimation, are shown in Figure C-19. Here there are 4 OCIs, each with the same average received power, either -15 dB or -18.2 dB. There are now 4 receiving antennas. Each of the two ICUs' pilots is interfered with by two OCIs' pilots, and each ICU's data is interfered with by the other ICU's data plus all 4 OCIs' data.

Also shown are FER results for perfect channel state information in two cases: (1) where the channels of all ICU and OCI users are known, and a linear equalizer suppresses all the OCIs as well as the in-cell interferer; (2) where only the channels of the ICUs are known (the OCIs still just add to the noise), and a linear equalizer or a IBDFE receiver detects ICUs. The OCIs are at -15 dB in each of these PCSI cases. With OCIs at this level, it is seen that knowing only the ICUs' channels causes about a 0.4 dB SNR penalty relative to the case where all channels are known and taken into account. The figure also shows a very substantial SNR penalty relative to perfect CSI (4.5 to 5 dB), for linear equalization when the ICU channels are estimated non-iteratively.

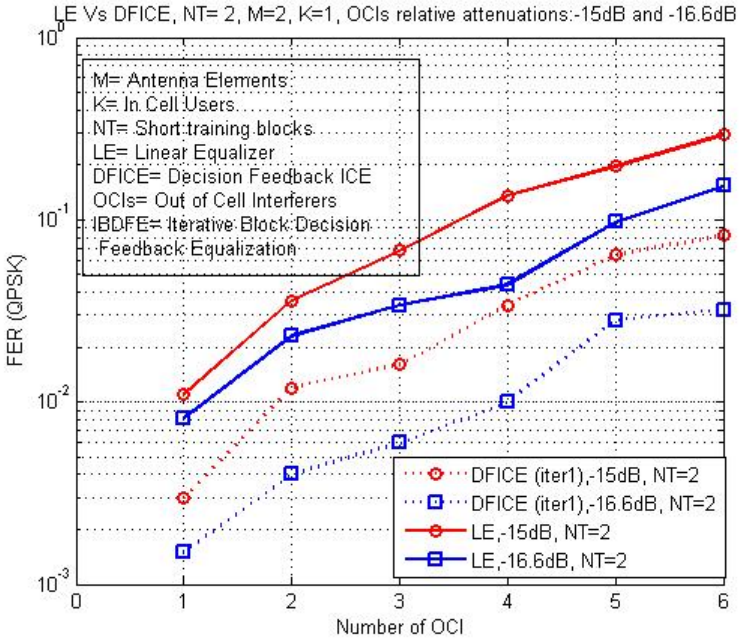

Figure C-18 Frame error rate for 1 in-cell user with 0dB average received power, variable number of out-of-cell users, each at -15 dB or -16.6 dB average received power, 2 receiving antennas. Serial modulation. Linear frequency domain with 2X1D pilot interpolation (LE) or IBDFE equalization with decision feedback iterative channel estimation (DFICE) with 1 iteration. Four 256-symbol training blocks. SNR=6 dB at each receiving antenna. Rate ½ constraint length 7 convolutional code, QPSK modulation. Independent C2 channel model on each antenna to antenna link. 50 km./hr. mobility.

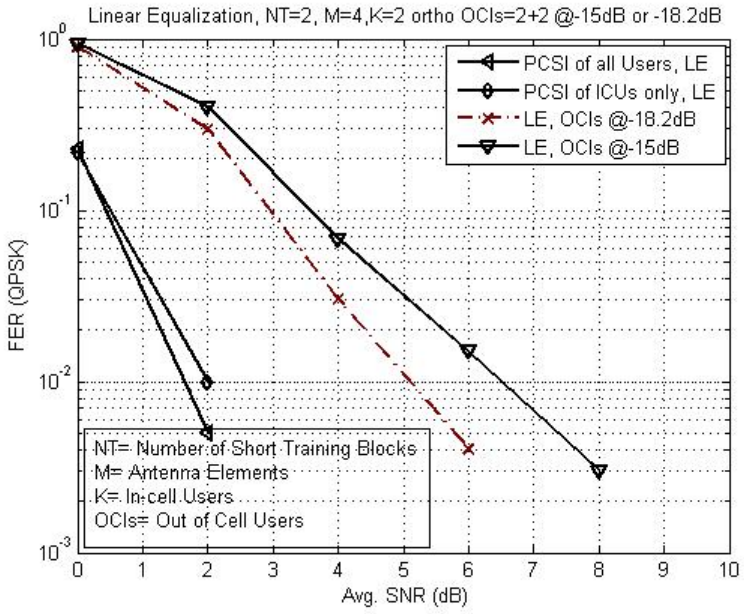

Figure C-19 Frame error rate for 2 in-cell users with 0dB average received power, 4 out-of-cell users, each at -15 dB or -18.2 dB average received power, 4 receiving antennas. Serial modulation. Linear frequency domain equalization with 2X1D pilot interpolation. Four 256-symbol training blocks. Rate ½ constraint length 7 convolutional code, QPSK modulation. Independent C2 channel model on each antenna to antenna link. 50 km./hr. mobility.

Figure C-20 shows frame error rate results, under the same interference conditions, for IBDFE equalization with four iterations, with 2X1D Wiener interpolation or decision feedback iterative channel estimation (DFICE) with one or two iterations. There is an improvement over the linear equalization, non-iterative channel estimation case; the SNR penalty relative to perfect CSI is now about 3 dB at 10^{-2}

frame error rate, for the 4 OCIs at -15 dB. The figure also shows the case where there are no OCIs: the SNR penalty attributable to the presence of the 4 OCIs is about 1.5 dB.

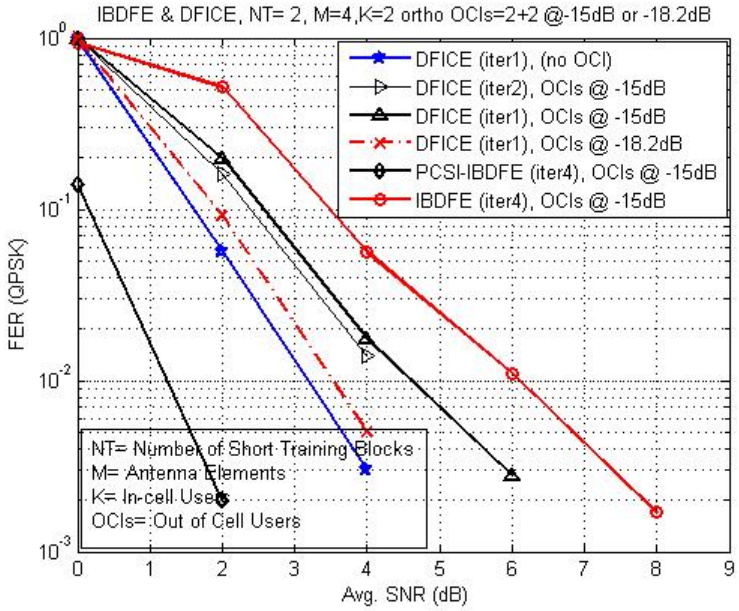

Figure C-20 Frame error rate for 2 in-cell users with 0dB average received power, 4 out-of-cell users, each at -15 dB or -18.2 dB average received power, 4 receiving antennas. Serial modulation. IBDFE equalization with 2X1D pilot interpolation or decision feedback iterative channel estimation (DFICE) with 1 or 2 iterations. Four 256-symbol training blocks. Rate ½ constraint length 7 convolutional code, QPSK modulation. Independent C2 channel model on each antenna to antenna link. 50 km./hr. mobility.

The effect of adding the least squares forward filter updating described in Section 4.3.2 is shown in Figure C-21. Comparison with Figure C-20 shows a SNR improvement of 0.5 to 1 dB for four OCIs at -15 dB each.

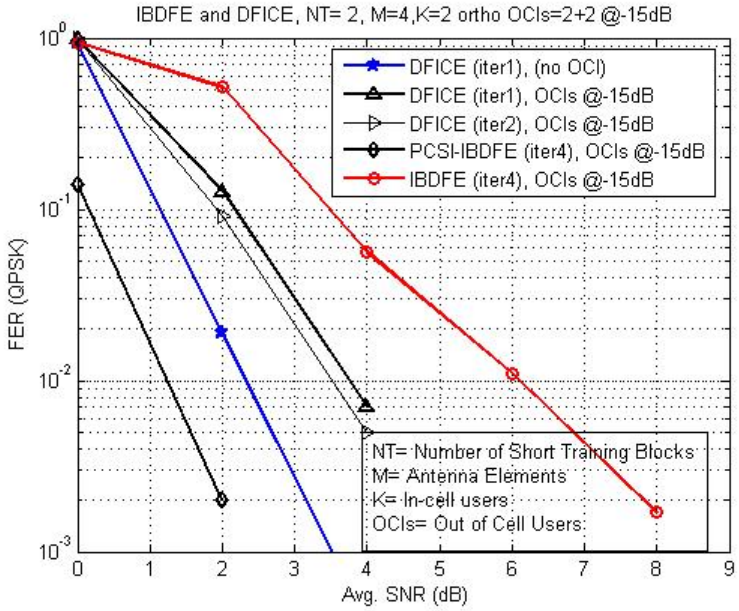

Figure C-21 Frame error rate for 2 in-cell users with 0dB average received power, 4 out-of-cell users, each at -15 dB average received power, 4 receiving antennas. Serial modulation. IBDFE equalization with 2X1D pilot interpolation or decision feedback iterative channel estimation (DFICE) with 1 or 2 iterations, and also least squares updating of forward equalizer to mitigate OCIs. Four 256-symbol training blocks. Rate ½ constraint length 7 convolutional code, QPSK modulation. Independent C2 channel model on each antenna to antenna link. 50 km./hr. mobility.

C.5 Performance Assesment of Kalman filter

Figure C-22 shows the MSE as a function of the SNR, for the Kalman filtering approach and few reference approaches. MSE is averaged over all chunks within superframe. Observed performance represents a lower bound since it is assumed that all chunks of the superframe belong to one user. In Figure C-22, ICG and ECG denote cases when ideal or estimated channel information is obtained from the preamble, respectively. Furthermore, KALMAN denotes observed approach, EXTRAPOL case when channel information from the preamble is exptrapolated without using correction step of the Kalman filter, and NO EST case when channel information from the preamble is kept throughput the superframe. Mobile speed is set to 50 km/h and C1 channel model is used. It can be seen that only with Kalman filtering the MSE of 0.1 is approached. Such MSE can be considered sufficient for the purposes of CQI.

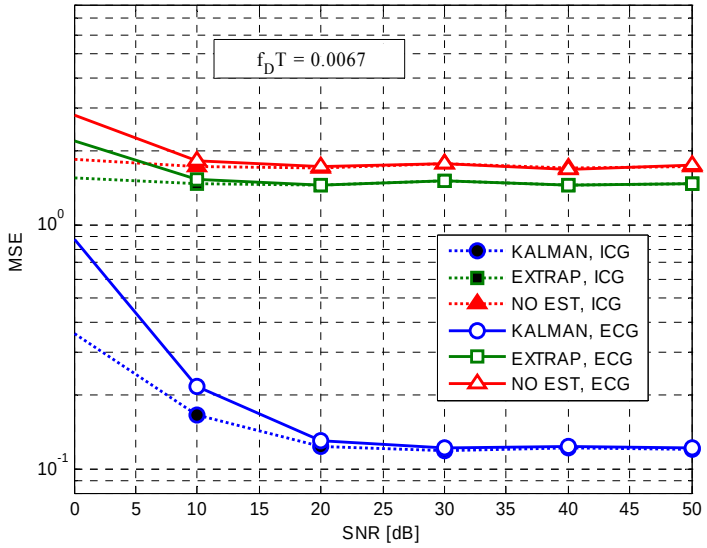

Figure C-22 MSE versus SNR performance for proposed Kalman filtering and other approaches.

Figure C-23 shows the MSE as a function of the Doppler frequency for Kalman filtering method and for SNR=10 dB. Again, MSE is averaged over all chunks within superframe. As expected, MSE performance worsens with increasing Doppler frequency However, even for considered mobile speeds above 50 km/h the MSE performance is below 0.2.

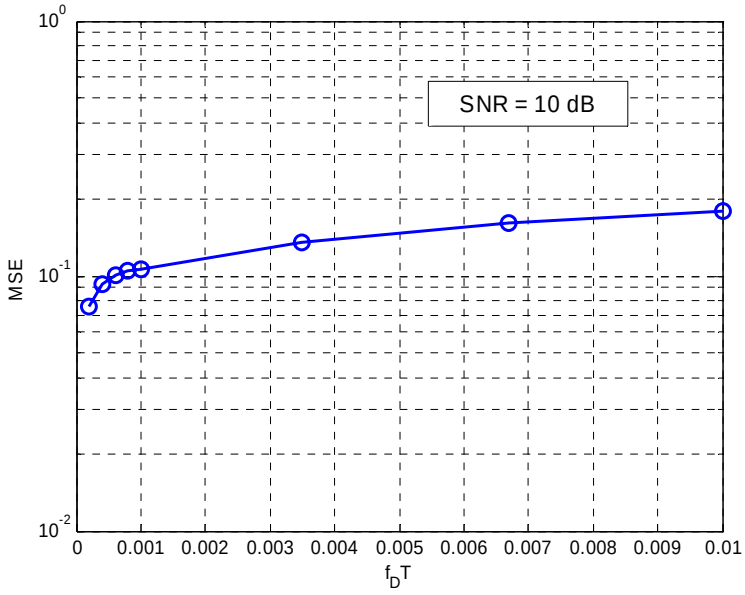

Figure C-23 MSE versus SNR performance for proposed Kalman filtering and other approaches.

Appendix D. Assessment of Genetic Algorithm Assisted Iterative Channel Estimation for MIMO-OFDM Uplink

D.1 Evaluation in WINNER Metropolitan Area (MA)

In this section, the performance of a 4QAM MIMO OFDM system using the proposed GA-ICE technique of Section 4.3.1 is quantified. The simulated scenario was the WINNER B1 channel [WIN1D54] associated with the TDD mode Metropolitan Area (MA) environment. The power delay profile of the channel is summarized in Table D-1. A frame size of N_F = 15 OFDM symbols, each constituted by K=2048 number of subcarriers, and a cyclic prefix of 128 samples were used [WIN2D6137]. The complex-valued channel envelope was assumed to remain unchanged within one OFDM symbol duration, but varied from one OFDM symbol to another.

As a simple example, N_t = 2 uplink users were supported by N_r = 2 BS receiver antennas, while each UT employs a single transmit antenna. The UTs were assumed to travel at a speed of 70km/h, corresponding to an OFDM symbol normalized Doppler frequency of 0.006. The fading envelope of the $N_t \times N_r$ number of UT-receiver channel links were assumed to be uncorrelated. Each user's associated transmit power or signal variance was assumed to be unity. The WINNER TDD orthogonal pilot pattern [WIN2D6137] was used, where the resultant pilot overhead[7] is ε =6.7%.

A half-rate Low Density Parity Check (LDPC) code proposed for WINNER systems [WIN1D210], [TZH+06] was employed, where the codeword size was set to 576 bits. Iterative decoding was performed by Min-Sum algorithm with a scaling factor of 0.8, horizontal scheduling, and a maximum iteration of 20 [WIN1D210], [TZH+06]. The above-mentioned simulation configurations and parameters are summarized in Table D-2.

Table D-1: Power delay profile of the WINNER B1 channel [WIN1D54].

Delay (ns)	0	10	40	60	85	110	135
Power (dB)	-1.25	0	-0.38	-0.10	-0.73	0.63	1.78
Delay (ns)	165	190	220	245	270	300	325
Power (dB)	-4.07	-5.12	-6.34	-7.35	-8.86	-10.1	-10.5
Delay (ns)	350	375	405	430	460	485	
Power (dB)	-11.3	-12.6	-13.9	-14.1	-15.3	-16.3	

Table D-2: Simulation parameters used in Appendix D.

FEC	Codec	LDPC [WIN1D210], [TZH+06]
	Code rate	1/2
	Decoding algorithm	Min-Sum (scaling factor 0.8)
	Scheduling	Horizontal
	Maximum number of iterations	20
	Codeword length	576 bits
System	Modulation	4QAM
	Number of users N_t	2
	Number of receivers N_r	2
	Subcarriers K	2048
	Cyclic prefix	128
	Frame size N_F	15 OFDM symbols
	Channel estimator	GA-ICE
	Pilot overhead ε	6.7%
	UT speed	70km/h

[7] The pilot overhead ε is defined by $\varepsilon = (N_t N_P)/(KN_F)$, where N_P is the total number of pilots used by each user in one frame.

	Number of inner iterations I_i	0-3
	Number of outer iterations I_o	0-3
Channel	Model	WINNER B1 [WIN1D54]
	Number of paths	20
	Power delay profile	See Table D-1

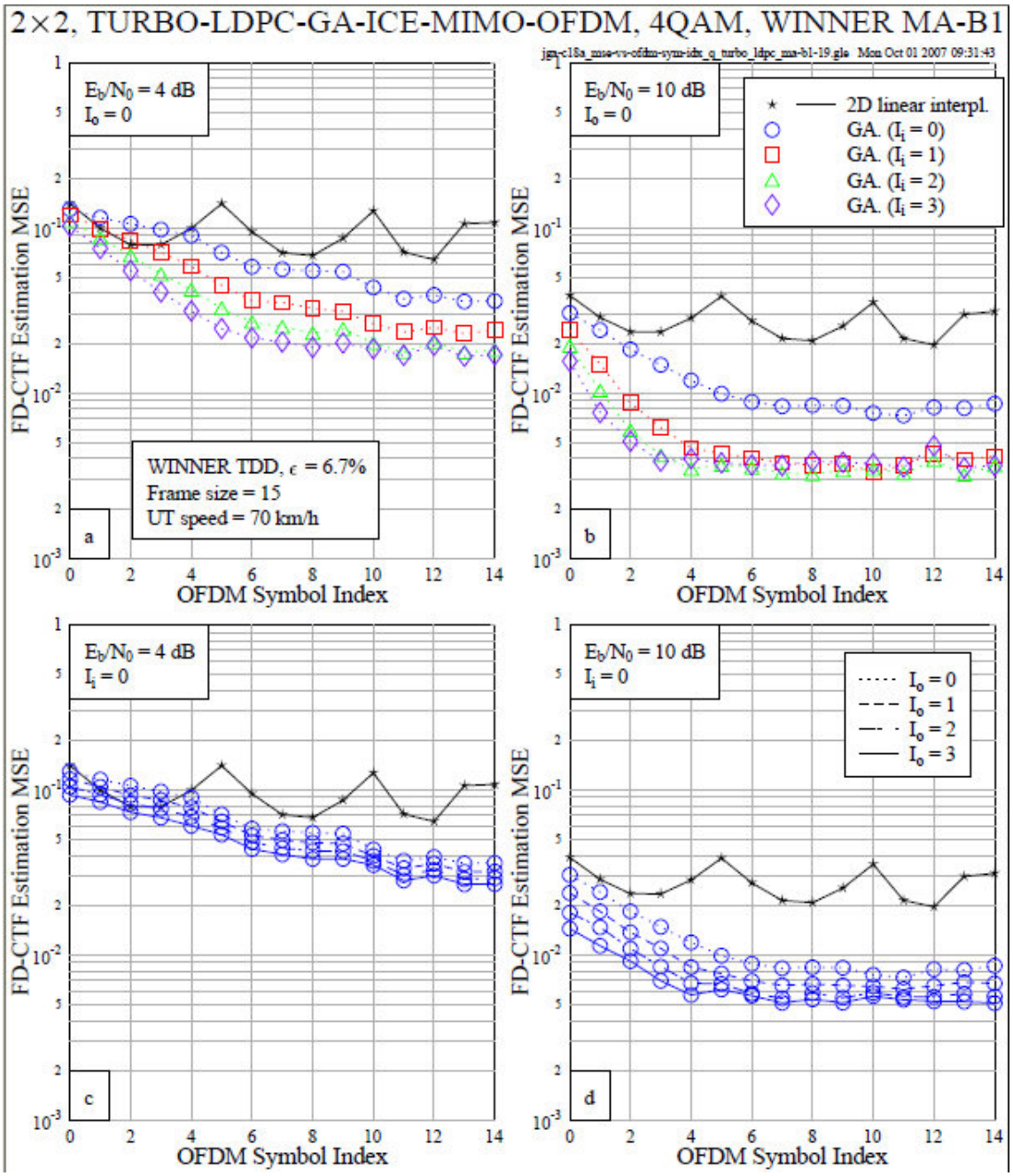

Figure D-1: FD-CTF estimation MSE performance versus OFDM symbol index of the GA-ICE recorded at E_b/N_0 = 4dB and 10dB in the WINNER B1 channel. The outer iteration I_o was fixed to 0 in subfigures (a) and (b), while the inner iteration I_i was fixed to 1 in subfigures (c) and (d), respectively. The performance of the 2D linear interpolation based channel estimation is also provided as reference.

As the first investigation, in Figure D-1 we provide the FD-CTF estimation Mean Square Error (MSE) performance of GA-ICE recorded across all the OFDM symbols within one frame. As a reference, the MSE performance of a simple 2D linear interpolation based channel estimator is also given. More specifically, the number of outer iterations I_o was fixed to 0 in Figure D-1(a) and (b), while the number of

inner iterations I_i was fixed to 1 in Figure D-1(c) and (d), respectively. In addition, two E_b/N_0 values were tested, namely 4dB in Figure D-1(a) and (c), and 10dB in Figure D-1(b) and (d), respectively. It can be seen from Figure D-1 that GA-ICE keeps improving its performance during the initial few OFDM symbol durations, before reaching a stable lower MSE bound. This is because the FD-CTF estimates optimized by GA-ICE for a previous OFDM symbol, which are more accurate than the initial estimates provided by interpolation, are used for assisting the estimation process for the next OFDM symbol. As a result, the MSE performance of the linear interpolator is significantly improved by GA-ICE, especially in the higher-SNR scenario, as shown in Figure D-1. It is also noticed increasing the value of I_i rather than I_o can provide a better MSE performance, since the beneficial impact on channel estimation from the outer loop is delivered by the improved symbol estimates, and thus not being as direct as that from the inner loop, or more explicitly from the GA-ICE.

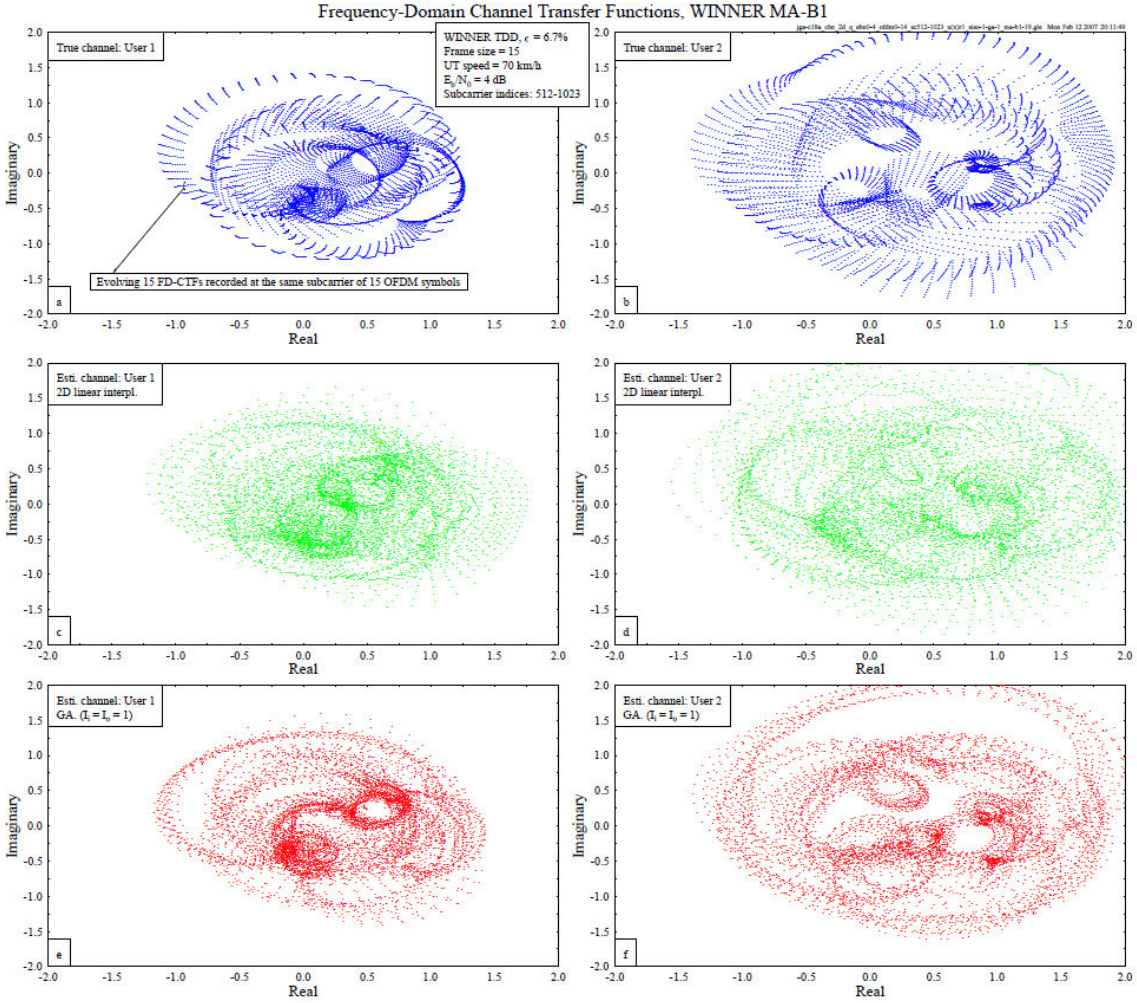

Figure D-2: A snapshot of the FD-CTF estimation performance of the GA-ICE recorded at E_b/N_0 = 4dB in the WINNER B1 channel. The GA-ICE estimated FD-CTFs of subfigures (e) and (f) associated with n = 1, …, 15 consecutive OFDM symbols within one frame at the $n_r = 1^{st}$ receiver antenna are plotted, and compared with the FD-CTFs estimated by the 2D linear interpolator of subfigures I and (d) as well as the true FD-CTFs of subfigures (a) and (b). The left-hand side subfigures (a), (c), and (e) represent the results for user 1, while the right-hand side subfigures (b), (d), and (f) represent user 2. Note that as an example only the FD-CTFs associated with subcarriers having indices within the range of [512, 1023] are plotted.

A visual comparison of the true, the 2D linear interpolator estimated, and the GA-ICE estimated FD-CTFs is portrayed in the top, middle, and bottom of Figure D-2, respectively, where a configuration of $I_i = I_o = 1$ was used for GA-ICE. More specifically, the $N_t = 2$ users' FD-CTFs associated with a specific receiver antenna element during a block of 15 consecutive OFDM symbols, i.e. one full frame, are plotted at a E_b/N_0 value of 4dB, as represented by the left- and right-hand side of Figure D-2, respectively. Each dot of the curves plotted in Figure D-2 represents a complex-valued FD-CTF at a specific subcarrier within the range of [512, 1023]. By observing the perfect channel-knowledge based illustration in Figure D-2(a) and (b), we can see that the FD-CTF at each subcarrier evolves over the duration of the 15 OFDM

symbols, where the thickness of the varied ring-shaped formations indicates the amount of FD-CTF change across the corresponding neighbourhood subcarrier zones during the time interval of one frame. The full perimeter of all the connected, variously-sized rings is constituted by the 512 spoke-like formations corresponding to the 512 subcarriers considered, as shown in Figure D-2(a) and (b). Explicitly, the shapes of the FD-CTF rings associated with the two user-receiver channel links are substantially different. This is because each individual link is subjected to independent fading, and although the Doppler frequency encountered at the four links is identical, their short-term envelope fluctuation observed over the 15 OFDM symbol durations is different. However, by comparing the subfigures at the top and bottom of Figure D-2, we can find that the FD-CTF estimates generated by GA-ICE closely match their true values, resulting in a similar FD-CTF contour for each of the two channel links. By contrast, the estimates provided by the 2D linear interpolator shown in Figure D-2(c) and (d) appear in a more dispersive manner, deviating from the true channel. This implies that GA-ICE is capable of *simultaneously* capturing the fading envelope changes of each individual user-receiver link, regardless of its instant variety of fading. Since an equally good performance was attained over all the user-receiver links, this demonstrates the global robustness of the proposed approach for MIMO scenarios.

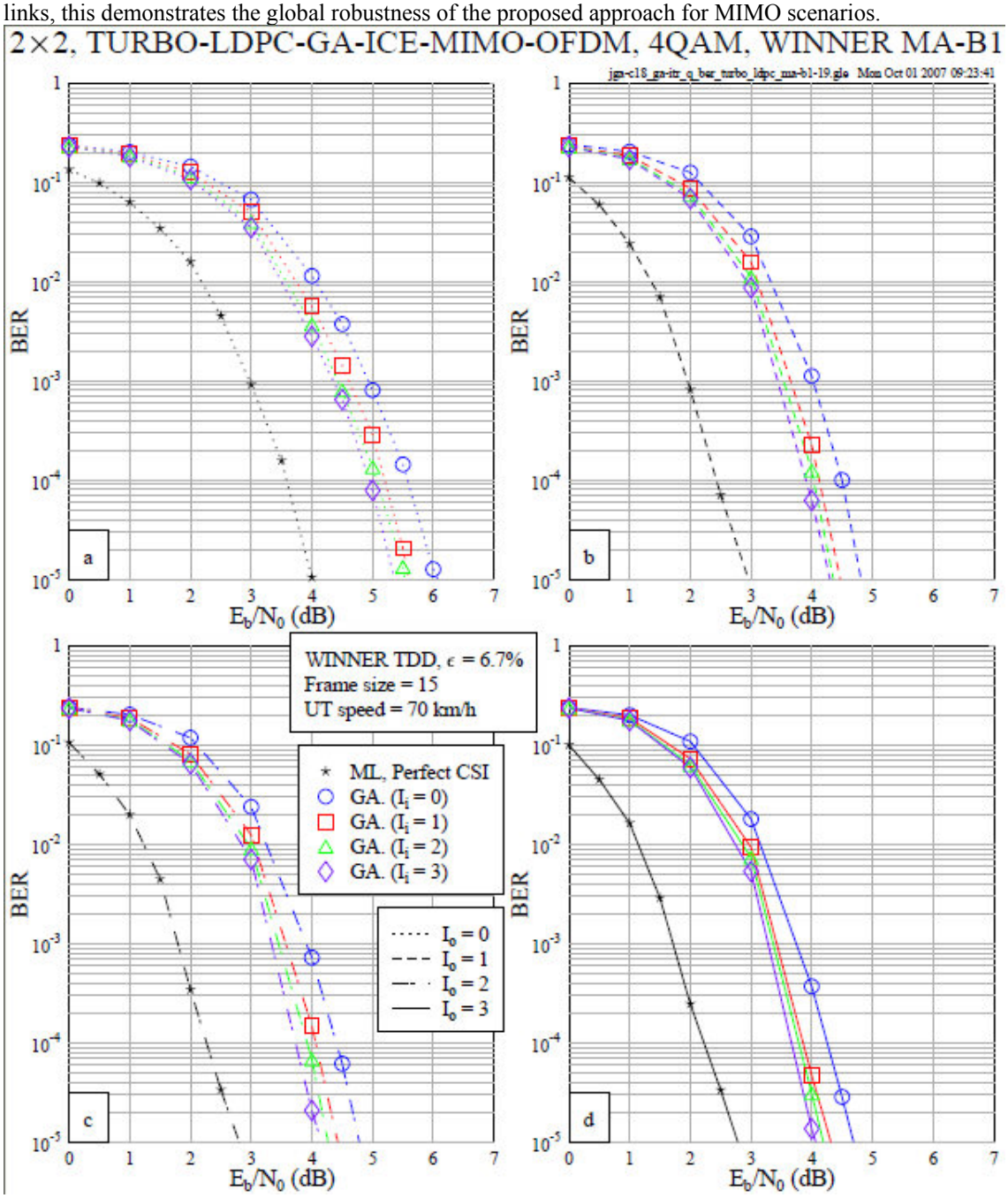

Figure D-3: BER versus E_b/N_0 performance of the LDPC-coded GA-ICE assisted multi-user turbo MIMO OFDM system in the WINNER B1 channel. The outer iteration I_o was fixed to 0-3 in subfigures (a)-(d), respectively.

In Figure D-3 we show the Bit Error Ratio (BER) versus E_b/N_0 performance of the LDPC-coded GA-ICE assisted multi-user turbo MIMO OFDM system, focusing on the effect of employing different inner iterations I_i. The performance of the system employing the optimum Maximum Likelihood (ML) MUD is also offered as a reference, where perfect Channel State Information (CSI) is assumed. Note that in Figure D-3(a)-(d) the number of outer iterations I_o was fixed to 0-3, respectively. It is seen from Figure D-3 that despite the high UT speed of 70km/h, the E_b/N_0 gap between the proposed GA-ICE aided scheme and the perfect CSI assisted optimum arrangement can be as small as about 1.2dB at the BER of 10^{-5}.

Another finding from Figure D-3 is that the system's performance becomes better, as the number of inner iterations I_i increases, regardless of the number of outer iterations I_o. This implies that the channel estimates provided by the meritorious GA-ICE can be consistently improved, when a higher value of I_i is used. It results in a channel estimation related E_b/N_0 reduction of about 0.4-0.7dB at the BER of 10^{-5}, in comparison with the scheme associated with $I_i = 0$. Note that however the largest portion of the attainable gain is achieved at the first iteration, i.e. $I_i = 1$, while the gain provided by the succeeding inner iterations becomes smaller, as I_i advances from 1 to 3. Similar findings can also be observed from Figure D-4, where the Frame Error Ratio (FER) performance of the proposed system with same configurations is shown.

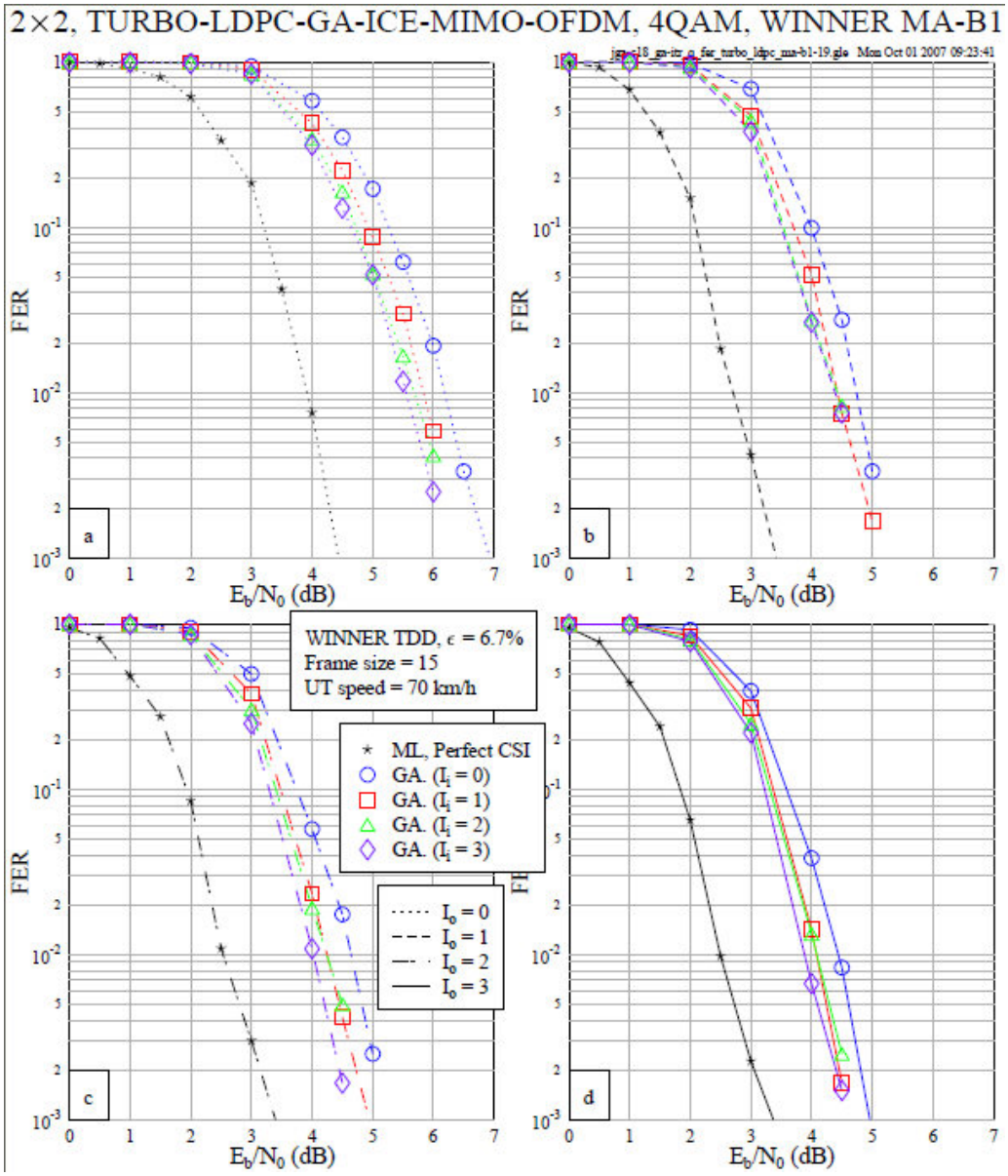

Figure D-4: FER versus E_b/N_0 performance of the LDPC-coded GA-ICE assisted multi-user turbo MIMO OFDM system in the WINNER B1 channel. The outer iteration I_o was fixed to 0-3 in subfigures (a)-(d), respectively.

As a comparison, the BER and FER performances of the system are re-plotted in Figure D-5 and Figure D-6, respectively, from the perspective of the number of outer iterations I_o. More specifically, we respectively fixed the number of inner iterations I_i to 0-3 in the subfigures (a)-(d) of both Figure D-5 and Figure D-6. Similar to Figure D-3 and Figure D-4, it is found from Figure D-5 and Figure D-6 that when the number of outer iterations I_o is increased, a consistent improvement in the system performance is recorded, although the first iteration offers most of the potential performance benefits. Moreover, compared with the reference non-iterative scheme associated with $I_i = I_o = 0$, a higher E_b/N_0 reduction is achieved by increasing I_o rather than I_i. As expected, since the outer iteration routine involves the LDPC decoder, a higher value of I_o results in that more contribution from the LDPC decoder is available, thus accelerating the convergence speed of the overall enhancement in the achievable system performance.

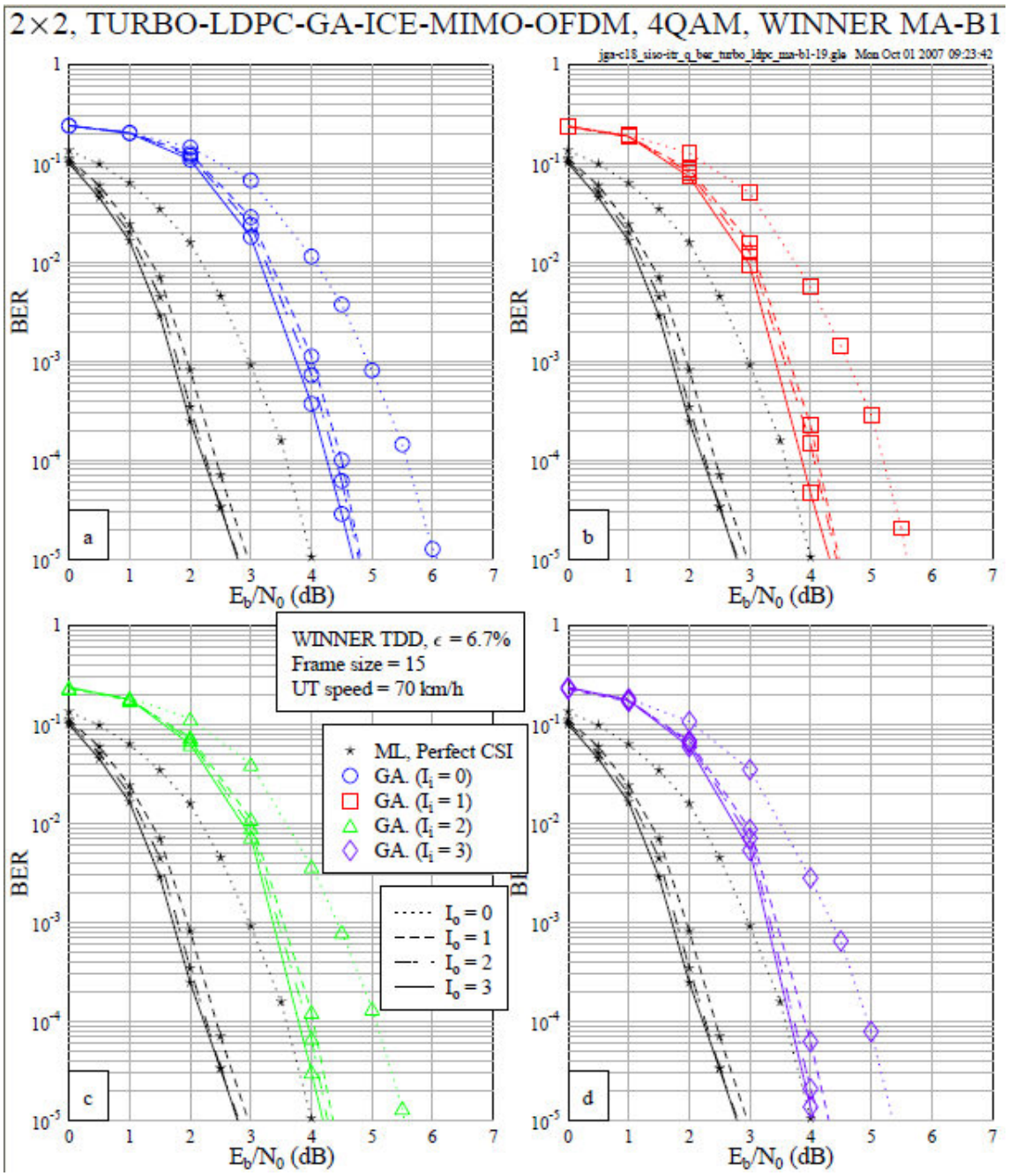

Figure D-5: BER versus E_b/N_0 performance of the LDPC-coded GA-ICE assisted multi-user turbo MIMO OFDM system in the WINNER B1 channel. The inner iteration I_i was fixed to 0-3 in subfigures (a)-(d), respectively.

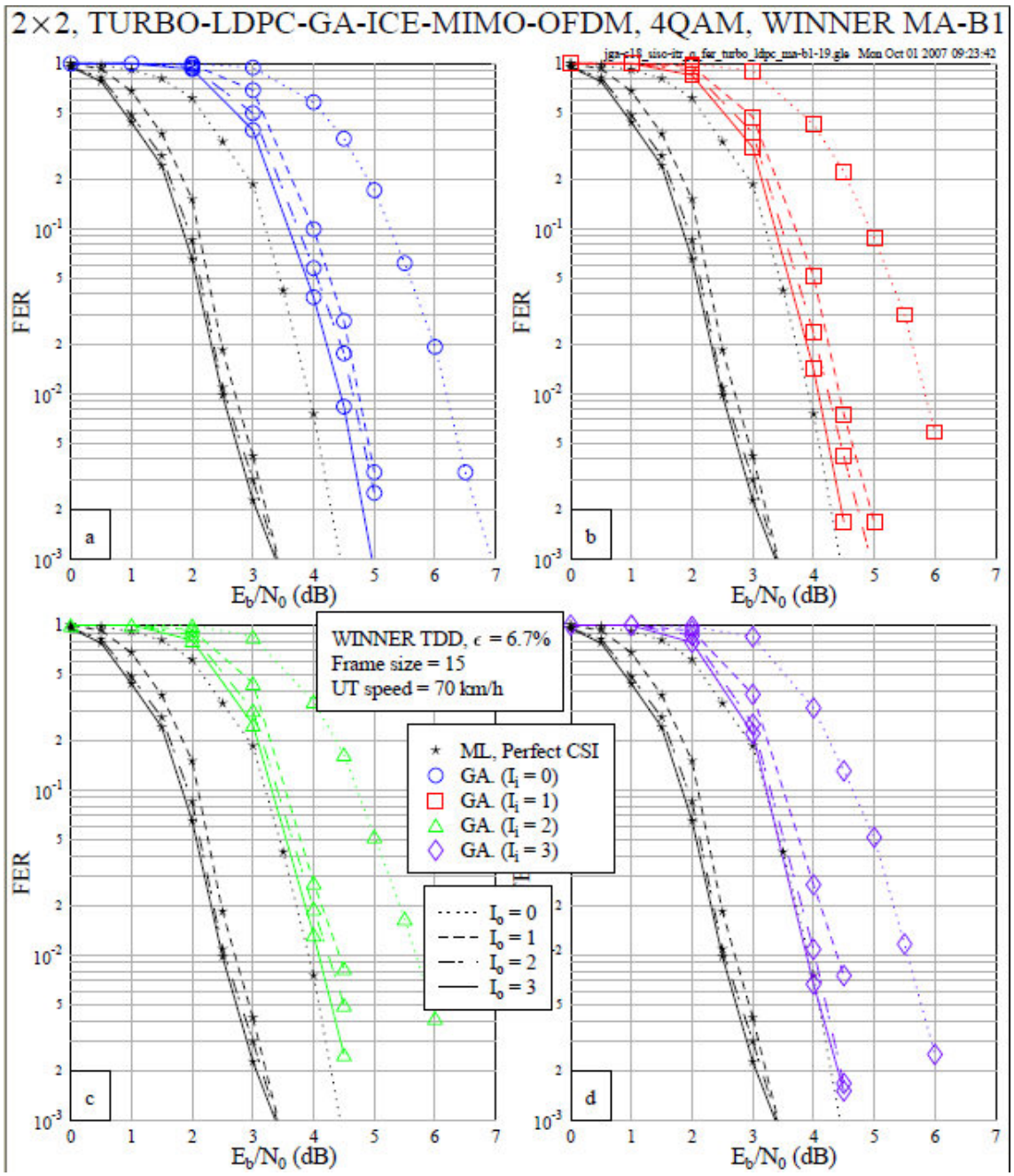

Figure D-6: FER versus E_b/N_0 performance of the LDPC-coded GA-ICE assisted multi-user turbo MIMO OFDM system in the WINNER B1 channel. The inner iteration I_i was fixed to 0-3 in subfigures (a)-(d), respectively.

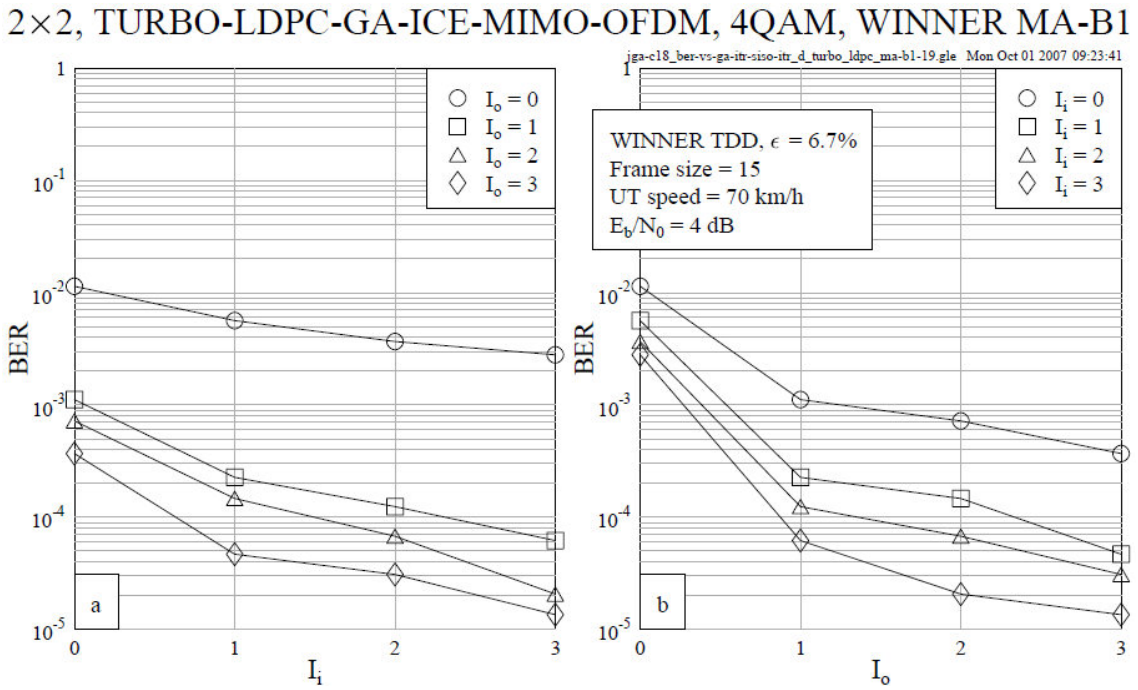

Figure D-7: BER versus I_i (left) and I_o (right) performance of the LDPC-coded GA-ICE assisted multi-user turbo MIMO OFDM system in the WINNER B1 channel. An E_b/N_0 value of 4dB was assumed.

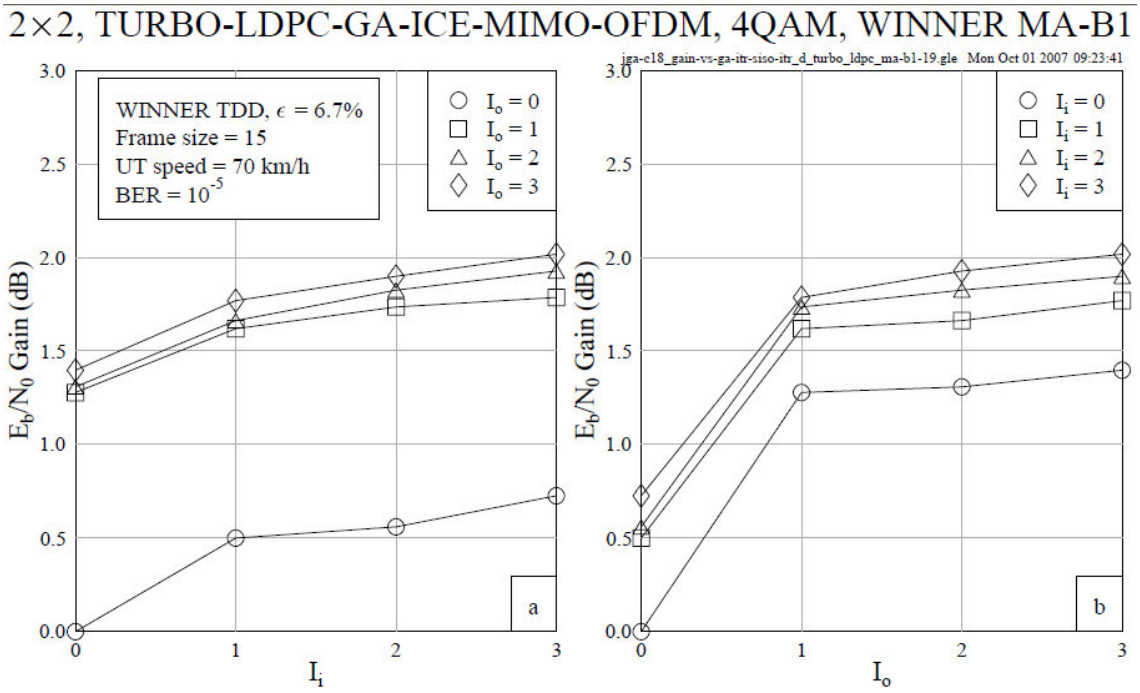

Figure D-8: E_b/N_0 versus I_i (left) and I_o (right) performance of the LDPC-coded GA-ICE assisted multi-user turbo MIMO OFDM system in the WINNER B1 channel. The target BER was 10^{-5}.

The benefit from the inner and outer iterative processing is further revealed by Figure D-7, where the BER performances recorded at an E_b/N_0 value of 4dB against I_i and I_o are given in subfigures (a) and (b), respectively. As shown in Figure D-7(b), the BER is reduced by up to two magnitudes when I_o is increased from 0 to 1. Accordingly, the corresponding E_b/N_0 gain achieved by the first outer iteration is about 1-1.3dB, regardless of different number of inner iterations, as shown in Figure D-8(b). The E_b/N_0 gain here is defined as the E_b/N_0 difference recorded at the BER of 10^{-5} between the reference non-iterative scheme with $I_i = I_o = 0$, and the schemes using different values of I_i and/or I_o. By contrast, as previously discussed, the BER reduction and E_b/N_0 gain achieved by increasing the number of inner iterations I_i are relatively moderate, as evidenced by Figure D-7(a) and Figure

D-8(a). The best performance is offered by the scheme using with $I_i = I_o = 3$ with a resultant E_b/N_0 gain of 2dB.

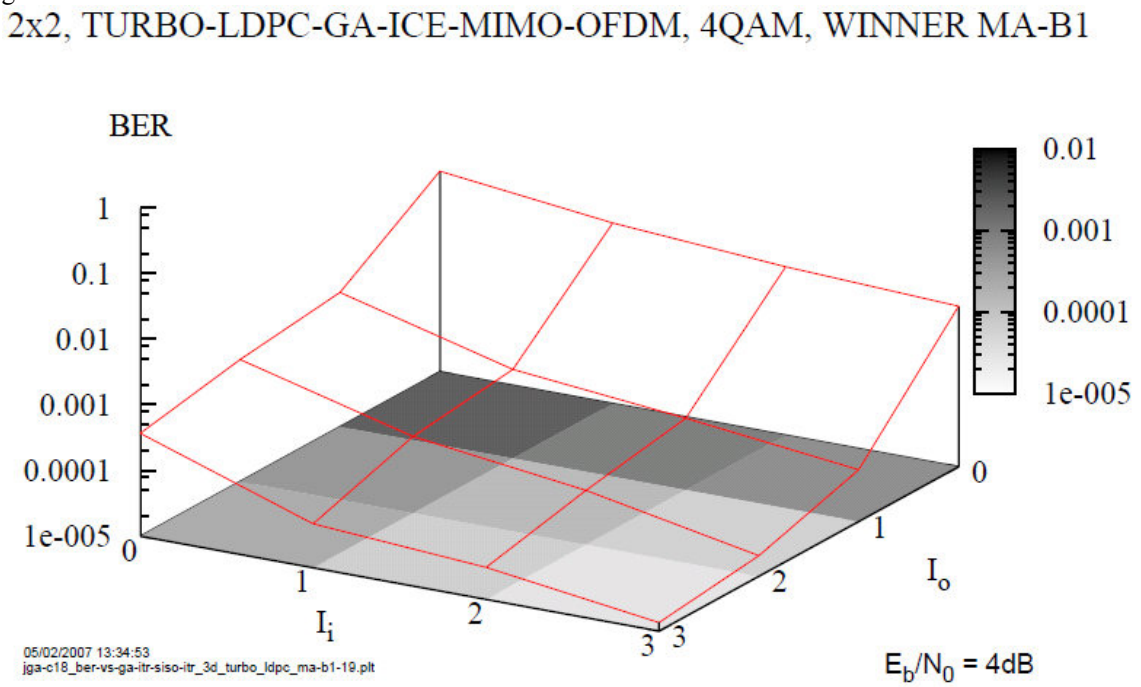

Figure D-9: The 3D BER versus I_i/I_o performance of the LDPC-coded GA-ICE assisted multi-user turbo MIMO OFDM system in the WINNER B1 channel. An E_b/N_0 value of 4dB was assumed.

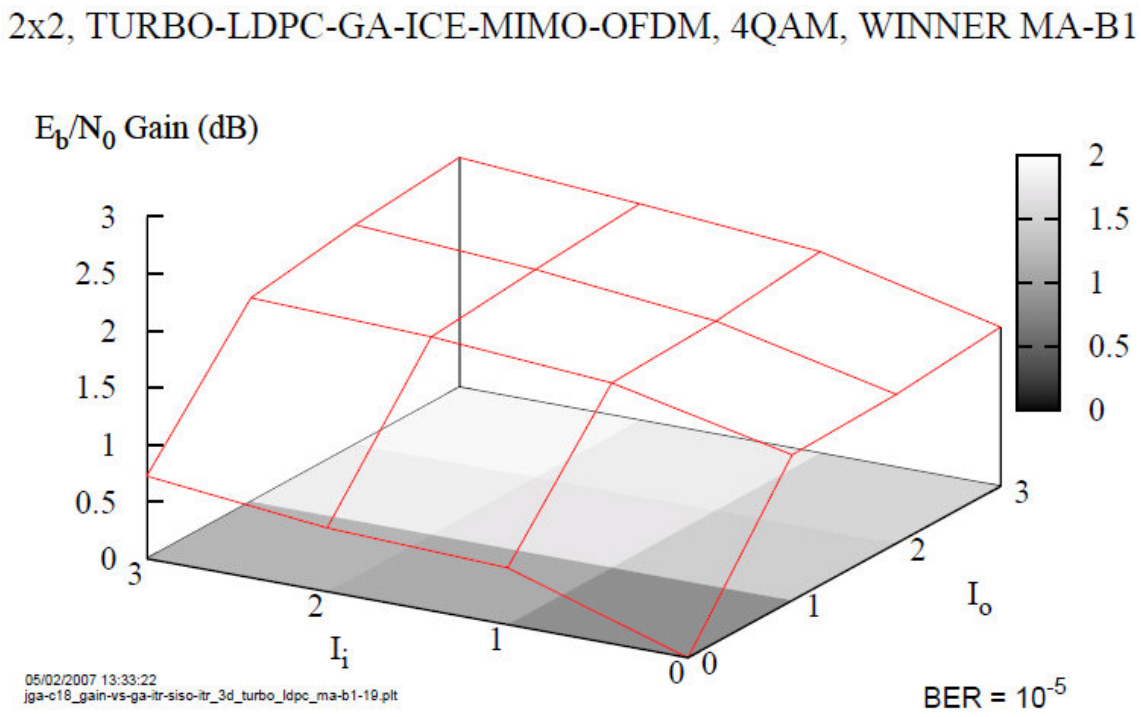

Figure D-10: The 3D E_b/N_0 gain versus I_i/I_o performance of the LDPC-coded GA-ICE assisted multi-user turbo MIMO OFDM system in the WINNER B1 channel. The target BER was 10^{-5}.

As a further investigation on the collaborative contribution from both the inner and outer iterations to the overall system performance improvement, the BER and the E_b/N_0 gain performances as a function of I_i and I_o are visualized in Figure D-9 and Figure D-10, respectively. Thanks to the beneficial interaction between the inner and outer iterations, the system performance is correspondingly enhanced, as the combination of (I_i, I_o) advances from (0, 0) to (3, 3), while the overall performance improvement is biased by I_o, as illustrated by the projected greyscale zones observed in both Figure D-9 and Figure D-10.

D.2 Evaluation in WINNER Local Area (LA)

In this section, the simulation results achieved in the WINNER Local Area (LA) scenario are provided. Accordingly, the WINNER A1 channel model [WIN1D54] associated with LA was employed, whose power delay profile is summarized in Table D-3. The speed of UTs was assumed to be 5km/h, corresponding to an OFDM symbol normalized Doppler frequency of 0.0005. Other simulation parameters used are the same as those specified in Table D-2.

Table D-3: Power delay profile of the WINNER A1 channel [WIN1D54].

Delay (ns)	0	5	10	15	20	25	30
Power (dB)	0	-0.9	-1.5	-1.6	-2.0	-2.6	-3.4
Delay (ns)	35	40	45	50	55	65	75
Power (dB)	-4.5	-5.5	-5.5	-5.0	-4.7	-5.4	-9.0
Delay (ns)	85	95	105	115	125	135	
Power (dB)	-11.3	-12.5	-13.6	-15.1	-16.8	-18.7	

In Figure D-11, Figure D-12, Figure D-13 and Figure D-14, we show the BER and FER versus E_b/N_0 performances of the LDPC-coded GA-ICE assisted multi-user turbo MIMO OFDM system, where the effects of varying inner and outer iterations, i.e. I_i and I_o, are highlighted respectively. Again, the performance of the perfect CSI-aided system employing the optimum ML MUD is offered as a benchmarker. Similar observations can be found as those documented in Section D.1 in the context of MA, and these confirm the effectiveness of the proposed scheme also in LA scenario.

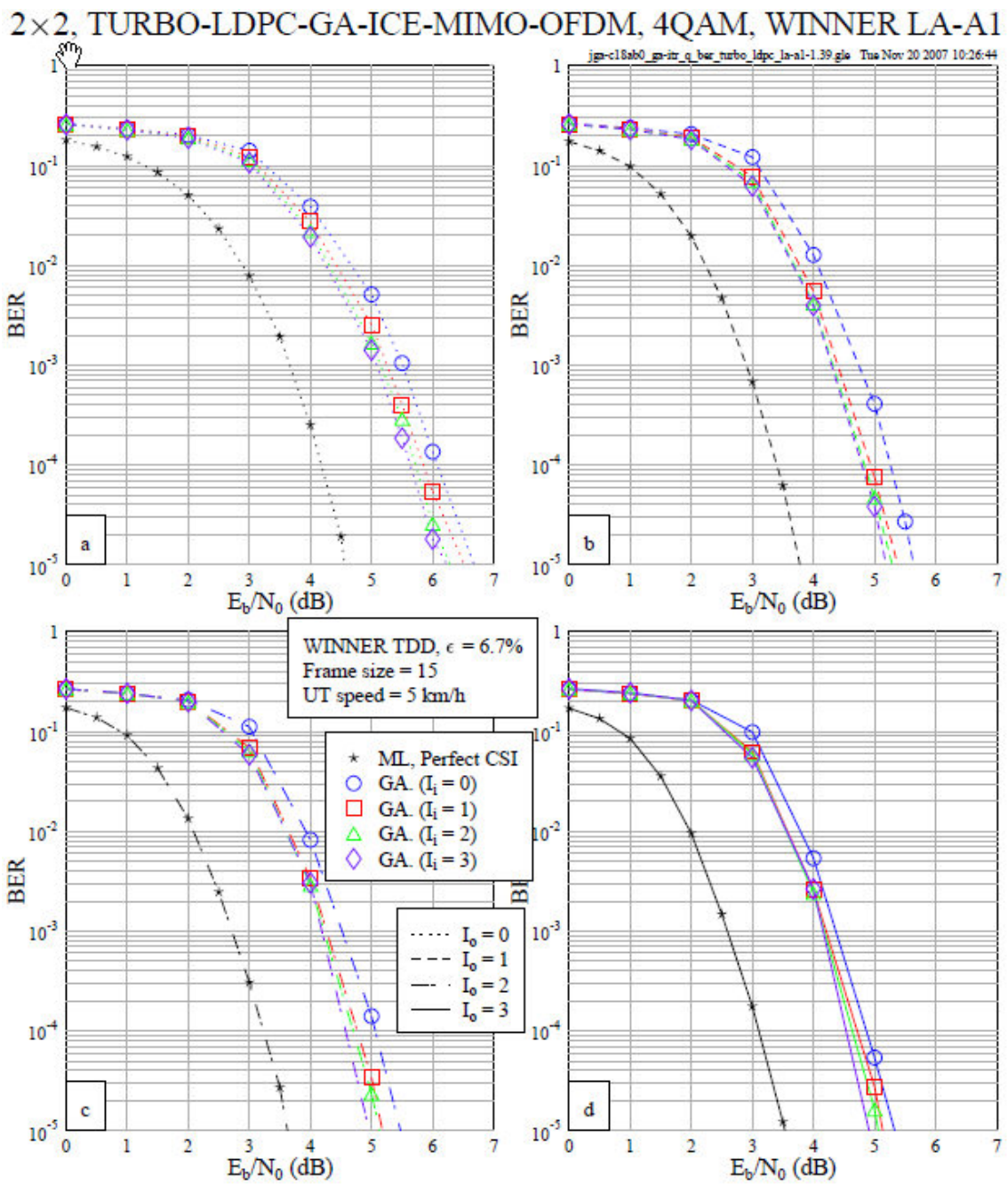

Figure D-11: BER versus E_b/N_0 performance of the LDPC-coded GA-ICE assisted multi-user turbo MIMO OFDM system in the WINNER A1 channel. The outer iteration I_o was fixed to 0-3 in subfigures (a)-(d), respectively.

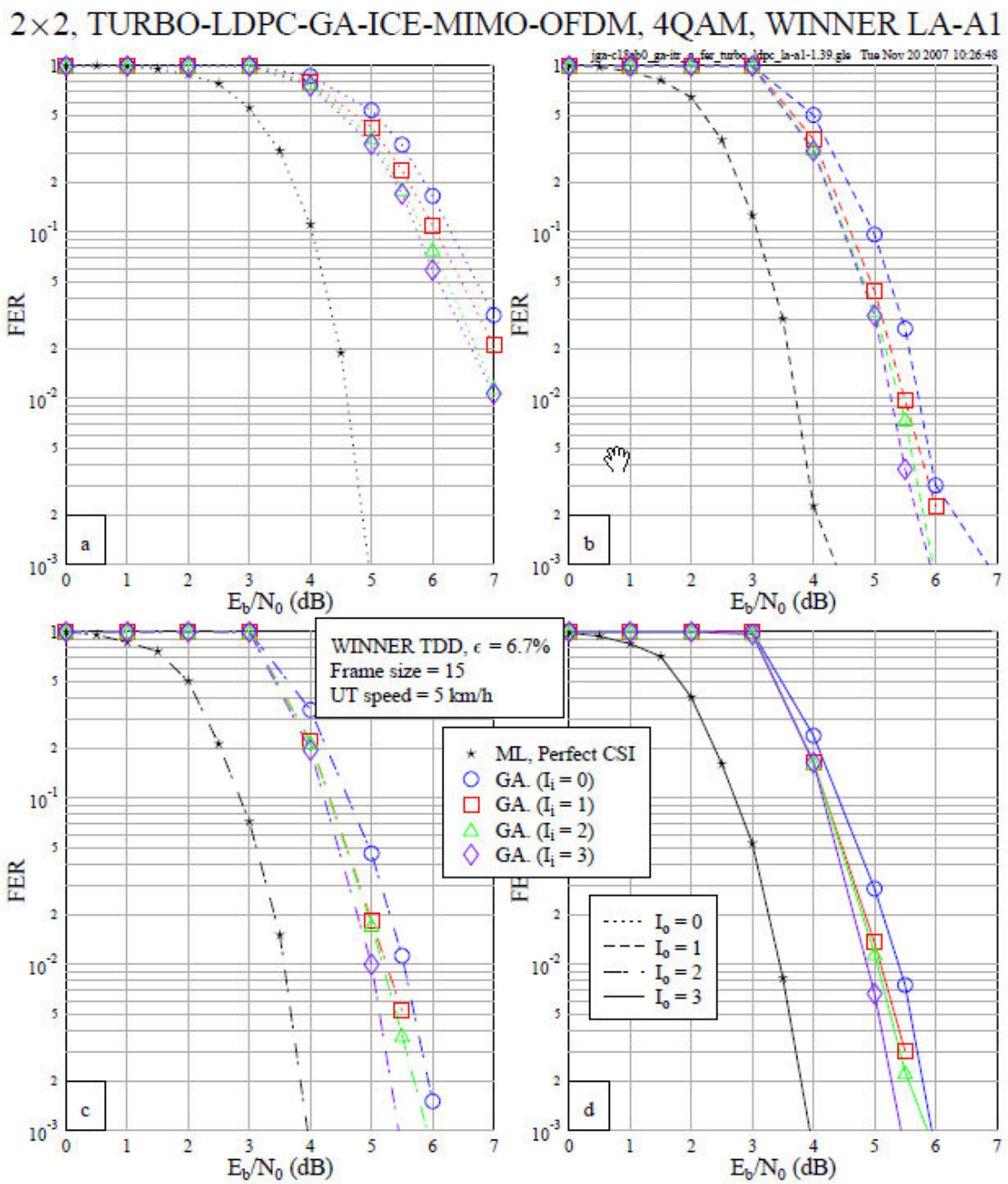

Figure D-12: FER versus E_b/N_0 performance of the LDPC-coded GA-ICE assisted multi-user turbo MIMO OFDM system in the WINNER A1 channel. The outer iteration I_o was fixed to 0-3 in subfigures (a)-(d), respectively.

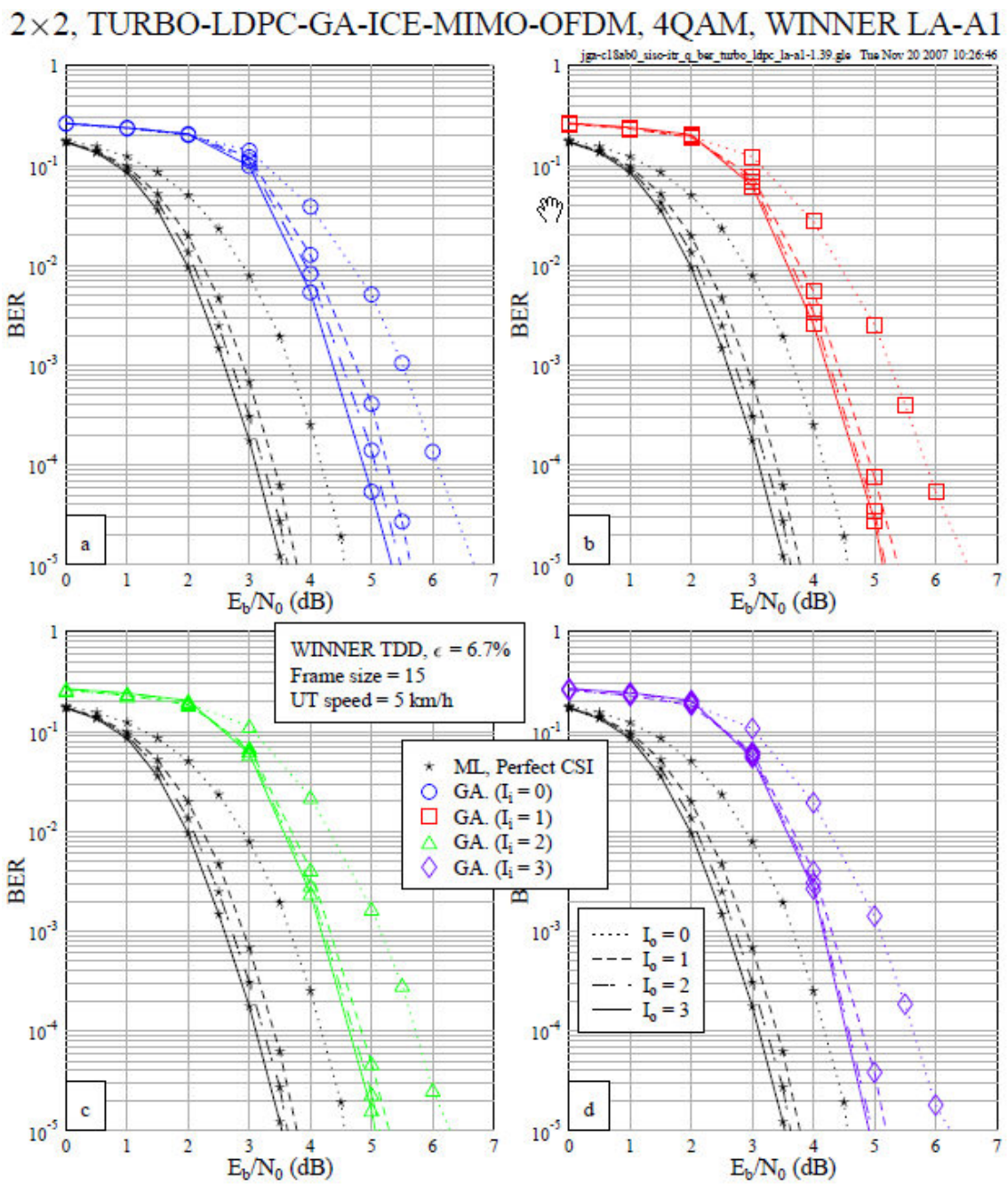

Figure D-13: BER versus E_b/N_0 performance of the LDPC-coded GA-ICE assisted multi-user turbo MIMO OFDM system in the WINNER A1 channel. The inner iteration I_i was fixed to 0-3 in subfigures (a)-(d), respectively.

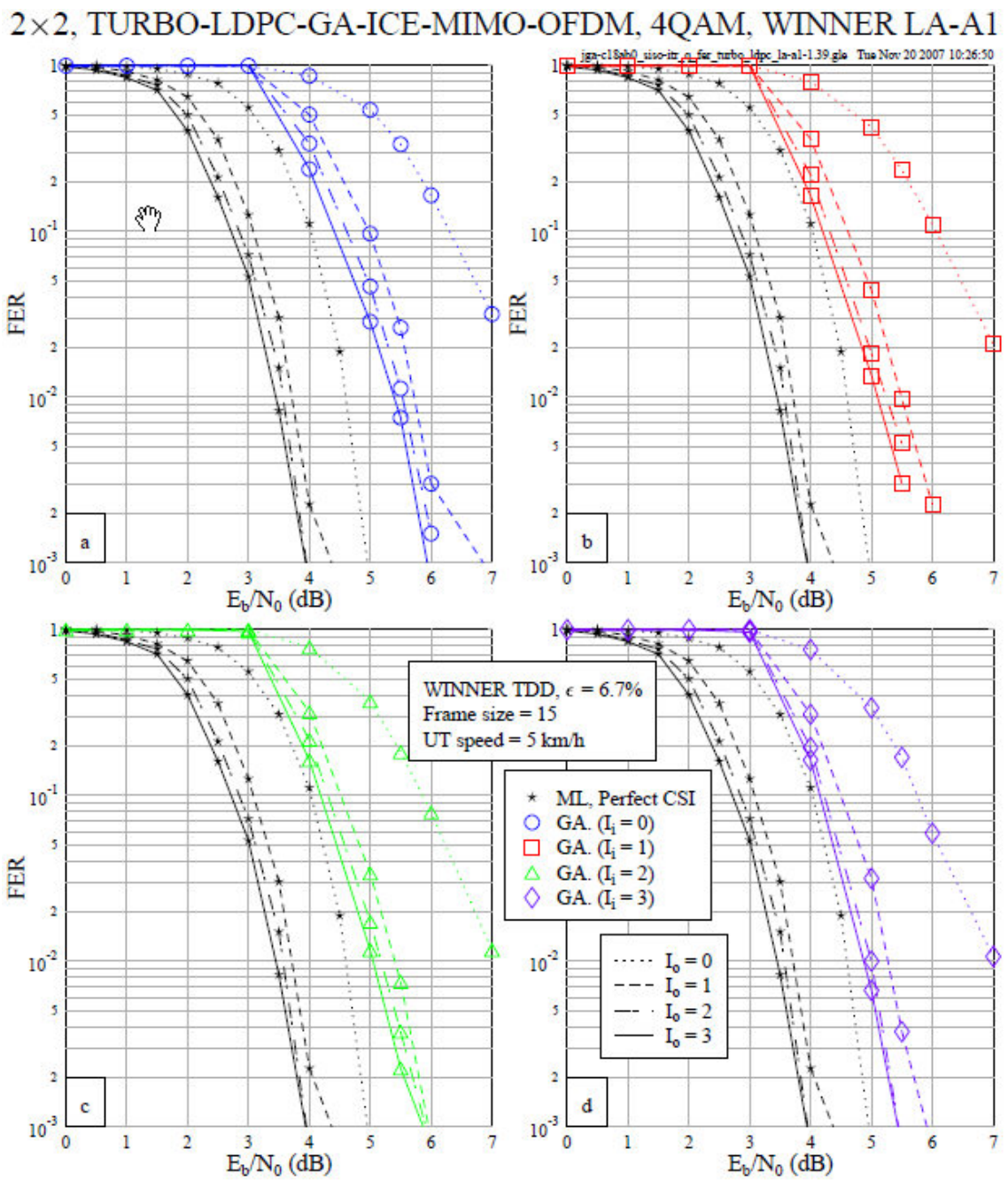

Figure D-14: FER versus E_b/N_0 performance of the LDPC-coded GA-ICE assisted multi-user turbo MIMO OFDM system in the WINNER A1 channel. The inner iteration I_i was fixed to 0-3 in subfigures (a)-(d), respectively.

Appendix E. Signalling: Impact of Quantisation Errors on Two Transmission Schemes

E.1 Dominant Eigenmode Transmission

We have simulated the dominant eigenmode transmission with quantisation errors at transmit side by quantising the right singular vector **w** using RVQ scheme with 8 bits. The quantised version of **w** is then fed back to the transmitter. 1000 channel realisations are generated for both the i.i.d. complex Gaussian channels and WINNER C1 LOS channel model. 16-QAM modulation has been used in the simulations. Note that we have only simulated systems with one single carrier here. For OFDM systems, **w** needs to be fedback to the transmitter for either all subcarriers or part of the subcarriers depends on the channel frequency selectivity. The latter is more practical but degrades the system performance.

Figure E-1 and Figure E-2, show the BER performance for a 4×4 system using the i.i.d. complex Gaussian channel model and the WINNER C1 LOS channel model respectively. Both figures clearly show the degradation when quantisation errors exist at the transmitter. Since the receiver knows quantisation error, there is no error floor on BER when a zero-forcing receiver is used.

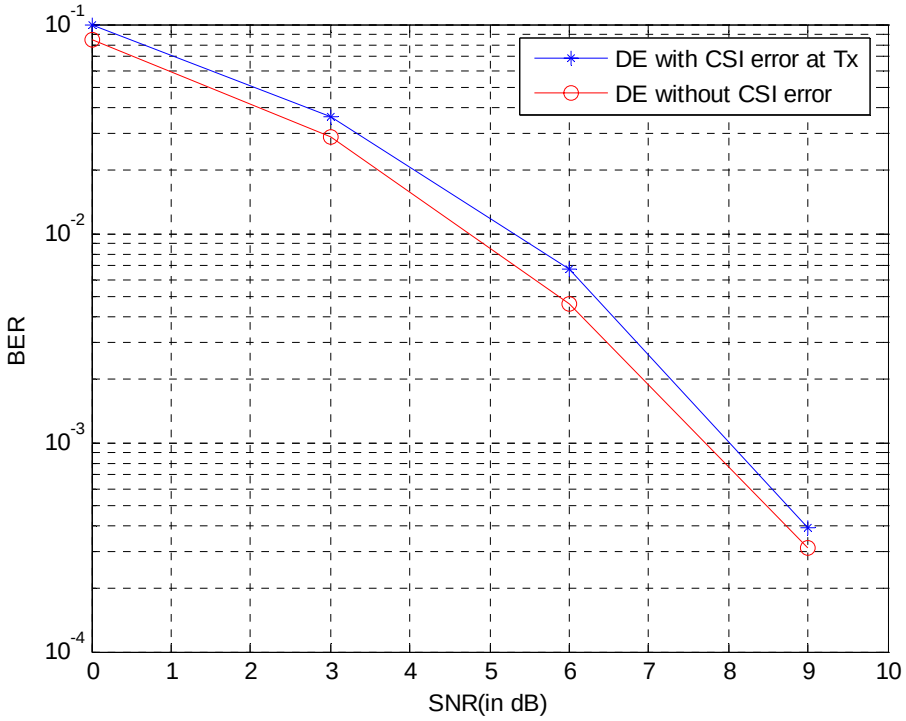

Figure E-1 DE transmission for 4×4 system with and without channel quantisation errors at the transmit side, $\rho_{tx} = \rho_{rx} = 0$ and the number of RVQ bits is 8.

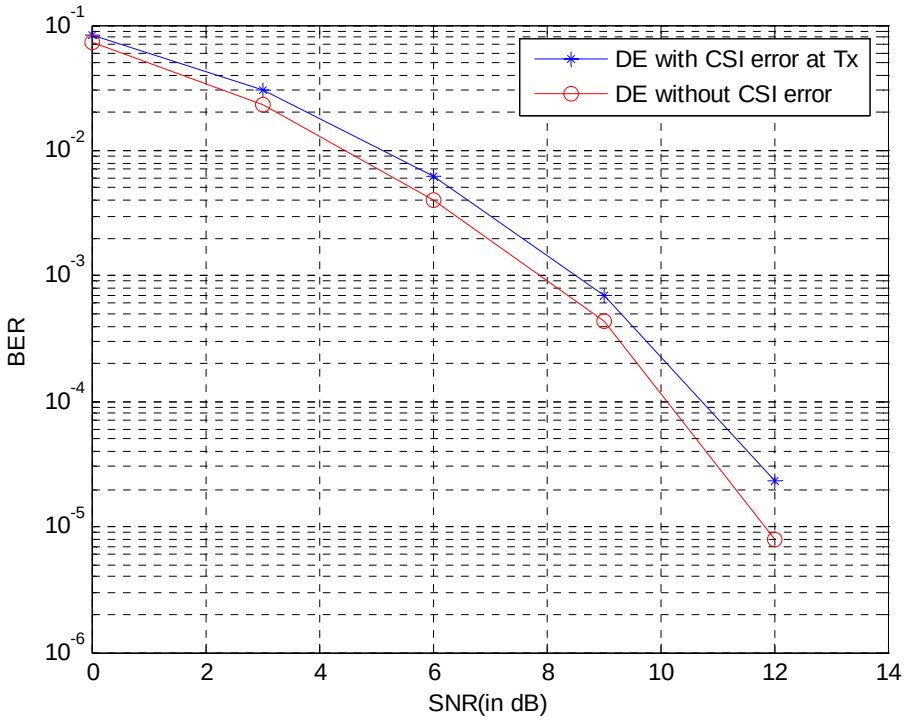

Figure E-2 DE transmission schemes for 4×4 system with and without channel quantisation errors at the transmit side, WINNER C1 LOS scenario, the number of RVQ bits is 8

E.2 MMSE Precoding for Multi-user Downlink Transmission

We simulate one base station (equipped with 4 transmit antennas) that communicates with 2 users each equipped with one receive antenna. We assume each user estimate the CSI perfectly and feed back the quantised CSI to the transmitter. The WINNER B1 NLOS scenario is simulated. We study both the system throughput and BER performance (assuming 4-QAM modulation). Here, we have only simulated systems with one single carrier. For OFDM systems, each user needs to feedback its channel state information to the transmitter for either all subcarriers or part of the subcarriers depends on the channel frequency selectivity. The latter degrades the system performance but is more realistic.

Figure E-3 and Figure E-4 show the BER performance and the system throughput using 12 bits RVQ respectively. The performance and throughput for the system with perfect CSI at the base station are also plotted as references. Unlike the results shown in the single user transmission case, the BER for the multi-user downlink transmission achieves an error floor in the high SNR region. This is because the user only knows its own channel perfectly, but not the CSI for the other user. Therefore it is not possible to cancel the interference caused by the transmission to the other user using quantised CSI at the base station. Due to the same reason, the throughput for the whole system achieves a floor at around 3 bit/s/Hz.

Figure E-5 and Figure E-6 show the performance using different quantisation bits (4/8/12/16/20 bits). It is clearly shown that as the quantisation bits increases, both the BER performance and the system throughput improve.

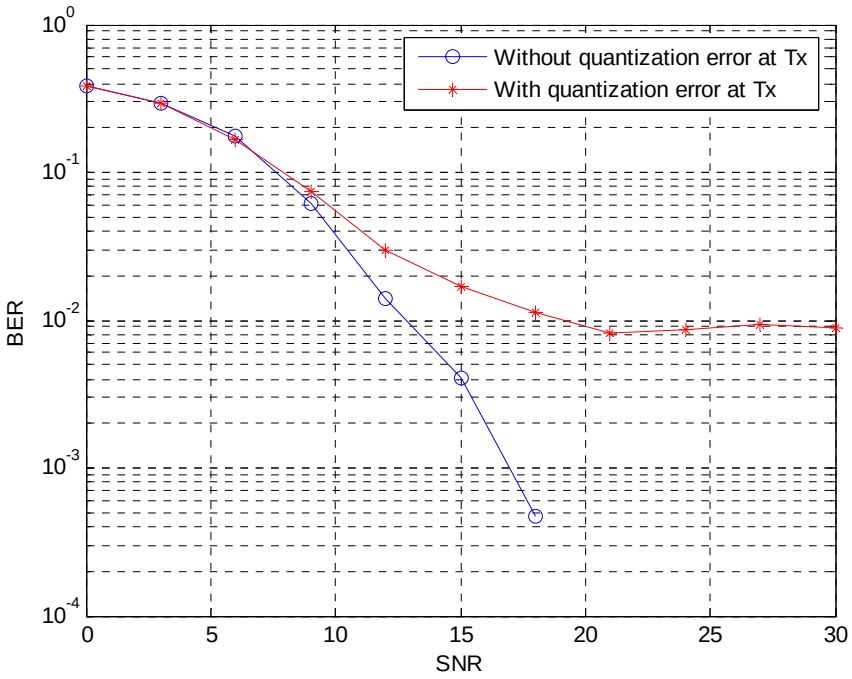

Figure E-3 BER performance of multi-user downlink transmission for two 4×1 channels with and without channel quantisation errors, WINNER B1 NLOS scenario, the number of RVQ bits is 12.

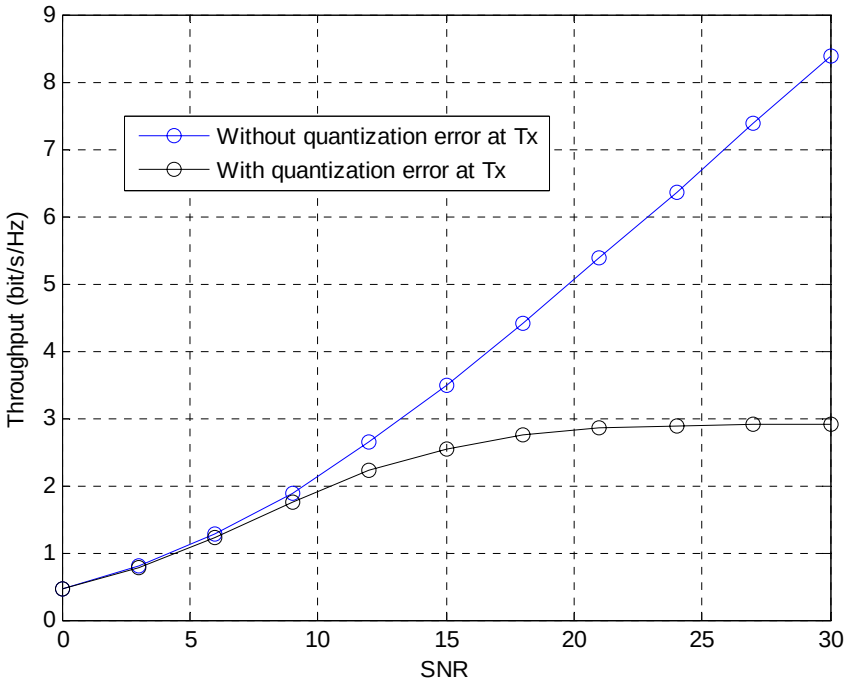

Figure E-4 Throughput of multi-user downlink transmission for two 4×1 channels with and without channel quantisation errors, WINNER B1 NLOS scenario, the number of RVQ bits is 12.

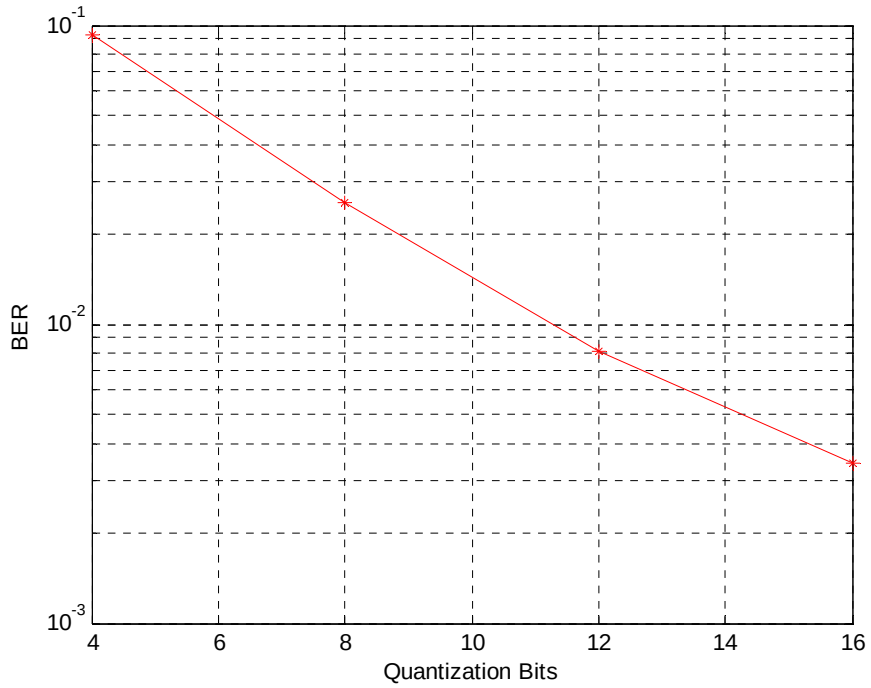

Figure E-5 BER performance of multi-user downlink transmission for two 4×1 channels with different RVQ bits, WINNER B1 NLOS Scenario, SNR equals 21dB.

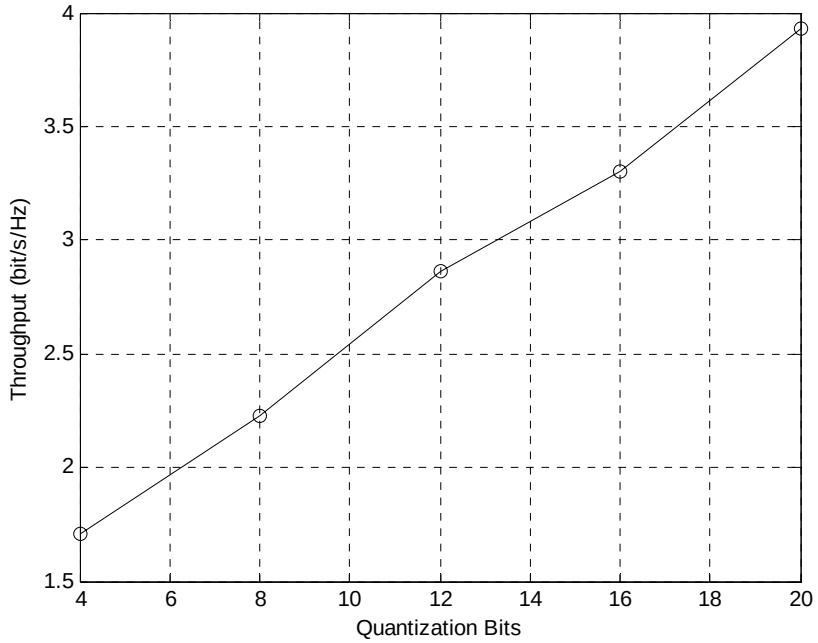

Figure E-6 Throughput of multi-user downlink transmission for two 4×1 channels with different RVQ bits, WINNER B1 NLOS Scenario, SNR equals 21dB.

Appendix F. Assessment of RF Impairments

F.1 Phase Noise

The proposed algorithm was tested under WINNER TDD parameter. The initial CPE correction is based on the known pilots using the defined pilot grid. As for the channel code a rate 1/2 convolutional code with generator polynomial $G=[133, 171]_8$ was used. An estimate of the transmitted symbols based on the correction of the common phase error only is not very reliable. Hence, an additional estimation of higher order phase noise components is necessary in order to further improve the systems performance.

Figure F-1 shows the performance results in terms of frame error rates for a 16-QAM system with a relative oscillator linewidth of 0.1 percent. Compensation of the phase noise up to the 3rd harmonic (ICI_3) provides a significant performance improvement compared to the single common phase error correction. Figure F-2 presents the intercarrier interference correction for a relative oscillator linewidth of $5*10^{-5}$. Only two detector-decoder iterations are sufficient to achieve almost the phase noise free transmission performance. Finally, the correction of phase noise using modulation is given in Figure F-3. High order modulation schemes are more sensitive against phase noise. Nevertheless, a significant reduction of the error floor while increasing the estimation order is visible.

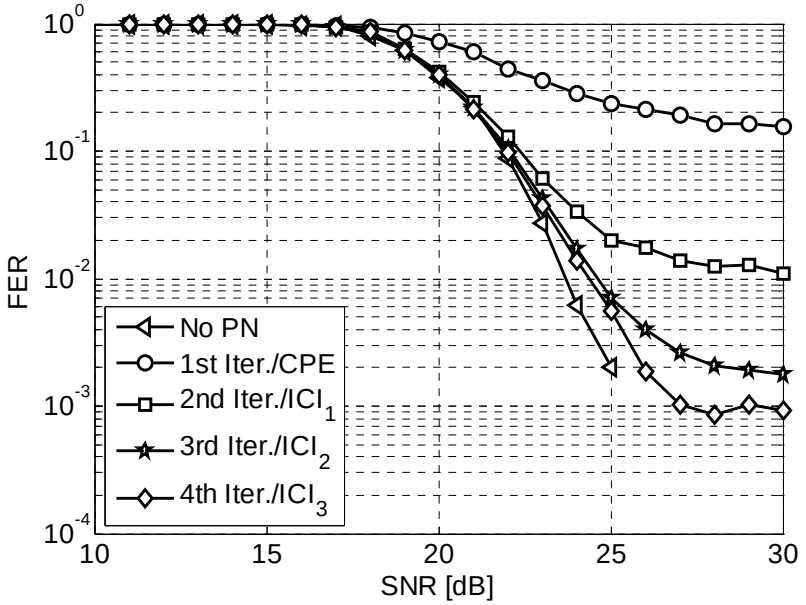

Figure F-1 Phase Noise compensation, 16-QAM, TDD Mode, A1 NLOS, Memory 6 Convolution Code, δ_{3dB}=0.001

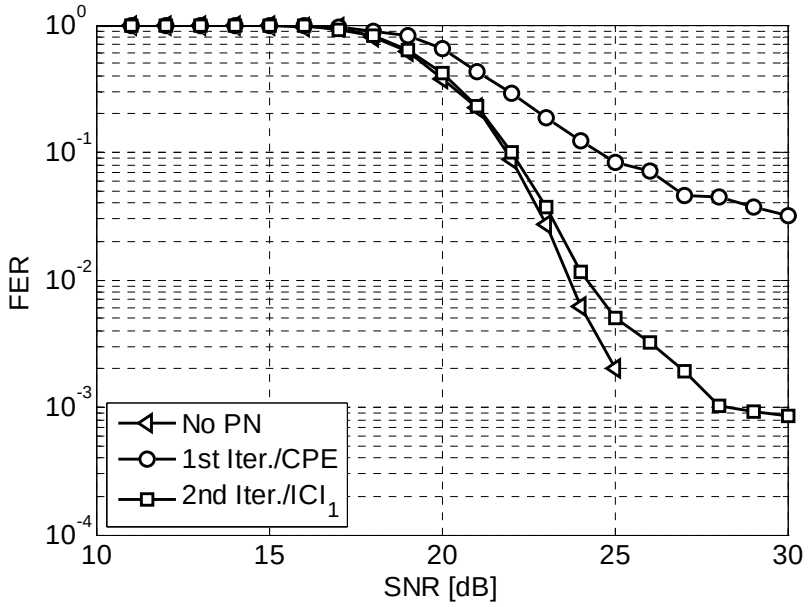

Figure F-2 Phase Noise compensation, 16-QAM, TDD Mode, A1 NLOS, Memory 6 Convolution Code, δ_{3dB}=0.0005

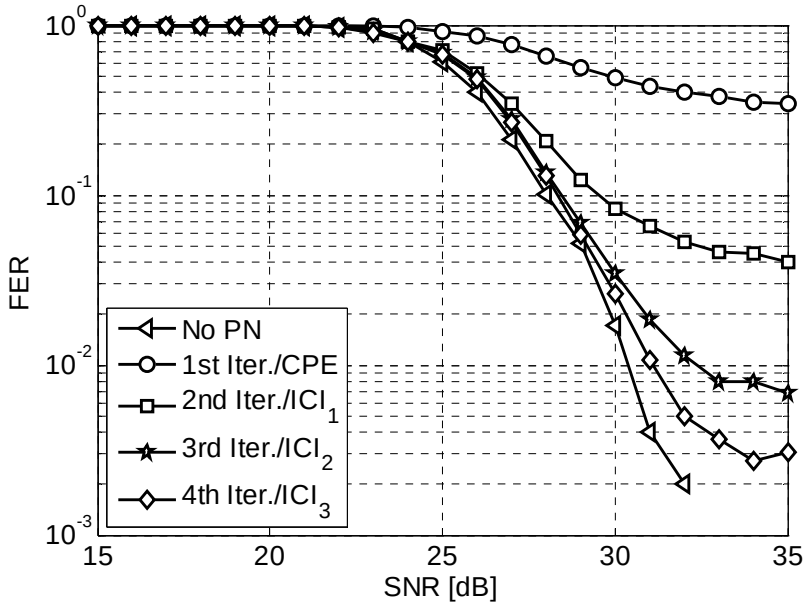

Figure F-3 Phase Noise compensation, 64-QAM, TDD Mode, A1 NLOS, Memory 6 Convolution Code, δ_{3dB}=0.0005

F.2 DFT-Precoded OFDM (Single Carrier) Systems

The decision-directed approach combined with turbo equalisation, described in 6.4.1 was used**.** The code used here is a regular (3,6) LDPC code with a 504 X 1008 parity check matrix. The Belief Propagation (BP) algorithm is used for decoding. The number of iterations in the LDPC decoder and the number of iterations in the turbo equalizer are 4. The code block length is *N*=1008. The FFT length is also 1008. The bandwidth is 40 *MHz* and the channel is the C2 channel.

Figure F-4 presents the BER achieved for QPSK versus E_b/N_0.. $\delta f \cdot T$ is the frequency offset, normalised to the FFT block duration (the subcarrier spacing). $\delta f \cdot T = 0.1$ represents a large frequency offset: 10% of the subcarrier spacing. The value of $\gamma^2 = 0.001$ corresponds to a phase noise power spectrum bandwidth of about 6.4 KHz. These represent very severe degrees of frequency offset and phase

noise, but the compensation approach results in a performance loss of only about 1 to 1.5 dB. Further studies to be conducted will employ other phase noise spectra, and will show comparisons with OFDM.

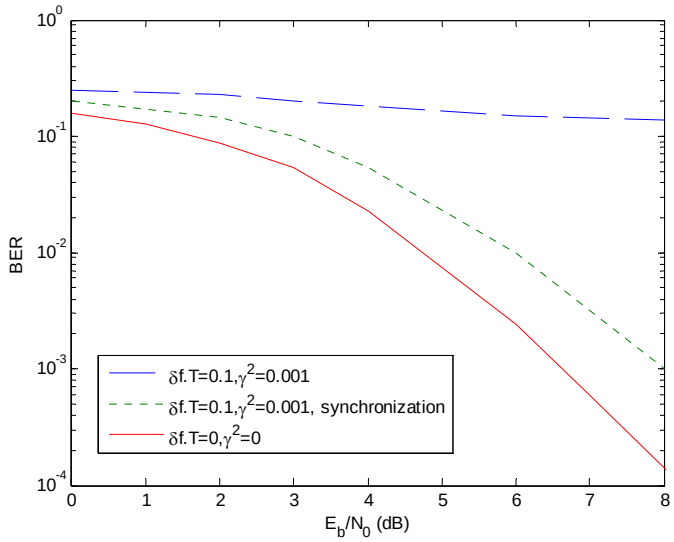

Figure F-4 Phase Noise and frequency offset compensation, QPSK

As mentioned in 6.4.1 frequency-interleaved user signals, such as those of IFDMA, will mutually interfere due to the effects of frequency offset and phase jitter [DLF04a], [DLF04b]. Figure F-5 illustrates the SNR loss as a function of frequency offset (normalised by intercarrier spacing) for IFDMA, with a total of 32 subcarriers per user, spaced at 32-subcarrier intervals. Four cases are shown: (1) P=1 user signal, so no adjacent channel interference; (2) P=8 users, occupying 8 adjacent subcarriers, where the SNR degradation is measured for the user signal on the edge of the group of 8 (I_d=1); (3) P=8 users, occupying 8 adjacent subcarriers, where the SNR degradation is measured for the user signal in the middle of the group of 8 (I_d=4); (4) P=32 adjacent users. Cases (3) and (4) have similar degradation, since most of the interference to the user signal of interest comes from immediately adjacent user signal subcarriers on both sides. In case 2, the user of interest only experiences interference on one side, and in case (1) there is no interference. These results show that SNR degradation to IFDMA is about 0.5 dB or less as long as the frequency offset is below about 2% of the inter-subcarrier spacing.

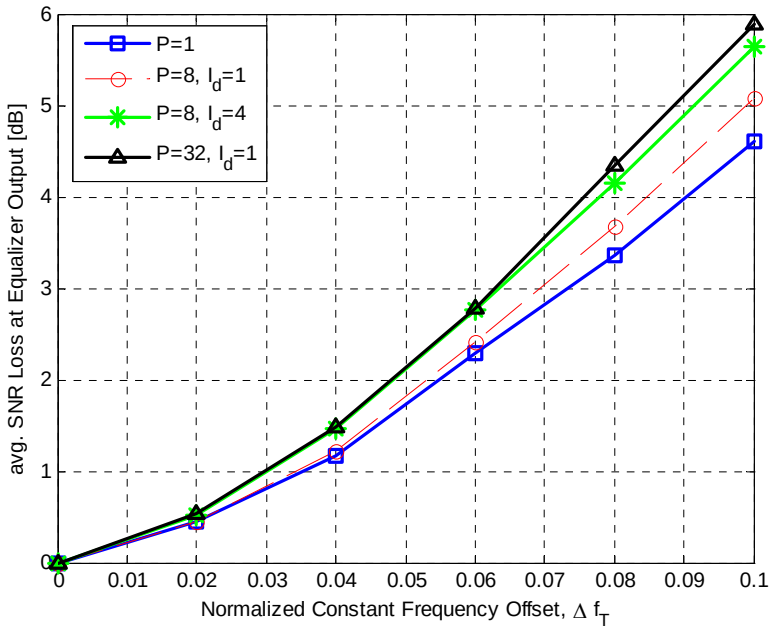

Figure F-5 SNR degradation due to frequency offset for P frequency-interleaved and adjacent IFDMA signals. Each user signal cosists of 32 subcarriers spaced 32 subcarriers apart.

The effect of phase noise, modelled as in 6.3.2, is shown in Figure F-6 for the same signal parameters. The SNR degradation is less than about 0.5 dB if the 3 dB normalised oscillator linewidth is less than about 0.25%.

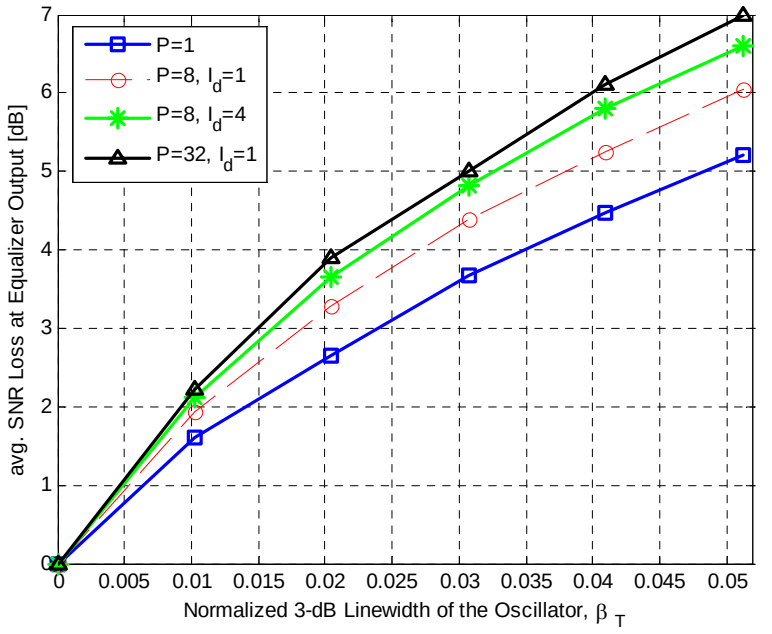

Figure F-6 SNR degradation due to phase noise for P frequency-interleaved and adjacent IFDMA signals. Each user signal consists of 32 subcarriers spaced 32 subcarriers apart.

Appendix G. Data-difference covariance matrix derivation

Consider a general form of the transmitted signal

$$x(n)=\sum_{i=-\infty}^{\infty} x_i(n-n_0)\,rect_N(n-iN-n_0) \tag{G.1}$$

where is a random time offset normalized by sampling time. The *i*–th data symbol is defined by

$$x_i(n)=\frac{1}{\sqrt{N}}\sum_{k=0}^{N-1} X_{i,k}e^{j\omega_N kn} \tag{G.2}$$

Assuming that the autocorrelation function $R_{i,j}^{x}(n+m,n)$ of $x(n)$ depends on *n* it can be described as

$$\begin{aligned} R_{i,j}^{x}(n,n+m)= \\ &= E\left\{\sum_{i=-\infty}^{\infty} x_i(n-n_0)rect_N(n-iN-n_0)\sum_{j=-\infty}^{\infty} x_j^*(n+m-n_0)rect_N(n+m-jN-n_0)\right\} \\ &= E\left\{\sum_{i=-\infty}^{\infty}\sum_{j=-\infty}^{\infty} x_i(n-n_0)x_j^*(n+m-n_0)rect_N(n-iN-n_0)rect_N(n+m-jN-n_0)\right\} \end{aligned} \tag{G.3}$$

Substituting $j=i+l$ into (G.3) the autocorrelation function takes the form

$$\begin{aligned} R_{i,j}^{x}(n,n+m)= \\ &= E\left\{\sum_{i=-\infty}^{\infty}\sum_{l=-\infty}^{\infty} x_i(n-n_0)x_{i+l}^*(n+m-n_0)rect_N(n-iN-n_0)rect_N(n+m-iN-lN-n_0)\right\} \\ &= \sum_{l=-\infty}^{\infty} E_x\left\{x_i(n-n_0)x_{i+l}^*(n+m-n_0)\right\}\sum_{i=-\infty}^{\infty}\frac{1}{N}\sum_{n_0=0}^{N-1} rect_N(n-iN-n_0)rect_N(n+m-iN-lN-n_0) \end{aligned} \tag{G.4}$$

The time samples of two different OFDM symbols are statistically independent if the OFDM modulated data are statistically independent. Thus, the autocorrelation function is non-zero only if $l=0$, i.e. $i=j$. Substituting $p=n_0+iN$ (G.4) reduces to

$$\begin{aligned} R_{i,j}^{x}(n,n+m)= \\ &= E_x\left\{x_i(n-n_0)x_i^*(n+m-n_0)\right\}\frac{1}{N}\sum_{p=-\infty}^{\infty} rect_N(n-p)rect_N(n+m-p) \\ &= E_x\left\{x_i(n-n_0)x_i^*(n+m-n_0)\right\}\Lambda_N(m) \end{aligned} \tag{G.5}$$

where

$$\Lambda_N(m)=\begin{cases}\dfrac{N-|m|}{N}, & \text{for } |m|\le N \\ 0, & \text{for } |m|>N\end{cases} \tag{G.6}$$

Substituting (G.2) into (G.5) the autocorrelation function can be written as

$$\begin{aligned} R_{i,j}^{x}(n,n+m)&=\frac{1}{N}E_x\left\{\sum_{k=0}^{N-1} X_{i,k}e^{j\omega_N k(n-n_0)}\sum_{q=0}^{N-1} X_{i,q}^*e^{-j\omega_N k(n+m-n_0)}\right\}\Lambda_N(m) \\ &=\frac{1}{N}\Lambda_N(m)E_x\left\{\sum_{k=0}^{N-1}\sum_{q=0}^{N-1} X_{i,k}X_{i,q}^*e^{j\omega_N k(n-n_0-n-m+n_0)}\right\},\quad \text{for } |m|\le N \end{aligned} \tag{G.7}$$

Under the assumption of statistical independence and the zero mean of input data symbols the expected value $E_x\left\{X_{i,k}\cdot X_{i,q}^*\right\}=0,\ \forall k\ne q$. Thus,

$$\begin{aligned} R_{i,j}^{X}(n,n+m)&=\frac{1}{N}\Lambda_N(m)\sigma_X^2\sum_{k=0}^{N-1} e^{-j\omega_N km}=\frac{1}{N}\Lambda_N(m)\cdot\sigma_X^2 2\sum_{k=k_{\min}}^{k_{\max}}\frac{e^{-j\omega_N km}+e^{-j\omega_N(N-k)m}}{2} \\ &=\frac{2}{N}\Lambda_N(m)\sigma_X^2\sum_{k=k_{\min}}^{k_{\max}}\cos(\omega_N km) \end{aligned} \tag{G.8}$$

where $k_{\min}$ and $k_{\max}$ are the minimum and the maximum indices of used subcarrier as shown in Figure G-1.

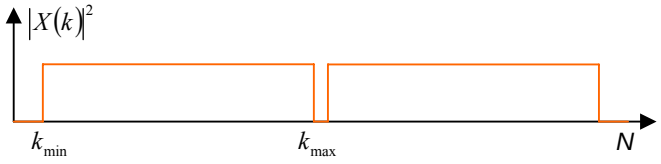

Figure G-1 OFDM symbol band

Finally, the autocorrelation function receives the form

$$R_{i,j}^{X}(m)=\begin{cases}\dfrac{2}{N}\Lambda_N(m)\sigma_X^2\displaystyle\sum_{k=k_{\min}}^{k_{\max}}\cos(\omega_N km), & \text{for } i=j\\ 0, & \text{for } i\neq j\end{cases} \tag{G.9}$$

Further derivation will be performed for the case when the previous OFDM symbol interferes with the desired one. The derivation for the second case is identical and gives the same results, thus, it will not be presented here.

Let us recall the definition of the data-difference covariance matrix

$$\Phi_{\mathbf{s}}=E\left\{\begin{bmatrix}\mathbf{s}_{i1}\\ \mathbf{s}_{i2}\end{bmatrix}\begin{bmatrix}\mathbf{s}_{i1}^H & \mathbf{s}_{i2}^H\end{bmatrix}\right\} \tag{G.10}$$

where

$$\begin{aligned}\mathbf{s}_{i1}&=\left[x_i(N-L_{ch}-\gamma),\ldots,x_i(N-N_G-1)\right]-\left[x_{i-1}(N-\Delta),\ldots,x_{i-1}(N-1)\right]\\ \mathbf{s}_{i2}&=\left[x_i(N-N_G),\ldots,x_i(N-1),x_i(0),\ldots,x_i(N-1)\right]-\\ &\quad\left[x_i(N-N_G),\ldots,x_i(N-1),x_i(0),\ldots,x_i(N-1)\right]=[0,\ldots,0]_{1\times L_{tot}}\end{aligned} \tag{G.11}$$

Since in the considered case $\mathbf{s}_{i2}$ is a zero vector, the data-difference covariance matrix simplifies to

$$\Phi_{\mathbf{s}}=E\left\{\mathbf{s}_{i1}\mathbf{s}_{i1}^H\right\} \tag{G.12}$$

and can be further modified as follows

$$\Phi_{\mathbf{s}}=\begin{bmatrix}R(0,0) & \ldots & R(0,\Delta)\\ \ldots & \ldots & \ldots\\ R(\Delta,0) & \ldots & R(\Delta,\Delta)\end{bmatrix} \tag{G.13}$$

where

$$\begin{aligned}R(a,b)&=E\left\{\left[x_i(n+a)-x_{i-1}(m+a)\right]\left[x_i(n+b)-x_{i-1}(m+b)\right]^*\right\}\\ &=E\left\{x_i(n+a)x_i^*(n+b)\right\}-E\left\{x_{i-1}(m+a)x_i^*(n+b)\right\}-\\ &\quad E\left\{x_i(n+a)x_{i-1}^*(m+b)\right\}+E\left\{x_{i-1}(m+a)x_{i-1}^*(m+b)\right\}\end{aligned} \tag{G.14}$$

where $n=N-L_{ch}-\gamma$ and $m=N-\Delta$. Since the autocorrelation function (G.9) is wide-sense stationary, after substituting $c=b-a$, $d=n+b-m-a$, and $e=m+b-n-a$, (G.14) can be expressed by

$$\begin{aligned}R(a,b)&=E\left\{x_i(n)x_i^*(n+c)\right\}-E\left\{x_{i-1}(m)x_i^*(m+d)\right\}-\\ &\quad E\left\{x_i(n)x_{i-1}^*(n+e)\right\}-E\left\{x_{i-1}(m)x_i^*(m+c)\right\}\\ &=R_{i,i}^X(c)-R_{i,i-1}^X(d)-R_{i-1,i}^X(e)+R_{i-1,i-1}^X(c)\end{aligned} \tag{G.15}$$

According to (G.9) the autocorrelation function is equal to zero when $j\neq i$, thus,

$$\begin{aligned}R(a,b)&=R_{i,i}^X(b-a)+R_{i-1,i-1}^X(b-a)\\ &=\frac{2}{N}\Lambda_N(b-a)\sigma_X^2\sum_{k=k_{\min}}^{k_{\max}}\cos(\omega_N k(b-a))+\frac{2}{N}\Lambda_N(b-a)\sigma_X^2\sum_{k=k_{\min}}^{k_{\max}}\cos(\omega_N k(b-a))\\ &=\frac{4}{N}\Lambda_N(b-a)\sigma_X^2\sum_{k=k_{\min}}^{k_{\max}}\cos(\omega_N k(b-a))\end{aligned} \tag{G.16}$$

For $b = a$ the sum in the above formula is equal to $\frac{N_U}{2}$, thus, large N the autocorrelation function receives the form

$$R(a,b) \cong \begin{cases} 2\frac{N_U}{N}\sigma_X^2, & \text{for } a = b \\ 0, & \text{for } a \neq b \end{cases} \tag{G.17}$$

Finally, the data-difference covariance matrix $\Phi_{\mathbf{s}}$ is equal to

$$\Phi_{\mathbf{s}} \approx 2\frac{N_U}{N}\sigma_X^2 \mathbf{I}_{l\times l} \tag{G.18}$$

The data-difference covariance matrix for the case when the preceding OFDM symbol interfere with the desired one is derived in the same way. The method of derivation of the data covariance matrix $\Phi_{\mathbf{x}}$ is exactly the same. However, the data vector should be used instead of the data-difference vector. Thus, the data covariance matrix is equal to

$$\Phi_{\mathbf{X}} \approx \frac{N_U}{N}\sigma_X^2 \mathbf{I}_{l\times l} \tag{G.19}$$

Both covariance matrices are used in Appendix H where the SNR degradation due to IBI is derived.

Appendix H. SNR Degradation Due to Interference

H.1 Inter-Block Interference (IBI)

The received OFDM symbols are distorted by *Inter-Block Interference* when the samples from previous or subsequent OFDM symbols are added to the desired samples. There are two mainsprings of IBI occurrence, i.e.

- excessively large timing synchronisation error,
- the maximum channel length longer then the cyclic prefix length.

As a result the Signal-to-Noise Ratio (SNR) of the received signal is reduced. In this section the SNR degradation due to IBI is estimated.

Recall that an OFDM system transmits information as a series of *N*-point OFDM symbols defined by

$$x_i(n) = \frac{1}{\sqrt{N}} \sum_{k=0}^{N-1} X_{i,k} e^{j\omega_N kn} rect(n) \tag{H.1}$$

where $\omega_N = \frac{2\pi}{N}$, *i* denotes the OFDM symbol index, and $rect_N(n) = \begin{cases} 1, & 0 \le n < N \\ 0, & \text{otherwise} \end{cases}$. Data are transmitted on $K_U < N$ subcarriers, i.e., $X_{i,k} = X_{i,N-k} = 0$ if $k \notin \langle k_{\min}, k_{\max} \rangle$, where $k_{\min}$ and $k_{\max}$ represent the lowest and the highest used subcarrier index. The last N_G samples of $x_i(n)$ are copied at the beginning of the OFDM symbol creating a cyclic prefix. Thus, the total length L_{tot} of the OFDM transmit block $\mathbf{p}_i$ is equal to $L_{tot} = N + N_G$, where

$$\mathbf{p}_i = [p_i(0), ..., p_i(L_{tot}-1)] = [x_i(N-N_G), ..., x_i(N-1), x_i(0), ..., x_i(N-1)] \tag{H.2}$$

Ignoring the additive channel noise the received signal $y_i(n)$ is equal to

$$y_i(n) = \sum_{i=-\infty}^{\infty} p_i(n - iL_{tot}) \otimes h_i(n) \tag{H.3}$$

where $\otimes$ is the convolution operator and $h_i(n)$ is the channel impulse response represented as

$$h_i(n) = \sum_{k=0}^{L_{ch}-1} h_{i,k} \delta(n-k) \tag{H.4}$$

As far as the WINNER scenarios are concerned, the impulse response lengths of all channels are assumed to be shorter then the length of the cyclic prefix, i.e. $L_{ch} < N_G$. In this case the received OFDM symbol can be affected by *Inter-Block Interference* (IBI) only if timing synchronisation is erroneous. However, assuming that receiver should be synchronised to the first channel path, error γ within range $\gamma \in \langle -(N_G - L_{ch}), 0 \rangle$ will not cause IBI. Any error outside this range will be the reason for IBI. In further calculations case "a" will denote the interference caused by the synchronisation error $\gamma < -(N_G - L_{ch})$, and case "b" will denote the interference caused by the synchronisation error $\gamma > 0$. Thus, in fact case "a" is related to IBI due to the preceding OFDM symbol, whereas case "b" is related to IBI due to the succeeding OFDM symbol.

Let us consider the hypothetical case when signal $p_i(n)$ consists of the shifted replicas of $x_i(n)$. Thus (H.3) can be rewritten as [Ce101]

$$d_i(n) = \sum_{l=-\infty}^{\infty} x_i(n - lN + N_i) \otimes h_i(n), \; N_i = (iL_{tot} + N_G) \bmod N \tag{H.5}$$

where symbol $d_i(n)$ denotes the desired received signal. In this situation the received signal is IBI free and will be used as the reference signal during interference calculation.
The interference $q_i(n)$ affecting *i*-th received symbol can be interpreted as a difference between the *i*-th desired received signal $d_i(n)$ of (H.5) and the real received signal $y_i(n)$ of (H.3) [Ce101].

$$q_i(n) = d_i(n) - y_i(n), \text{ for } n = 0, ..., L_{tot} \tag{H.6}$$

The vector form of the above equation is given by

$$\mathbf{q}_i = \mathbf{H}\mathbf{s}_i \tag{H.7}$$

where $\mathbf{H}$ is the channel convolution matrix of size $N \times (N + L_{ch} + \gamma)$ for case "a" and $N \times (N + N_G + \gamma)$ for case "b", and it has the following form

$$\mathbf{H} = \begin{bmatrix} h_{L_{ch}-1} & \dots & h_{L_{ch}-\Delta} & \dots & h_0 & 0 & \dots & \dots & 0 \\ 0 & \dots & \dots & \dots & \dots & \dots & \dots & \dots & \dots \\ 0 & \dots & h_{L_{ch}-1} & \dots & \dots & \dots & h_0 & \dots & 0 \\ 0 & \dots & \dots & \dots & \dots & \dots & \dots & \dots & 0 \\ 0 & \dots & \dots & \dots & h_{L_{ch}-1} & \dots & h_\gamma & \dots & h_0 \end{bmatrix}, \quad \Delta = L_{ch} + \gamma - N_G \tag{H.8}$$

The vector $\mathbf{s}_i = [\mathbf{s}_{i1}, \mathbf{s}_{i2}]$ is the vector of differences between the desired received samples and the real received samples, i.e., for the case when the previous symbol interferes with the desired one. Both components are described by the formula

$$\begin{aligned} \mathbf{s}_{i1} &= [x_i(N - L_{ch} - \gamma), \dots, x_i(N - N_G - 1)] - [x_{i-1}(N - \Delta), \dots, x_{i-1}(N - 1)] \\ \mathbf{s}_{i2} &= [x_i(N - N_G), \dots, x_i(N-1), x_i(0), \dots, x_i(N-1)] - \\ &\qquad [x_i(N - N_G), \dots, x_i(N-1), x_i(0), \dots, x_i(N-1)] = [0, \dots, 0]_{1\times L_{tot}} \end{aligned} \tag{H.9}$$

and when the succeeding symbol interferes with the desired one the vector components are

$$\begin{aligned} \mathbf{s}_{i1} &= [x_i(N - N_G), \dots, x_i(N-1), x_i(0), \dots, x_i(N-1)] - \\ &\qquad [x_i(N - N_G), \dots, x_i(N-1), x_i(0), \dots, x_i(N-1)] = [0, \dots, 0]_{1\times L_{tot}} \\ \mathbf{s}_{i2} &= [x_i(0), \dots, x_i(\gamma - 1)] - [x_{i+1}(N - N_G), \dots, x_{i+1}(N-1), x_{i+1}(N-1), \dots, x_{i+1}(\gamma - N_G - 1)] \end{aligned} \tag{H.10}$$

Since $\mathbf{s}_{i2}$ for case "a" and $\mathbf{s}_{i1}$ for case "b" are zero vectors the covariance matrix of $\mathbf{q}_i$ can be expressed by

$$\Phi_{\mathbf{q}} = E\{\mathbf{q}_i \mathbf{q}_i^H\} = \hat{\mathbf{H}} \Phi_{\mathbf{s}} \hat{\mathbf{H}}^H \tag{H.11}$$

where H is Hermitian transpose, $\hat{\mathbf{H}}$ is the channel convolution matrix consisting of the first Δ columns of matrix $\mathbf{H}$ in case "a", and the last γ columns of matrix $\mathbf{H}$ in case "b". The data-difference covariance matrix $\Phi_{\mathbf{s}}$ is defined as

$$\Phi_{\mathbf{s}} = E\left\{ \begin{bmatrix} \mathbf{s}_{i1} \\ \mathbf{s}_{i2} \end{bmatrix} \begin{bmatrix} \mathbf{s}_{i1}^H & \mathbf{s}_{i2}^H \end{bmatrix} \right\} \tag{H.12}$$

The total power of IBI may be estimated by means of autocorrelation function of $q(n)$, i.e.

$$P_{IBI} = r_q(0) = E\{q(n) q^*(n)\} \tag{H.13}$$

In general this autocorrelation function is given by [Cel01]

$$r_q(m) = E\{q(n) q^*(n+m)\} = \frac{1}{N} \sum diag(\Phi_{\mathbf{q}}, m), \quad |m| < N \tag{H.14}$$

where $\sum diag(\Phi_{\mathbf{q}}, 0)$ is the trace of the matrix, and $\sum diag(\Phi_{\mathbf{q}}, m)$ is the sum of the elements on the m-th diagonal above or below the main diagonal. If the number of subcarriers is large, the data-difference covariance matrix $\Phi_{\mathbf{s}}$ is almost diagonal (see Appendix G) and then

$$\Phi_{\mathbf{s}} \approx 2 \frac{N_U}{N} \sigma_X^2 \mathbf{I}_{l\times l} \tag{H.15}$$

where $N_U = 2(k_{\max} - k_{\min} + 1)$ is the number of the used subcarriers, and l is the number of columns of channel convolution matrix $\hat{\mathbf{H}}$. Thus, the power of the interference is equal to

$$P_{IBI} = r_q(0) = 2 \frac{N_U}{N} \sigma_X^2 P_h^{IBI}(\tau) \tag{H.16}$$

where $P_h^{IBI}(\tau) = \frac{1}{N} \left[\sum_{j=0}^{\tau-1} (j+1) |h(L_{ch} - \tau + j)|^2 \right]$ and $\tau = \Delta$ for case "a", and $P_h^{IBI}(\tau) = \frac{1}{N} \left[\sum_{j=0}^{\tau-1} (j+1) |h(\tau - 1 - j)|^2 \right]$ and $\tau = \gamma$ for case "b".

The total received power can be described as

$$P_{tot} = r_y(0) = E\{y(n)y^*(n)\} = \frac{1}{N}\sum diag(\Phi_y, 0) \tag{H.17}$$

where, in turn the received data covariance matrix $\Phi_{\mathbf{y}}$ is

$$\Phi_{\mathbf{y}} = E\{\mathbf{y}_i \mathbf{y}_i^H\} = \mathbf{H}\Phi_{\mathbf{x}}\mathbf{H}^H \tag{H.18}$$

with $\Phi_{\mathbf{x}} = E\{\mathbf{x}_{i,IBI}\mathbf{x}_{i,IBI}^H\}$. When the received OFDM symbol is distorted by the samples of a previous OFDM symbol (case "a") the vector $\mathbf{x}_{i,IBI}$ is defined as follows

$$\mathbf{x}_{i,IBI} = [x_{i-1}(N-\Delta), ..., x_{i-1}(N-1), x_i(N-N_G), ..., x_i(N-1), ..., x_i(0), ..., x_i(N-1)] \tag{H.19}$$

In the other case, when the received OFDM symbol is distorted by the samples of succeeding OFDM symbol (case "b"), the vector $\mathbf{x}_{i,IBI}$ receives the form

$$\mathbf{x}_{i,IBI} = [x_i(N-N_G), ..., x_i(N-1), ..., x_i(0), ..., x_i(N-1), x_{i+1}(N-N_G), ..., x_{i+1}(N-\gamma)] \tag{H.20}$$

For a large number of subcarriers the covariance matrix $\Phi_{\mathbf{x}}$ is, similarly as $\Phi_{\mathbf{s}}$, almost diagonal (see Appendix G), thus

$$\Phi_{\mathbf{x}} \approx \frac{N_U}{N}\sigma_X^2 \mathbf{I}_{l\times l} \tag{H.21}$$

where $l = N + N_G + \Delta$ for case "a" and $l = N + N_G + \gamma$ for case "b".
Substitution of (H.21) into (H.18) and (H.18) into (H.17) results in

$$P_{tot} = \frac{N_U}{N}\sigma_X^2 P_h \tag{H.22}$$

where P_h is the average power of channel coefficients. Thus, the Signal-to-Noise Ratio (SNR) of the received signal distorted by IBI is defined as

$$SNR_{IBI}(\tau) = \frac{P_{tot} - P_{IBI}}{P_{IBI} + \sigma_z^2} = \frac{\frac{N_U}{N}\sigma_X^2 P_h - 2\frac{N_U}{N}\sigma_X^2 P_h^{IBI}(\tau)}{2\frac{N_U}{N}\sigma_X^2 P_h^{IBI}(\tau) + \sigma_z^2} \tag{H.23}$$

Knowing that $SNR = \frac{\frac{N_U}{N}\sigma_X^2 P_h}{\sigma_z^2}$ is the SNR of the received signal without IBI and denoting $K(\tau) = \frac{P_h^{IBI}(\tau)}{P_h}$, expression (H.23) simplifies to

$$SNR_{IBI}(\tau) = \frac{SNR - 2\cdot SNR\cdot K(\tau)}{2\cdot SNR\cdot K(\tau) + 1} \tag{H.24}$$

Thus, the SNR degradation due to Inter-Block Interference is defined by

$$D(\tau) = \frac{SNR}{SNR_{IBI}(\tau)} = \frac{2\cdot SNR\cdot K(\tau) + 1}{1 - 2\cdot K(\tau)} \tag{H.25}$$

Let us stress that the above equation is valid only for large number of subcarriers as it occurs in the WINNER scenarios. Curves with SNR degradation values for different timing synchronisation errors and A1 NLOS, A1 LOS, B1 NLOS, B1 LOS and C2 NLOS channels are presented in Appendix L.

H.2 Inter-Carrier Interference (ICI)

The quality of the OFDM transmission highly depends on the carrier frequency offset because it destroys the orthogonality between subcarriers. There are two main sources of the carrier frequency offset, i.e., the Doppler shift and the mismatch between frequencies of the transmit and receive oscillators. The carrier frequency offset attenuates the desired signal and causes that the *Inter-Carrier Interference* (ICI) further decreases the SNR of the received OFDM signal.

Let us assume perfect time synchronisation and the case when the channel impulse response length is shorter then the cyclic prefix length. Both assumptions ensure that there is no Inter-Block Interference. Thus, the *i*-th received OFDM symbol is defined by

$$y_i(n) = s_i(n)\left[p_i(n) \otimes h_i(n) + z_i(n)\right] \tag{H.26}$$

where $z_i(n)$ is the sample of additive white Gaussian noise of variance σ_z^2. The frequency offset Δf induced by the mismatch between the oscillators is represented as a phase shift $s_i(n)$ in time domain, i.e.,

$$s_i(n) = e^{j[2\pi\,\Delta f\,(n+i(N+N_G))T+\theta]} \tag{H.27}$$

where T is the sampling period and θ is an unknown phase offset between the transmitter and receiver carriers.

In case of the OFDM signal the frequency offset Δf can be considered as normalized by the subcarrier spacing. Thus, the normalized frequency offset ε is given by

$$\varepsilon = \Delta f NT \tag{H.28}$$

After substituting (H.28) into (H.27) the new formula of the phase shift can be written as [LLTC04]

$$\widetilde{s}_i(n) = \frac{1}{\sqrt{N}} e^{j\left[2\pi\frac{\varepsilon}{NT}(n+m(N+N_G))T+\theta\right]} = \frac{1}{\sqrt{N}} e^{j\omega_N n\,\varepsilon} e^{j2\pi\,\varepsilon\,m\left(1+\frac{N_G}{N}\right)} e^{j\theta} \tag{H.29}$$

where as previously $\omega_N = \frac{2\pi}{N}$. Thus, the received signal (H.26) is equal to

$$y_i(n) = \sqrt{N}\cdot\widetilde{s}_i(n)\left[p_i(n) \otimes h_i(n)\right] + s_i(n) z_i(n) \tag{H.30}$$

In the frequency domain the received signal (H.30) is expressed by the formula

$$Y_i(k) = \widetilde{S}_i(k) \otimes \left[X_i(k) H_i(k)\right] + \widetilde{Z}_i(k) \tag{H.31}$$

where $\widetilde{Z}_i(k)$ is the discrete Fourier transform of the noise $\widetilde{z}_i(n) = z_i(n) s_i(n)$, which is a zero-mean Gaussian complex variable with variance $\widetilde{\sigma}_z^2 = \sigma_z^2$. The DFT $\widetilde{S}_i(k)$ of the phase shift $\widetilde{s}_i(n)$ factor is defined as [LLTC04]

$$\begin{aligned}
\widetilde{S}_i(k) &= \frac{1}{\sqrt{N}} \sum_{n=0}^{N-1} \widetilde{s}_i(n) e^{-j\omega_N nk} \\
&= \frac{1}{\sqrt{N}} \sum_{n=0}^{N-1} \frac{1}{\sqrt{N}} e^{j\varpi_N \varepsilon\, n} e^{j2\pi\varepsilon m\left(1+\frac{N_G}{N}\right)} e^{j\theta} e^{-j\omega_N nk} \\
&= \frac{1}{N} e^{j2\pi\,\varepsilon\,m\left(1+\frac{N_G}{N}\right)} e^{j\theta} \sum_{n=0}^{N-1} e^{jn(\varepsilon-k)\frac{2\pi}{N}} \\
&= \frac{1}{N} e^{j2\pi\,\varepsilon\,m\left(1+\frac{N_G}{N}\right)} e^{j\theta} \frac{1-e^{j2\pi(\varepsilon-k)}}{1-e^{j2\pi(\varepsilon-k)/N}} \\
&= \frac{1}{N} \frac{\sin(\pi(\varepsilon-k))}{\sin(\pi(\varepsilon-k)/N)} e^{j\pi(\varepsilon-k)(1-1/N)} e^{j2\pi\,\varepsilon\,m\left(1+\frac{N_G}{N}\right)} e^{j\theta}
\end{aligned} \tag{H.32}$$

The normalized frequency offset (H.28) can be expressed by its integer and fractional part as

$$\varepsilon = l + \widetilde{\varepsilon},\ \ \left|\widetilde{\varepsilon}\right| \le 0.5 \tag{H.33}$$

Then the received signal in the frequency domain is equal to

$$Y_i(k) = \widetilde{S}_i(l) X_i(k-l) H_i(k-l) + \sum_{j\neq l} \widetilde{S}_i(j) X_i(k-j) H_i(k-j) + \widetilde{Z}_i(k) \tag{H.34}$$

The first term in (H.34) represents the attenuated signal received on the (*k*-*l*)-th subcarrier instead of the *k*-th one, caused by frequency offsets that exceed *l* times the subcarrier spacing, denoted as the *integer frequency offset*. The second term is the Inter-Carrier Interference and the last term is the Gaussian noise. The integer frequency offset does not change the SNR of the received signal, thus, in order to simplify calculations it is assumed that $l = 0$.

The received signal can be divided into the desired signal part and the distortion part as [LLTC04]

$$\begin{aligned} Y_i(k) &= U_i(k) + I_i(k) + \widetilde{Z}_i(k) \\ U_i(k) &= \widetilde{S}_i(0) X_i(k) H_i(k) \\ I_i(k) &= \sum_{j=1}^{N-1} \widetilde{S}_i(j) X_i(k-j) H_i(k-j) \end{aligned} \tag{H.35}$$

The signal-to-noise ratio (SNR) of the signal received on *k*-th subcarrier is defined by

$$\begin{aligned} SNR(k) &= \frac{E\left\{U_i(k)U_i^*(k)\right\}}{E\left\{I_i(k)I_i^*(k)\right\} + E\left\{\widetilde{Z}_i(k)\widetilde{Z}_i^*(k)\right\}} \\ &= \frac{E\left\{\left|\widetilde{S}_i(0)X_i(k)H_i(k)\right|^2\right\}}{E\left\{\left|I_i(k)\right|^2\right\} + E\left\{\left|\widetilde{Z}_i(k)\right|^2\right\}} \end{aligned} \tag{H.36}$$

It is further assumed that channel coefficients are mutually uncorrelated and the data symbols are mutually independent, i.e.

$$\begin{aligned} E\left\{h_i(n)h_i^*(q)\right\} &= \delta(n-q)E\left\{\left|h_i(n)\right|^2\right\} \\ E\left\{X_i(k-r)X_i^*(k-r)\right\} &= \delta(s-r)\frac{N_U}{N}\sigma_X^2 \end{aligned} \tag{H.37}$$

Since the channel coefficient $H_i(k)$ is independent of data symbols, the power of the desired signal is equal to [LLTC04]

$$E\left\{\left|\widetilde{S}_i(0)X_i(k)H_i(k)\right|^2\right\} = \left|\widetilde{S}_i(0)\right|^2 \frac{N_U}{N}\sigma_X^2 E\left\{\left|H_i(k)\right|^2\right\} \tag{H.38}$$

where

$$\left|\widetilde{S}_i(0)\right|^2 = \left[\frac{\sin(\pi\varepsilon)}{N\sin(\pi\varepsilon/N)}\right]^2 = I^2(\varepsilon) \tag{H.39}$$

In order to estimate the average power of the channel coefficients the property (H.37) is used

$$\sum_{k=0}^{N_U-1} E\left\{\left|H_i[k]\right|^2\right\} = E\left\{\sum_{n=0}^{L_{ch}-1}\sum_{p=0}^{L_{ch}-1} h_i(n)h_i^*(p)e^{-j\omega_N(n-p)k}\right\} = \sum_{n=0}^{L_{ch}-1} E\left\{\left|h_i(n)\right|^2\right\} = P_h \tag{H.40}$$

The average power of the ICI is defined by

$$\begin{aligned} E\left\{\left|I_i(k)\right|^2\right\} &= E\left\{\sum_{r=1}^{N-1}\sum_{p=1}^{N-1}\widetilde{S}_i(r)\widetilde{S}_i^*(p)H_i(k-r)H_i^*(k-r)X_i(k-r)X_i^*(k-r)\right\} \\ &= \sum_{r=1}^{N-1}\left|\widetilde{S}_i(r)\right|^2 E\left\{\left|H_i(k-r)\right|^2\right\}\sigma_X^2 = \sum_{r=1}^{N-1}\left|\widetilde{S}_i(r)\right|^2 P_h\sigma_X^2\frac{N_U}{N} \end{aligned} \tag{H.41}$$

Using the Parseval's theorem the power of $\widetilde{S}_i$ can be estimated as

$$\sum_{r=0}^{N-1}\left|\widetilde{S}_i(r)\right|^2 = \sum_{n=0}^{N-1}\left|\widetilde{s}_i(n)\right| = 1 \tag{H.42}$$

Thus, the power of the ICI can be expressed as

$$E\left\{\left|I_i(k)\right|^2\right\} = \left(1-\left|S_i(0)\right|^2\right)P_h\sigma_X^2\frac{N_U}{N} \tag{H.43}$$

After substituting (H.43), (H.41), (H.40), (H.39) and (H.38) into the SNR is equal to

$$SNR(\varepsilon) = \frac{I^2(\varepsilon)P_h\sigma_X^2\frac{N_U}{N}}{\left(1-I^2(\varepsilon)\right)P_h\sigma_X^2\frac{N_U}{N} + \sigma_z^2} \tag{H.44}$$

Using substitution $SNR = \dfrac{\frac{N_U}{N}\sigma_X^2 P_h}{\sigma_z^2}$ expression (H.44) simplifies to

$$SNR(\varepsilon) = \frac{I^2(\varepsilon) SNR}{\left(1 - I^2(\varepsilon)\right) SNR + 1} \tag{H.45}$$

Finally the SNR degradation due to the frequency offset can be estimated

$$D(\varepsilon) = \frac{SNR}{SNR(\varepsilon)} = \frac{\left(1 - I^2(\varepsilon)\right) SNR + 1}{I^2(\varepsilon)} \tag{H.46}$$

Curves with SNR degradation values for different frequency synchronisation errors and A1 NLOS, A1 LOS, B1 NLOS, B1 LOS and C2 NLOS channels are presented in Appendix L.

H.3 IBI and ICI

In case of perfect time and frequency synchronisation the received signal will not be distorted neither by ICI nor IBI, and its total useful power will be equal to the total received power defined by (H.22). If both phenomena take place jointly the signal can be treated as first distorted by IBI due to the channel conditions, then the resulting signal is a subject of ICI due to the mismatch of the frequency of the transmit and receive oscillators. Thus, the useful power at the receiver input is equal to the difference between the total received power and the power of IBI. Moreover, it is further reduced by the factor $\left|\widetilde{S}_i(0)\right|^2$ due to ICI, i.e.

$$P_U = \left|\widetilde{S}_i(0)\right| \left(P_{tot} - P_{IBI}\right) \tag{H.47}$$

The frequency offset influences also the interfering signal as well. However, according to (H.42) the power of the time-interfering signal is not changed. Thus the total power of interference is equal to the sum of the powers of ICI and IBI. The signal-to-noise ratio of the received signal is equal to

$$SNR(\varepsilon, \tau) = \frac{I^2(\varepsilon)\left(P_h \sigma_X^2 \frac{N_U}{N} - 2 \frac{N_U}{N} \sigma_X^2 P_h^{IBI}(\tau) \right)}{\left(1 - I^2(\varepsilon)\right)\left(P_h \sigma_X^2 \frac{N_U}{N} - 2 \frac{N_U}{N} \sigma_X^2 P_h^{IBI}(\tau) \right) + 2 \frac{N_U}{N} \sigma_X^2 P_h^{IBI}(\tau) + \sigma_z^2} \tag{H.48}$$

Substituting $SNR = \frac{\frac{N_U}{N} \sigma_X^2 P_h}{\sigma_z^2}$ and $K(\tau) = \frac{P_h^{IBI}(\tau)}{P_h}$ (H.48) simplifies to

$$SNR(\varepsilon, \tau) = \frac{I^2(\varepsilon)\left(SNR - 2SNRK(\tau)\right)}{\left(1 - I^2(\varepsilon)\right)\left(SNR - 2 \cdot SNRK\right) + 2SNRK(\tau) + 1} = \frac{SNRI^2(\varepsilon)\left(1 - 2K(\tau)\right)}{SNR\left[1 - I^2(\varepsilon)\left(1 - 2K(\tau)\right)\right] + 1} \tag{H.49}$$

Finally, the SNR degradation due to IBI and ICI is expressed as

$$D(\varepsilon, \tau) = \frac{SNR}{SNR(\varepsilon, \tau)} = \frac{\left[1 - I^2(\varepsilon)\left(1 - 2 \cdot K(\tau)\right)\right] SNR + 1}{I^2(\varepsilon)\left(1 - 2K(\tau)\right)} \tag{H.50}$$

Curves presenting SNR degradation values for different timing synchronisation errors, frequency synchronisation errors and A1 NLOS, A1 LOS, B1 NLOS, B1 LOS and C2 NLOS channels are presented in Appendix L.

Appendix I. Performance of Link Level Synchronisation Techniques

I.1 Performance of Link Level Synchronisation Techniques: Licensed Case

In this section, simulation results of timing and frequency synchronisation algorithms described in Section 7.3 are presented. Simulations were performed for the system parameters presented in Appendix A, i.e.,

- Base Coverage Urban scenario with Frequency Division Duplex (FDD) and C1 NLOS channel model, maximum velocity of UT equal to 70 km/h;
- Micro-cellular scenario with Time Division Duplex (TDD) and B1 NLOS/LOS channel models, maximum velocity of UT equal to 70 km/h;
- Indoor scenario with TDD and A1 NLOS/LOS channel models, maximum velocity of UT equal to 5 km/h.

The OFDM symbol utilised for the timing and frequency synchronisation was designed according to Figure 7-2. In order to demodulate the received synchronisation symbol, FFT of size 512 was utilised. The size of the IFFT used for channel impulse response estimation during fine timing estimation was also equal to 512. The results of timing synchronisation with strongest channel path detection, using decision formula (7.17), are shown in Figure I-1 for both A1 channel models, in Figure I-2 for both B1 channel models and in Figure I-3 for C2 NLOS channel mode. These figures illustrate the timing synchronisation error probability versus SNR for the coarse and fine timing synchronisation algorithms.

The fine timing synchronisation algorithm slightly improves the synchronisation quality for A1 NLOS, A1 LOS and B1 LOS channel models. However, for B1 NLOS and C2 NLOS channel models the algorithm proves its usefulness.

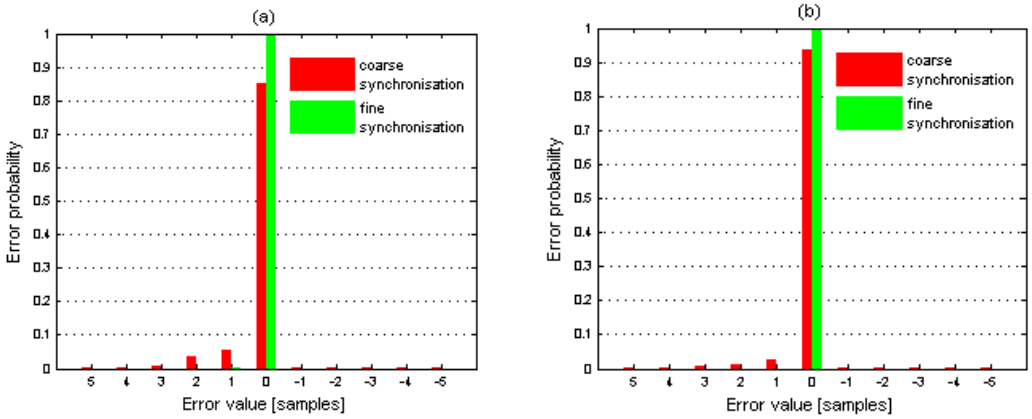

Figure I-1 Timing synchronisation error probability for A1 (a) LOS, (b) NLOS channel. Synchronisation with the strongest path detection.

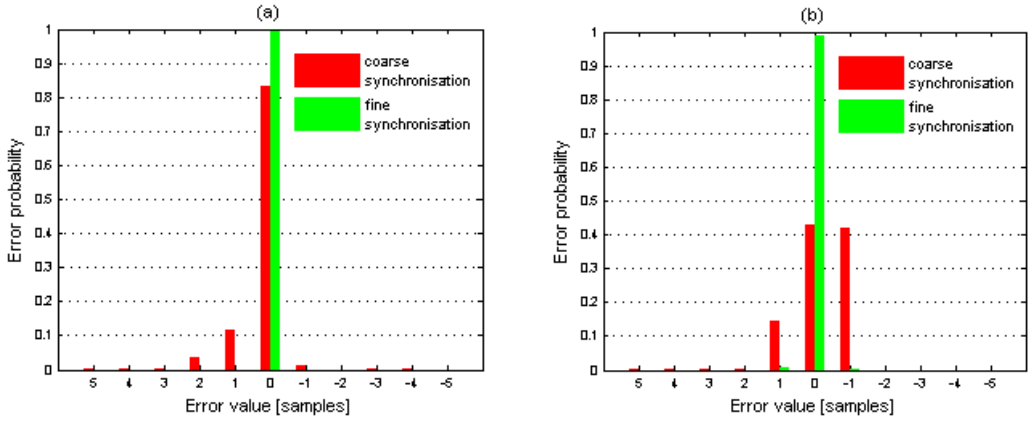

Figure I-2 Timing synchronisation error probability for B1 (a) LOS, (b) NLOS channel. Synchronisation with the strongest path detection.

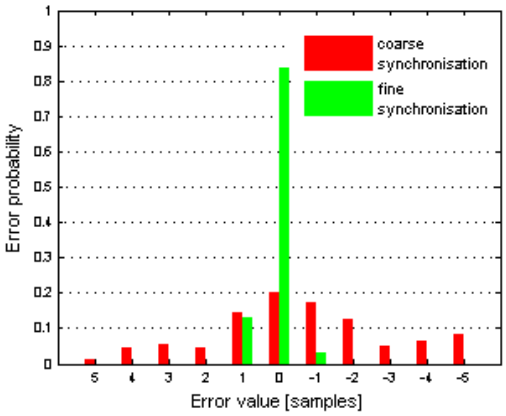

Figure I-3 Timing synchronisation error probability for C2 NLOS channel. Synchronisation with the strongest path detection

The results presented above prove that the algorithm finds the strongest path very well. The accuracy of the timing synchronisation ensures that, in case of WINNER channels, there will be no Inter-Block Interference with the preceding OFDM symbol. However, one cannot be sure at all that there will not be any IBI with a succeeding OFMD symbol (see Appendix L).

Finding the first path of the power exceeding a certain threshold should solve the above problem. The results of the timing synchronisation using decision formula (7.18) are shown in Figure I-4 for A1 channel models, in Figure I-5 for B1 channel models and in Figure I-6 for C2 NLOS channel model. These figures present the timing synchronisation error probability for different values of scaling factor α, which determines the detecting threshold in (7.18).

One can see that the accuracy of this approach is much worse than of the one presented earlier. However, the range of synchronisation errors in all cases is smaller than the timing error IBI-free range (

). Thus, left-shifting the FFT window by the assumed maximum of the timing error will guarantee the IBI-free reception of the signal.

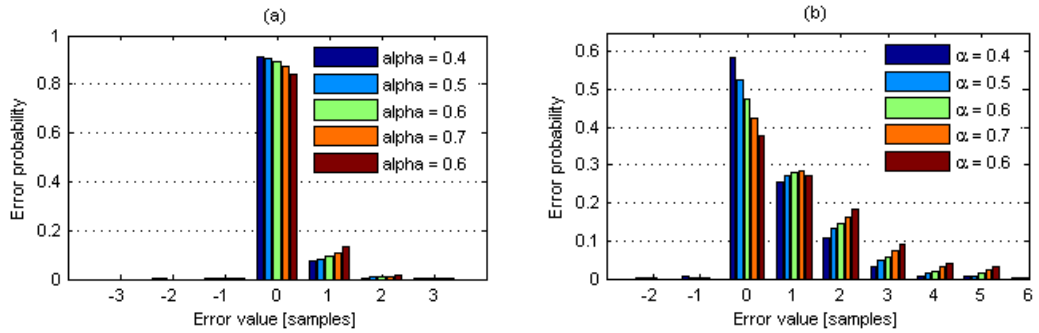

Figure I-4 Timing synchronisation error probability distribution for A1 (a) LOS (b) NLOS channel. Detection of the first path of the power exceeding the threshold depended on "alpha".

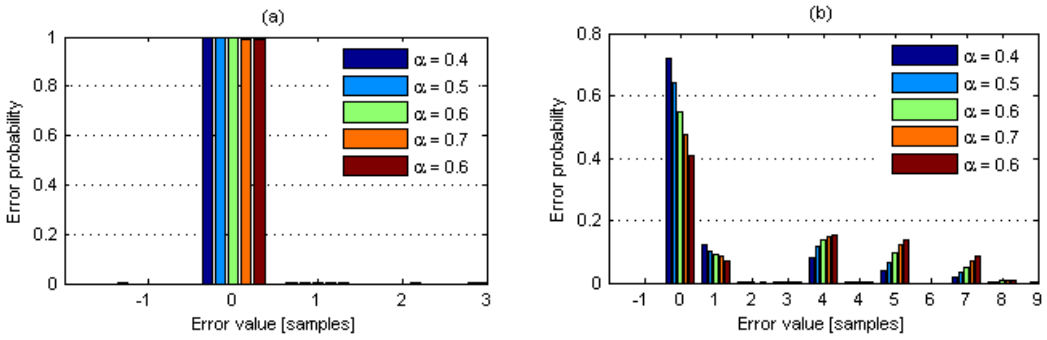

Figure I-5 Timing synchronisation error probability distribution for B1 (a) LOS, (b) NLOS channel. Detection of the first path of the power exceeding the threshold depended on "alpha".

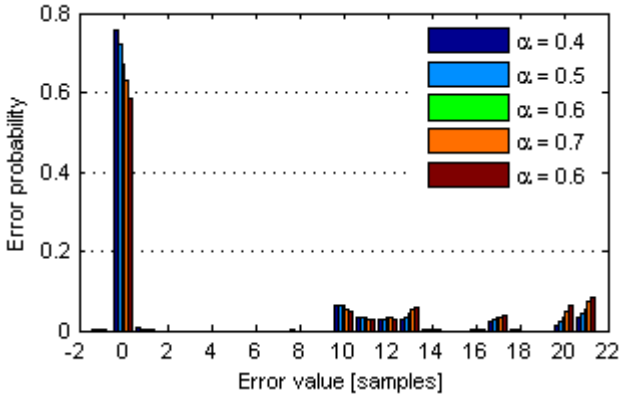

Figure I-6 Timing synchronisation error probability distribution for C2 NLOS channel. Detection of the first path of the power exceeding the threshold depended on "alpha".

Results of fine frequency offset estimation are presented in Figure I-7 for A1 channel models, in Figure I-8 for B1 channel and in Figure I-9 for C2 NLOS channel model. The implemented algorithm of fine frequency offset estimation is able to estimate frequency offsets within the range $\pm 2\Delta f$, where Δf is the subcarrier distance. Its performance was tested with three frequency offsets equal to 0.5, 1.0 and 1.99 Δf . The results are presented as the Mean Squared Error (MSE) of the frequency offset estimation versus SNR. It can be seen that the accuracy of the algorithm is independent of the frequency offset.

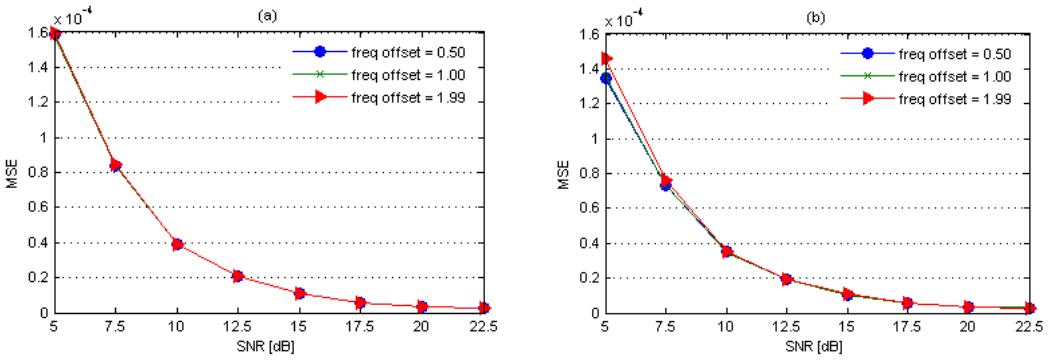

Figure I-7 Frequency synchronisation Mean Squared Error for A1 (a) LOS, (b) NLOS channel.

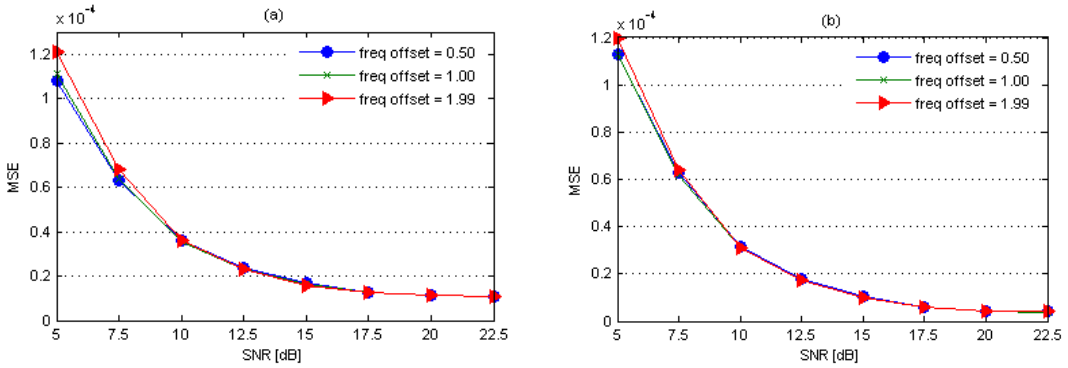

Figure I-8 Frequency synchronisation Mean Squared Error for B1 (a) LOS, (b) NLOS channel.

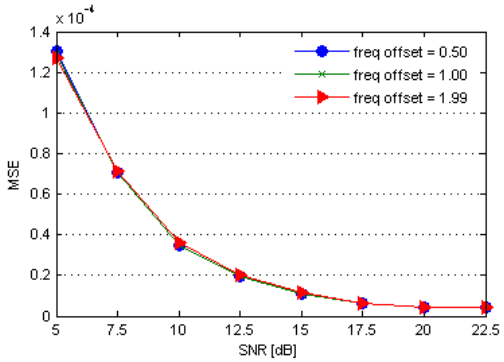

Figure I-9 Frequency synchronisation Mean Squared Error for C2 NLOS channel.

In order to improve frequency offset estimates the algorithm computes the mean of previously estimated offsets, as stated in Section 7.3.2. The comparison of accuracy of the algorithm with and without averaging is illustrated in Figure I-10 for A1 channels, in Figure I-11 for B1 channel models and in Figure I-12 for C2 NLOS channel model. Simulations were performed for the frequency offset equal to 1.99 of the subcarrier distance, i.e., the maximum frequency offset possible to estimate by the algorithm. Simulations proved that utilising the averaging significantly decreases the MSE of the frequency offset. For all SNR values used during simulation the MSE was decreased approximately by the factor of 2.

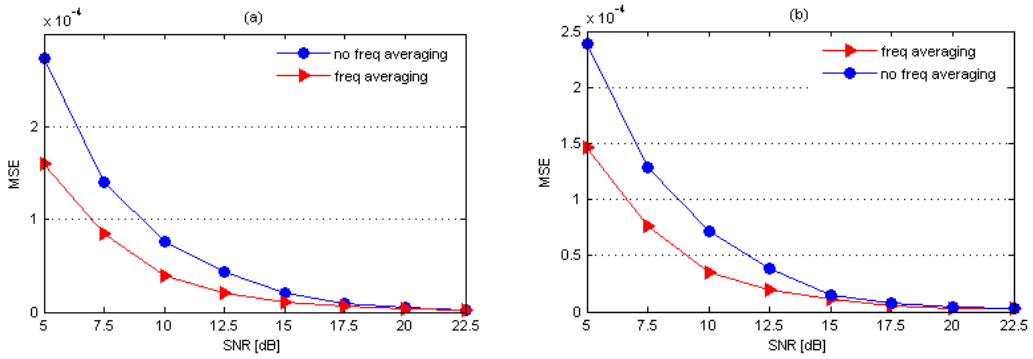

Figure I-10 Frequency synchronisation Mean Squared Error versus frequency averaging for A1 (a) LOS, (b) NLOS channel.

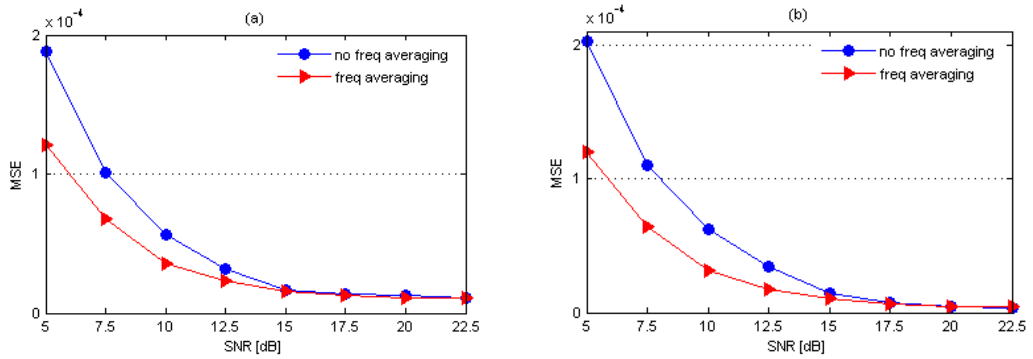

Figure I-11 Frequency synchronisation Mean Squared Error versus frequency averaging for B1 (a) LOS, (b) NLOS channel.

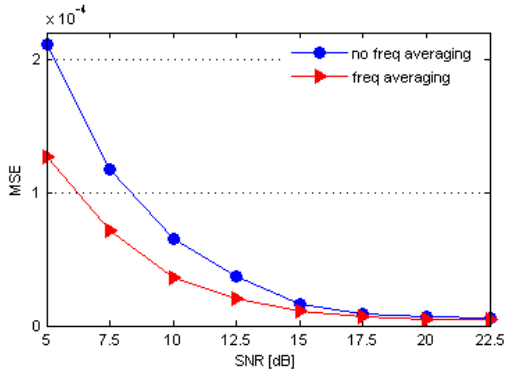

Figure I-12 Frequency synchronisation Mean Squared Error versus frequency averaging for C2 NLOS channel.

If the frequency offset is larger than twofold subcarrier distance, the integer frequency offset estimation is required. In the analysed system the estimation was performed with formula (7.12) and was tested for frequency offsets equal to four times and eight times the subcarrier distance. Simulation results for integer frequency synchronisation are presented in Table I.1. Since the simulation results for both frequency offsets were the same only one table is shown. The table presents the probability of successful synchronisation for the given SNR and channel model.

channel	SNR [dB]							
	5	7,5	10	12,5	15	17,5	20	22,5
A1 LOS	1	1	1	1	1	1	1	1
A1 NLOS	1	1	1	1	1	1	1	1
B1 LOS	1	1	1	1	1	1	1	1
B1 NLOS	1	1	1	1	1	1	1	1
C2 NLOS	1	1	1	1	1	1	1	1

Table I.1 Performance of the integer frequency offset synchronisation algorithm

All synchronisation algorithms designed for synchronisation process were performed during one OFDM symbol giving satisfying results. However, in order to investigate if the time consumed by computations does not exceed the OFDM symbol duration, the complexity of these algorithms should be estimated. The number of real multiplications was chosen as a measure of the algorithm complexity and its estimation is shown in Table I.2.

Process	number of real multiplications
coarse timing synchronisation	6912
fine frequency synchronisation	8704
frequency offset correction	8192
FFT-512	9216
IFFT-512	9216
power delay profile estimation	1024
Other	1344
TOTAL	44608
IFFT-2048	45056

Table I.2 The estimated complexity of applied algorithms.

Since the total amount of real multiplications required for synchronisation is lower than the amount of real multiplications performed during IFFT of size 2048, the proposed synchronisation scheme seems to be reasonable solution for WINNER link level synchronisation.

I.2 Performance of Link Level Synchronisation Techniques: License Exempt and Spectrum Sharing Case

Performance with algorithm that applies NBI cancellation

This section evaluates the performance of the proposed NBI cancellation algorithm. The results have been obtained in the presence of several randomly located NBI interferers modelled as pulse amplitude modulated signals, each occupying a bandwidth of 1MHz. The signal to interference ratio (SIR) is defined as the ratio of the average power received over a sub-carrier of the desired signal and the power of the interfering signal. Indoor scenario described by the parameters from Appendix A and NLOS channel A1 are used for subsequent simulations.

Figure I-13-Figure I-15 show the timing histograms obtained without interference, with interference and with interference cancellation, respectively. Correct synchronisation is achieved if the timing estimate lies inside the range $[CP_{length} - L, 0]$ where L is the channel length. Results show that in absence of interference cancellation, synchronisation in presence of strong interferers is impossible. On the other hand, Figure I-15 shows that timing histograms measured after cancellation are very close to the ideal optimum of the interference-free case.

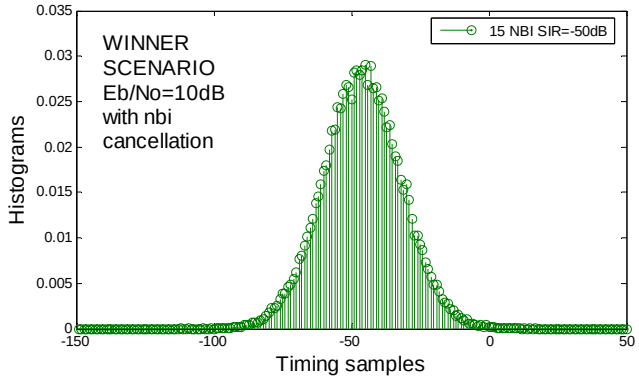

Figure I-13: Histogram of timing estimator without NBI.

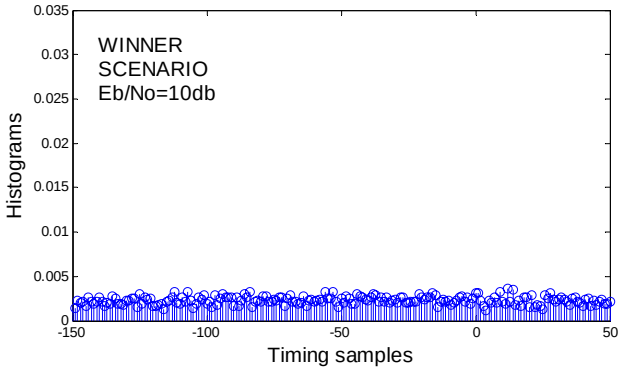

Figure I-14: Histogram of timing estimator with NBI without cancellation.

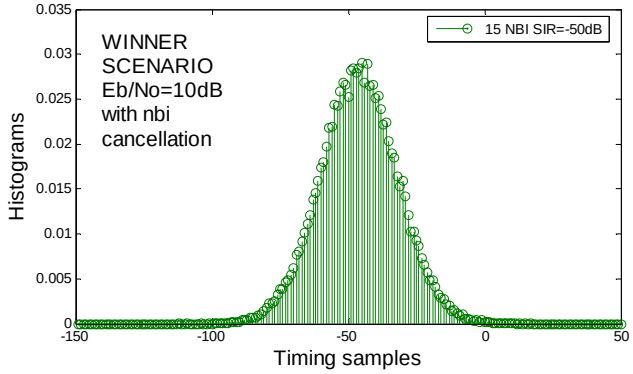

Figure I-15: Histogram of timing estimator with NBI cancellation.

Figure I-16 shows the carrier frequency MSE. The MSE has been computed assuming perfect timing estimation. Once again, estimation performance is very poor without interference cancellation. Residual interference due to the spectral leakage gives an error floor in the performance of the frequency estimation algorithm after NBI cancellation. Nonetheless, this floor is sufficiently low in the simulation scenarios that we have investigated.

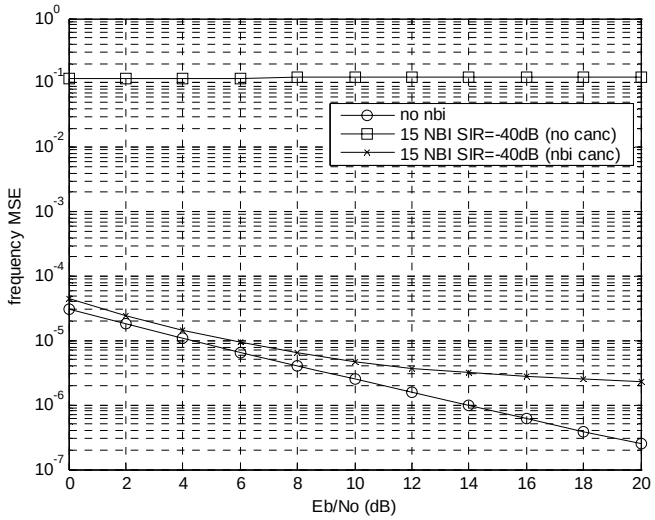

Figure I-16: Carrier frequency estimation mean square error.

Performance of T-Pilot-based synchronisation algorithm

In this section, simulation results of *T-pilot*-based timing and frequency synchronisationion algorithms in presence of narrowband interference are presented. Note that this algorithm does not try to take into account possible presence of NBI. The bandwidth of each interfering signal was equal to 1 MHz, and synchronisationion was tested for 1, 2, 4, 8 and 16 interfering signals. The Signal-to-Interference Ratio (SIR) was defined as the ratio of the average power of the desired signal transmitted over a subcarrier and the power of the interfering signal on that subcarrier. The following set of SIR was used, i.e. –3, -6, -12, -15, -18, -21 and –24 dB. Two configurations were simulated, i.e. the transmitted signal had parameters used in Base Coverage Urban (BCU) and in Micro-cellular (MC) scenarios. In both configurations AWGN channel was used.

The influence of the interference on the Mean-Squared Error of the frequency offset estimation is shown in Figure I-17 for BCU and in Figure I-18 for MC. It can be seen that the frequency synchronisation is immune to the interference only for high SIR. For low SIR values MSE rises rapidly even if there is only one interfering signal.

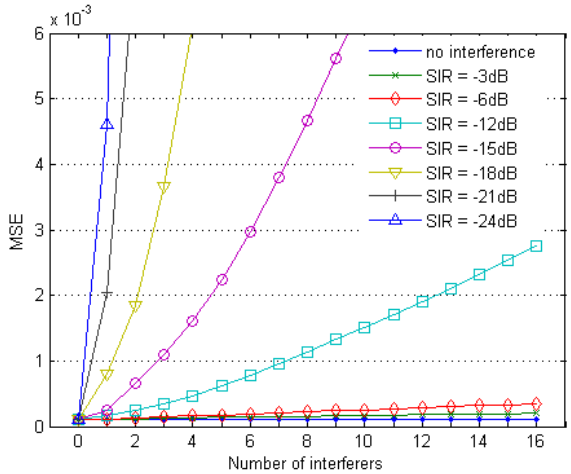

Figure I-17 Frequency synchronisation Mean Squared Error. Signal parameters of Base Coverage Urban scenario.

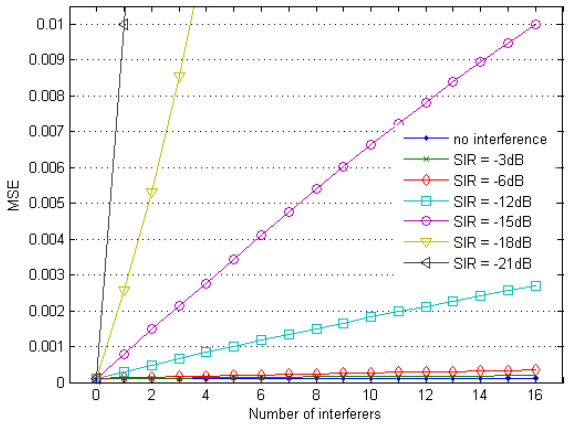

Figure I-18 Frequency synchronisation Mean Squared Error. Signal parameters of Micro-cellular and Indoor scenarios.

The influence of the interference on the time synchronisation is presented in Figure I-19 and Figure I-20 for BCU and MC respectively. On both figures a probability of the time synchronisation error "e" equal to 0 is presented. The results were obtained for real frequency synchronisation. It should be stressed that the lower probability of the error free time synchronisation the higher probability of time synchronisation failure where time synchronisation failure means the time offset estimate error causing Inter-Block Interference.

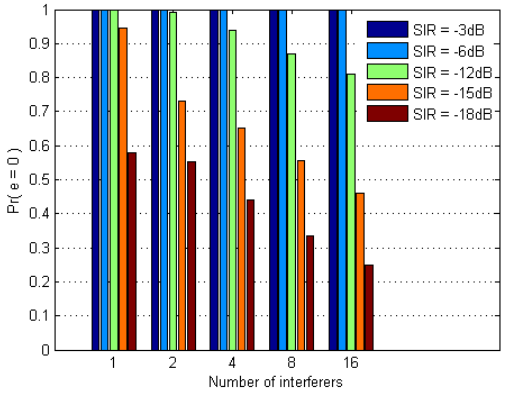

Figure I-19 Time synchronisation performance with non perfect frequency synchronisation. Signal parameters of Base Coverage Urban scenario.

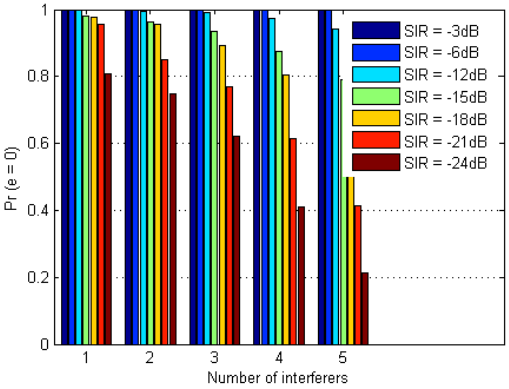

Figure I-20 Time synchronisation performance with non perfect frequency synchronisation. Signal parameters of Micro-cellular and Indoor scenarios.

The degradation of the time synchronisation performance was caused by both large frequency synchronisation error due to the narrowband interference and by the narrowband interference itself. In order to test timing synchronisation robustness simulations with perfect frequency synchronisation were

performed. Results are presented in Figure I-21 for BCU and in Figure I-22 for MC. One can see that the results are better then the previous ones, however, the performance degradation is mainly related with the presence of the interference especially in BCU case.

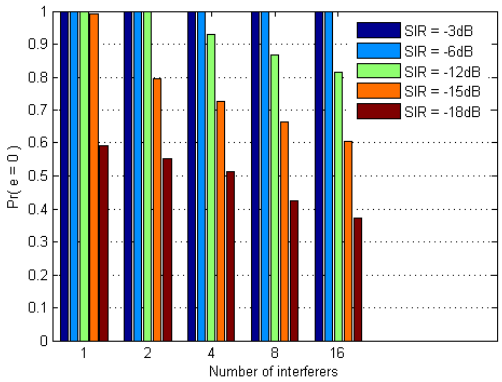

Figure I-21 Time synchronisation performance with perfect frequency synchronisation. Signal parameters of Base Coverage Urban scenario.

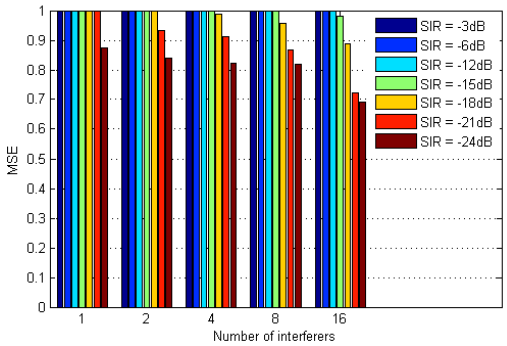

Figure I-22 Time synchronisation performance with non perfect frequency synchronisation. Signal parameters of Micro-cellular and Indoor scenarios.

Simulation results show that *T-Pilot*-based synchronisation algorithms robustness to narrowband interference is limited only to higher SIR values. If stronger interference signals are expected the interference detection and cancellation should be implemented.

Appendix J. Performance of Self-Organised Network Synchronisation

To assess the validity of the proposed scheme simulations are conducted. Simulations assess the convergence of the algorithm, and more precisely the time taken by a given network to perform slot synchronisation.

J.1 Local Area

The local area scenario considers that four antenna arrays are placed within corridors. The network topology considered for simulations for 15 user terminals participating to the network synchronisation is depicted in Figure J-1.

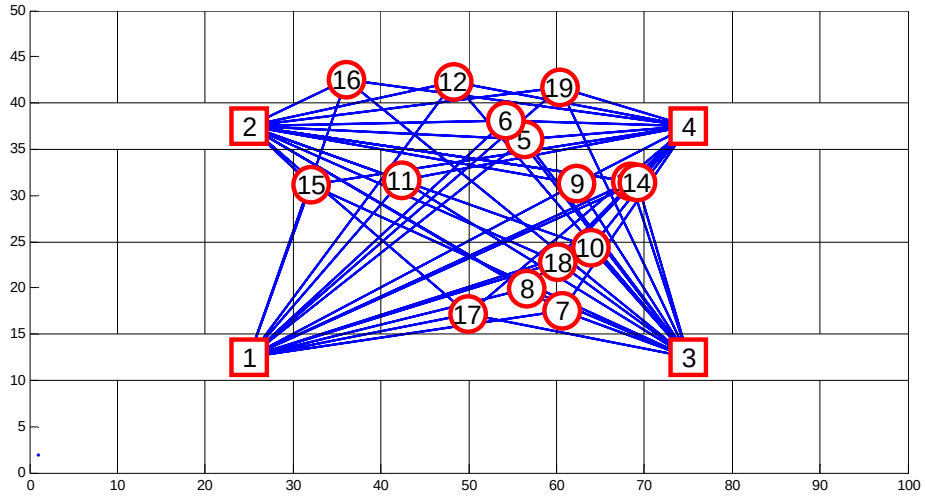

Figure J-1: Considered Network Topology for 15 UTs

To accelerate the synchronisation process, it is useful to limit the number of user terminals that participate to the synchronisation process. In Figure J-1 user terminals, which are marked as circles, can communicate directly with all base stations, which are marked as squares, and cannot communicate directly. User terminals that do not participate to the network synchronisation procedure do not transmit the "UL Sync" word, and adjust their slot oscillator based on received "DL Sync" words.

The following simulation results look at the time needed for the entire network to synchronise, i.e. all user terminals fire simultaneously before all base stations fire simultaneously. The time to synchrony T_{sync} is normalised to the duration a super-frame T_{SF}, and is evaluated for 5,000 sets of initial conditions, i.e. all participants initially commence with a uniformly distributed random clock value, as the coupling value at user terminals α_{UT} varies. Base stations parameters are set to: $\alpha_{\text{BS}} = 1.1$, $\beta_{\text{BS}} = 0.01$ for the coupling, and $T_{\text{refr,DL}} = 10 \cdot T_{\text{s}}$ where T_{s} is the duration of an OFDM symbol (see Appendix A). User terminal parameters are set to $\beta_{\text{UT}} = 0.01$ and $T_{\text{refr,UL}} = 10 \cdot T_{\text{s}}$. Figure J-2 through Figure J-5 show the cumulative distribution function of the normalised time to synchrony as the number of participating user terminal augments.

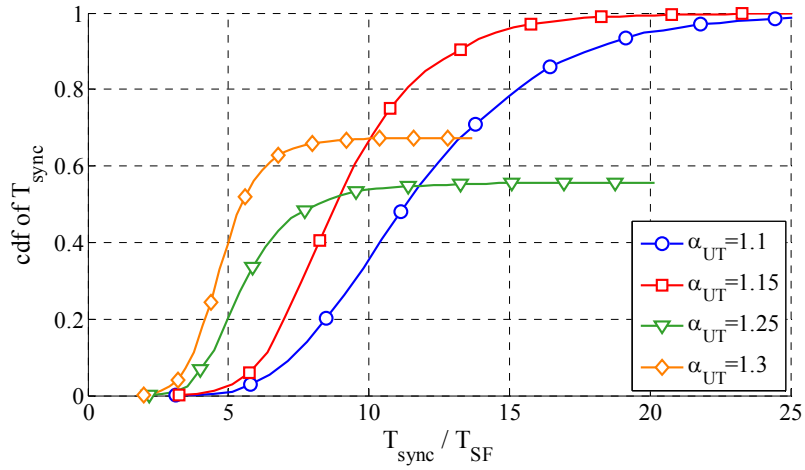

Figure J-2: Local Area Results for 10 UTs.

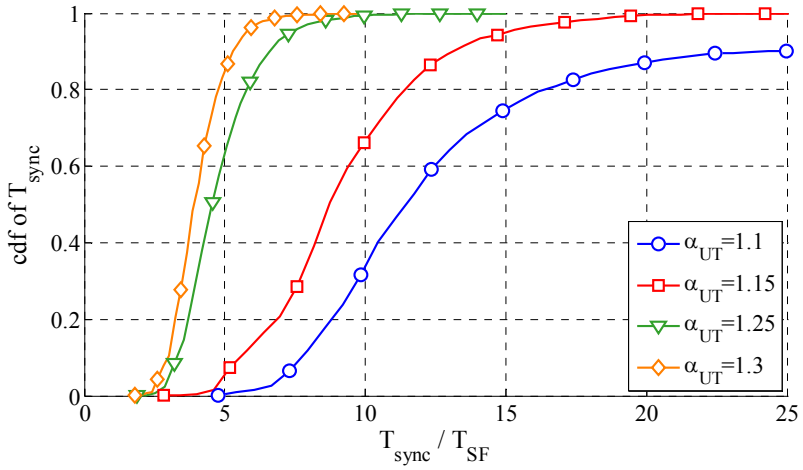

Figure J-3: Local Area Results for 15 UTs.

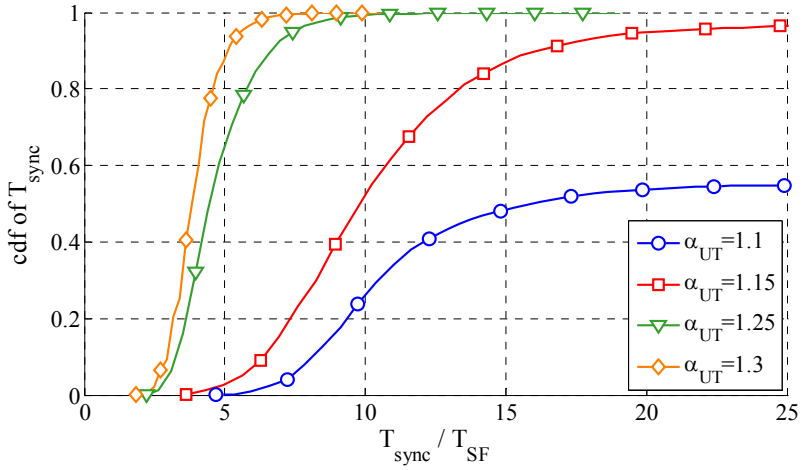

Figure J-4: Local Area Results for 20 UTs.

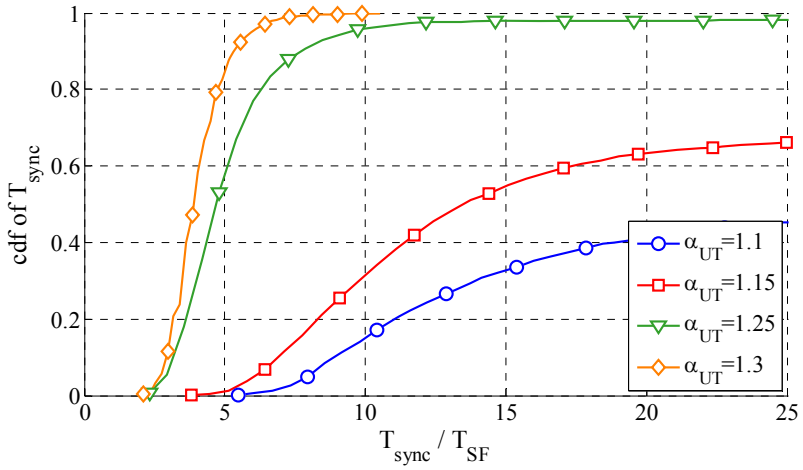

Figure J-5: Local Area Results for 25 UTs.

From these figures, the performance of the proposed slot synchronisation algorithm augments as the number of nodes in the system increases.

For 10 user terminals, low coupling values is preferable, as synchronisation is always reached for $\alpha = 1.1$ and $\alpha = 1.15$. For higher coupling values, synchronisation is not always reached, but convergence is quicker.

As the number of user terminals increases, the results for high coupling improve: synchronisation is always reached for $\alpha = 1.25$ and $\alpha = 1.3$ and the time to synchrony is always below 10 super-frames. For 90% of initial conditions, T_{sync} is equal to 5 periods when $\alpha = 1.3$.

J.2 Metropolitan Area

In the metropolitan area scenario, base stations and user terminals are placed on a grid. This changes the topology of the network, and several hops are needed to communicate from one base station to the other. In order to make sure that the network is connected, i.e. there is a path between any pair of nodes, only user terminals that are placed at intersections participate to the network synchronisation scheme and transmit the UL Sync word. These nodes are able to link at least two base stations which are not in line of sight. An example of the considered topology is shown in Figure J-6 for a three-by-three (3x3) grid. Base stations, indicated as clock dots, are placed according to the pattern given in [WIN2D6137], and 45 user terminals, marked as red dots are placed randomly at intersections. Links are shown between connected BSs and UTs.

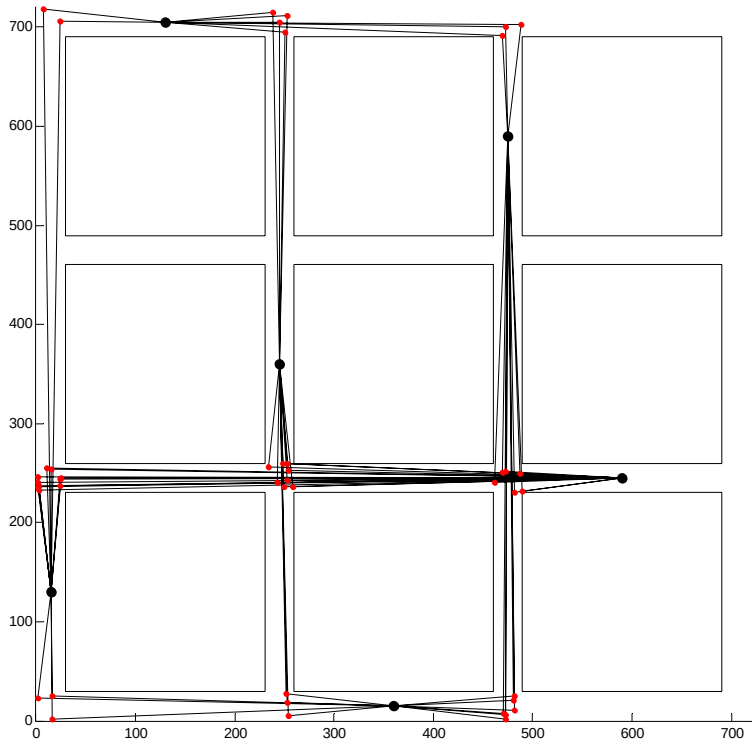

Figure J-6: Considered Network Topology for a 3x3 blocks network and 45 UTs.

The following simulation results look at the time needed for the entire network to synchronise, i.e. all user terminals fire simultaneously before all base stations fire simultaneously, when nodes are placed on a grid of 3x3, 4x4 and 5x5 blocks. The time to synchrony T_{sync} is normalised to the duration a super-frame T_{SF}, and is evaluated for 5,000 sets of initial conditions, i.e. all participants initially commence with a uniformly distributed random clock value, as the coupling value at user terminals α_{UT} varies. Base stations parameters are set to: $\alpha_{\text{BS}} = 1.03$, $\beta_{\text{BS}} = 0.01$ for the coupling, and $T_{\text{refr,DL}} = 40 \cdot T_{\text{s}}$ where T_{s} is the duration of an OFDM symbol (see Appendix A). User terminal parameters are set to $\beta_{\text{UT}} = 0.01$ and $T_{\text{refr,UL}} = 30 \cdot T_{\text{s}}$. Figure J-7 through Figure J-10 show the cumulative distribution function of the normalised time to synchrony as the number of participating user terminal augments.

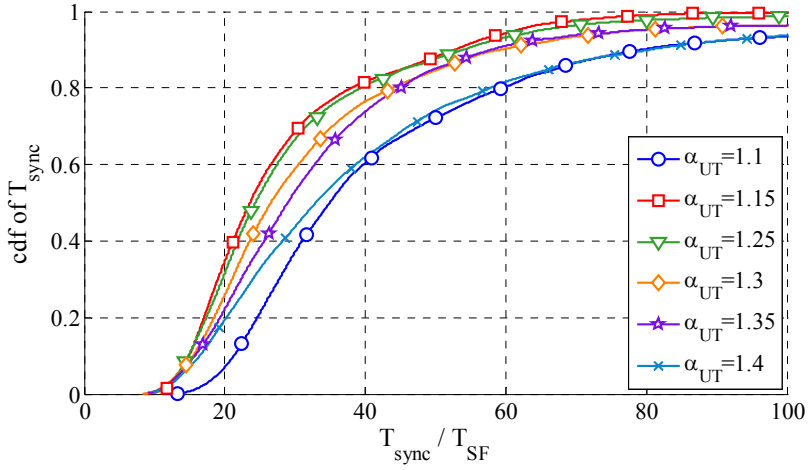

Figure J-7: Metropolitan Area Results for a 3x3 grid and 60 UTs.

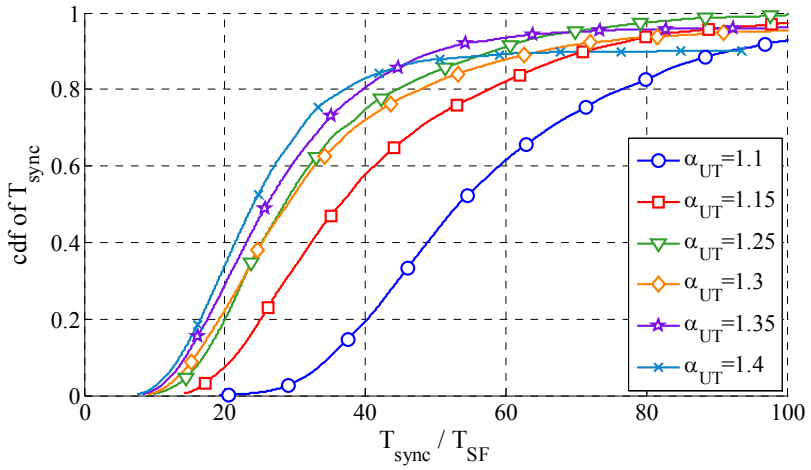

Figure J-8: Metropolitan Area Results for a 4x4 grid and 60 UTs.

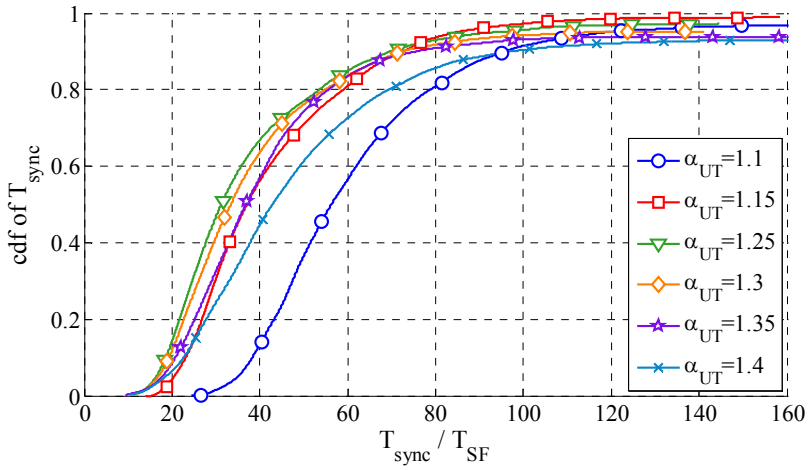

Figure J-9: Metropolitan Area Results for a 4x4 grid and 80 UTs.

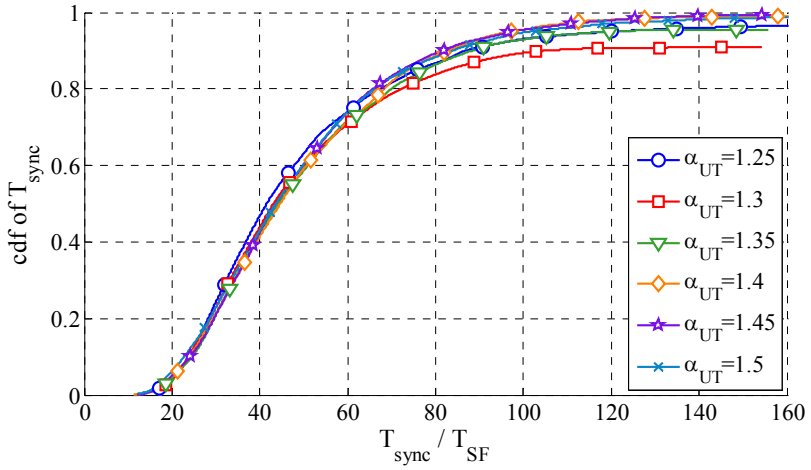

Figure J-10: Metropolitan Area Results for a 5x5 grid and 80 UTs.

As the network size increases, the time to synchrony also rises. For a 3x3 grid, synchrony is reached within 50 periods in 90% of initial conditions, whereas it requires 80 periods for a 5x5 grid. In all cases, the time to synchrony can be considered to be relatively high, especially compared to the local area scenario, where synchrony is reached within 10 periods. Thus it is necessary to place reference nodes within each 3x3 block, so that nodes can acquire a timing reference more quickly. As a rule of thumb, one reference base station for 10 normal base stations would drastically reduce the time to synchrony.

J.3 Wide Area

In the wide area scenario, given the large propagation delays, the main concern for the network synchronisation scheme is the achieved accuracy. Thus the following simulations investigate the misalignment in time between base stations and user terminals, and the misalignment between base stations, rather than the time needed for a network to synchronise.

The accuracy is defined as follows. Let $\tau_{\mathrm{UT},i}$ and $\tau_{\mathrm{BS},j}$ respectively denote the firing instant of user terminal *i* and base station *j*, which are marked in Figure 8-6 at the end of listen periods in each state machine. From Figure 8-6, it is clear that when nodes are synchronised, there is a constant misalignment between UTs and BSs, which is equal to the durations of the UL,Sync word and the RAC. Thus, the accuracy between the *i*th UT and the *j*th BS is defined as:

$$\text{accuracy} = \left| \tau_{\mathrm{UT},i} - \left(\tau_{\mathrm{BS},j} - \left(T_{\mathrm{UL,Sync}} + T_{\mathrm{RAC}} \right) \right) \right| \quad .$$

Given this definition, if the nodes are perfectly aligned in time, the accuracy is equal to zero. However, given the propagation delay between two nodes, it is rarely the case.

In the following, the accuracy of the self-organised network synchronisation scheme is verified considering seven loaded cells with 150 user terminals distributed in the network and participating to the network synchronisation procedure by transmitting the UL Sync word. Participating UTs are chosen if their distance from their own base station is superior to $d_{\mathrm{selection}}$. Such a topology is represented in Figure J-11 for a cell radius of 1000 metres and a selection range of $d_{\mathrm{selection}} = 950\mathrm{m}$.

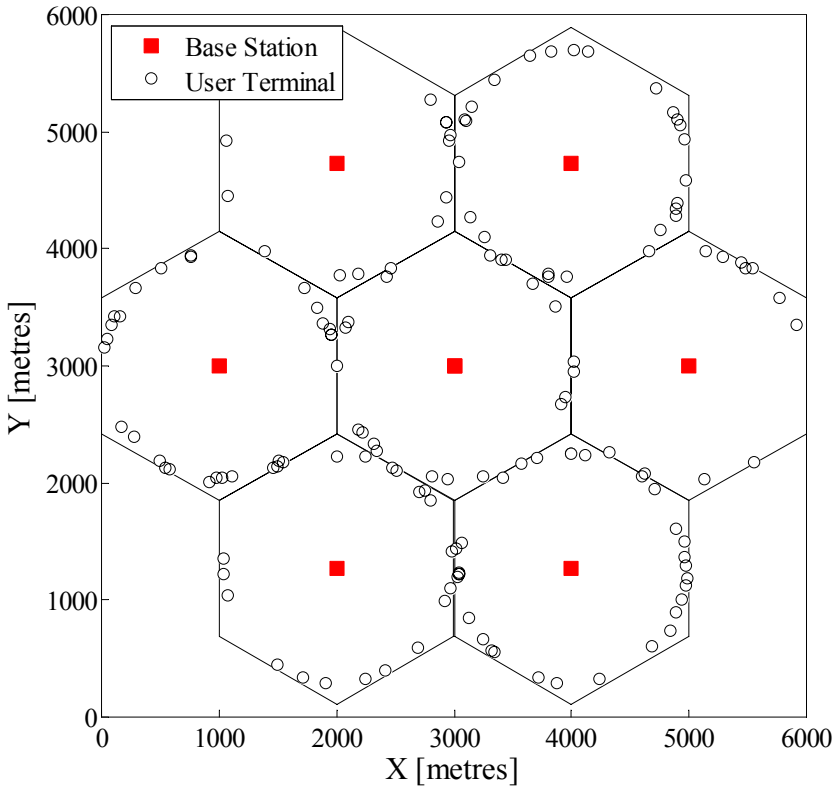

Figure J-11: Example of a network topology for 7 BSs and 150 participating UTs.

Simulations are conducted as follows. Initially nodes start from a random misalignment that is restricted to $T_{\mathrm{UL},sync}$ for user terminals and $T_{\mathrm{DL},sync}$ for base stations with an average spacing of $T_{\mathrm{UL,Sync}} + T_{\mathrm{RAC}}$ between the two groups. This way, nodes synchronise more quickly than if the misalignment is as large as the super-frame duration. Base stations parameters are set to: $\alpha_{\mathrm{BS}} = 1.20$, $\beta_{\mathrm{BS}} = 0.01$ for the coupling, and $T_{\mathrm{refr,DL}} = 25 \cdot T_{\mathrm{s}}$ where T_{s} is the duration of an OFDM symbol (see Appendix A). User terminal parameters are set to $\alpha_{\mathrm{BS}} = 1.40$, $\beta_{\mathrm{UT}} = 0.01$ and $T_{\mathrm{refr,UL}} = 15 \cdot T_{\mathrm{s}}$. Figure J-12 plots the synchronisation accuracy between user terminals and base stations versus the propagation delay between them.

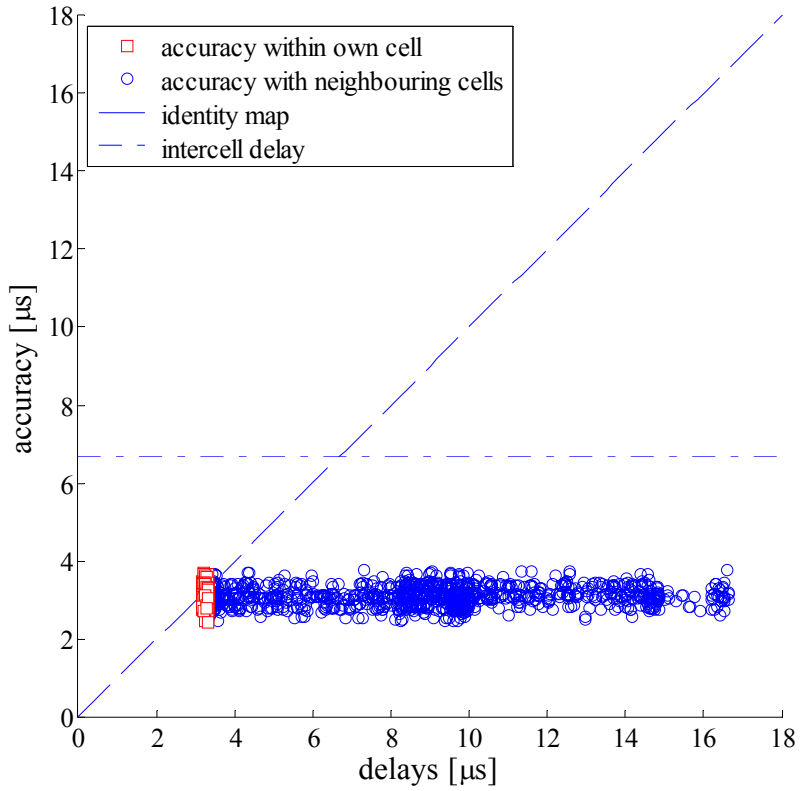

Figure J-12: Network synchronisation accuracy without compensation of propagation delays.

In Figure J-12 two accuracy groups are considered: the accuracy between the UTs and their closest base station (accuracy within own cell), and the accuracy between these users and the six surrounding base stations (accuracy within neighbouring cells) for a selection range of $d_{\text{selection}} = 950\text{m}$.

In both cases, the accuracy is much lower than the inter-BS delay, denoted intercell delay, which is constant between the central base stations and the six surrounding ones, and is equal to $2000/3\cdot10^{8} \approx 6.67\mu s$. The achieved accuracy of nodes with their own base station is centred on their respective propagation delay, as shown with the identity map. Surprisingly, the accuracy with surrounding base stations is also centred on this value. Therefore when compensating by the propagation delay, the accuracy should centre on zero.

To verify the accuracy in the case of timing advance, the timing reference instant of user terminals $\tau_{\text{UT},i}$ is advanced by the propagation delay with their own base station $\theta_{\text{UT},i,\text{BS(i)}}$, so that the new definition for the accuracy is equal to:

$$\text{accuracy}_{\text{TA}} = \left|\tau_{\text{UT},i} - \theta_{\text{UT},i,\text{BS(i)}} - \left(\tau_{\text{BS},j} - \left(T_{\text{UL,Sync}} + T_{\text{RAC}}\right)\right)\right|$$

Figure J-13 plots the synchronisation accuracy when advancing the timing references of user terminals.

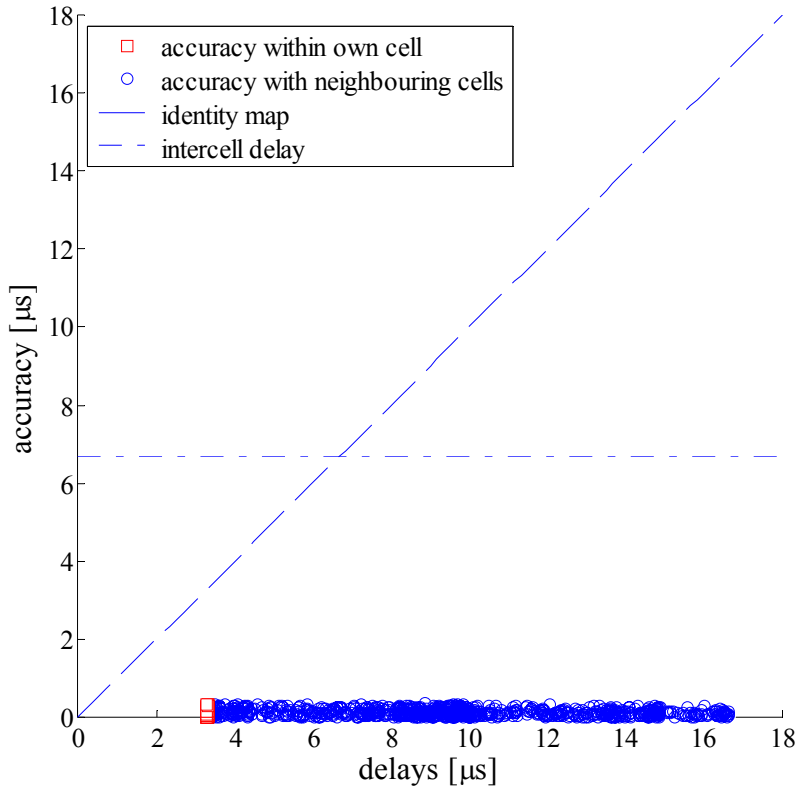

Figure J-13: Network synchronisation accuracy with compensation of propagation delays.

Compensation of the propagation delay within the own cell effectively greatly improves the accuracy between user terminals and base stations. From Figure J-13 the accuracy is always below $1\mu s$.

Another important result for the network synchronisation is the misalignment among base stations, which is measured by looking at the time difference between the firing instants of base stations:

$$\text{accuracy}_{\text{BS}} = \left|\tau_{\text{BS},i} - \tau_{\text{BS},j}\right|$$

In Figure J-14 the inter-base station accuracy is plotted as a function of the propagation delay between them for a selection range of $d_{\text{selection}} = 950\text{m}$ based on 100 generated networks. As the position of base stations is fixed and BSs are disposed in an hexagonal fashion as shown in Figure J-11, only three propagation delays are possible, namely $6.67\mu s$, $11.4\mu s$ and $13.3\mu s$, and respectively correspond to inter-BS distances 2000 m, 3409 m and 4000 m.

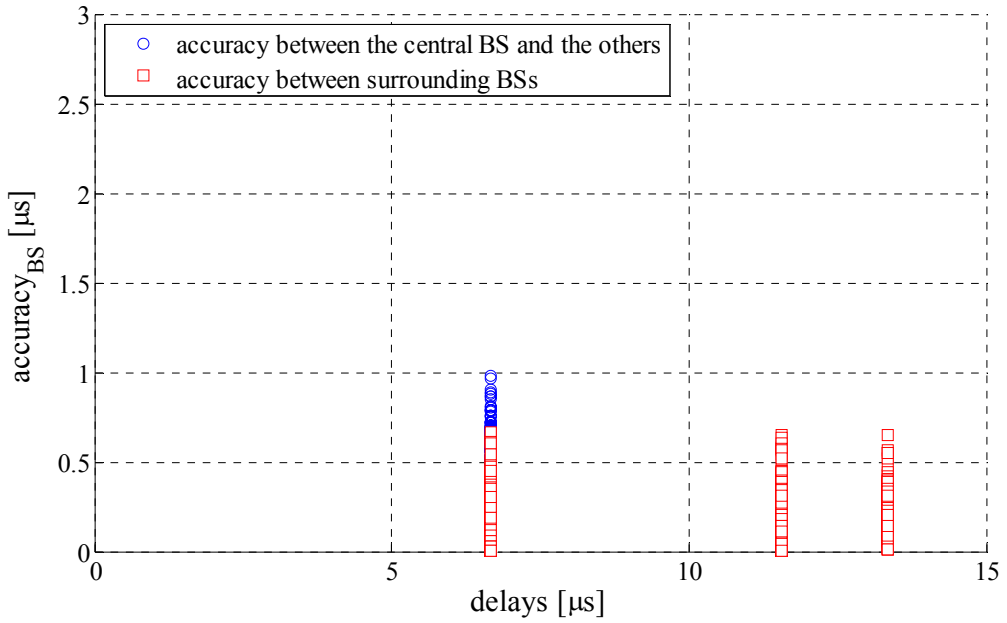

Figure J-14: Inter-Base Station Accuracy when $d_{selection}$=950 m.

From Figure J-14 the maximum misalignment between two base stations is $1\mu s$ and concerns for the central cell. Surprisingly base stations that are further apart are better aligned than the central one.

So far the achieved accuracy was examined for a selection distance of 950 metres. Figure J-15 plots the maximum misalignment between a UT and a BS with and without timing advance.

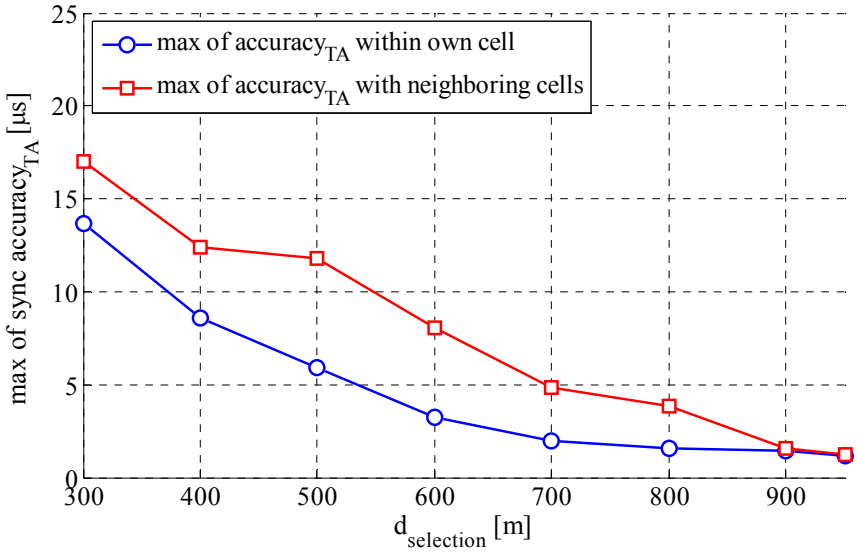

Figure J-15: Maximum misalignment as a function of the selection distance $d_{selection}$ for N_{UT}=150.

From Figure J-15 the selection range $d_{selection}$ is an important parameter for the accuracy of the network synchronisation algorithm. For a low range, the worse achieved accuracy is around $15\mu s$, and performing timing advance does not improve this, because timing references are spread too far apart. Increasing the selection range enables to reduce the spread in timing references, and forces nodes to form one group, as observed in Figure J-12. Thus relying on the cell edge users, i.e. $d_{selection} < 900\text{m}$, to perform network synchronisation presents the advantage that the synchronisation accuracy is far lower than if the selection range is low, and an accuracy in the range of $1\mu s$ can be achieved. Furthermore transmissions from UTs that are close to their BS is less likely to be heard by surrounding BSs than transmissions from cell edge UTs.

Appendix K. Pilot Design Optimization

In the chunk-based OFDMA uplink, chunk placement for each user is flexible. Users should perform the channel estimation based on their own dedicated pilots. The channel estimation for a single chunk is much demanded. This is because chunks for the specific user may not be adjacently placed along the time-frequency direction, for instance the interleaved OFDMA. Therefore, the optimization of pilot placement for a certain band, particularly a single chunk, becomes very important. The LMMSE based scheme and LS based non-ideal interpolation, e.g. linear interpolation, can be considered as the channel estimation approaches for the uplink scenario. However, the LMMSE scheme itself needs relatively high computation cost. Furthermore, as shown in Appendix B.1 the interpolation error is impossibly separated from the thermal noise for LMMSE-based scheme in the uplink situation. The corresponding optimum pilot placement highly relies on the specific system setup and channel environments. Consequently, LS-based scheme becomes the better choice. To find the optimum pilot solution for LS based non-ideal interpolation channel estimation turns to be very important and meaningful. In the following contents, we first show the optimum solution for the time-frequency direction of a single chunk. Then, the proposed solution is carefully applied in the multi-antenna systems, the performance is evaluated. Followed by, a sub-optimum pilot placement is presented and evaluated for the consecutive chunks scenario.

K.1 Optimum Pilot Placement for Single Chunk Scenario

Consider a chunk comprising n_{sub} subcarriers and n_{symb} OFDM symbols. Its frequency-domain version at the receiver is expressible as

$$y_{n,m} = \widetilde{h}_{n,m} s_{n,m} + v_{n,m}, \qquad \begin{matrix} \overline{N}_o \le n < \overline{N}_o + n_{symbl} \\ \overline{M}_o \le m < \overline{M}_o + n_{sub} \end{matrix} \tag{K-1}$$

where the subscript n, m ,denotes the time and frequency index respectively, s the information-bearing symbols with variance σ_s^2 (s can also be replaced by p , which stands for the pilot symbol), y the received symbols, v the white Gaussian noise with variance σ_v^2, $\widetilde{h}$ the channel frequency response. To clarify the presentation, we let $\overline{N}_o = \overline{M}_o = 0$ for convenience. The objective of channel estimation of single chunk is to estimate the $n_{sub} \times n_{symb}$ channel matrix $\mathbf{H} = [\widetilde{\mathbf{h}}_{\mathbf{0}}, \widetilde{\mathbf{h}}_{1}, \cdots, \widetilde{\mathbf{h}}_{n_{symb}-1}]$, in which $\widetilde{\mathbf{h}}_n = [\widetilde{h}_{n,0}, \widetilde{h}_{n,1}, \cdots, \widetilde{h}_{n,n_{sub}-1}]^T$ (^{T} for the transpose). Since the channel within a chunk should be time-frequency non-selective, two pilots for each direction are enough to track the channel coefficients via linear interpolation. (i.e., here we are mainly concerned on the FDD adaptive case)

Define a 2×2 matrix $\mathbf{Y}$, which contains the received pilot symbols of a chunk. The estimation of the corresponding channel matrix $\mathbf{H}$ is implemented a

$$\hat{\mathbf{H}} = \widetilde{\mathbf{W}} \mathbf{Y} \overline{\mathbf{W}} \tag{K-2}$$

where, $\widetilde{\mathbf{W}}$ is a $n_{sub} \times 2$ frequency filtering matrix and $\overline{\mathbf{W}}$ is a $2 \times n_{symb}$ time filtering matrix. Eqn. **(K-2)** implies the channel estimation can be carried out separately for frequency and time direction. According to the above assumptions, the channel estimation along either the frequency or time direction can be based on a same universal mathematical model as below

$$\mathbf{y} = \mathbf{D}(\mathbf{p})\widetilde{\mathbf{h}} + \mathbf{v} \tag{K-3}$$

where, $\mathbf{y}, \mathbf{p}, \widetilde{\mathbf{h}}, \mathbf{v}$ are the corresponding 2×1 vectors standing for the received pilots, transmitted pilots, channel frequency coefficients and noise respectively, $\mathbf{D}(\mathbf{a})$ is the diagonal matrix with vector $\mathbf{a}$ on the diagonal.

Since the channel is almost linearly varying within a chunk, the channel vector $\widetilde{\mathbf{h}}$ can be expressed as the following linear model

$$\widetilde{\mathbf{h}} = \underbrace{[\mathbf{g}_{K_1}^T ; \mathbf{g}_{K_2}^T]}_{\mathbf{G}} \mathbf{a} , \tag{K-4}$$

where, $\mathbf{a}=[a_0,a_1]^T$ stands for the coefficient for the linear model and $\mathbf{g_k}=[k,1]^T$ (^{T} denotes the transpose), $\{K_1, K_2 = K_1+\boldsymbol{\delta}\}$ are the pilots allocations and $\boldsymbol{\delta}$ is the corresponding pilot spacing (PS). Therefore, the least-square channel estimation can be implemented as

$$\hat{\tilde{h}}_k = \mathbf{g_k}\boldsymbol{\Gamma}^{+}\mathbf{y} \quad , \quad k \in \{0, K-1\} \tag{K-5}$$

where $\boldsymbol{\Gamma}=\mathbf{D(p)G}$ ($^+$ denotes the pseudo inverse), $K=n_{symb}$ for the time direction or $K=n_{sub}$ for the frequency direction. So that, the average mean-square-error (MSE) of the channel estimate can be calculated as follows

$$MSE = \frac{1}{K}\sum_{k=0}^{K-1}\left\|\hat{\tilde{h}}_k - \tilde{h}_k\right\|^2 . \tag{K-6}$$

To measure the exact the estimation error, especially the interpolation error, we need to know the actual channel. Unfortunately, finding the actual model is really a very big challenge. Therefore, the investigation here is focused on the difference between the linear model and some well-recognized near-actual channel model.

K.1.1 MSE Performance analysis

Along frequency direction, the estimation error is analyzed by comparing the linear model with the frequency response of an FIR channel. The later one is a well-recognized near-actual channel model, and has been employed for most of analytical analysis in wireless communications. Based on this idea, the channel coefficient $\tilde{h}_k$ (along frequency direction) can be expressed as the following form

$$\tilde{h}_k = \mathbf{f}_k^T\mathbf{h}, \tag{K-7}$$

where $\mathbf{f}_k=[1,\exp(-j2\pi k/M),\cdots,\exp(-j2\pi(L-1)/M)]^T$ is Fourier transfer vector, M is the DFT size and $\mathbf{h}=[h_0,h_1,\cdots,h_{L-1}]^T$ is the channel impulse response (L the upper bound of the channel order). So, the MSE in (K-6) can be rewritten as

$$MSE = \frac{1}{K}\sum_{k=0}^{K-1}\left(\tilde{\boldsymbol{\alpha}}_k^H\mathbf{R}_{hh}\tilde{\boldsymbol{\alpha}}_k + \sigma_v^2\left\|\boldsymbol{\beta}_k\right\|^2\right), \tag{K-8}$$

where, $\tilde{\boldsymbol{\alpha}}_k = \mathbf{g}_k^T\mathbf{G}^{+}\mathbf{F}-\mathbf{f}_k^T$, $\boldsymbol{\beta}_k=\mathbf{g_k}^T\boldsymbol{\Gamma}^{+}$, $\mathbf{R}_{hh}=E\{\mathbf{hh^H}\}$ (^{H} denotes the Hermitian) and $\mathbf{F}=[\mathbf{f}_{K_1}^T;\mathbf{f}_{K_2}^T]$
Hence, the channel estimator error has two parts, i.e., the interpolation error (the first term t the right hand of (K-8) and the noise-induced error (the second term at the right hand of (K-8)).

Along the time direction, Jakes' model can offer an excellent description for the channel time-selectivity. However, it is a continuous function in the Doppler domain, which can not be straightforwardly employed for our analysis. Therefore we choose the Fourier basis expansion model (FBEM) for analyzing the issues along time direction.
Consider a Doppler spectrum consisting of $(2Q+1)$ samples. Denote $f_{\max}$ to be the maximum Doppler shift normalized by the OFDM duration. The channel coefficient $\tilde{h}_k$ (along time direction) can be expressed as [Ma07]

$$\tilde{h}_k = \mathbf{b}_\mathbf{k}^T\boldsymbol{\gamma} \ , \tag{K-9}$$

where, the $(2Q+1)\times 1$ vector $\boldsymbol{\gamma}$ is the Doppler component, and $\mathbf{b}_\mathbf{k}^T$ is a $(2Q+1)\times 1$ vector, whose q th element is given by $b_{k,q}=\exp(j2\pi k(q-Q)/N)$, where N is a sufficient large value such that $\frac{Nf_{\max}}{Q}\approx\left\lceil\frac{Nf_{\max}}{Q}\right\rceil=1$. It is clear that the $\mathbf{b}_\mathbf{k}^T$ is an IDFT vector. Similar to the analysis for the frequency direction, we can obtain the MSE of estimation error along time direction as below

$$MSE = \frac{1}{K}\sum_{k=0}^{K-1}\left(\bar{\boldsymbol{\alpha}}_k^H\mathbf{R}_{\gamma\gamma}\bar{\boldsymbol{\alpha}}_k + \sigma_v^2\left\|\boldsymbol{\beta}_k\right\|^2\right), \tag{K-10}$$

where, $\bar{\boldsymbol{\alpha}}_k = \mathbf{g}_k^T\mathbf{G}^{+}\mathbf{B}-\mathbf{b}_k^T$, $\mathbf{R}_{\gamma\gamma}=E\{\boldsymbol{\gamma}\boldsymbol{\gamma}^\mathbf{H}\}$ and $\mathbf{B}=[\mathbf{b}_{K_1}^T;\mathbf{b}_{K_2}^T]$

It is clear that estimation error along time direction (K-10) is also composed by two terms, i.e., the interpolation error and noise-induced error. Compared to the frequency direction MSE (K-8), the only

difference is the term of interpolation error, which actually is caused by the linear model and two different near-actual channel models.

K.1.2 Impact on the optimum pilot placement

The object of optimum pilot placement is to minimize the channel estimation error. It is related to find the optimum pilot location K_1^{opt} (or K_2^{opt}) as well as the optimum PS ($\boldsymbol{\delta}^{opt}$). This optimization problem can be solved by studying the partial derivative of MSE with respect to the variables K_1 or $\boldsymbol{\delta}$. However the state-of-the –art approaches were only focused on minimizing the noise-induced error. The result was that the pilots should be placed at ends of a chunk (e.g., [Ma07]). For example, two pilots along frequency direction should be placed on $\{0, n_{sub}-1\}$ th sub-carriers. To see the impact of interpolation error, we need investigate the pilot placement of minimizing the interpolation error.

Along frequency direction, the channel matrix $\mathbf{R}_{\mathbf{hh}}$ can be assumed to be a diagonal matrix, i.e., $\mathbf{R}_{\mathbf{hh}} = \mathrm{diag}\{\boldsymbol{\sigma}_0^2, \boldsymbol{\sigma}_1^2, ..., \boldsymbol{\sigma}_{L-1}^2\}$. This is a reasonable assumption when the wireless fading channel is rich in scattering [Ohno04]. So that, by studying the partial derivative of the term of interpolation error (= MSE_i) with respect to the K_1, the optimum pilot location based on the interpolation error is shown as below

$$K_1^{opt} = \frac{K-1-\boldsymbol{\delta}}{2}. \tag{K-11}$$

The above equation shows the K_1^{opt} is a function of the PS $\boldsymbol{\delta}$. Analogously, by taking the above result and investigating the partial derivative of MSE_i with respect to $\boldsymbol{\delta}$, optimum PS can be obtained by

$$\boldsymbol{\delta}^{opt} = \sqrt{\frac{K^2-1}{3}} \approx \frac{K}{\sqrt{3}}. \tag{K-12}$$

The approximation in above equation is due to $K^2 >> 1$ in the practical systems. However, $\boldsymbol{\delta}^{opt}$ is usually not an integer, so we can use the round function to offer the near-optimum setup, i.e., $\boldsymbol{\delta} = \mathrm{Round}\{\boldsymbol{\delta}^{opt}\}$. Obviously, from (K-11) and (K-12), the optimum pilot placement set is actually regardless of the channel information, and just decided by the chunk size.

Along time direction, the channel time correlation matrix $\mathbf{R}_{\gamma\gamma}$ can be approximate to a diagonal matrix as well, i.e., $\mathbf{R}_{\gamma\gamma} = diag\{o_o^2, o_1^2, ..., o_{2Q}^2\}$. This is also a reasonable assumption while the channel is rich in scattering. In this case, the difference between the analysis of frequency and time direction is the matrices $\mathbf{B}$ and $\mathbf{F}$. Interestingly, $\mathbf{F}$ is formed by the DFT series and $\mathbf{B}$ is formed by IDFT series. It can be easily justified that this difference can not change the convexity of the MSE performance. Therefore the optimum set derived for the frequency direction is also valid for minimizing the interpolation error along time direction.

The analysis has shown that the pilot placement optimized for the interpolation error is not the optimum design for the noise-induced error. In the large-SNR range (i.e., noise impact is negligible), the time-frequency optimum pilot placement should be in line with the proposal above. However, while the noise becomes the dominate impact for instance in the small-SNR range, the optimum pilot should minimize the noise impact. Therefore, the optimum pilot placement can be different with respect to different SNR setup. Moreover, the optimum pilot placement is also related to the channel selectivity. The channel frequency selectivity is related to the ratio $\frac{L}{M}$, which is around 1/8 or 1/16 for the practical system. The channel time selectivity is related to the ratio $\frac{2Q+1}{N}$, which is around 1/100 for the typical vehicle communication (e.g., FDD adaptive case, C2 channel, 50-70 km/h velocity). Therefore, the impact of interpolation error along the time-direction may not be as significant as that along the frequency direction. Based on the above concolusion, the performance evaluation for WINNER reference adaptive FDD structure under the SISO case has been displayed in the following section, i.e., section K.1.3. It clearly shows that, the pilot placement solutions with PS=11 along time direction and PS=5 along frequency direction can be regarded as the best placement solution within a chunk for the specific practical communication scenario. These results are well matched to the corresponding theoreticall analysis shown above.

K.1.3 Peformance evaluation of the single chunk scenario (SISO)

The MSE and BER performance related to the frequency direction have first been evaluated in Figure K-1. It shows a good match to the corresponding analysis in section K.1.2. For example, in the high SNR range (i.e., $\mathrm{SNR} > 16\mathrm{dB}$), where the interpolation error dominates the performance, the optimum pilot spacing (PS) solution is the case of PS=5, which is $\mathrm{Round}\left\{\frac{1}{\sqrt{3}}\right\}$ of the chunk size; On the other hand, in the small SNR range (i.e., $\mathrm{SNR} < 10\mathrm{dB}$), the solution with the case of PS=7 shows the best performance, which means two pilots should be placed on the both edges of each chunk. However, even in the small and moderate SNR range ((i.e. $\mathrm{SNR} \le 16\mathrm{dB}$), the performance of the case of PS=5 is very close the optimum one (e.g., PS=7) in terms of both MSE and BER. So, it is reasonable to conclude that the pilot placement with the case of PS=5 is the best one along frequency direction for the FDD cases.

Next, we examine the proposed pilot placement along the time direction. The pilot placement along frequency direction is set to the above best one, i.e., $K_1 = 1, \boldsymbol{\delta} = 5$. Figure K-2 a) illustrates the interpolation error with respect to various PS along time direction. The first pilot location is according to (K-11) since it is a function of PS. It is observed that, in the case of low velocity, e.g. speed is 20 km/h, the interpolation error is almost identity for PS setups. This is because the channel is almost time-invariant within a chunk. Therefore, the partial derivative of interpolation error with respect to $\boldsymbol{\delta}$ is lways close to zero. In this case, the optimum PS can be arbitrary value. On the other hand, the performance difference for various PS becomes considerable with increasing the velocity. For example, at the velocity of 120-300 km/h, the channel can be considerably time-selective within a chunk. According to the analysis, the optimum PS should be $\boldsymbol{\delta} = \mathrm{Round}\{12\} = 7$, this is confirmed by the simulation. The above explanation can also be valid for explaining the phenomena in (b), where the noise is considered as well (the SNR is set to 16 dB). In the velocity range from 20km/h – 70km/h, we can observe the case of PS=11 is the optimum one. With the velocity increases, the optimum PS stars to vary and finally becomes to 7 for the large velocity >250 km/h. In practical systems, when the velocity is large enough, we should consider the FDD non-adaptive case, i.e., one more pilot is inserted to track the channel variance. However, even for the non-adaptive case, the above conclusion is still valid when considering the linear interpolation via two pilots. Therefore, based on this, we can conclude, for the practical systems the optimum PS should be targeted on minimizing the noise impact. The case of PS=11 is the best one for FDD adaptive case.

The corresponding BER performance is shown in Figure K-3. It also shows that PS=11 is the optimum PS for the velocity range of 20-70 km/h. Even for the range of 120km/h to 170 km/h, it still provides the very close performance to the corresponding optimum ones. This proves the above conclusion again.
Generally, based on the above analysis, we can regard the pilot placement solutions with PS=11 along time direction and PS=5 along frequency direction can be regarded as the best placement solution along within a chunk for this specific communication scenario, i.e., FDD adaptive case.

Since the difference between the proposed scheme and WINNER reference FDD scheme is along frequency direction ((i.e., $K_1 = 1, \boldsymbol{\delta} = 5$) for proposed scheme and $K_1 = 1, \boldsymbol{\delta} = 4$ for WINNER). Therefore, in Figure K-4 and Figure K-5, we compare their performance along frequency direction in terms of MSE and BER respectively. The estimation method is actually LMMSE-based approach (i.e., wiener filter). It shows even with the LMMSE-based scheme, the proposed pilot placement still outperforms the WINNER reference scheme. There is around 1 dB BER performance gain at large SNR range ($\mathrm{SNR} \ge 20$ dB).

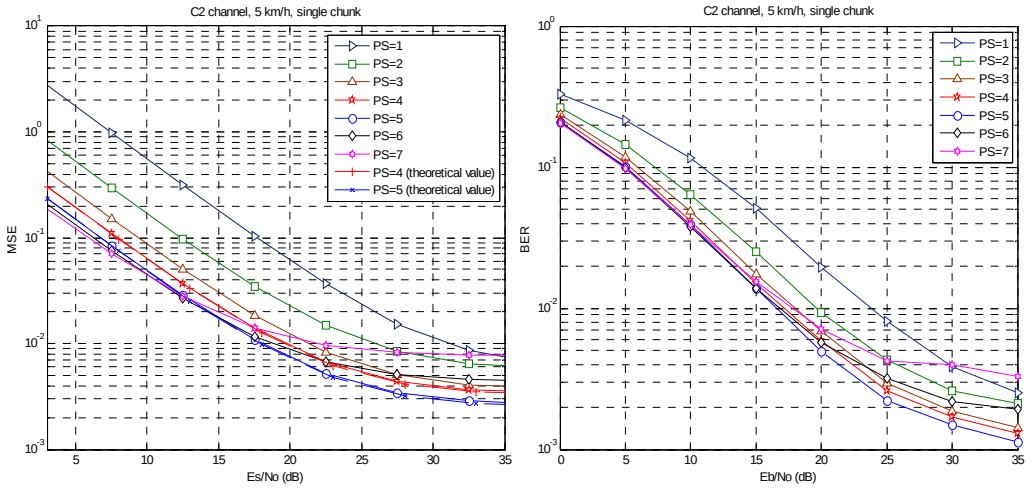

Figure K-1 : Optimum Pilot Spacing (PS) along frequency direction (a) MSE performance (b) BER performance

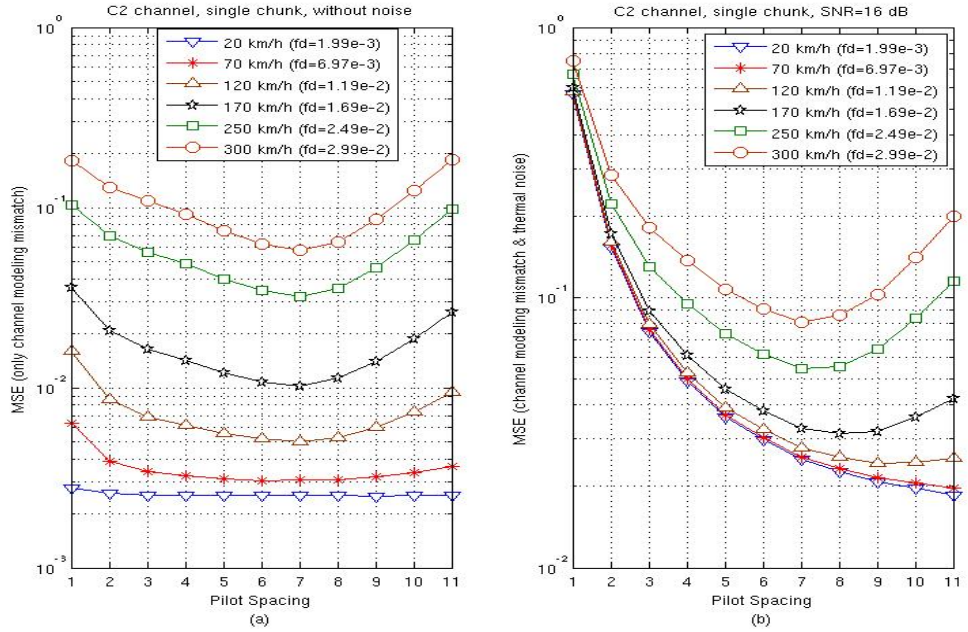

Figure K-2 : MSE performance along time direction (a) interpolation error (b) interpolation error and noise

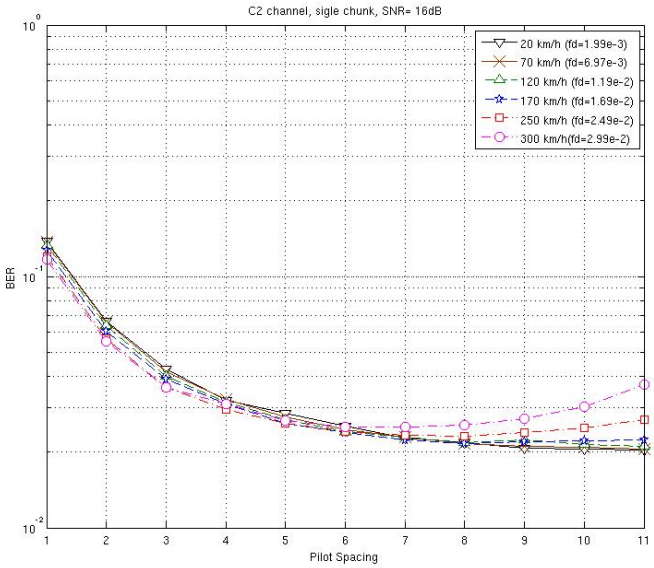

Figure K-3: BER performance along time direction

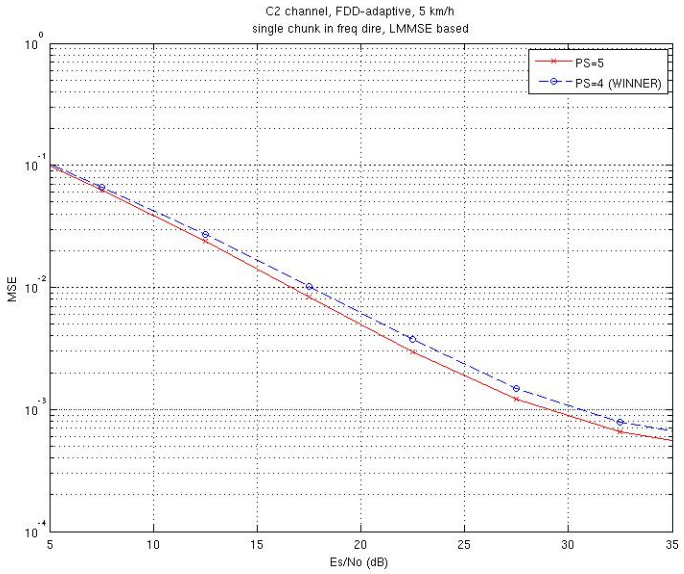

Figure K-4: MSE performance for LMMSE-based scheme

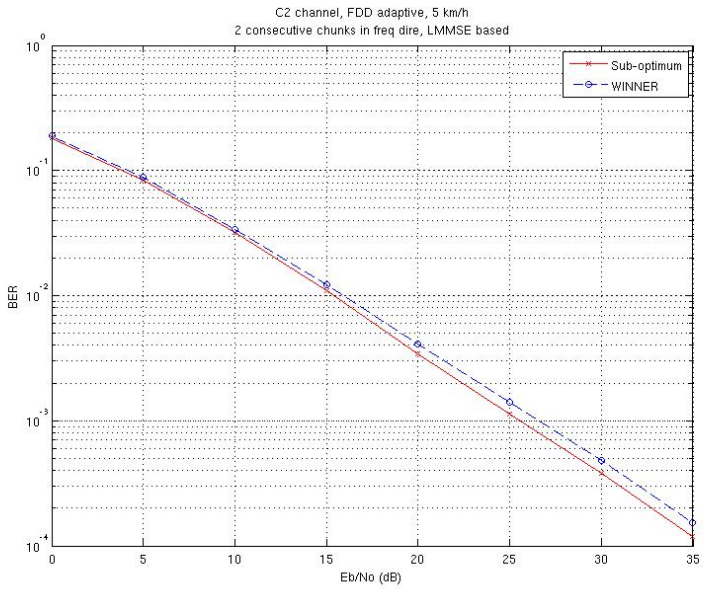

Figure K-5: BER performance for LMMSE-based scheme

K.1.4 Pilot placement solutions for Multiple-transmitters scenario

In the uplink communications, the sender is usually equipped with up to two transmit-antennas. Since the channel estimation can be carried out individually for each receive antenna, we can consider the pilot placement for the system with two transmit-antennas and one receive antenna. In this scenario, the pilot symbols should be placed to avoid the inter-antenna interference. This is usually realized by sending zero symbols on the corresponding tones.

As an example of FDD adaptive case shown in Figure K-6, one antenna sends the zero symbols on the tones, where the other sends the pilot symbols. This can introduce the pilot orthogonality between two antennas, but loss the optimality for the single-chunk scenario. In this scenario, we consider two pilot placement schemes as depicted in Figure K-6 (b-1) and (b-2). The basic idea is to change the pilot spacing either along the frequency direction (b-1) or along the time direction (b-2). For the consideration of fairness, the pilot pattern for two antennas should be symmetric.

To evaluate the two schemes, their BER performance with respect to different velocities is plotted in Figure K-7. The Alamouti scheme [Ala98] is employed to simplify the receiver architecture. Compared to the best solution of SISO case (Figure K-6 (a)), the pilot placement shown in Figure K-6 (b-1) (here called "FreqAdjust") adjusts the frequency direction PS from the case of PS=5 to the case of PS=4, and keeps the time direction PS unchanged, i.e., the case of PS=11 Correspondingly, the pilot placement shown Figure K-6 (b-2) (here called "TimeAdjust") only adjusts the time direction PS from the case PS=11 to PS=10 for each antenna. The objective of this evaluation is to find which kind of pilot placement is the best trade-off between the pilot optimality and channel identifiability. Generally, the velocity only has slight impact on the performance in the case of the same pilot placement scheme. However, for the same velocity, the "TimeAdjust" scheme always outperforms the "FreqAdjust" scheme. There is up to 2 dB improvement achieved by the "TimeAdjust" scheme in the large SNR range (e.g., SNR $\geq$ 23 dB). This indicates that the performance is affected by channel frequency selectivity more than the time selectivity in practice. Therefore, the pilot placement design for the multiple transmit-antennas scenario should pay more attention to the frequency direction issues. And the scheme (b-2) is the better choice for this case.

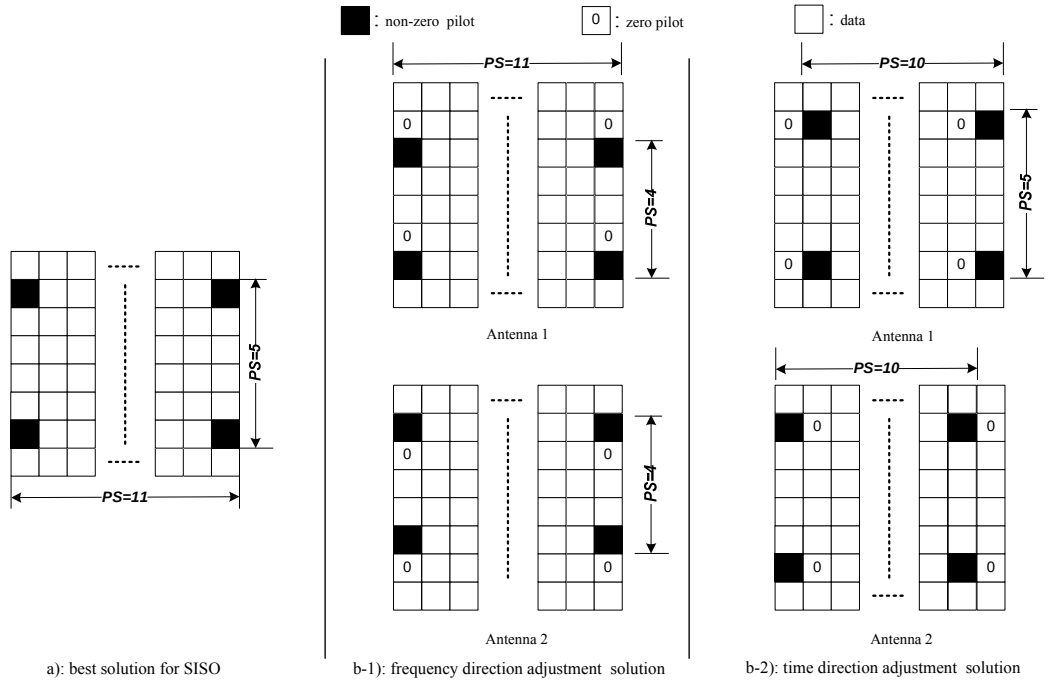

Figure K-6: Pilot placements for multiple transmitter scenario: a) best placement for SISO case; b-1) frequency direction adjustment scheme; b-2) Time direction adjustment scheme

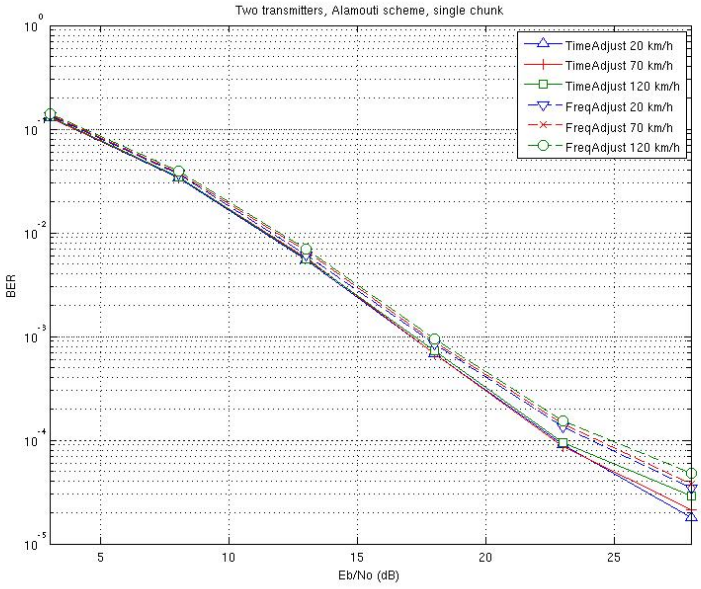

Figure K-7: BER performance multiple transmitters scenario

K.2 Sub-Optimum Pilot Placement for Multiple Consecutive Scenario

The chunk placement for each user can be adjacent or not. When some consecutive chunks are allocated to one user, more pilots are available for channel estimation. In another words, the pilots inside the neighboring chunk can assist the channel estimation on the desired chunk with higher order interpolation method. This scenario is here defined as consecutive chunks scenario. In [Ma07] , an optimum approach has been proposed while adjacent chunks are placed along time direction. In this section, we only consider the scenario that adjacent chunks are placed along frequency. For this scenario, the current WINNER structure (i.e., with equal-spaced pilot placement, shown in Figure K-8 (a)) can only provide

the optimum performance based on the impact of the noise. Here, we proposed a sub-optimum scheme, which can reduce both impact of the noise and the interpolation error. Here, the objective is to investigate the pilot placement in the presence of interpolation error.

As described previously, the estimation error (including interpolation error and noise) is not white over sub-carriers. Using the WINNER structure, the estimation error on edge sub-carriers can be considerably larger than that on the other sub-carriers among non-zero pilots when employing the polynomial interpolation schemes. Such loss can seriously affect the overall performance, and so is called edge effect. Fortunately, the edge effect can be significantly mitigated while a pilot is placed on an edge sub-carrier. In contrast with WINNER structure, the proposed structure in Figure K-8 (b) requires one of the two pilots placed at the edge of each chunk. Meanwhile, a total of three pilots are needed in the last chunk; two of them are placed on the edge sub-carriers. Based on this basic structure, the channel estimation carried out for each individual chunk can be the second order interpolation over three pilots. Then the objective becomes where the optimum location for the rest pilot within each chunk is, in another words, if the equal-spaced placement used in WINNER structure is still optimum for minimizing the interpolation error.

Figure K-8 (b) shows that the N_c adjacent chunks are obviously divided in two parts. Part one consists of the first $N_c - 1$ chunks, where each chunk has two pilots. When the channel estimation is performed, one pilot in next chunk is used to assist. The pilot from neighboring chunk is allocated just next to the edge of objective chunk, this helps mitigate the edge effect, meanwhile hold the channel among these three pilots still close to be linear, which can further benefit to improve the estimation accuracy. Part two is N_c th chuck consisting of three pilots. In general, the three pilots used for channel estimation of each chunk are placed on $\{K_1 = 0, K_2 = K_1 + \zeta, K_3\}$, where $\{K_3 = n_{sub}\}$ for part one and $\{K_3 = n_{sub} - 1\}$ for part two).

Based on the second order interpolation and FIR frequency channel modeling, the average MSE along frequency direction over all the consecutive chunks can be described as below

$$MSE = \frac{N_c - 1}{N_c n_{sub}} \sum_{k=0}^{n_{sub}-1} \left(\tilde{\boldsymbol{\alpha}}_k^{1\,H} \mathbf{R}_{hh} \tilde{\boldsymbol{\alpha}}_k^1 + \sigma_v^2 \left\| \boldsymbol{\beta}_k^1 \right\|^2 \right) + \frac{1}{N_c n_{sub}} \sum_{k=0}^{n_{sub}-1} \left(\tilde{\boldsymbol{\alpha}}_k^{2\,H} \mathbf{R}_{hh} \tilde{\boldsymbol{\alpha}}_k^2 + \sigma_v^2 \left\| \boldsymbol{\beta}_k^2 \right\|^2 \right), \qquad \text{(K-13)}$$

where, the subscript {1,2} on the right up of $\boldsymbol{\alpha}, \boldsymbol{\beta}$ is the index of different part, i.e., part one or part two; $\boldsymbol{\alpha}, \boldsymbol{\beta}$ are the corresponding ones in (K-8) with replaced by the second-order channel coefficients and three pilots. To find the optimum PS, the partial derivative of MSE of the part of interpolation error (i.e., MSE_i) with respect to various ζ is studied and the following conclusion results:

$$\zeta^{opt} = \text{Round}\{\frac{K_3}{2}\} \qquad \text{(K-14)}$$

This result indicates that the equal-spaced pilot placement is also optimized in terms of the interpolation error. With this PS, the proposed structure can be reasonably regarded as a sub-optimum solution for this scenario.

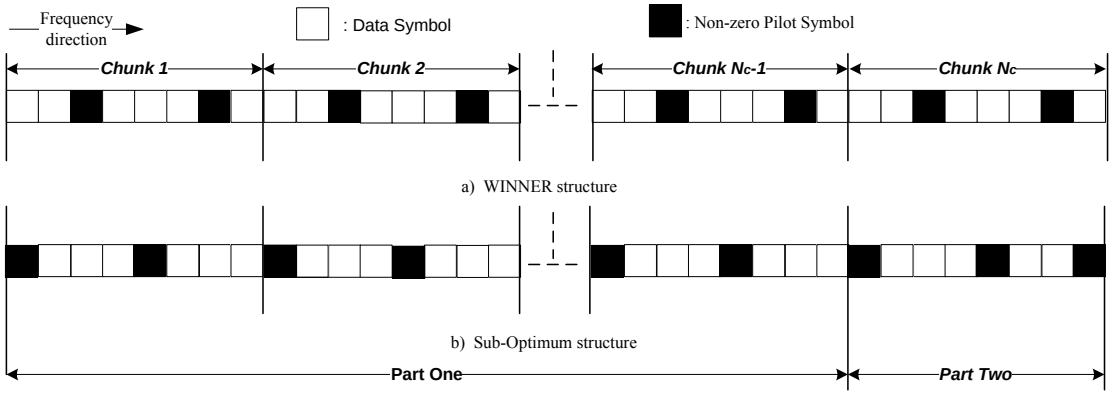

Figure K-8: Sub-optimum placement for consecutive chunks scenario along frequency direction

The BER performance of the sub-optimum pilot placement is evaluated in Figure K-9. The WINNER reference adaptive FDD structure is considered for comparison. The second-order interpolations as well as the linear interpolation via 2 (and 3) pilots are employed. It shows the sub-optimum scheme always

outperforms the WINNER structure in the case of same interpolation scheme. The second order interpolation significantly outperforms the linear interpolation in larger SNR range (SNR>15 dB), but a bit worse in small SNR range. This is because linear interpolation is good at de-noising but the second-order interpolation is more robust to the accuracy of the interpolation error. However, the performance loss in small SNR range is so small that the proposed placement with second order interpolation can still be regarded as the best choice in this scenario.

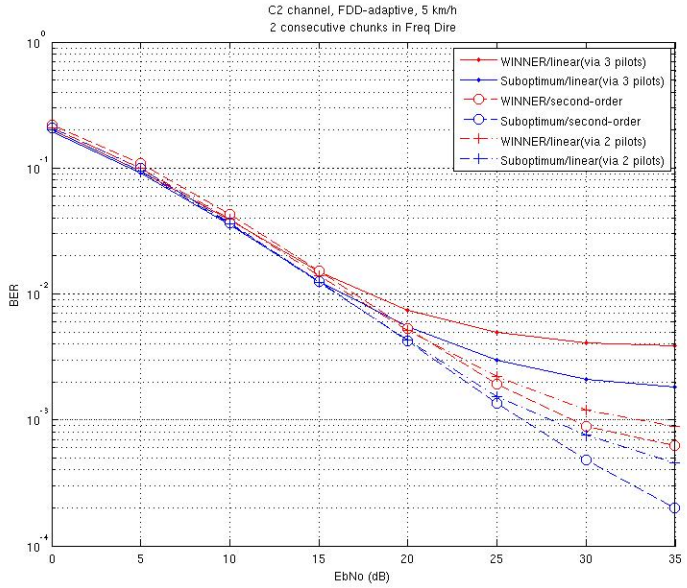

Figure K-9: BER comparison between WINNER structure and sub-optimum structure

K.3 Capacity-Achieving Pilot Design

As shown in Appendix B, an appropriate channel estimator model can describe estimator performance with only 2 parameters, i.e.,

- the estimations error and
- the overhead in terms of transmit power dedicated to pilot symbols. This overhead is also known as pilot insertion loss.

Such model enables analytical optimization of the pilot boost, pilot distance and the number of transmit antennas in MIMO case. As parameter to maximize we choose system capacity due to the fact that it inherently takes into account both spectral efficiency and power loss. Optimizing pilot parameters with respect to, e.g., SNR loss (which does not inherently take into account spectral efficiency loss) would lead to trivial solutions in which pilot distance is one, i.e., whole chunks are dedicated to pilot and no data is transmitted.

In the following two subsections the above mentioned analysis is performed for both SISO and MIMO case.

K.3.1 SISO System

The ergodic SISO channel capacity that includes channel estimation and pilot insertion losses in the case when channel is not known at the transmitter can be lower bounded by

$$C \geq (1-\Omega_P) E\left[\log_2\left(1+\left|H_{n,\ell}\right|^2 \gamma/\Delta\gamma\right)\right] \qquad \text{(K.15)}$$

where the expectation is taken over the CTF $H_{n,\ell}$, and $\Delta\gamma$ is given by (2-10) or **(B-8)**.

K.3.1.1 Pilot Boost

The effect of a pilot boost is twofold: first, the estimation error decreases; second, the power dedicated to pilot symbols increases. So, there clearly exists an optimum pilot boost S_p that minimizes $\Delta\gamma$ and

consequently maximizes capacity C. For the parameterized estimation error model, the optimum pilot boost is obtained by differentiating $\Delta\gamma$ from **(B-8)** with respect to S_p and setting the result to zero

$$S_{\mathrm{p,opt}} = \sqrt{\frac{1-\Omega_p}{\Omega_p G_n}} \tag{K.16}$$

Inserting $S_{\mathrm{p,opt}}$ into **(B-8)** yields the minimum SNR penalty for a certain estimator and pilot grid

$$\Delta\gamma_{\min} = \left(\sqrt{1-\Omega_P} + \sqrt{\Omega_P / G_n}\right)^2 + \gamma_0 \sigma_i^2 \tag{K.17}$$

The capacity in (K.15) only depends on the pilot boost S_p through the SNR penalty $\Delta\gamma$. Hence, for a given pilot overhead Ω_p, the optimum pilot boost $S_{\mathrm{p,opt}}$ maximizes (K.15). Maximization subject to Ω_p yields the overall maximum capacity

$$C_{\max} \geq \max_{\Omega_P} \left\{ (1-\Omega_P) E\left[\log_2\left(1 + \left|H_{n,\ell}\right|^2 \gamma / \Delta\gamma_{\min}\right)\right]\right\} \tag{K.18}$$

Unfortunately, it is far from obvious which combination of Ω_p, G_n and σ_i^2 maximizes (K.18), since both G_n and σ_i^2 are dependent on Ω_p. By approximating the estimator by an ideal low-pass interpolation filter (LPIF), as done in the following subsection, a relation between these parameters is established, and the maximum capacity is derived in closed form. In the general case where a closed form solution is difficult, a semianalytical procedure is suggested.

K.3.1.2 Ideal Lowpass interpolation filter (LPIF)

Applied to the parametrazied MSE analysis performed here, an ideal LPIF has some interesting properties. Provided that all CIR components pass through the filter undistorted, i.e. $\tau_{\mathrm{w}} \geq \tau_{\max}$, and $f_{\mathrm{D,w}} \geq f_{\mathrm{D,max}}$, the estimator gain for the ideal LPIF is independent of the channel model as well as the SNR. Moreover, the interpolation error diminishes, $\overline{\sigma}_{\mathrm{i}}^2 = 0$; so the estimator gain becomes $G_{\mathrm{est}} = G_{\mathrm{n}}$, being determined by the fraction of the AWGN suppressed by the filter. This is illustrated in Figure K-10 where the filter transfer function of an ideal LPIF is drawn in the time domain. The estimator gain per channel estimation dimension is found to be equivalent to the oversampling factor β_{f} and β_{t}, defined in (4.1). Since for 2×1 D-PACE the two FIR filters are independent, the total estimator gain becomes $G_{\mathrm{est}} = \beta_{\mathrm{f}} \beta_{\mathrm{t}}$.

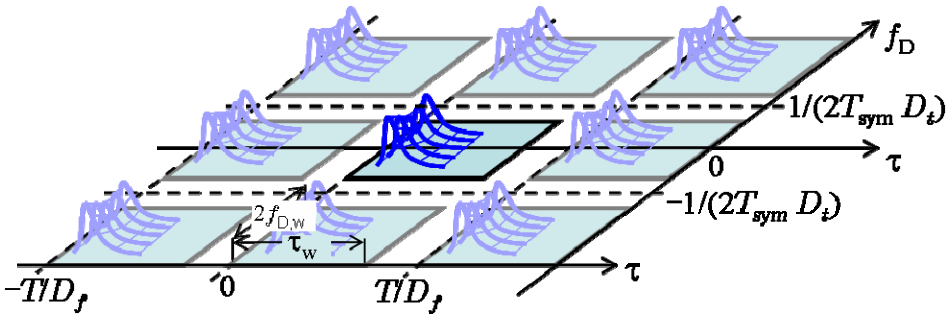

Figure K-10 Filter transfer function of an ideal 2D low-pass interpolation filter.

The oversampling factors are related to the pilot spacing by (4.1), which in turn determine the pilot overhead $\Omega_{\mathrm{p}} = 1/(D_{\mathrm{f}} D_{\mathrm{t}})$. Now the optimum pilot boost of (K.16) for an ideal LPIF can be conveniently expressed as

$$S_{\mathrm{p,opt}} = \sqrt{\frac{1-\Omega_p}{\Omega_p \beta_f \beta_t}} = c_w \frac{\sqrt{1-\Omega_p}}{\Omega_p} \tag{K.19}$$

where $c_w = \sqrt{2\tau_w f_{D,w} T_{sym}/T}$ and the involved parameters are defined in Section 4.2. We note that $S_{\mathrm{p,opt}}$ is dependent only on OFDM parameters, as well as the two filter specific parameters τ_{w} and $f_{\mathrm{D,w}}$. Hence, the dependency on the channel has disappeared. Although this is only valid for interpolation of infinite sequences, $G_{\mathrm{est}} = \beta_{\mathrm{f}}\beta_{\mathrm{t}}$ is a reasonable approximation for long filters in the low SNR regime, where the noise error $\bar{\sigma}_{\mathrm{n}}^2$ dominates the interpolation error $\bar{\sigma}_{\mathrm{i}}^2$.

The estimator gain $G_n = \Omega_p / c_w^2$ is found to be proportional to Ω_p. Inserting G_n into (K.17) and after some algebraic transformations the minimum SNR penalty yields $\Delta\gamma_{\min} = \left(\sqrt{1-\Omega_{P,\min}} + \sqrt{\Omega_{P,\min}}\right)^2$. This means that $\Delta\gamma_{\min}$ is minimized by the maximum pilot overhead Ω_p, i.e. all transmitted symbols are dedicated to pilots. However, since in this case no data is transmitted the capacity in (K.18) approaches zero. In fact, (K.18) is maximized by selecting the smallest pilot overhead $\Omega_{p,\min}$ which still satisfies the sampling theorem

$$C_{\max} \geq (1-\Omega_{P,\min}) E\left[\log_2\left(1 + \left|H_{n,\ell}\right|^2 \gamma \Big/ \left(\sqrt{1-\Omega_{P,\min}} + c_w\right)^2\right)\right] \quad \text{(K.20)}$$

where $\Omega_{p,\min} = 1/(D_{f,\max} D_{t,\max})$ is attained by the maximum pilot spacing which satisfy sampling theorem (cf. (4.1)), $D_{f,\max} = \left\lfloor \frac{T}{\tau_W} \right\rfloor$ and $D_{t,\max} = \left\lfloor \frac{1}{2 f_{D,w} T_{sym}} \right\rfloor$, where $\lfloor x \rfloor$ is the largest integer equal or smaller than x. To prove (K.20) it can be readily checked that $C_{\max}$ is a monotonically decreasing function with respect to Ω_p, with the global maximum at $\Omega_p = 0$. Hence, (K.20) is maximized by $\Omega_{p,\min}$, since $\Delta\gamma_{\min}$ is only valid for pilot grids which satisfy the sampling theorem in (4.1).

If rounding effects due to integer pilot spacing are ignored, we may write $D_{f,\max} D_{t,\max} \approx 1/c_w^2$. Now the effects of channel estimation errors for PACE are completely described by $\Omega_{p,\min} \approx c_w$. Interestingly, the estimator gain now approaches unity, $G_n = 1$. Moreover, as for virtually all existing OFDM systems $\Omega_{p,\min} << 1$, the SNR penalty becomes

$$\Delta\gamma_{\min} = \left(\sqrt{1-\Omega_{P,\min}} + \sqrt{\Omega_{P,\min}}\right)^2 \approx 1 + 2\sqrt{\Omega_{P,\min}},$$

and (K.20) can be approximated by

$$C_{\max} \approx (1-\Omega_{P,\min}) E\left[\log_2\left(1 + \left|H_{n,\ell}\right|^2 \gamma \Big/ \left(1 + 2\sqrt{\Omega_{P,\min}}\right)\right)\right] \quad \text{(K.21)}$$

However, the condition $\Omega_{p,\min} \approx c_w$ may be difficult to realize in practice, and we need to resort to a semi-analytical procedure presented in the next subsection.

K.3.1.3 Optimum Pilot Grid Design for PACE SISO OFDM

It was shown in previous section that for an ideal LPIF an unique optimum pilot grid exists which maximizes channel capacity. For realizable filters, we propose the following three-step procedure to assemble the optimum pilot grid:

a. Specify the filter parameters τ_W and $f_{D,w}$.

b. Choose maximum possible pilot spacings and the estimator dimensions M_f and M_t, which maintain a certain interpolation error σ_i^2. This determines the minimum pilot overhead $\Omega_{p,\min}$, and the estimator gain $G_n = 1/\mathbf{w}^H\mathbf{w}$.

c. Calculate the optimum pilot boost $S_{\mathrm{p,opt}}$ using (K.19).

Regarding a.; in a well designed OFDM system the maximum channel delay τ_W should not exceed the cyclic prefix (CP). Hence it is reasonable to assume $\tau_W = T_{CP}$. Furthermore, $f_{D,w}$ is set according to the maximum Doppler frequency expected in a certain propagation scenario, e.g. urban, rural or indoor. The condition in b. is imposed to keep σ_i^2 sufficiently low. The impact of σ_i^2 on the SNR penalty $\Delta\gamma$ in **(B-8)** becomes negligible if $\gamma_w \sigma_i^2 < \varepsilon_{th}$, where ε_{th} is a small positive constant and γ_w denotes the largest expected SNR. This condition effectively enforces a sufficient degree of oversampling, i.e. Ω_p is required to be larger than the theoretical minimum. Then, step c. assures that the capacity in (K.18) is maximized, given that M_f and M_t are sufficiently large. To quantify "large" with respect to M_f and M_t an appropriate measure is to compare the estimator gain, $G_n = 1/\mathbf{w}^H\mathbf{w}$, with the theoretical one of the ideal LPIF, $\beta_f\beta_t$. Hence, if $\beta_f\beta_t\mathbf{w}^H\mathbf{w} \approx 1$, (K.19) accurately determines $S_{\text{p,opt}}$ and the bound in (K.20) becomes tight.

However, edge effects due to finite length sequences imply that it is not possible to get arbitrarily close to the performance of an ideal LPIF. In particular, due to practical constraints such as latency, the choice of M_t is limited, as there may be only a few number of pilots in time direction.

K.3.2 MIMO System

The ergodic MIMO channel capacity that includes channel estimation and pilot insertion losses in the case when channel is not known at the transmitter can be lower bounded by

$$C \geq (1 - N_T\Omega'_P)E\left[\log_2 \det\left(\mathbf{I}_{N_R} + \frac{\mathbf{H}_{n,\ell}\mathbf{H}_{n,\ell}^H}{N_T}\frac{\gamma}{\Delta\gamma}\right)\right] \tag{K.22}$$

where $\mathbf{I}_{N_R}$ is the $N_R \times N_R$ identity matrix and the CTF is defined by

$$\mathbf{H}_{n,\ell} = \begin{pmatrix} H_{n,\ell}^{(1,1)} & H_{n,\ell}^{(2,1)} & \cdots & H_{n,\ell}^{(N_T,1)} \\ H_{n,\ell}^{(1,2)} & H_{n,\ell}^{(2,2)} & \cdots & H_{n,\ell}^{(N_T,2)} \\ \vdots & \ddots & \ddots & \vdots \\ H_{n,\ell}^{(1,N_R)} & \cdots & H_{n,\ell}^{(N_T-1,N_R)} & H_{n,\ell}^{(N_T,N_R)} \end{pmatrix}. \tag{K.23}$$

Furthermore, the expectation is taken over the frequency and time dimension of $\mathbf{H}_{n,\ell}$, i.e., over indices *n* and *l*. Substituting $\Delta\gamma$, given by (B-12) or (B-17), into (K.22) we obtain

$$C \geq (1 - N_T\Omega'_P)E\left[\log_2 \det\left(\mathbf{I}_{N_R} + \frac{\mathbf{H}_{n,\ell}\mathbf{H}_{n,\ell}^H}{N_T}\frac{\gamma}{(1 + N_T\Omega'_P(S_P - 1)) \cdot \left(1 + \frac{1}{G_n S_P}\right) + \sigma_i^2\gamma}\right)\right] \tag{K.24}$$

The capacity penalty due to the pilot aided channel estimation is characterized by two factors: the SNR loss due to estimation errors and the spectral efficiency loss due to pilot insertion.

In the following we focus on the problem of capacity maximization. By doing so we consider:

- pilot boost S_p,
- pilot overhead Ω'_p and
- number of transmit antennas N_T

as optimization parameters such that the capacity is maximized.

K.3.2.1 Pilot Boost

Analogous as in SISO case an optimum pilot boost S_p which minimizes $\Delta\gamma$ and consequently maximizes capacity C can be determined. Following the same procedure we obtain

$$S_{\text{p,opt}} = \sqrt{\frac{1-N_T\Omega'_p}{N_T\Omega'_p G_n}}, \tag{K.25}$$

$$\Delta\gamma_{\min} = \left(\sqrt{1-N_T\Omega'_P} + \sqrt{N_T\Omega'_P/G_n}\right)^2 + \gamma\sigma_i^2 \tag{K.26}$$

and

$$C \geq (1-N_T\Omega'_P)E\left[\log_2 \det\left(\mathbf{I}_{N_R} + \frac{\mathbf{H}_{n,\ell}\mathbf{H}_{n,\ell}^H}{N_T}\frac{\gamma}{\left(\sqrt{1-N_T\Omega'_P} + \sqrt{\frac{N_T\Omega'_P}{G_n}}\right)^2 + \sigma_i^2\gamma}\right)\right] \tag{K.27}$$

As in the case of an SISO system we resort to an ideal low-pass interpolation filter (LPIF) in order to derive pilot distance, boost and number of transmit antenna which maximize capacity.

K.3.2.2 Pilot Distance

Analogous as in SISO case maximum capacity is attained by the maximum pilot spacing which satisfy sampling theorem (cf. Section 4.2), $\Omega'_{p,\min} = 1/(D_{f,\max}D_{t,\max})$, whereas SNR loss and corresponding capacity loss equal

$$\Delta\gamma_{\min} = \left(\sqrt{1-N_T\Omega'_{p,\min}} + c_w\sqrt{N_T}\right)^2 \tag{K.28}$$

and

$$C \geq (1-N_T\Omega'_{P,\min})E\left[\log_2 \det\left(\mathbf{I}_{N_R} + \frac{\mathbf{H}_{n,\ell}\mathbf{H}_{n,\ell}^H}{N_T}\frac{\gamma}{\left(\sqrt{1-N_T\Omega'_{p,\min}} + c_w^2\sqrt{N_T}\right)^2}\right)\right] \tag{K.29}$$

K.3.2.3 Number of Transmit Antennas

Suppose that N'_T out of the N_T transmit antennas are used for communication between the transmitter and receiver. Under such circumstances, (K.29) can be transformed to

$$C \geq \max_{N'_T \leq N_T}(1-N'_T\Omega'_{P,\min})E\left[\log_2 \det\left(\mathbf{I}_{N_R} + \frac{\mathbf{H}_{n,\ell}\mathbf{H}_{n,\ell}^H}{N'_T}\frac{\gamma}{\left(\sqrt{1-N'_T\Omega'_{p,\min}} + \sqrt{N'_T\Omega'_{p,\min}}\right)^2}\right)\right] \tag{K.30}$$

By performing analogous considerations to those done for the block fading channel in [addref] and [addref], it can be concluded that at high SNRs the number of transmit antennas which maximizes channel capacity is given by

$$N'_T = \min\{N_T, N_R, 1/(2\Omega'_{P,\min})\}. \tag{K.31}$$

Several important conclusions with respect to the capacity maximization in MIMO-OFDM can be drawn from above equation:

- The number of transmit and receive antennas should be equal.
- The amount of training should not exceed half of the OFDM frame.
- If $N_T = N_R = 1/(2\Omega'_{P,\min})$, from the expression for the pilot boost it follows that pilots should not be boosted, i.e., they should be of equal power as the data symbols.

K.3.2.4 Optimum Pilot Grid Design for PACE MIMO OFDM

Similar as in SISO case the following procedure can be applied to determine the optimum pilot grid:

a. Specify the filter parameters.
b. Choose maximum possible pilot spacings and estimator dimensions that maintain a certain interpolation error. This determines the minimum pilot overhead and the estimator gain.
c. Determine the optimum pilot boost using.(K.25).
d. Calculate the optimum number of transmit antennas using (K.31).

K.3.3 Numerical example of pilot boost, pilot distance, and number of transmit antennas optimization

In this section, numerical results are given that illustrate the benefit of the pilot grid optimization presented in Appendix K.3.1and K.3.2 of a downlink SISO or MIMO OFDM system utilising common pilots.

The independent fading taps are generated using Jakes' model having a normalized maximum Doppler frequency of $f_{\mathrm{D,max}}T_{\mathrm{sym}}$ = 0.033, which corresponds to a velocity of around 300km/h at 5GHz carrier frequency.

For the results presented in this section QPSK mapping was used. The convolutional channel code is generated using the (octal) generator polynomial (133,171), with rate $r = 1/2$ and memory 6. A soft Max-Log MAP decoder was implemented.

The channel estimation unit is implemented by 2x1D PACE, consisting of two cascaded FIR interpolation filters as described in Section 4.2 and [WIN1D21]. The chosen filter in time and frequency is a mismatched Wiener interpolation filter as described in Section 4.2. The filter coefficients are generated with the following prior knowledge about channel statistics:

- The maximum delay of the channel is set equal to the CP-length, $\tau_{\mathrm{w}} = T_{CP} > \tau_{\max}$
- While the actual velocity for the typical urban macro channel model C2 is set to 50 km/h, the max. expected velocity for generating the filter coefficients is set to 300 km/h at 5GHz carrier frequency
- SNR is assumed to be γ_{w}=30 dB, corresponding to the maximum SNR required to decode all modulation formats of the WINNER system.

K.3.3.1 Performance of SISO System

With these parameters, the sampling theorem in (4.1) requires for the pilot spacings in frequency and time D_{f}<8 and D_{f}<13. For velocities to be expected in an urban environment, D_{t} is determined by the frame length rather than the sampling theorem, and is set to D_{t} = {4,8}. The filter order in time direction was set equal to the number of pilots per frame, so M_{t} ={17,9}. Trials suggested that in frequency direction appropriate values for the oversampling factor are between 20% and 100%. Thus, the pilot spacing in frequency direction will be set to D_{f} = {2,4,6}. In frequency direction the filter order was selected as a compromise between complexity and performance, set to M_{f}=16. Out of the possible combinations two parameter sets are selected, shown in Table K-1. Also shown in Table K-1 are the pilot overheads due to channel estimation, Ω_{p}, and the difference in total pilot transmit power, S_{p}, associated to these parameter sets. It is seen that the overhead, Ω_{p}, is roughly between 2% and 13%. Furthermore, the overall transmit power for pilot symbols of the denser pilot grid (b) is S_{p}=3 dB higher than grid (a). The parameters are summarized in Table K-1.

Table K-1: Selected pilot grids

	D_{f}	D_{t}	M_{f}	M_{t}	Ω_{p}	$S_{\mathrm{p,opt}}$
(a1)	6	8	16	9	2.3%	7.9dB
(a2)	4	8	16	9	3.5%	6.4dB
(a3)	2	8	16	9	6.9%	3.5dB
(b1)	6	4	16	17	4.4%	5.0dB
(b2)	4	4	16	17	6.5%	3.3dB
(b3)	2	4	16	17	13.1%	0.4dB
Ideal LPIF					0.8%	10.4dB

The accuracy to the channel estimation error model is validated in Figure K-11. The performance of an OFDM system with 2x1D PACE is plotted and compared to the proposed estimation error approximation. The BER curve for the receiver with perfect CSI is shifted according to (K.17), and is plotted together with a receiver having implemented a channel estimation unit. The proposed Gaussian approximation of estimation errors matches the simulation results very closely.

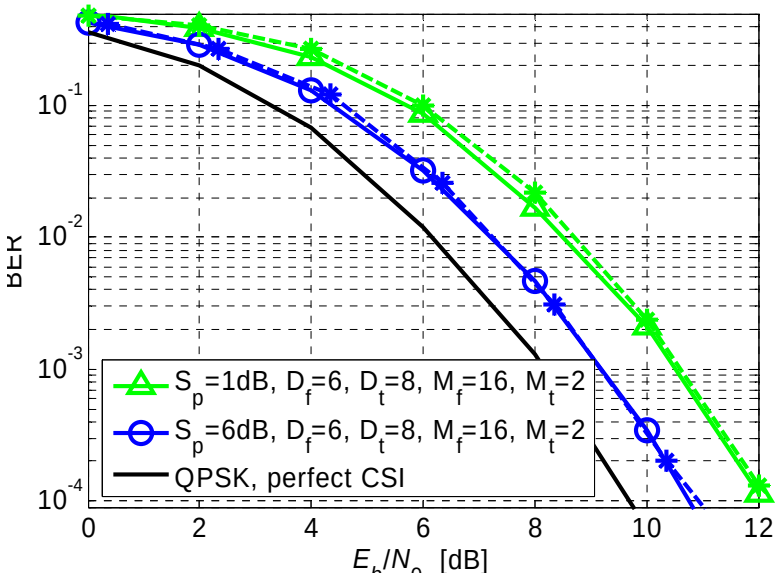

Figure K-11 Performance of an OFDM system with 2x1D PACE. Dashed lines show simulation results employing the channel estimation unit, while solid lines denote curves applying the Gaussian approximation of channel estimation errors.

In Figure K-12 the capacity in is plotted against the pilot boost S_p, at SNR $\gamma = 10\,\mathrm{dB}$, for the candidate pilot grids shown in Table K-1. Among the considered grids, the most bandwidth efficient grid a1 achieves the maximum capacity $C_{\max}$ at $S_p = S_{p,opt} = 7.9\,\mathrm{dB}$. Although grid a1 does not achieve the overall minimum $\Delta\gamma_{\min}$, grid a1 is optimum in the sense that it maximizes the channel capacity. For grids having similar pilot overhead Ω_p, the grid with higher estimator gain G_n always exhibits superior capacity, as seen by comparing grids a3 with b2. In any case, provided that $S_p = S_{p,opt}$ the decrease in capacity is negligible for Ω_p < 5% and modest for Ω_p < 10%. Furthermore, for a given Ω_p variations of the pilot boost S_p around $S_{p,\mathrm{opt}}$ have negligible impact on the capacity as long as $\left|S_p - S_{p,opt}\right| \le 2\,\mathrm{dB}$, offering some flexibility to adopt the pilot design to other system requirements, without sacrificing much capacity.

Also shown in Figure K-12 is the capacity of an ideal LPIF with $\Omega_p = c_w^2$, achieving the theoretical maximum capacity with the optimum pilot boost $S_{p,opt} = 10.4\,\mathrm{dB}$. It is seen that there is a significant gap between the theoretical maximum and the achievable capacity with a realizable filter. This gap is mostly due to a non rectangular filter transfer function, which requires extra oversampling, effectively reducing the estimator gain.

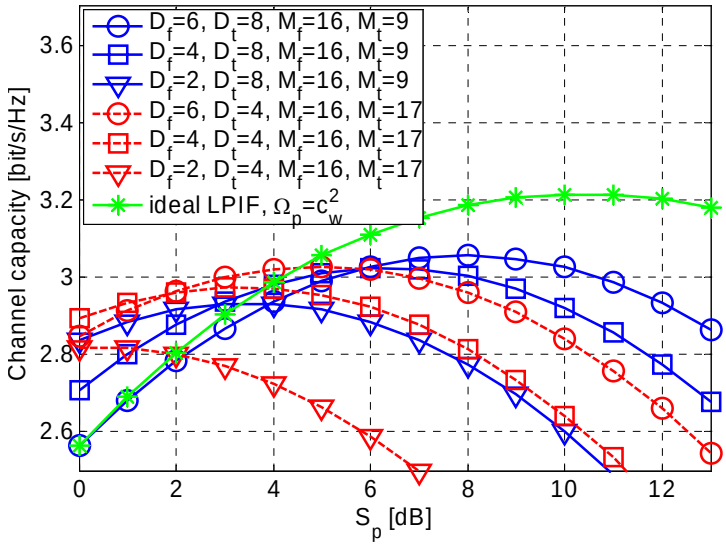

Figure K-12 channel capacity including channel estimation errors vs pilot boost S_{p}. Solid and dashed lines denote a SNR of $\gamma = 10$ dB and 30 dB.

K.3.3.2 Performance of MIMO System

In Figure K-13 the channel capacity versus pilot boost S_p for an 8×8 MIMO-OFDM system applying different pilot grids is depicted at SNR $\gamma = 10\,\mathrm{dB}$. As it can be seen, the most bandwidth efficient grid (D_f =6; D_t=8) maximizes capacity. Furthermore, maximum capacity $C_{\max}$ for each of the grids is achieved for those S_{p} that satisfy theoretically obtained optimal value. As reference, the capacity assuming an ideal LPIF is also plotted. A significant gap between the capacity using an ideal LPIF and with realizable filters is visible. This is mainly due to the fact that realizable filters do not exhibit a rectangular filter transfer function leading, inevitably reducing the estimator gain. This plot confirms the proposed semi-analytical procedure described in Section K.3.2.4.

The channel capacity versus pilot boost, S_p, for an $N \times N$ MIMO-OFDM system with pilot grid D_{f} =6; D_{t} = 8, M_{f} =16;M_{t} = 9 and for different number of transmit/receive antennas is depicted in Figure K-14. The plots where generated using the optimum pilot boost S_p that satisfy theoretically obtained optimal value. Again, the SNR is set to $\gamma = 10\,\mathrm{dB}$. Maximum capacity is achieved for $N_T = 21$ yielding $N_T \Omega_p \approx 0.5$ and $S_p = 0\,\mathrm{dB}$.

The channel capacity versus the number of transmit antennas N_T for an $N_T \times 8$ MIMO-OFDM system for grid $D_{\mathrm{f}} = 6$; $D_{\mathrm{t}} = 8$; $M_{\mathrm{f}} = 16$; and $M_{\mathrm{t}} = 9$ at SNR $\gamma = 10\,\mathrm{dB}$ is shown in Figure K-15. Again, the pilot boosting level is optimized according to the theoretical considerations. As a reference, capacity of the corresponding system assuming perfect channel estimation and no loss due to pilots is shown. It can be observed that for $N_T \approx 8$ maximum capacity is achieved. For higher values the reduction in available bandwidth due to the pilot insertion dominates, lowering the achievable capacity.

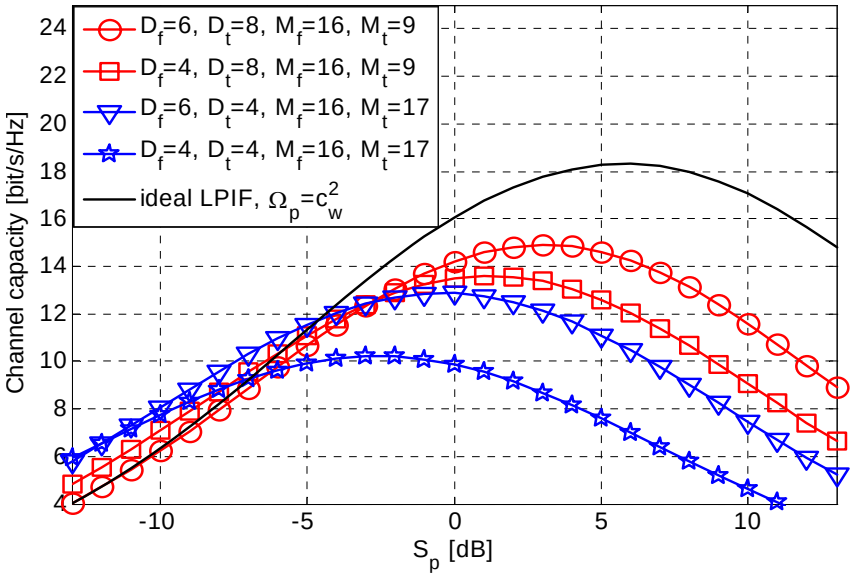

Figure K-13 Capacity versus pilot boost for 8 × 8 MIMO-OFDM system applying different pilot grids.

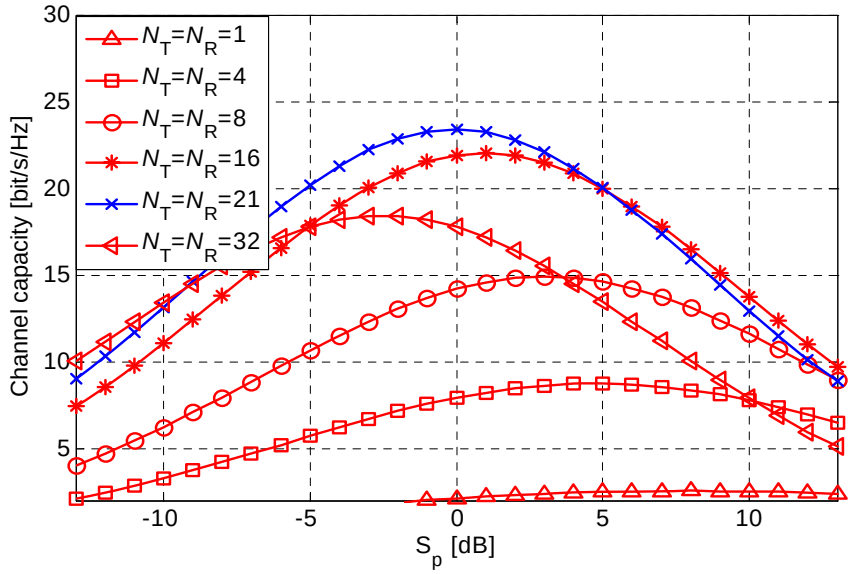

Figure K-14 Capacity versus pilot boost for *N* × *N* MIMO-OFDM system for different number of antennas N_T; $D_f = 6$; $D_t = 8$; $M_f = 16$; **and** $M_t = 9$.

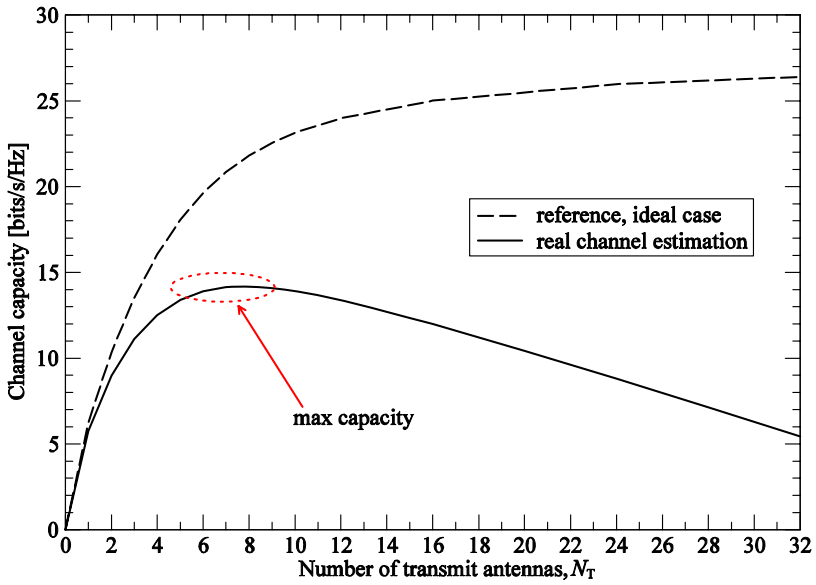

Figure K-15 Loss in channel capacity due to channel estimation vs pilot boost S_p. Solid and dashed lines denote a SNR of $\gamma = 10$ dB and 30 dB.

Appendix L. SNR degradation due to IBI and/or ICI – simulation results

In this section, results of estimated SNR degradation are presented. Simulations were performed for the system parameters presented in Appendix A, i.e.,

- Base Coverage Urban scenario with Frequency Division Duplex (FDD) and C1 NLOS channel model;
- Micro-cellular scenario with Time Division Duplex (TDD) and B1 NLOS/LOS channel models;
- Indoor scenario with TDD and A1 NLOS/LOS channel models.

The Inter-Carrier Interference occures when the frequency synchronisation algorithms are not able to estimate the exact value of the frequency offset caused by the Doppler shift and the mismatch between frequencies of the transmit and receive oscillators. The SNR degradation due to ICI versus normalised frequency synchronisation error is presented in Figure L-1[8]. Each curve was generated for different value of the desired SNR and is marked with its value and specific colour. Since the SNR degradation due to ICI expressed by (H.46) is independent of the channel model and system parameters Figure L-1 is valid for all WINNER scenarios. It can be easily seen that the OFDM system is very vulnerable to frequency offsets. The increase of the order of ten of the normalised frequency offset estimation error causes the increase of the SNR degradation in the order of one hundred. In the worst case the, i.e., when the frequency synchronisation error is equal to one-tenth of the subcarrier spacing, the desired signal-to-noise ratio of 30 dB is decreased by 15 dB.

The Inter-Block Interference (IBI) occurs only if timing synchronisation error is excessively large, or the channel impulse response is longer then the cyclic prefix. For the WINNER case only the first scenario takes place. As mentioned in Appendix L there is a range of timing synchronisation errors that will not cause IBI. The IBI-free ranges for different transmission modes and channel models are presented in

. The channel length counted in samples is computed for the transmitted signal sampling time.

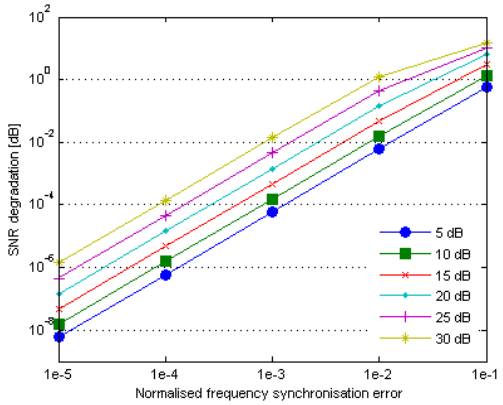

Figure L-1 SNR degradation vs normalised frequency synchronisation error

[8] Note that the vertical axis showing the SNR degradation in dB has a logarithmic scale for better visualisation of the results.

Table L.1 Timing synchronisation errors not causing IBI

Transmission mode	Prefix length (samples)	Channel model	Channel length (ns)	Channel length (samples)	IBI-free range
TDD	128	A1 LOS	75 ns	8	<-120, 0>
TDD	128	A1 NLOS	135 ns	14	<-114, 0>
TDD	128	B1 LOS	105 ns	11	<-117, 0>
TDD	128	B1 NLOS	485 ns	49	<-79, 0>
FDD	256	C2 NLOS	1420 ns	117	<-139, 0>

For the given system and channel parameters if the timing synchronisation error is within the above range then the SNR degradation is equal to 0 dB. Otherwise, the SNR degradation is greater then 0 dB and its value depends on the timing synchronisation error and on the SNR of the desired signal. The relationship between the SNR degradation and the timing synchronisation error is shown in Figure L-2 for TDD mode and A1 LOS channel, in Figure L-3 for TDD mode and A1 NLOS channel, in Figure L-4 for TDD mode and B1 LOS channel, in Figure L-5 for TDD mode and B1 NLOS channel and in Figure L-6 for FDD mode and C2 NLOS channel. All curves were generated for six desired SNR values, i.e., 5, 10, 15, 20, 25 and 30 dB. Figures marked with (a) show the SNR degradation when the desired signal interferes with the preceding one, and marked with (b) show the SNR degradation when the desired signal interferes with the succeeding one. It was also assumed that the timing synchronisation error is not greater than the cyclic prefix length for case "(a)" and the channel impulse response length for case "(b)".

It can be easily seen that the interference with the succeeding symbol causes greater SNR degradation than the interference with the preceding symbols. This is due to the fact that the interfering preceding symbol is transmitted through the most delayed and the weakest channel paths whilst the succeeding interfering symbol is transmitted through first and the strongest channel paths. Thus, the interference power in the first case is smaller than the interference power in the latter case.

Taking into account the range of IBI-free region and the SNR degradation due to the interference with the succeeding symbol the FFT window of the received symbol should not start after the cyclic prefix but few samples earlier, depending on the timing synchronisation algorithm accuracy.

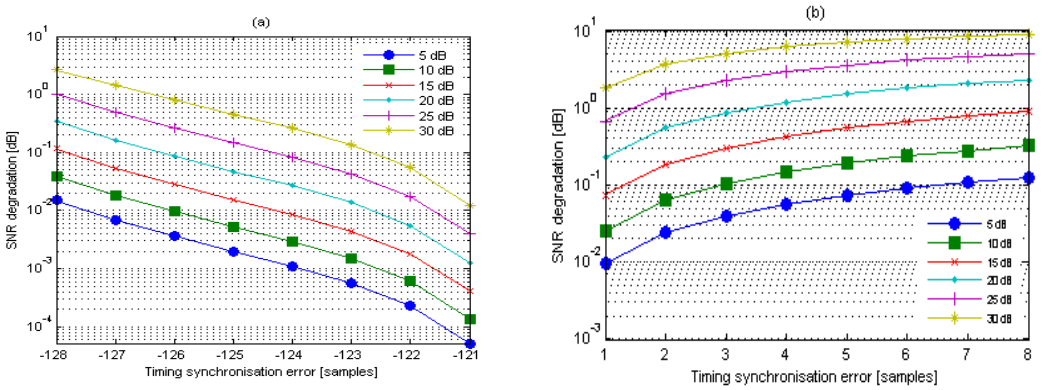

Figure L-2 A1 LOS channel, SNR degradation due to IBI vs timing synchronisation error, preceding symbol interferes with the desired one (a), succeeding symbol interferes with the desired one (b)

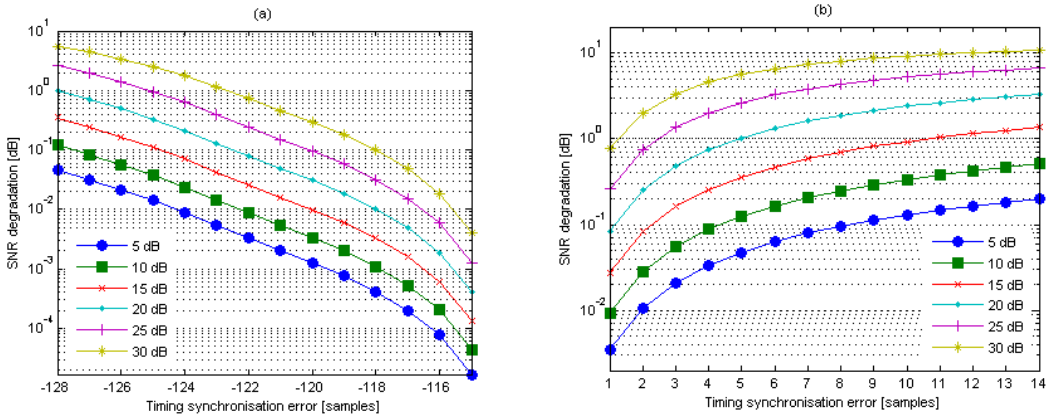

Figure L-3 A1 NLOS channel, SNR degradation due to IBI vs timing synchronisation error, preceding symbol interferes with the desired one (a), succeeding symbol interferes with the desired one (b)

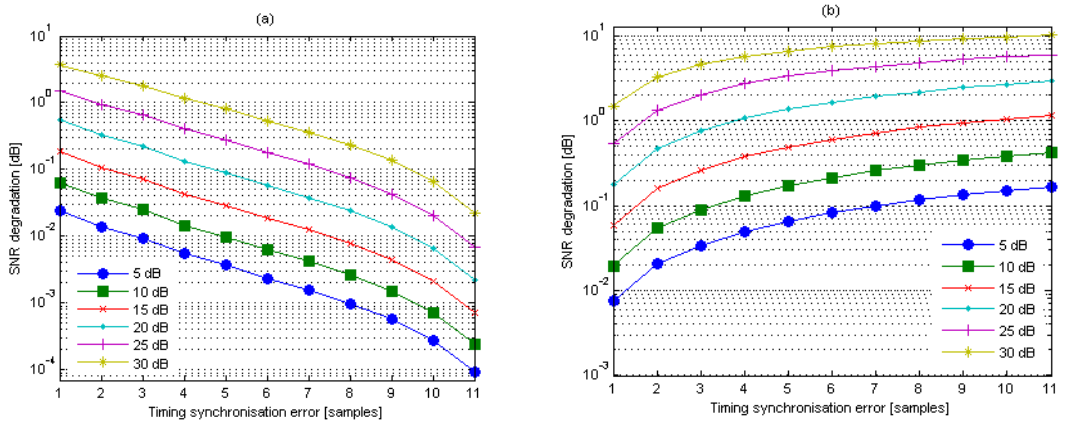

Figure L-4 B1 LOS channel, SNR degradation due to IBI vs timing synchronisation error, preceding symbol interferes with the desired one (a), succeeding symbol interferes with the desired one (b)

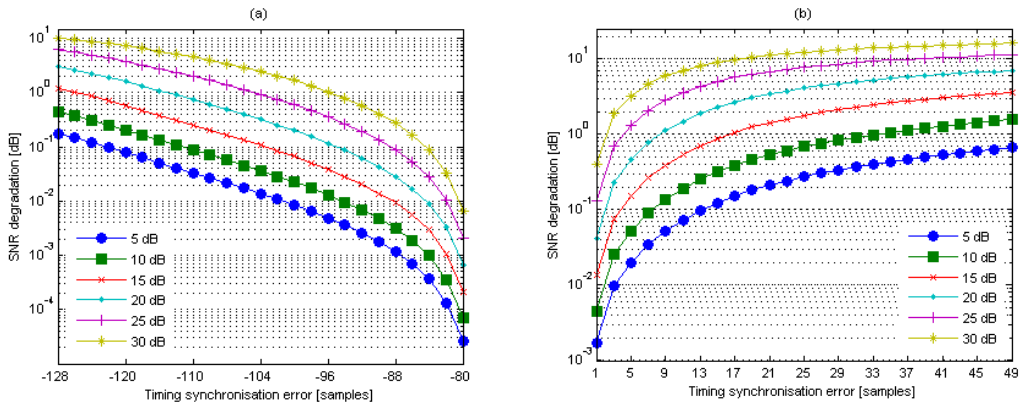

Figure L-5 B1 NLOS channel, SNR degradation due to IBI vs timing synchronisation error, preceding symbol interferes with the desired one (a), succeeding symbol interferes with the desired one (b)

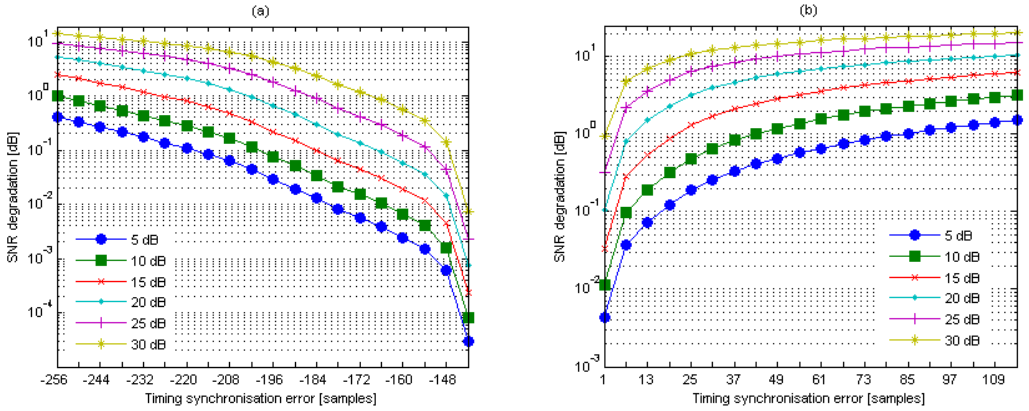

Figure L-6 C2 NLOS channel, SNR degradation due to IBI vs timing synchronisation error, preceding symbol interferes with the desired one (a), succeeding symbol interferes with the desired one (b)

In general, both phenomena, i.e., IBI and ICI can take place jointly as a result of timing and frequency synchronisation errors occurring simultaneously. The results of the estimated SNR degradation are presented in Figure L-7 for TDD and A1 LOS channel, in Figure L-8 for TDD mode and A1 NLOS channel, in Figure L-9 for TDD mode and B1 LOS channel model, in Figure L-10 for TDD and B1 NLOS channel and in Figure L-11 for FDD and C2 NLOS channel. All figures present the relationship between the SNR degradation and timing synchronisation errors obtained for five different frequency offset estimation errors normalised to the subcarrier distance, i.e., 1e-1, 1e-2, 1e-3, 1e-4 and 1e-5. SNR of the desired signal was equal to 30 dB in all cases. Figures marked with "(a)" show the SNR degradation due to ICI and IBI caused by the preceding symbol and figures marked with "(b)" present the SNR degradation due to ICI and IBI caused by the succeeding symbol.

Similar to the previous results, the SNR degradation is smaller for the case of interference with preceding symbol than for the case of interference with succeeding symbol. Moreover, in the first case the degradation is less dependent on timing synchronisation errors then on frequency synchronisation errors. When the succeeding symbol interferes with the desired one small frequency offset estimation errors have almost no influence on SNR degradation. For large frequency offset estimation errors, e.g., 1e-1, the SNR degradation is independent of IBI. Thus, these results prove that frequency synchronisation algorithms should be designed with special attention.

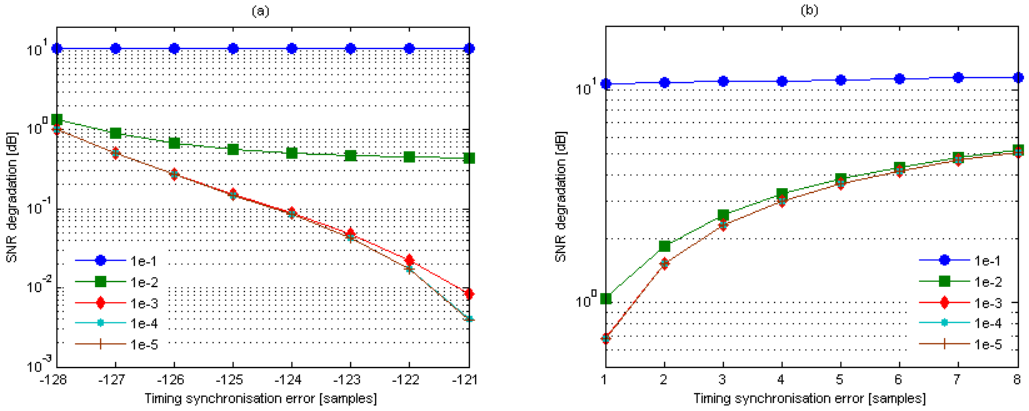

Figure L-7 A1 LOS channel, SNR degradation due to IBI and ICI vs timing synchronisation error, preceding symbol interferes with the desired one (a), succeeding symbol interferes with the desired one (b)

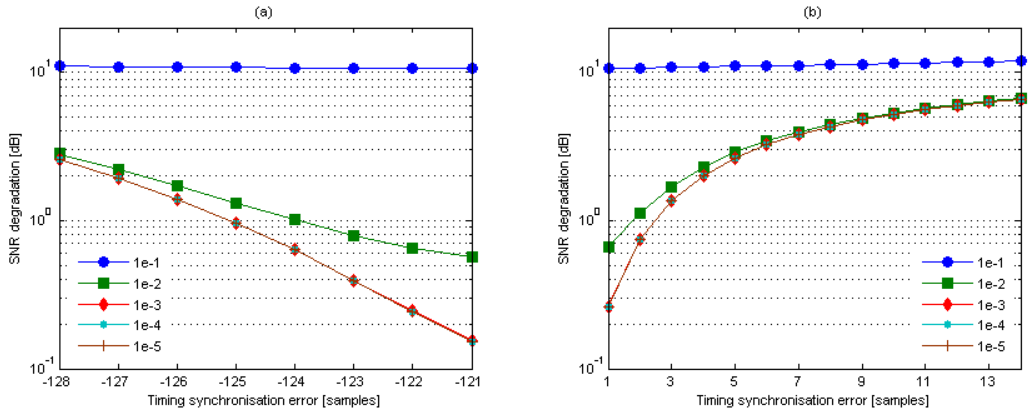

Figure L-8 A1 NLOS channel, SNR degradation due to IBI and ICI vs timing synchronisation error, preceding symbol interferes with the desired one (a), succeeding symbol interferes with the desired one (b)

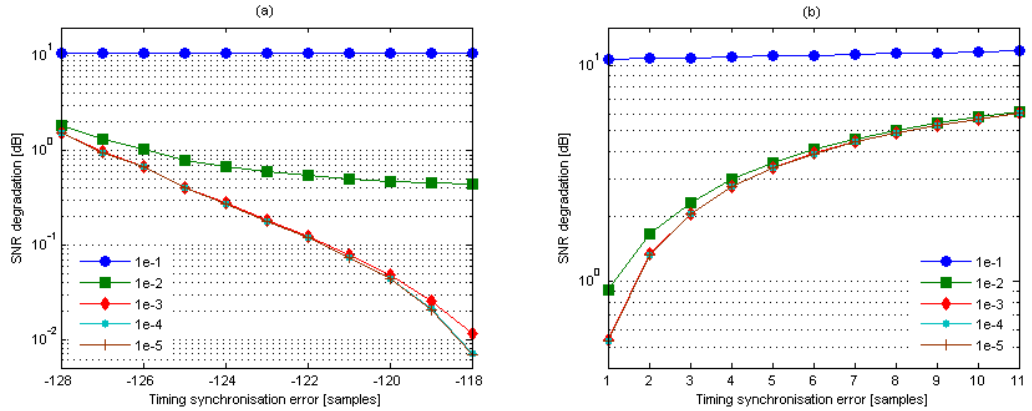

Figure L-9 B1 LOS channel, SNR degradation due to IBI and ICI vs timing synchronisation error, preceding symbol interferes with the desired one (a), succeeding symbol interferes with the desired one (b)

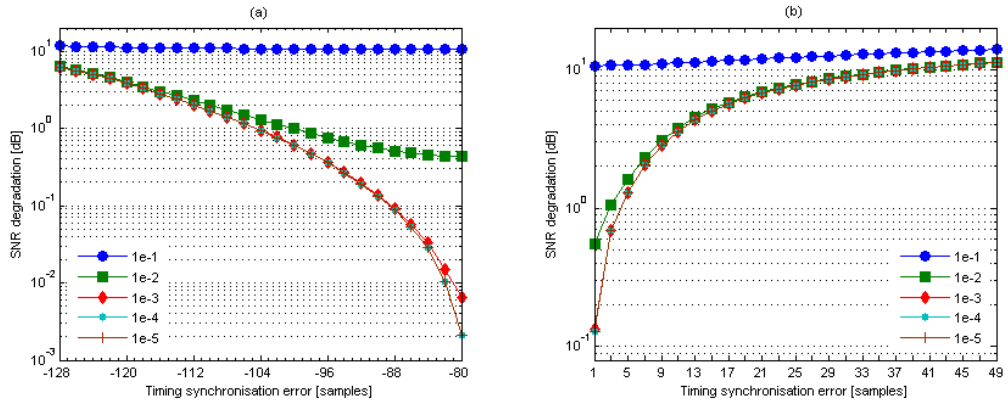

Figure L-10 B1 NLOS channel, SNR degradation due to IBI and ICI vs timing synchronisation error, preceding symbol interferes with the desired one (a), succeeding symbol interferes with the desired one (b)

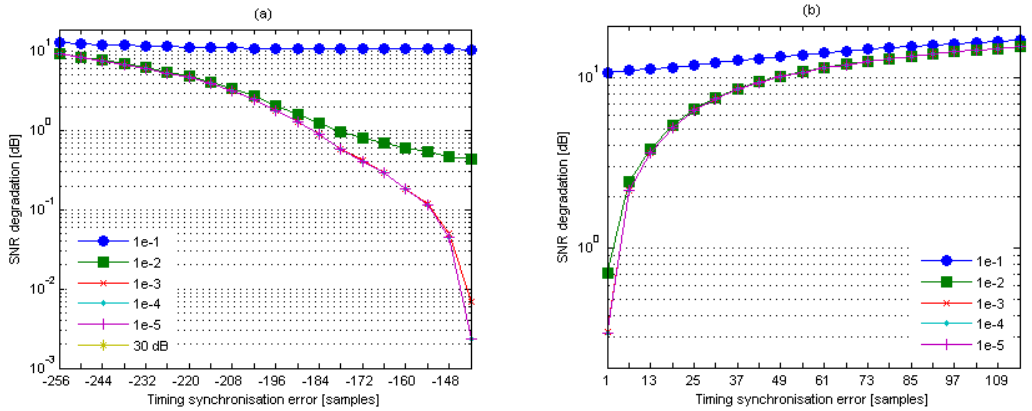

Figure L-11 C2 NLOS channel, SNR degradation due to IBI and ICI vs timing synchronisation error, preceding symbol interferes with the desired one (a), succeeding symbol interferes with the desired one (b)

References

[AB07] G. Auer and J. Bonnet, "Threshold Controlled Iterative Channel Estimation for Coded OFDM", in *Proc. IEEE VTC 2007 spring*, Dublin, Ireland, pp. 1737-1741, Apr. 2007.

[ADF+07] G. Auer, F. Danilo-Lemoine, D. Falconer and C-T Lam, "Design of Time and Frequency Domain Pilots for Generalized Multicarrier Systems", in *Proc. ICC 2007*, Glasgow, UK, June 2007.

[AH06a] J. Akhtman and L. Hanzo, "An Optimized-Hierarchy-Aided Maximum Likelihood Detector for MIMO-OFDM," in *Proc. IEEE Vehicular Technology Conference* (VTC '06 Spring), vol. 3, Melbourne, Australia, pp. 1526–1530, 7-10 May 2006.

[AH06b] J. Akhtman and L. Hanzo, "Low complexity approximate log-MAP detection for MIMO systems," in *Proc. IEEE Wireless Communications and Networking Conference* (WCNC '06), vol. 3, Las Vegas, USA, pp. 1759–1764, 3-6 April 2006.

[Ala98] S.M. Alamouti, "A Simple Transmit Diversity Technique for Wireless Communications", *IEEE Journal of Selected Areas in Communications*, Vol. 16, pp. 1451-1458, October 1998.

[Aro07] D. Aronsson, "Channel Estimation and Prediction from a Bayesian Perspective". Licentiate Thesis, Uppsala University, Sweden, June 2007.

http://www.signal.uu.se/Publications/abstracts/l071.html

[AS07] D. Aronsson and M. Sternad, "Kalman predictor design for frequency-adaptive sheduling of FDD OFDMA uplinks," *IEEE Conference on Personal, Indoor and Mobile Radio Communications (PIMRC)*, Athens, Greece, September 2007.

[BA06] J. Bonnet and G. Auer, "Optimized Iterative Channel Estimation for OFDM", *Proc. IEEE VTC fall* 2006, Montreal, Canada, pp. 1-5, Sept. 2006.

[BRF07] S. Bittner, W. Rave, G. Fettweis, "Phase Noise Suppression in OFDM with Spatial Multiplexing" in *Proc. VTC Spring 2007*, Dublin, Ireland, Apr. 2007

[BT02] N. Benvenuto and S. Tomasin, "On the Comparison Between ODFM and Single Carrier with a DFE using a Frequency Domain Feedforward Filter", in *IEEE Trans. Communications*, Vol. 50, No. 6, June 2002, pp. 947-955.

[CCA07] M. Carta, I. Cosovic and G. Auer, "Pilot design for MIMO-OFDM with beamforming", *Proc. Multi-Carrier Spread Spectrum Workshop* (MC-SS 2007) May 2007.

[Ce101] S. Celebi, "Interblock Interference (IBI) and Time of Reference (TOR) Computation in OFDM systems", *IEEE Trans. Commun.*, vol. 49, no. 11, pp. 1895-1900, Nov. 2001

[DLF04a] R. Dinis, C.T. Lam, D. Falconer, "On the Impact of Phase Noise and Frequency Offset on Block Transmission CDMA Schemes", in *Proc. ISCWS, Mauritius,* Sept. 2004

[DLF04b] R. Dinis, C.T. Lam and D. Falconer, "Carrier Synchronisation Requirements for CDMA Systems with Frequency-Domain Orthogonal Signature Sequences", in *Proc. ISSSTA, Sydney*, Sept. 2004

[DFL+07] F. Danilo-Lemoine, D. Falconer, C-T Lam, M. Sabbaghian and K. Wesołowski, "Power Backoff Reduction Techniques for Generalized Multicarrier Waveforms", in *EURASIP J. on Wireless Communications and Networking special issue on multicarrier systems*, Nov., 2007.

[DGE03] R. Dinis, A. Gusmao and N. Esteves, "On Broadband Block Transmission over Strongly Frequency-Selective Fading Channels", in *Proc. Wireless 2003*, Calgary, July 2003.

[Dlu02] Z. Dlugaszewski, "Simple Coarse Frequency Offset Estimation Scheme for OFDM Burst Transmission Using Specially Designed Preamble Symbols", in *Proc. International OFDM-Workshop 2002*, Hamburg, Germany, pp. 227-231, Sept. 2002

[Dlu03] Z. Dlugaszewski, "Methods of OFDM Transmission on Fading Channels," Doctoral Thesis, Poznan University of Technology, Poznan, 2003

[DMR00] A. Demir, A. Mehrotra and J. Roychowdhury, “Phase Noise in Oscillators: A Unifying Theory and Numerical Methods for Characterisation” *IEEE Transactions on Circuits and Systems-I* 47(5):655-674, 2000

[DW02] Z. Długaszewski, K. Wesołowski, “Simple Coarse Frequency Offset Estimation Schemes for OFDM Burst Transmission”, in *Proc. PIMRC 2002, Lisbon, Portugal*, pp. 567-571, Sep. 2002

[Ekm02] T. Ekman, Prediction of Mobile Radio Channels. Modelling and Design. Ph.D. Thesis, Signals and Syst., Uppsala Univ, 2002.

http://www.signal.uu.se/Publications/abstracts/a023.html

[ESA02] T. Ekman, M. Sternad and A. Ahlen, "Unbiased power prediction on broadband channels″ *IEEE VTC 2002-Fall*, Vancouver, Canada, Sept. 2002.

[EPG95] U. Ernst, K. Pawelzik, and T. Geisel, “Synchronisation induced by temporal delays in pulse-coupled oscillators”, Phys. Rev. Letters, 74(9):1570 – 1573, Feb. 1995.

[FDL+07a] D. Falconer, F. Danilo-Lemoine, C-T Lam and M. Sabbaghian, “Power Backoff Reduction for Generalized Multicarrier Waveforms”, in *Proc EUSIPCO 2007*, Poznan, Poland, Sept. 2007

[FOR93] S. Forrest, “Genetic Algorithms: Principles of Natural Selection Applied to Computation”, *Science*, vol. 261, no. 5123, pp. 872–878, August 1993.

[Fos96] G. J. Foschini, “Layered Space-Time Architecture for Wireless Communication in a Fading Environment when using Multiple Antennas”, *Bell Laboratories Technical Journal*, vol. 1, no. 2, pages 41-59, 1996.

[GB89] J. J. Grefenstette and J. E. Baker, “How Genetic Algorithms Work: A critical look at implicit parallelism,” in *Proc. International Conference on Genetic Algorithms*, J. D. Schaffer, Ed. California, USA: Morgan Kaufmann, 1989, pp. 20–27.

[GDGLP00] X. Guardiola, A. Diaz-Guilera, M. Llas, and C.J. Perez, “Synchronisation, diversity, and topology of networks of integrate and fire oscillators”, *Phys. Rev.* E, 62(4):5565–5570, Apr. 2000.

[GOL89] D. E. Goldberg, “Genetic Algorithms in Search, Optimization, and Machine Learning”, Reading, Massachusetts: Addison-Wesley, 1989.

[HK06] L. Hanzo and T. Keller, “An OFDM and MC-CDMA Primer”, IEEE Press - John Wiley & Sons Ltd., 2006.

[HKR97] P. Höher, S. Kaiser, and P. Robertson. Pilot-Symbol-Aided Channel Estimation in Time and Frequency. In *Proc. Communication Theory Mini-Conf. (CTMC) within IEEE Global Telecommun. Conf. (Globecom’97),* Phoenix, USA, pages 90–96, 1997.

[Hoe91] P. Höher. TCM on Frequency Selective Land-Mobile Radio Channels. In *Proc. 5th Tirrenia Int. Workshop on Dig. Commun.,* Tirrenia, Italy, pages 317–328, September 1991.

[HOL75] J. Holland, “Adaptation in Natural and Artificial Systems”, Ann Arbor, Michigan: University of Michigan Press, 1975.

[HS03] Y.-W. Hong and A. Scaglione, “Time synchronisation and reach-back communications with pulse-coupled oscillators for UWB wireless ad hoc networks”, in *Proc. IEEE Conference on Ultra Wideband Systems and Technologies 2003*, pp. 190–194, Nov. 2003

[JAG+06a] M. Jiang, J. Akhtman, F. Guo, and L. Hanzo, “Iterative Joint Channel Estimation and Multi-User Detection for High-Throughput Multiple-Antenna Aided OFDM Systems,” in *Proc. IEEE Vehicular Technology Conference* (VTC ’06 Spring), vol. 1, Melbourne, Australia, pp. 221–225, 7-10 May 2006.

[JAG+06b] M. Jiang, J. Akhtman, and L. Hanzo, “Iterative Joint Channel Estimation and Multi-User Detection for Multiple-Antenna Aided OFDM Systems,” *IEEE Transactions on Wireless Communications*, vol. 6, no. 8, pp. 2904–2914, August 2007.

[Kay93] S. M. Kay. *Fundamentals of Statistical Signal Processing: Estimation Theory*. Prentice Hall, Englewood Cliffs, NJ, 1993.

[Lar96] L.E. Larson, ed., *RF and Microwave Circuit Design for Wireless Communications*, Artech House, Norwood, MA., 1996.

[LFD07] C-T Lam, D. Falconer and F. Danilo-Lemoine, "PAPR Reduction Using Frequency Domain Multiplexed Pilot Sequences", in *Proc. WCNC 2007*, Hong Kong, March, 2007.

[LLTC04] J. Lee, H. L. Lou, D. Toumpakaris, J. M. Cioffi, "Effect of Carrier Frequency Offset on OFDM Systems for Multipath Fading Channels", in *Proc. on Globecom 2004*, Dallas, USA, pp. 3721-3725, Nov. 2004

[LWB06] P. Liu, S. Wu and Y. Bar-Ness, "A Phase Noise Mitigation Scheme for MIMO WLANs with Spatially Correlated and Imperfectly Estimated Channels" *IEEE Communicatios Letters*, 10(3):141-143, 2006

[Ma07] Y. Ma, and R. Tafazolli, "Channel estimation for OFDMA uplink: a hybrid of linear and BEM interpolation approach", *IEEE Trans. Signal Processing*, vol. 50, pp. 1568-1573, April 2007.

[MIT96] M. Mitchell, "An Introduction to Genetic Algorithms", Cambridge, Massachusetts: MIT Press, 1996.

[MUH91] H. Mühlenbein, "Foundations of Genetic Algorithms", G. Rawlins, Ed. California, USA: Morgan Kaufmann, 1991.

[MS90] R.E. Mirollo and S.H. Strogatz, "Synchronisation of pulse-coupled biological oscillators", *SIAM J. APPL. MATH*, 50(6):1645–1662, Dec. 1990

[NLF07] B. Ng, C-T Lam, and D. Falconer, "Turbo Frequency Domain Equalization for Single Carrier Broadband Wireless Systems", *IEEE Trans. Wireless Communications*, Vol. 6, No. 2, Feb., 2007

[NP02] K. Nikitopoulos, A. Polydoros, "Post-FFT Fine Frame Synchronisation of OFDM systems", in *Proc. IST Mobile Summit'02*, Thessaloniki, Greece, June 2002

[Ohno04] S. Ohno and G. B. Giannakis, "Capacity maximizing MMSE-optimal pilots for wireless OFDM over frequency-selective block Rayleigh-fading channels", in *IEEE Trans. Information Theory*, vol. 50, no. 9, pp. 2138-2145, Sep 2004.

[PNG03] A. Paulraj, R. Nabar, and D. Gore, "Introduction to Space-time Wireless Commnications", Cambridge University Press, May 2003.

[PRF04] D. Petrovic, W.Rave and G. Fettweis, "Intercarrier Interference due to Phase Noise in OFDM: Estimation and Suppression" in *Proc. IEEE VTC'04 fall*, Los Angeles, USA, pp 2191-2195, 2004

[PVM95] T. Pollet, M. Van Bladel and M. Moeneclaey, "BER Sensitivity of OFDM Systems to Carrier Frequency Offset and Wiener Phase Noise", in *IEEE Trans. Comm.*, Vol. 43, , pp. 191-193, Feb.-April, 1995

[SDF07] F. Siddiqui, F. Danilo-Lemoine and D. Falconer, "PIC-Assisted IBDFE-Based Iterative Spatial Channel estimation with Intra- and Inter-Cell Interference in SC-FDE System", in *Proc. VTC 2007 fall*, Baltimore, USA, Oct., 2007

[SC97] T.M. Schmidl and D.C. Cox, "Robust Frequency and Timing Synchronisation for OFDM", in *IEEE Trans. Comm.,* Vol. 45, No. 12, pp. 1613-1621, Dec. 1997

[SJ06] S. Schiffermüller and V. Jungnickel, „Practical Channel Interpolation for OFDMA", in *Proc. Globecom 2006*, San Francisco, USA, Nov. 2006.

[SF06] M. Sabbaghian, D. D. Falconer, "Comparison between Convolutional and LDPC Code based Turbo Frequency Domain Equalization", in *Proc. IEEE International Conference on Communications (ICC 2006)*, vol. 1, Istanbul, Turkey, pp. 5432-5437, June 2006.

[SS06] S. Sezginer, H. Sari, "OFDM Peak Power Reduction with simple amplitude predistortion", in *IEEE Comm.Letters*, vol. 10, issue 2, pp. 65-67, February 2006

[Sto98] J. Stott, "The Effects of Phase Noise in COFDM", *European Broadcasting Union Review Technical,* No. 276, pp. 12-25, 1998

[SA03] M. Sternad and D. Aronsson, "Channel estimation and prediction for adaptive OFDM downlinks," *IEEE VTC 2003-Fall*, Orlando, Fla, Oct. 2003.

[SA05] M. Sternad and D. Aronsson, ”Channel estimation and prediction for adaptive OFDMA/TDMA uplinks, based on overlapping pilots”, *International Conference on Acoustics, Speech and Signal Processing (ICASSP 2005)*. Philadelphia, PA, USA, March 19-23 2005.

[SEA01] M. Sternad, T. Ekman and A. Ahlén, “Power prediction on broadband channels”, *IEEE Vehicular Technology Conference VTC01-Spring*, Rhodes, Greece, May 6-9 2001. [SFS06] T. Svensson, S. Falahati and M. Sternad, “Coding and Resource Scheduling in Packet Oriented Adaptive TDMA/OFDMA Systems”, *Proceedings IEEE Vehicular Technology Conference Spring*, Melbourne, Australia, May 2006.

[SLA02] M. Sternad, L. Lindbom and A. Ahlén, "Wiener design of adaptation algorithms with time-invariant gains," *IEEE Transactions on Signal Processing*, vol. 50, pp. 1895-1907, August 2002.

[SSO+07] M. Sternad, T. Svensson, T. Ottosson, A. Ahlen, A. Svensson and A. Brunström, “Towards systems beyond 3G based on adaptive OFDMA transmission”, Invited paper, *Proceedings of the IEEE*, Special Issue on Adaptive Transmission, vol. 95, no. 12, Dec. 2007.

[SFF+07] T. Svensson, T, Frank, D. Falconer, M. Sternad, E. Costa and A. Klein, ”B-IFDMA – A power efficient multiple access sceme for non-frequency adaptive transmission”. IST Mobile and Vehicular Summit, Budapest, July 2007.

[STSF04] T.C.W. Schenk, X-J Tao, P.F.M Smulders and E.R. Fledderus, “Influence and Suppression of Phase Noise in Multi-Antenna OFDM”, in *Proc. IEEE VTC’04 fall*, Los Angeles, USA, pp. 1443-1447, 2004

[STSF05] T.C.W. Schenk, X-J Tao, P.F.M Smulders and E.R. Fledderus, “On the Influence of Phase Noise Induced ICI in MIMO OFDM Systems”, in *IEEE Electronics Letters*, 9(8):682-684, 2005

[TA07] A. Tyrrell, and G. Auer, “Imposing a Reference Timing onto Firefly Synchronisation in Wireless Networks”, in *Proc. IEEE VTC Spring 2007,* Dublin, Ireland, Apr. 2007

[TAB06] A. Tyrrell, G. Auer, and C. Bettstetter, “Fireflies as Role Models for Synchronisation in Ad Hoc Networks”, in *Proc. Bionetics 2006,* Calvalese, Italy, Dec. 2006

[TFF07] M. Trivellato, F. Boccardi, and F. Tosato, “User Slection Schemes for MIMO Broadcast Channels with Limited Feedback”, in *Proc. IEEE VTC Spring 2007,* Dublin, Ireland, pp. 2089-2093, Apr. 2007.

[TJC99] V. Tarokh, H. Jafarkhani, A.R. Calderbank, “Space-Time Block Codes from Orthogonal Designs”, in *IEEE Transactions on Information Theory*, vol. 45, n°5, pp. 1456-1467, July 1999.

[TZH+06] T. Lestable, E. Zimmerman, M.-H. Hamon, and S. Stiglmayr, “Block-LDPC Codes vs Duo-Binary Turbo-Codes for European Next Generation Wireless Systems”, in *Proc. IEEE Vehicular Technology Conference* (VTC ’06 Fall), Montreal, Canada, 25-28 September 2006.

[WB02] S. Wu and Y. Bar-Ness, “A Phase Noise Suppression Algorithm for OFDM based WLANs”, in *IEEE Communications Letters,* 6(12):535-537, 2002

[WFG+98] P. W. Wolniansky, G. J. Foschini, G. D. Golden, and R. A. Valenzuela, “V-BLAST: an Architecture for Realizing Very High Data Rates over the Rich Scattering Wireless Channel”, in *Proc. URSI International Symposium on Signals, Systems and Electronics*, 1998, pages 295-300.

[WHI94] D. Whitley, “A Genetic Algorithm Tutorial,” Statistics and Computing, vol. 4, no. 2, pp. 65–85, June 1994.

[WIN1D21] IST-2003-507581 WINNER, “D2.1 Identification of Key Radio-Link Technologies”, June, 2004.

[WIN1D22] IST-2003-507581 WINNER “D2.2 Feasibility of Multi-Bandwidth Transmissions”, October, 2004.

[WIN1D23] IST-2003-507581 WINNER, “D2.3 Assessment of Radio-Link Technologies”, February, 2005.

[WIN1D24] IST-2003-507581 WINNER, “D2.4 Assessment of adaptive transmission technologies”, February, 2005.

[WIN1D25] IST-2003-507581 WINNER “D2.5 Duplex Arrangements for Future Broadband Radio Interface”, Oct., 2004.

[WIN1D27] IST-2003-507581 WINNER, “D2.7 Assessment of Advanced Beamforming and MIMO Technologies”, February 2005.

[WIN1D210] IST-2003-507581 WINNER, “D2.10 Final Report on Identified RI Key Technologies, System Concept, and Their Assessment”, December 2005.

[WIN1D42] IST-2003-507581 WINNER, “D4.2 Impact of cooperation schemes between RANs (incl. Complexity estimate)”, February 2005.

[WIN1D541] IST-2003-507581 WINNER. D5.4 Final Report on Link Level and System Level Channel Models, September 2005.

[WIN1D54] IST-2003-507581 WINNER, “Final Report on Link Level and System Level Channel Models”, November, 2005.

[WIN1D71] IST-2003-507581 WINNER, “D7.1 System Requirements”, July 2004

[WIN1D76] IST-2003-507581 WINNER, “D7.6 WINNER System Concept Description”, Oct. 2005

[WIN2D112] IST-4-027756 WINNER II., D1.1.2 “WINNER II Channel Models, Part I Channel Models”, September, 2007.

[WIN2D223] IST-4-027756 WINNER II., D2.2.3 “D2.2.3 Modulation and Coding schemes for the WINNER system”, November, 2007.

[WIN2D341] IST-4-027756 WINNER II. D3.4.1 “The WINNER II Air Interface: Refined Spatial-Temporal Processing Solutions”, November, 2006.

[WIN2D353] IST-4-027756 WINNER II. D3.5.3 “Final assessment of relaying concepts for all CGs scenarios under consideration of related WINNER L1 and L2 protocol functions”, November, 2007

[WIN2D461] IST-4-027756 WINNER II. D4.6.1 “The WINNER II Air Interface: Refined Multiple Access Concepts”, November, 2006.

[WIN2D471] IST-4-027756 WINNER II, “D4.7.1 Interference Averaging Concepts“, June, 2007.

[WIN2D472] IST-4-027756 WINNER II, “D4.7.2 Interference Avoidance Concepts“, June, 2007.

[WIN2D473] IST-4-027756 WINNER II, “D4.7.3 Smart Antenna Based Interference Mitigation“ June 2007.

[WIN2D482] IST-4-027756 WINNER II, “D4.8.2 Cooperation schemes validation”, June 2007.

[WIN2D6131] IST-4-027756 WINNER II. D6.13.1 WINNER II Test Scenarios and Calibration Cases Issue 1, June 2006

[WIN2D6137] IST-4-027756 WINNER II, "D6.13.7 WINNER II Test Scenarios and Calibration Cases Issue 2," November 2006.

[WIN2D61311] IST-4-027756 WINNER II, "D6.13.11 Final CG "metropolitan area" description for integration into overall System Concept and assessment of key technologies”, October 2007.

[WIN2D61314] IST-4-027756 WINNER II, "D6.13.14 WINNER II system concept description“, November 2007.

[YLCC00] B. Yang, K.B. Letaief, R.S. Cheng and Z. Cao, “Timing Recovery for OFDM Transmission”, in *IEEE Journal on Selected Areas in Comm.* Vol. 18, no. 11, pp. 2278-2291, Nov. 2002

[ZO03] X. Zhang and B. Ottersten, “Performance analysis of V-BLAST structure with channel estimation error,” in *Proc. IEEE Workshop on Signal Processing Advances in Wireless Communications (SPAWC 2003)*, Rome, Italy, pp. 487–491, 2003.